THE EFFECT OF SURFACE RENEWAL ON MASS TRANSFER IN AGITATED CONTACTORS

by

Adil Ahmed Awedh Al-Hemiri

A thesis submitted to the University of Aston in Birmingham for the degree of Doctor of Philosophy

Department of Chemical Engineering,
The University of Aston in Birmingham.

November, 1973.

SUMMARY

The literature on the hydrodynamics and mass transfer characteristics of liquid extraction in rotary agitated columns has been reviewed.

A 4 inch diameter, 6 feet high Rotating Disc Contactor was constructed, and operated, to investigate droplet hydrodynamics and mass transfer efficiencies with a range of 5 liquid-liquid systems. High speed still and ciné photography were used for drop size and oscillation time measurements; solute concentrations were measured by refractive indices.

Hold-up and volumetric capacity were found to vary with operating parameters as previously reported. Axial point hold-ups were determined directly and correlated by,

$$X = \left[0.0013N+0.38(V_d-1)-1\right](h-h^2)+0.076(1-1/V_d)$$

Mean drop size decreased with column height and the results were correlated by,

$$d_{32}/R = 4.7 \times 10^{17} \left(\frac{NR^2\rho_c}{\mu_c}\right)^{-3.33} \left(\frac{\mu_d}{\mu_c}\right)^{0.23} \left(\frac{NR\mu_c}{\sigma_i}\right)^{2.0} (X)^{0.225} \text{EXP.}\left[0.4\left(\frac{n}{z}\right)\right]$$

Correlations of similar form were obtained with discs selected to be 'wetted' by the dispersed phase and with 'wetted' cones. The latter novel design employed polypropylene cones to eliminate the dispersed liquid vortex produced by enhanced coalescence when solute transfer was out of this phase.

Original observations were made of phase inversion phenomena and a model proposed resulting in the criteria for inversion,

$$V_c/V_d = 1-\left[1/X\right]-\left[1/aX^2\right]+2\sum_{j=3}^{j}\left\{b^{j-3}/a^{j-1}X^j\right\}$$

where a = 4.1, b = 2.1 and j = 3,4,5 to j dependant upon the system physical properties and design geometry.

Mass transfer data were interpreted by comparing observed mass transfer coefficients with values calculated assuming the stagnant drop, circulating drop, oscillating drop and fresh surface models. Generally best agreement was obtained with the latter two models. For the transfer direction dispersed → continuous phase, a mechanism of surface renewal was indicated and 'surface ageing' postulated for the opposite direction. In the former case sheet and vortex formations and a coalescence-redispersion mechanism occurred. Mass transfer under such conditions was the sum of the contributions of the individual periods,

$$\sum_{n=1}^{n}\left[\sum_{i=1}^{i}\int\left[\frac{dc}{(c-c^*)}\right]_i\right]_n = \sum_{n=1}^{n}\left[\sum_{i=1}^{i} A_i/V_i\int K_i\,dt\right]_n$$

where n is the total number of compartments and i refers to the particular period, viz. formation, free rise, etc.

Disc wetting properties had no significant effect on efficiency. Compared to non-mass transfer operation, axial mixing in both phases was greatly reduced when transfer was from the dispersed to the continuous phase because of enhanced coalescence and greater with transfer in the opposite direction due to inhibition.

A single 12 inch RDC compartment was designed to investigate the effect of disc 'wettability' on droplet break-up mechanisms; with wetted discs redispersion of dispersed phase was by rim disintegration or, at high flow rates, by sheet rupture.

A 4 inch spray column was used to demonstrate the phenomena of stagnant, circulating, and pulsating drops undergoing mass transfer during formation. Schlieren photography and 'density matching' techniques were employed for this purpose.

Further studies have been initiated into phase inversion and droplet impaction and coalescence on wetted surfaces.

ACKNOWLEDGEMENT

The author wishes to thank:

The Iraqi Ministry of Oil for awarding the Scholarship for this research;

Professor G. V. Jeffreys for supplying the equipment and for his interest in the subject of this study;

Dr. C. J. Mumford for his supervision and interest;

The Laboratory and Technical Staff of the Department of Chemical Engineering for their assistance in fabricating equipment throughout the period of this research;

Miss P. Sage for the drawings; and finally

Mrs. C. Meredith and Miss E. Broughton of 'The Secretary Byrds' for their patience and excellent quality of the typing and photocopying.

CONTENTS

APPENDICES

NOMENCLATURE

REFERENCES

1. INTRODUCTION

In liquid-liquid extraction the components of a liquid mixture are separated by treatment with a solvent in which one or more of them is preferentially soluble. The process entails the dispersion of one liquid as droplets into a continuous phase followed by solute transfer to or from the droplets, and finally separation of the dispersed phase by flocculation and coalescence.

The rate of solute transfer in moles per unit time may be expressed as the product of an overall mass transfer coefficient K, the interfacial area A, and a concentration driving force ΔC,

$$N = K A \Delta C \qquad (1.1)$$

The overall coefficient is dependent on the series resistance to diffusion inside the drop, outside the drop and at the interface. Neglecting the latter term,

$$\frac{1}{K} = \frac{1}{k_d} + \frac{1}{mk_c} \qquad (1.2)$$

where m is the distribution coefficient. The total interfacial area is a function of the droplet size and dispersed phase hold-up in the contactor. Assuming that the drops are spherical and can be represented by a mean value $d_{vs.}$, (1).

$$A = \frac{6}{d_{vs}} \quad x \qquad (1.3)$$

where x is the dispersed phase hold-up.

This, however, is an idealised picture which takes no account of the roles of molecular and eddy diffusional mechanisms, which exist dependent upon the hydrodynamic regime. Three regimes have been recognised, viz., laminar, transitional, and turbulent. Whilst molecular diffusion predominates in the laminar and transition regions the main mechanism in the turbulent region is eddy diffusion (1,2). Furthermore, a wide distribution of droplet size exists in practical contactors, dependent upon the degree of turbulence which results in break-up and recoalescence effects. The flow patterns inside and outside the individual drops, also differ, These determine, whether a droplet is 'stagnant', 'circulating' or 'oscillating'. The different film coefficients for each mode of transfer are reviewed in Chapter 4.

In practice the extent of droplet interaction and its promotion by interfacial turbulence may be significant. Moreover the driving force is always reduced, to some extent, by the effect of axial mixing.

Mass transfer rates higher than those predicted from Equations 1.1 to 1.3 have been achieved in practice. This can be attributed to droplet interaction and the continual introduction of fresh interface due to a repeated coalescene-redispersion mechanism, termed 'surface renewal' (3,4). The concept of surface renewal has been the subject of many studies in recent years, in both liquid-liquid (3,4,5) and vapour-liquid (5,6) processes, in an attempt to provide a better understanding of the mechanisms involved and to assist equipment design.

Three possible surface renewal mechanisms may be distinguished in liquid-liquid mass transfer operations:

1) Eddies of uniform solute concentrations, emanate from a turbulent bulk and arrive at the interface, where they remain for a short time, undergo steady state penetration of solute by molecular diffusion, and are swept away to be replaced by others (7). This leads to,

$$N_A = \sqrt{D_{AS}} \ (C_{Ai} - C_{Ao}) \qquad (1.4)$$

2) Interfacial turbulence, mostly appearing in the form of erratic oscillation and violent internal circulation (1,8).

3) Both the above mechanisms consider liquid on a micro scale. The third mechanism concerns surface renewal effects caused by induced turbulence by agitation or impaction leading to repeated coalescence and break-up. The same mechanism is applicable to the coalescence and redispersion in perforated plate contactors.

Surface renewal, may be promoted or inhibited by the following factors which therefore affect the rate of mass transfer,

i) The degree of turbulence from agitation and its effect upon the frequency of break-up;

ii) The use of packing or plates, e.g., as in Scheibel (9) and perforated plate (1) columns, to increase coalescence and redispersion;

iii) Wettability of the column internals, which may result in increased coalescence;

iv) Direction of mass transfer. This may either increase or reduce the interfacial turbulence and the droplet interaction associated with it; and

v) The presence of surfactants. This is, strictly, a special case of (iv).

Factors (i), (ii) and (iii) apply to mechanism type 3, while factors (iv)and (v) apply to mechanisms 1 and 2.

In this work factors pertaining to mass transfer rates and volumetric capacities of continuous contactors are reviewed. Most attention is given to agitated columns, wherein surface renewal effects would be expected to be predominant, and in particular, in Chapter 3, to the R.D.C. upon which the experimental investigations were based.

The design and construction of a 4 inch R.D.C. is described in Chapter 7.

Methods employed to evaluate surface renewal effects, dependent upon:-

(a) wettability of discs,

and (b) direction of mass transfer,

are described in Chapter 8. The results have been compared and mass transfer models presented in Chapters 9 and 10.

In addition the little reported phenomena of phase inversion was also studied, and a mathematical model describing it in counter-current agitated contactors is presented in Chapter 9.

2. LIQUID-LIQUID EXTRACTION EQUIPMENT

There are two major categories of equipment for liquid extraction.

(A) Stagewise contactors, in which the liquids are mixed, extracted and separated in discrete stages. The mixer-settler range of equipment is included in this class.

(B) Differential, continuous contact, extractors, in which the equivalent of many stages may be incorporated into a single apparatus. These may be categorised as follows:

(1) Gravity operated extractors, which include:

(a) Non-mechanical dispersion

(I) Baffle plate columns

(II) Wetted wall columns

(III) Spray columns

(IV) Packed columns

(V) Perforated-plate columns

(b) Mechanically agitated extractors

(I) Pulsed columns

(II) Rotary agitated columns, which include:

(i) The Schiebel column

(ii) The Oldshue-Rushton column

(iii) The Rotating Disc Contactor

(iv) The Assymetric rotating disc contactor

(v) Other rotary extractors

(2) Centrifugal extractors

2.1 ROTARY AGITATED COLUMNS

2.1.1 The Oldshue-Rushton Column (Fig.2.1)

The Oldshue-Rushton extractor (27,28), was introduced in 1945, but has only recently achieved commercial status outside North America. The extractor consists of a vertical column divided into compartments by horizontal stator rings; each compartment has four vertical baffles and is agitated by a turbine impeller driven by a central shaft. The column diameter is normally three times that of the impeller and twice the height of a compartment (29), although different column geometries have been employed (27,28,30,31).

Gutoff (30) confirmed that the purpose of the stators is to reduce the interstage mixing; by decreasing the stator diameter the interstage mixing was reduced. Clearly this can only be achieved at the expense of capacity. Gutoff (30) and later Ingham (32), showed that interstage mixing was small at low agitator speeds, but increased rapidly and linearly with speed once the turbulent region ($Re > 2.5 \times 10^4$) was reached. Other workers (27,28), demonstrated that an optimum speed exists for any flow rate.

Flooding characteristics of the Oldshue-Rushton column were found to be similar to those of other extraction columns (27). Although little work has been carried out to investigate hold-up, it was claimed to be correlated with the column parameters by the expression (33)

$$\frac{V_d}{x} + \frac{V_c}{1-x} = \overline{V}_N(1-x) \exp.\ [x\ (Z/_M - 4.1)] \qquad (2.1)$$

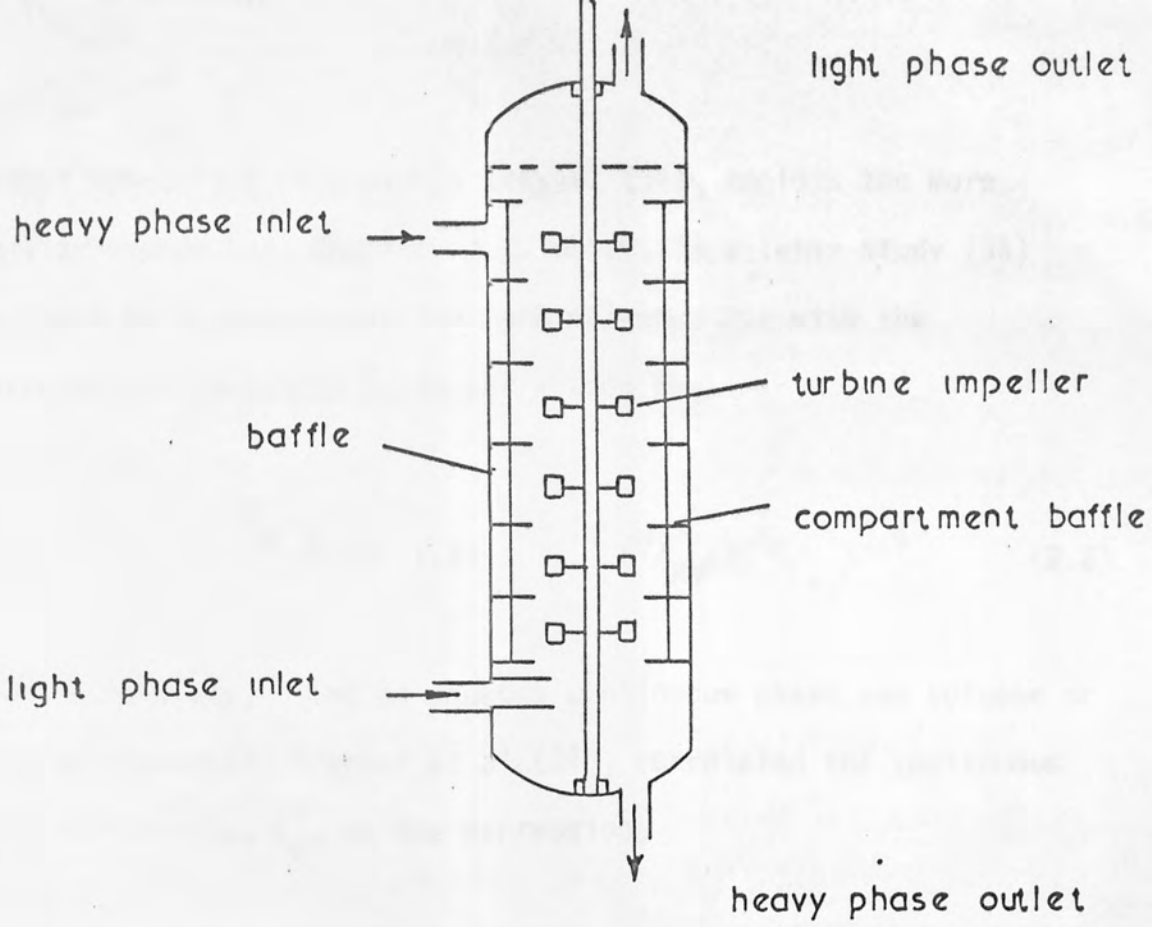

Fig. 2.1. Oldshue Rushton column

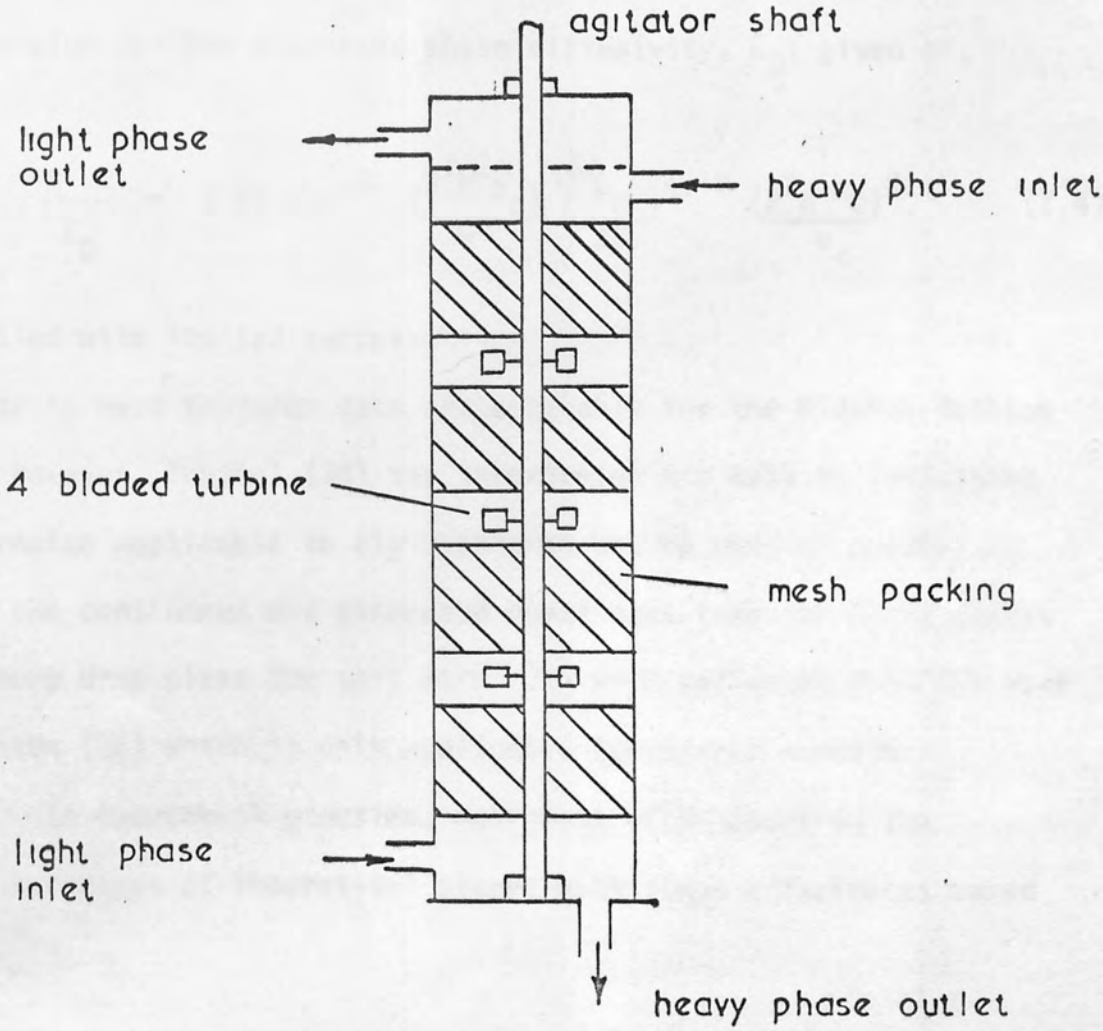

Fig. 2.2. Original scheibel column (8)

Another expression proposed by Treybal (34), employs the more familiar expression, Equation 3.1, which, in a later study (35) was found to be unsuitable for such columns; but with the characteristic velocity $\overline{V}_N$ is correlated by,

$$\frac{\overline{V}_N \mu_c}{\sigma} = 1.77 \times 10^{-4} \left(g/_{RN2}\right)\left(\Delta\rho/_{\rho_c}\right)^{0.9} \qquad (2.2)$$

In the same study, using an aqueous continuous phase and toluene or kerozine dispersed, Treybal et al (34), correlated the continuous phase diffusivity, E_c', in the expression,

$$\frac{X E_c'}{V_c H} = -0.14 + 0.0268 \frac{R N X}{V_c} \qquad (2.3)$$

An expression for the dispersed phase diffusivity, E_D'; given as,

$$\frac{R^2 N}{E_D'} = 3.93 (10^{-8}) \left(\frac{R^3 N^2 \rho_c}{\sigma}\right)^{1.54} \left(\frac{\rho_c}{\Delta\rho}\right)^{4.18} \left(\frac{R^2 N \rho_c}{\mu_c}\right)^{0.61} \qquad (2.4)$$

was applied with limited success.

Little or no mass transfer data are available for the Oldshue-Rushton column, however, Treybal (34) has interpreted his data as indicating that formulae applicable to rigid spheres can be used to predict K_c and K_d, the continuous and dispersed phase mass transfer coefficients. Furthermore drop sizes for this work (34) were estimated from the work of Thornton (36) which is only applicable to stirred vessels.

In commercial practice, design is often based on the erroneous concept of theoretical stages with stage efficiences based

on experience (29). The phase ratios employed in such columns have been of the order of 0.6 to 1:1 (27,28), although in practice a wider range, similar in order to that of a R.D.C., may be possible albeit with lower total throughputs. Finally, mass transfer characteristics of a pilot-scale Oldshue-Rushton column are currently under study (37).

Modified Designs

In a modified form of the Oldshue-Rushton column,the impeller is arranged eccentrically and small pipes are provided for interstage flow (38). This design reduced the amount of backmixing, albeit at the expense of capacity.

A central draft tube, to reduce axial mixing, was introduced, in a later study (32). This modification offered no improvement in practice.

2.1.2 The Scheibel Column (Fig.2.2)

The Scheibel column consists of an alternate sequence of mixing and packed sections in a vertical column. Each mixing section is agitated by a turbine impeller supported on a central shaft. Open knitted mesh is used in the packed compartments. The column does not operate as a mixer-settler since droplets persist throughout the packed sections (39,40). Thus, although some phase separation does occur in the packing, its main function is to isolate the mixing sections. The wetting properties of the packing have a profound effect on the droplet behaviour and column capacity (35). The relative height of packed and mixing zones may be varied to suit the particular duty.

The capacity of the column is limited by the permissible flowrate through the packing. The interstices size of the mesh packing is below the critical packing size, calculable for any system, for which capacity correlations have been established (41,42), and the hydrodynamics of flow through such packings is only now receiving attention (43). The total hold-up comprises a dynamic and a static hold-up. The latter is the dispersed phase retained in the packing after shut down. The hold-up was found to increase linearly with agitator speed, when the organic (light) phase was dispersed (39,44). However when the aqueous (heavy) phase was dispersed, the hold-up was found to pass through a maxima.

In normal operating conditions of the Scheibel column, a coalescence-redispersion mechanism has been found predominant. Due to the globules formation, the mean interfacial area in both the mixing and packed zones of the column is unpredictable (35). In the same study (35) it was suggested that, for systems with surface tension >9.7 dyne/cm., omission of the packing was desirable. Earlier Scheibel (45) proposed replacement of the packing with baffled calming zones for systems with high viscosity and interfacial tension.

To effect good phase separation knitmesh packings used in the calming zone are normally selected to be preferentially wetted by the dispersed phase. However, recently, it was found that enhanced coalescence occurred at the junction of a high and low energy surface (46). By using packings made of dissimilar materials, one a high energy surface and a second low energy surface, e.g., D.C. packing, the efficiency of separation of both oil-water and water-oil dispersions was significantly enhanced (46).

Modified Designs

Several modifications of the Scheibel column design have been proposed. One such design has ring shaped baffles supported immediately above and below the impeller. Compartment baffles are attached to the column shell (45). For systems of low viscosity and interfacial tension, using columns below 3 ft in diameter the mixing section may be isolated by the usual woven mesh sections. Scheibel, also used knitted mesh sections between the inner baffle plates.

A design similar to the latter Scheibel modification has been reported to have improved scale-up characteristics. The rotor speed for optimum extraction was correlated by (47),

$$ND^{0.9} = \text{const.} \qquad (2.5)$$

Another modification has been described by Tudose (48), where the packed sections were replaced by baffled calming zones.

2.1.3 The Rotating Disc Contactor

Because the basic R.D.C. design is fundamental to this work it was considered appropriate to discuss it fully in Chapter 3. However, in an attempt to reduce axial mixing effects, or possibly to circumvent the Shell patent position, many designs have been proposed which represent in part modifications of the basic arrangement of stators and rotors; these are discussed in 2.1.4 and 2.1.5 below.

2.1.4 The Asymmetric Rotating Disc Contactor (Fig.2.3)

The A.R.D.C. is the most important modification of the R.D.C. It was proposed by Misek (49,50), and has the agitated compartments placed off-centre. Next to the agitated zones is a transfer section, separated from it by a baffle, which permits flow between the zones only via passages near the periphery. A set of horizontal settling-zone baffles may be positioned at any height with respect to the firm position of the set of mixing zone baffles (51). It is claimed to inhibit unfavourable flow behaviour such as axial mixing. Nevertheless in scaling up from 1m to 2m diameter it is necessary to allow for an increase in the 'nominal H.E.T.S.' from 1.2m to 1.75m. Some loss in efficiency probably occurs due to phase entrainment in the settling zones. The design appears therefore to offer no practical advantage over the conventional R.D.C. considering the increased column diameter required. An approximate relation for the estimation of extractor capacity has been published (50,51,52). One known application is in caprolactam extraction but several are claimed to be in operation in typical R.D.C. applications (50).

2.1.5 Other Rotary Extractors

Less common rotary extractors are considered here. These are, basically, modifications of the extractors discussed earlier.

One such extractor, a modified R.D.C. design by Reman (53), has two or more rotors in the column shell. This is claimed to minimise instability of the vortex flow pattern in large diameter columns but there is no record of its industrial use.

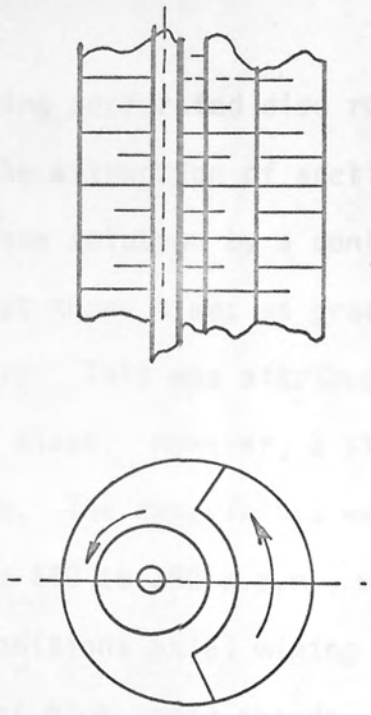

Fig. 2.3. The A.R.D.C.

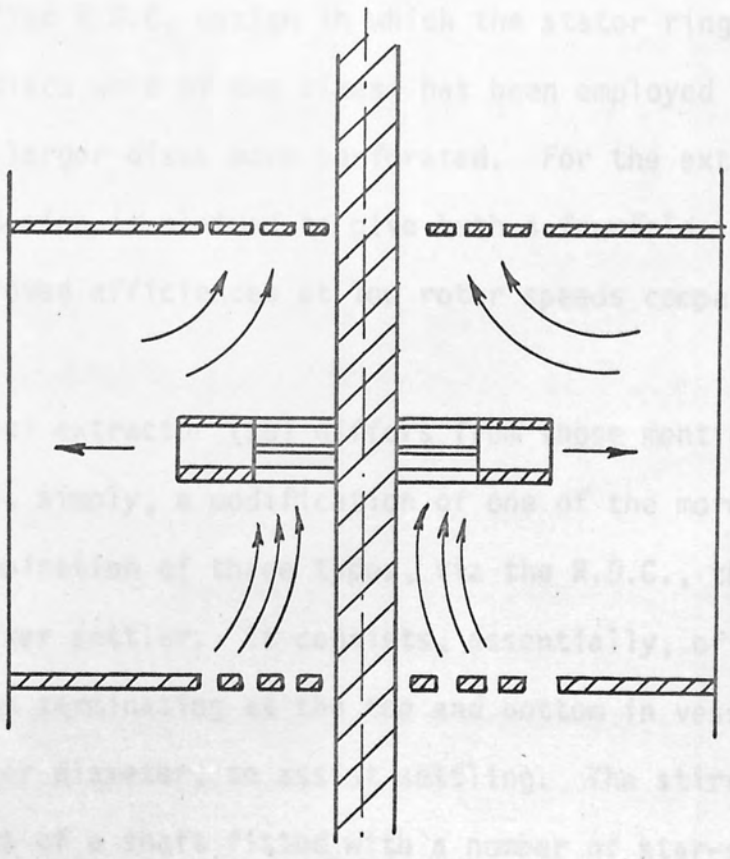

Fig. 2.4. The khuni extractor

A design employing perforated disc rotors has been tested on a pilot scale (54,55). The extraction of acetic acid from a dilute (3-5% w/w) dispersed benzene solution by a continuous aqueous phase gave mass transfer at least three times as great as with a conventional R.D.C. of the same geometry. This was attributed to the substantial reduction in average drop sizes. However, a significant reduction in capacity was also observed. The experiments were carried out at low rotor speeds, ranging from 140 to 350 r.p.m., with discs 52mm in diameter. Under these conditions axial mixing effects were insignificant. These may be troublesome at high rotor speeds.

Similar results have been obtained, with the system benzene-acetone-water, employing a design in which the discs were replaced by rotors comprising 4, 60° arcs (56).

A modified R.D.C. design in which the stator rings were omitted and the discs were of two sizes, has been employed by Sokov et al (57). The larger discs were perforated. For the extraction of aromatics, this design is claimed to give both a fourfold increase in capacity and improved efficiences at low rotor speeds compared with the R.D.C.

The Ziehl extractor (58) differs from those mentioned above in that it is not, simply, a modification of one of the more common designs but a combination of three types, viz the R.D.C., the pulsating column and the mixer settler. It consists, essentially, of a vertical, cylindrical column terminating at the top and bottom in vessels of considerably larger diameter, to assist settling. The stirring mechanism consists of a shaft fitted with a number of star-shaped impellers. By means of special gears through which the motor drives the shaft, vertical reciprocal as well as rotary motion is imposed on

the impellers so that they move in a sinus curve. Use of star shaped impellers gives the column a free cross-sectional area of 65-75% which allows very large throughputs to be handled by the extractor. Theoretical efficiencies were claimed to have been attained in the manufacture of phenol formaldehyde resins, from 1.4% phenol solution contaminated with formaldehyde and various other impurities. Crude naphtha was used as a solvent (58).

The Khuni extractor (59), Fig.2.4, incorporates the principles of the R.D.C., the Oldshue-Rushton and Sieve plate columns. It consists of a cylindrical shell with a relatively larger diameter at the top and bottom, to assist settling. The column is divided into compartments by plates perforated only at the centre so that the flow, from one compartment to the next, is directed towards the agitator. Each compartment has four vertical baffles and is agitated by an impeller, sandwiched between two washer type discs. Such a design would give low throughputs.

Recently a patent was issued for a design in which annular ring stators alternated with centrally located stators. Agitation was provided by a rotating cylinder. This design is a combination of the older laboratory annular extractor and the disc and doughnut column (60).

Finally, a column design has been patented, in which, the rotors were replaced by vertical perforated baffles. The motion of the baffle was oscillatory. HTU values obtained for this column, using the system carbon tetrachloride-acetic acid-water, compared favourably with those for the R.D.C. (61).

The above review indicates some of the wide variety of modifications possible with agitated contactors. It would appear however that these have no practical advantages over the conventional designs, and therefore an R.D.C. was constructed for the present study.

2.2 OTHER LIQUID-LIQUID EXTRACTORS

A wide variety of extractor designs exists within the earlier classification. However, since they are not directly relevant to this investigation, only their main characteristics will be summarised.

(i) Mixer-Settlers. These are stagewise contact units in which operation may be batch or continuous. The mixer generally comprises a baffled tank with a four or six bladed turbine agitator. In continuous operation the flow from the mixer is transferred into a larger settler vessel, usually 2.5 times the size of the mixer, to effect coalescence and phase separation (1,10,11,12,13).

(ii) Non-Mechanical Dispersion Extractors. These consist of vertical cylindrical shells, generally containing internal flow restrictions, e.g., baffled plates, packings and perforated plates and are classified accordingly. Spray columns and wetted wall columns are also included in this category. For packed and plate columns the mass transfer efficiency has been found to be significantly affected by the "wettability" of the column internals (16,17,18,19,20), and this will be discussed in Chapter 5.

(iii) Pulsed Columns. In this type of column the liquid phases are interdispersed by giving the continuous phase a pulsed motion. This may be induced by either a diaphragm pump or the introduction of compressed air. They have found particular use in handling radioactive solutions, since no moving parts are present within the extractor, and they may be located behind heavy radiation shields without the necessity for maintenance (1,21,22,23). Mass transfer data for such columns have been reported by various authors (1,24, 25,26). However power requirements of pulsed columns are relatively high.

(iv) Centrifugal Extractors. Unlike ordinary extractors in which countercurrent flow is maintained by the force of gravity, centrifugal contactors utilise large centrifugal forces to induce high velocities; consequently small extractor volumes are possible (1,10). High initial, maintenance and operating costs are the main disadvantages of these extractors. However the small extractor size for high flow capacities results in space savings and reduction in amount of solvent. The Podbeielniak (62,63,64) and the Luwesta extractors (65,66), have found useful applications in the pharmaceutical industry.

3. THE ROTATING DISC CONTACTOR (Fig.3.1)

The rotating disc contactor, was first introduced by Reman in 1951 (31). It consists of a vertical cylindrical shell divided into a number of compartments by a series of stator rings; a rotating disc supported on a central shaft is located in each compartment. The feed inlets, at each end of the column, are arranged tangentially in the direction of rotation. The outlets are usually through the top and bottom plates of the column. The dense phase is introduced into the top of the column and the light phase into the bottom, so that, countercurrent flow is established by gravity. One of the phases is dispersed by the action of the rotating discs. At the ends of the column there are settling zones for phase separation. Flat rotor discs without protrusions are generally used to create uniform shearing conditions and hence obtain as small a spread in droplet sizes as possible.

Originally used in the furfural extraction of petroleum lubricating oils, the R.D.C. has now found extensive use in almost all petroleum extraction processes including propane deasphalting and naphtha sweetening, as well as in the by-product coke, food,metal separation, and organic chemical industries. It has also been used for the separation of oxy-compounds from Fischer-Tropsch synthesis oil (67) and in the U.S.S.R. for the extraction of caprolactam (68). For the latter application it is claimed to be more economic than centrifugal extractors and superior in flexibility of operation and in insensitivity to solid phase impurities. Use of the R.D.C. as a continuous reactor has also been reported (69).

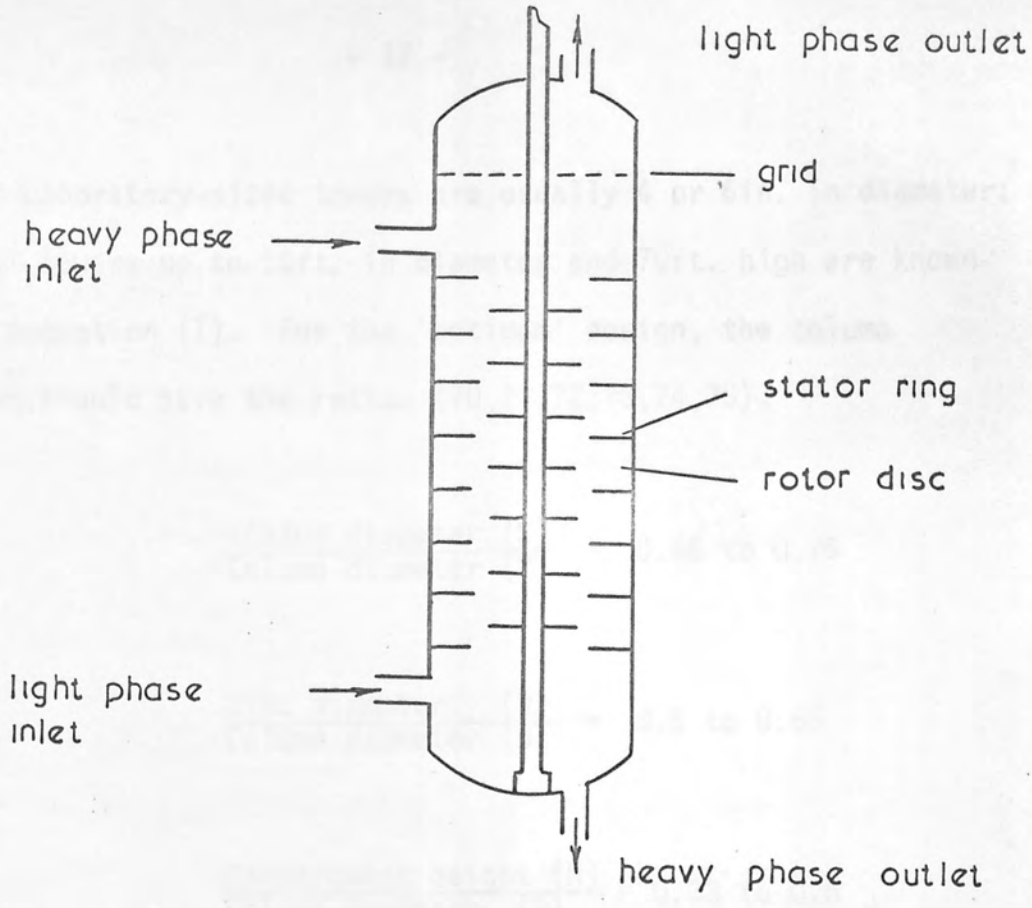

Fig. 3.1. Rotating disc contactor (31)

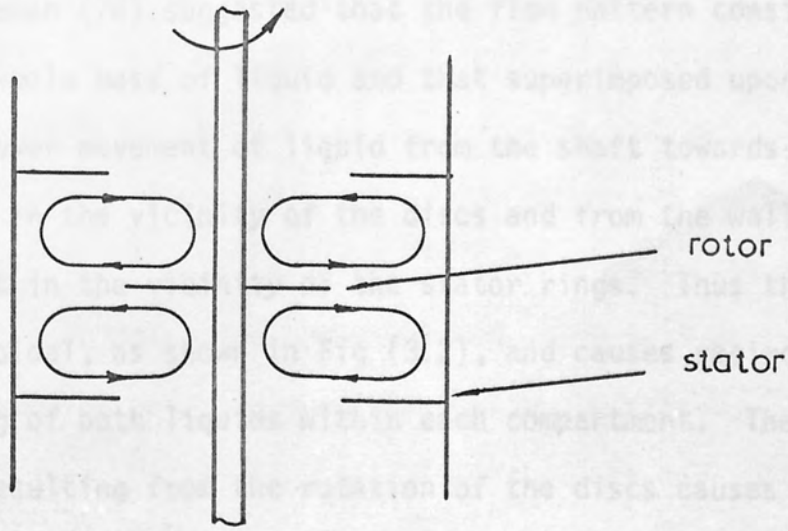

Fig. 3.2. Idealised flow pattern in a rotating disc contactor (76)

Laboratory-sized towers are usually 4 or 6in. in diameter; industrial towers up to 10ft. in diameter and 70ft. high are known to be in operation (1). For the 'optimum' design, the column dimensions should have the ratios (70,71,72,73,74,75),

$$\frac{\text{stator diameter (S)}}{\text{Column diameter (D)}} = 0.66 \text{ to } 0.75$$

$$\frac{\text{Disc diameter (R)}}{\text{Column diameter (D)}} = 0.5 \text{ to } 0.66$$

$$\frac{\text{Compartment height (H)}}{\text{Column diameter (D)}} = 0.33 \text{ to } 0.5$$

3.1 COLUMN BEHAVIOUR

The overall flow of the liquids in an R.D.C. is counter-current, being established by virtue of the difference in densities of the two phases. Reman (76) suggested that the flow pattern consists of a rotation of the whole mass of liquid and that superimposed upon this rotation is a slower movement of liquid from the shaft towards the wall of the contactor in the vicinity of the discs and from the wall back towards the shaft in the vicinity of the stator rings. Thus the resulting flow is toroidal, as shown in Fig (3.2), and causes recirculation and backmixing of both liquids within each compartment. The flow of the liquids resulting from the rotation of the discs causes one of them to be dispersed as droplets because of the accompanying shear stresses. For a given column geometry the size of drops formed in each compartment is controlled by the rotor speed (71).

Kung and Beckmann (71) also observed two general patterns of flow, one with very little back mixing below a rotor speed of 300ft/min. as shown in Fig.(3.3). Above this rotor speed, there was very marked back mixing, as shown in Fig (3.4).

In a later study Mumford (35) found that a critical minimum rotor speed existed, below which a layer of dispersed phase droplets built up beneath the rotor discs. This was found to be approximately

285 ft/min for toluene-water system,
240-265 ft/min for M.I.B.K.-water system and
285-305 ft/min for trimethylpentane-water system

3.2 HYDRODYNAMICS

3.2.1 Hold-up

In the calculation of mass transfer, the interfacial area in Equation (1.1) is estimated as the product of the drop surface area and the number of drops in the column. Hence it is necessary to predict either (i) the drop residence times in the extractor, or (ii) the fraction of the column volume occupied by the dispersed phase. It is difficult to estimate the droplet velocity in agitated extractors and it is, therefore, usual to determine the dispersed phase hold-up.

It has been generally reported that the hold-up increases with increasing rotor speed and dispersed phase flow rate. In a 3-inch diameter R.D.C. Logsdail et al (72) concluded from visual observations that the size of the dispersed phase droplets was independent of the phase flow rates and the dispersed phase hold-up. This study covered a wide range of column geometries and rotor speeds. Using water as the continuous phase and dispersed phases of toluene, butyl acetate, iso-

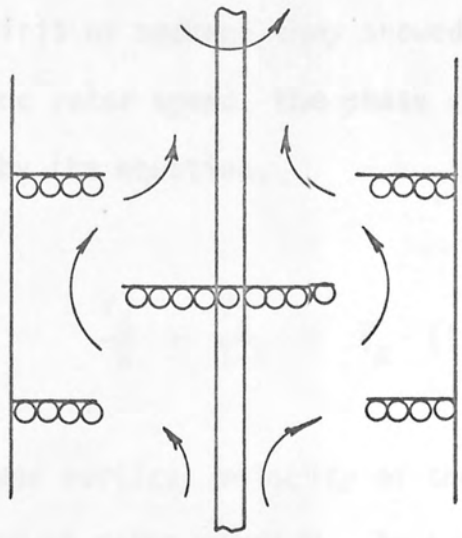

Fig. 3.3. Dispersed phase flow pattern
< 300 ft/min. paripheral speed (71)
R.D.C. system toluene - water

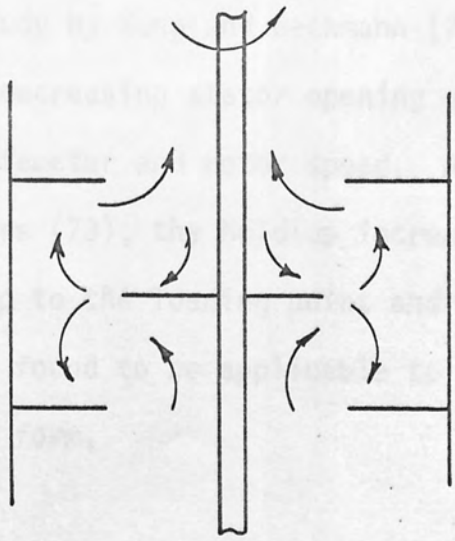

Fig. 3.4. Dispersed phase flow pattern
<300 ft/min peripheral speed (71)
R.D.C. system toluene - water

-octane, white spirit or benzene they showed that for a given system, column geometry and rotor speed, the phase flow rates and hold-up could be related by the equation,

$$\frac{V_d}{x} + \frac{V_c}{1-x} = \overline{V}_N \ (1-x) \qquad (3.1)$$

where $\overline{V}_N$ is the mean vertical velocity of the droplets at substantially zero flow rates and at rotor speed N. An expression relating $\overline{V}_N$ to the physical properties of the system, the column diameter and the rotor speed, was then developed by dimensional analysis. This expression has the form,

$$\frac{\overline{V}_N \ \mu_c}{\sigma} = 0.012 \left(\frac{\Delta\rho}{\rho_c}\right)^{0.9} \left(\frac{g}{RN^2}\right)^{1.0} \left(\frac{S}{R}\right)^{2.3} \left(\frac{H}{R}\right)^{0.9} \left(\frac{R}{D}\right)^{2.7} \qquad (3.2)$$

Both equations gave good agreement with experimental results.

In a study by Kung and Beckmann (71), the hold-up was found to increase with decreasing stator opening and compartment height and increasing disc diameter and rotor speed. As was reported earlier by Vermijs and Kramers (73), the hold-up increased linearly with dispersed phase flow rate up to the loading point and then increased more sharply. Equation 3.1, was found to be applicable to a wide range of column geometries in the form,

$$\frac{V_d}{x} + \frac{K_1 \ V_c}{1-x} = \overline{V}_N \ (1-x) \qquad (3.3)$$

where coefficient K_1 had the value 1.0 at $(S-R)_{/D} > {}^1/_{24}$ or 2.1 at $(S-R)_{/D} \leq {}^1/_{24}$. At rotor speeds less than 300 ft/min. the characteristic velocity $\overline{V}_N$ was found to remain constant, while at higher speeds $\overline{V}_N$ was correlated by the modification of Equation 3.2,

$$\frac{\overline{V}_N \mu_c}{\sigma} = K_1 \left(\frac{\Delta\rho}{\rho_c}\right)^{0.9} \left(\frac{g}{RN^2}\right)^{1.0} \left(\frac{S}{R}\right)^{2.3} \left(\frac{H}{R}\right)^{0.9} \left(\frac{R}{D}\right)^{2.6} \qquad (3.4)$$

where K_1 had the value 0.012 at $(S-R)_{/D} > {}^1/_{24}$ and 0.0225 at $(S-R)_{/D} \leq {}^1/_{24}$.

The equations discussed above make no allowance for coalescence and break-up in the column but Misek (77) proposed a modified form of Equation 3.1 to allow for such effects, viz.,

$$\frac{V_d}{x} + \frac{V_c}{1-x} = \overline{V}_N (1-x) \exp. \left[x \left(\frac{Z}{M} - 4.1\right)\right] \qquad (2.1)$$

in which Z is the 'coalescence coefficient'. The theoretical basis of this equation is summarised elsewhere (Appendix 5). Results for a water-toluene system with an interfacial tension of 24.5 dynes/cm. showed poor agreement; there was better correlation, however, for systems with lower interfacial tension. Deviations are particularly noticeable at low hold-up where coalescence effects would be expected to be least pronounced.

3.2.1.1 Hold-up profile

In most studies only the average value of hold-up has been determined (70,71,72). In more comprehensive studies, however, the

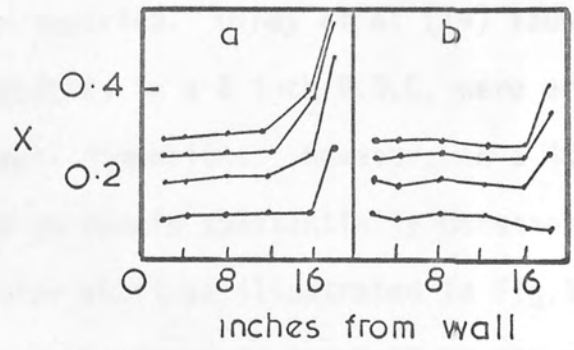

compartment. 9

a. 2·5 inch above stator
b. 2·5 inch below stator

rotor speeds 130, 150, 160 & 170 r.p.m

Fig. 3.5 Radial profile of hold-up
42. inch. R.D.C. system water-toluene

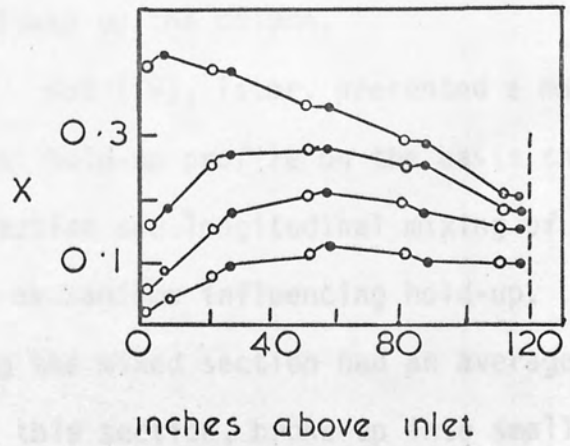

o — 2·5 inches above stators

• — 2·5 inches below stators

rotor speeds 130, 150, 160 & 170 r.p.m

Fig. 3.6 Axial profile of hold-up (74)
42 inch R.D.C system water-toluene

variation of hold-up values along the radial and axial directions have been reported. Olney et al (74) found that the results for radial profiles in a 6 inch R.D.C. were erratic, presumably due to the small dimensions. However, in a 42 inch R.D.C. the hold-up was found to remain substantially constant except in the vicinity of the rotor shaft as illustrated in Fig.3.5. In the axial direction, the hold-up was found to increase up the column, probably because a finite time is required for drop break-up. Towards the end of the column the hold-up decreased; this may be due to the competing effects of axial diffusion of drops in the contact zone and of drop discharge into the settling zone from the top compartment. Fig. 3.6 shows the axial profile in a 42 inch R.D.C. (74).

Similar results were reported by Roskos (78), e.g., axial profiles in an industrial R.D.C. used for phenol extraction with butylacetate, and furfural raffination of minerals oils are represented in Figs. 3.7 and 3.8. Generally, results show a maximum value at a point midway up the column.

Rod (79), later, presented a mathematical model describing the axial hold-up profile on the basis that droplet break-up in the mixed section and longitudinal mixing of the dispersion constituted the two mechanisms influencing hold-up. It was assumed that drops entering the mixed section had an average size d_1, but whilst passing through this section, broke-up into smaller drops of size d_2. Furthermore both sizes existed at any point in the mixing zone.

The diffusional model of Van de Vusse (80) was used to describe the longitudinal mixing and the same value of dispersion coefficient was used for both drop sizes.

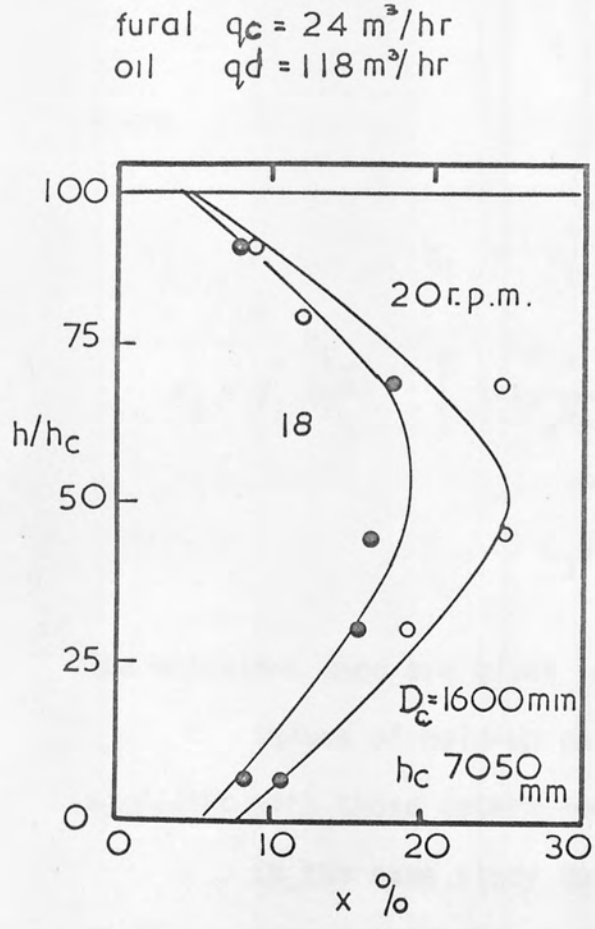

Fig. 3.7

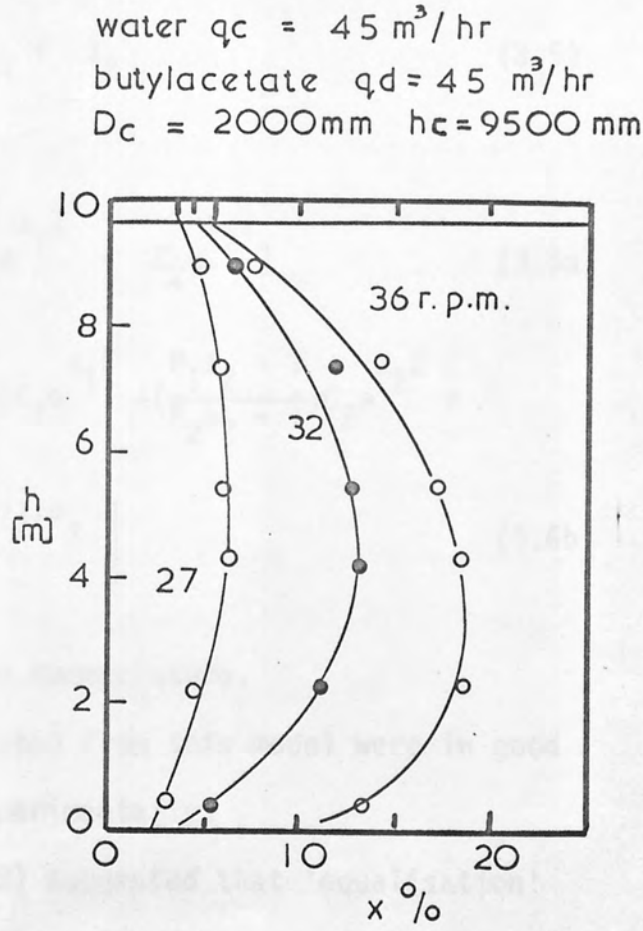

Fig. 3.8

Hold - up profile in an R.D.C.

The total hold-up was assumed to consist of two individual hold-ups, viz., one contributed by the fraction of larger drops X_1, and the other by smaller ones X_2.

i.e.,

$$X = X_1 + X_2 \tag{3.5}$$

where

$$X_1 = X_1^{\circ} \left[C_1 e^{\lambda_1 Z} + C_2 e^{\lambda_2 Z}\right] \tag{3.6a}$$

$$X_2 = X_1^{\circ} \left(\frac{P_2}{P_1}\right) \left[1-\left(\frac{P_1\lambda_1 - 1}{P_2\lambda_2 - 1}\right)C_1 e^{\lambda_1 Z} -\left(\frac{P_1\lambda_2 - 1}{P_2\lambda_2 - 1}\right)C_2 e^{\lambda_2 Z} + C_3 e^{-(1-Z)/P_2} \right] \tag{3.6b}$$

The notations used are given in the nomenclature.

Values of hold-up calculated from this model were in good agreement with those determined experimentally.

In the same study Rod (79) suggested that 'equalisation' or flattening of the hold-up profile to its maximum value should yield maximum transfer efficiency, due to the potential increase in interfacial area. However this may be invalid since maximum efficiency does not necessarily correlate with maximum hold-up, i.e., small drops have lower mass transfer coefficient values (1).

Nevertheless, the model indicates that flattening of the hold-up profile can be achieved by:-

(1) the use of an efficient distributor, producing a dispersion such that the mean size of drops does not decrease during passage through the mixed section.

This would increase the hold-up in the inlet part of the section, and

(2) the reduction of free cross-section at the outlet, e.g., by making the last stator opening smaller. This would reduce the superficial outlet velocities of the drops, and hence compensate for the tendency for rapid escape of drops from the mixed section, due to longitudinal mixing, thus preventing a reduction in hold-up at the outlet of this section.

Finally it is of interest to note that, according to the model, flooding or phase inversion would be expected to occur first at a point midway up the column, i.e., the point of maximum hold-up. Conversely the proposed modifications, leading to a constant hold-up along the column, should yield a design in which flooding or phase inversion is reached simultaneously throughout the column.

3.2.2 Flooding

One of the characteristics of differential contactors is that for each flow rate of one of the liquids there is a maximum possible flow rate for the other, governed by the liquid properties, the design of the device and the gravitational force. If the flow rate of either liquid is increased past this point, one of the liquids will be rejected by the equipment, which is then said to be "flooded". This maximum condition can be introduced into Equation 3.1 by differentiating and setting $(\frac{d V_d}{dx})$ and $(\frac{d V_c}{dx})$ equal to zero (72). This yields,

$$V_{d(f)} = 2\,\overline{V}_N\,x^2_f\,(1-x_f) \qquad (3.7)$$

$$V_{c(f)} = \overline{V}_N\,(1-x_f)^2\,(1-2x_f) \qquad (3.8)$$

Elimination of $\overline{V}_N$ from Equations 3.7 and 3.8 gives an expression relating the hold-up at flooding x_f and flow ratio $L = \frac{V_{d(f)}}{V_{c(f)}}$, thus,

$$X_f = \frac{(L^2 + 8L)^{0.5} - 3L}{4(1-L)} \qquad (3.9)$$

However, this method is not strictly applicable when the mean drop size, and hence V_N, are not constant over the entire hold-up region involved, e.g., in the presence of mass transfer, which could lead to increased drop sizes by virtue of enhanced coalescence. In the absence of mass transfer Thornton et al (72) evaluated $\overline{V}_N$ from their flooding rate data using Equations 3.8 and 3.7 and found good agreement with values obtained by inserting experimental X_f values in Equation 3.1.

Similar work was carried out by Strand et al (84) who, also, included a constriction factor C_R [C_R is the minimum of the three area ratios $(\frac{S}{D})^2$, $[1-(\frac{R}{D})^2]$, $[(\frac{S+R}{D})\sqrt{(\frac{S-R}{D})^2 + (\frac{H}{D})^2}]$] in their analysis, and found the procedure to be valid for columns up to 42 inch in diameter.

The same method can be applied to the modified Equation 2.1 proposed by Misek (75).

In other studies by Reman (31,70,76,81) the effect of the different variables on the limiting capacity was determined experimentally, to be as follows:

1. The capacity decreased with,

    a - Increasing rotor speed

    b - Increasing disc diameter

    c - Increasing dispersed to continuous flow rate ratio

2. The capacity increased with,

    a - Increasing stator opening

    b - Increasing compartment height

Successful correlation of capacity data was obtained by taking the energy input per unit volume $\frac{N^3R^5}{HD^2}$ as determining the drop size of the dispersed phase. To allow for the effect of constrictions on settling of the drops, the observed capacity values were divided by the factor C_R. Unfortunately this method for general correlation is of doubtful validity since it does not refer to the physical properties of the system, particularly interfacial tension. However a rough guide to power input group operating range has been given, which is shown in Fig.3.9 (82).

3.2.3 Phase Inversion

The phenomena of phase inversion has not been studied extensively. The phase ratio is the first factor determining which phase will be dispersed in a binary mixture of immisible liquids. However, power input, physical properties of the system and influences of mass transfer and surfactants, are also relevant factors.

In a study using an agitated tank, 2.3L in volume, Quinn and Sigloh (83) found that for a fixed impeller speed the inversion concentration ϕ expressed as volume fraction in the organic phase was given by,

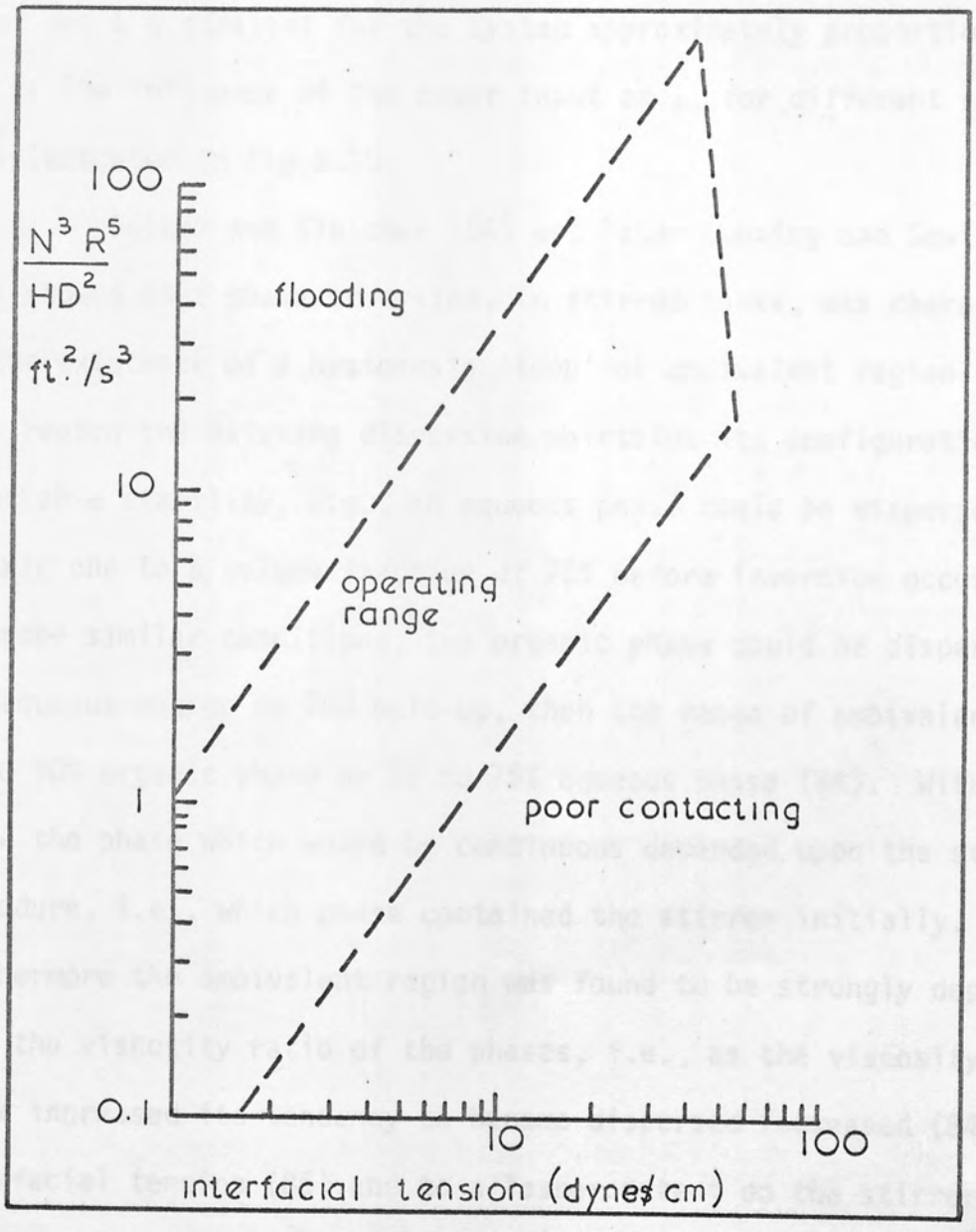

Fig. 3.9 R.D.C. power input group operating range (82)

$$\phi = \phi_o + b/p \qquad (3.10)$$

where ϕ_o was the asymptotic value for high energy input, p the energy input and b a constant for the system approximately proportional to σ/ρ_c. The influence of the power input on ϕ, for different systems is illustrated in Fig.3.10.

Selker and Sleicher (84) and later Luhning and Sawistowski (85) showed that phase inversion, in stirred tanks, was characterised by the existence of a hysteresis 'loop' or ambivalent region. Within this region the existing dispersion maintains its configuration with remarkable stability, e.g., an aqueous phase could be dispersed in an organic one to a volume fraction of 75% before inversion occurred, and, if under similar conditions, the organic phase could be dispersed in the aqueous one up to 90% hold-up, then the range of ambivalence is 25 to 90% organic phase or 10 to 75% aqueous phase (84). Within this range the phase which would be continuous depended upon the starting procedure, i.e., which phase contained the stirrer initially. Furthermore the ambivalent region was found to be strongly dependent upon the viscosity ratio of the phases, i.e., as the viscosity of a phase increased its tendency to become dispersed increased (84), the interfacial tension (85) and to a lesser extent on the stirrer speed (84,85). The presence of a solute under conditions of phase equilibrium, increased the range of ambivalence, while mass transfer (dispersed ↔ continuous) considerably narrowed it (85). The solute used in the above study (85) was propionic acid and the binary systems were benzene-water and p-xylene-water.

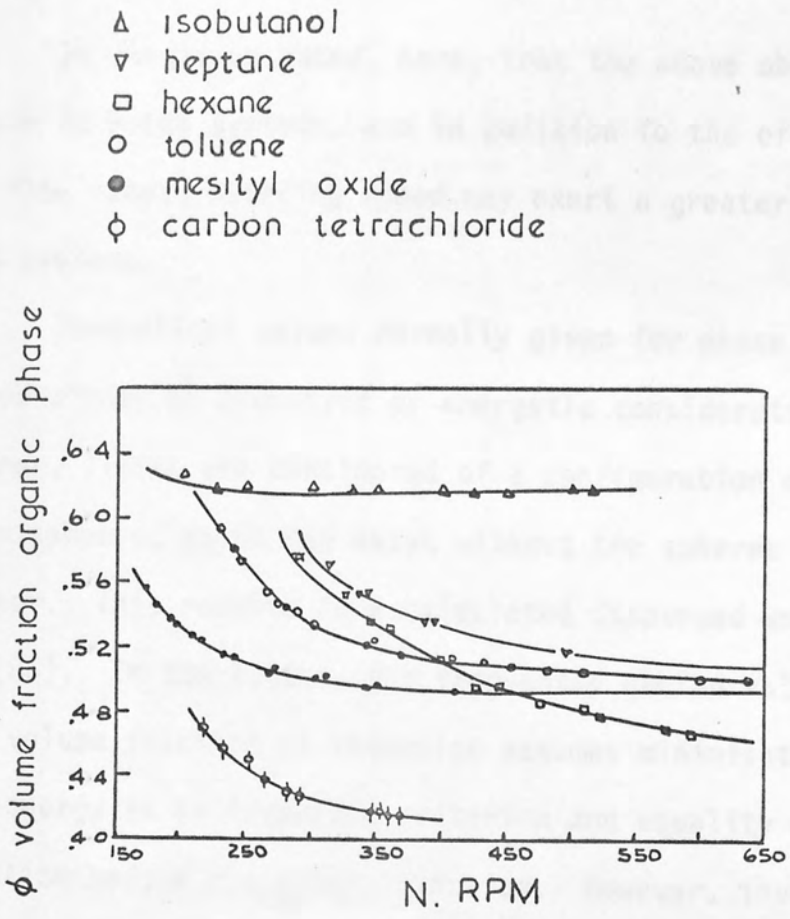

Fig. 3.10. Phase inversion curves for a four-bladed flat paddles impeller 3 1/8 in diameter (8.3)

It should be noted, here, that the above observations were made in batch systems, and in addition to the effect of the phase flow rates, stirring speed may exert a greater influence in flow systems.

Theoretical values normally given for phase inversion are based either on geometric or energetic considerations. In the former, limits are considered of a configuration of spheres, or deformed spheres, which can exist without the spheres touching each other. This results in a calculated dispersed volume of 74.02% (86). In the latter, the frequently quoted value of 50% for the volume fraction at inversion assumes minimisation of surface energy as an inversion criterion and equality of drop size distribution before and after inversion. However, inversion can be accompanied either by an increase or by a decrease in interfacial energy (85). Therefore consideration of surface energy minimisation, for purposes of theoretical modelling would require the introduction of certain assumptions concerning the hydrodynamic behaviour of the dispersion. In the limit the applicability of Kolomogoroff's theory of local isotropy may be assumed with the drop diameter as the characteristic linear dimension of the turbulent field. The mean drop size at inversion was reported to be similar in magnitude to the Kolomogoroff's length scale (85).

An expression to characterise phase inversion, was proposed by Yeh et al (86), in which the phase volume ratio at the point of inversion was equal to the square root of the ratio of the viscosity of the respective phases at the interface. It was found to be of limited use and may not be applicable if,

(i) One or both phases are strongly non-Newtonian

(ii) A large density difference exists

(iii) Inertia force rather than viscous force is dominant.

It must be remembered that all the above mentioned studies were carried out in a non-flow system using a turbine type agitator. Therefore phase inversion characteristicswould be expected to be different in flow systems, and with different type of agitators, e.g. rotating discs. Apart from the present study the phenomena of phase inversion is being further investigated in an Oldshue-Rushton column (37) and as an extension to this study, as mentioned later in Chapter 12.

Finally, it is of interest to note that in countercurrent extractors the onset of phase inversion may sometimes be confused with 'flooding' proper. Depending on the wetting properties of the column internals, the physical properties of the system and the design geometry, droplet rejection from the mixing zone, i.e., 'flooding', may set in before phase inversion or vice versa, thus giving rise to some confusion. This is discussed in more detail in Chapter 10.

3.3 DROPLET PHENOMENA

3.3.1 Drop Formation

In pilot plant extractors, the dispersed phase is generally introduced via an orifice plate. In order to produce drops of fairly uniform size, these plates must be designed with the following features,

1) The material of construction of the plate should not be wetted by the dispersed phase (19,87). The effect of plate wettability on drop formation is discussed later in Chapter 5.

2) The orifice should have a sharp chamfered end (1).

3) The nozzle velocity should not exceed 0.5ft/sec (88).

The volume, V of a drop released from a nozzle may be presented as a function of the time of formation, t_F in the form shown in Fig.3.11 (93).

In region (I), the drop volume, V_{min}, is independent of the time of formation, and can be estimated with fair accuracy by a method by Harkins and Brown (89). Region (II) has been the subject of extensive studies and many correlations have been proposed, e.g., those of Treybal and Howarth (90) and Null and Johnson (91). However, both correlations have been found to be unsatisfactory over a wide range of liquid properties and nozzle geometries, errors of the order of 380% being observed (92).

Heertjes and de Nie (93) working with unsaturated systems proposed the following expression for drop volume.

$$V_{dr} = V_{min} + \phi_v t_{RL} \qquad (3.11)$$

where ϕ_v was the rate of drop formation, assumed constant, and t_{RL} the release time.

For systems, with which comparitively small drops were formed an empirical correlation for t_{RL} was proposed (93),

$$t_{RL} = \frac{t_F}{1+(P+\frac{q}{d_n})\, t_F} \qquad (3.12)$$

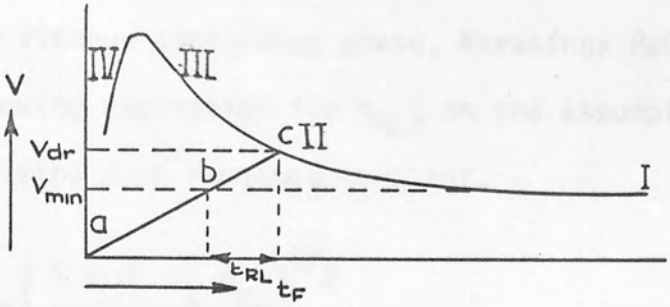

Fig. 3.11 The relation between drop volume and time of formation

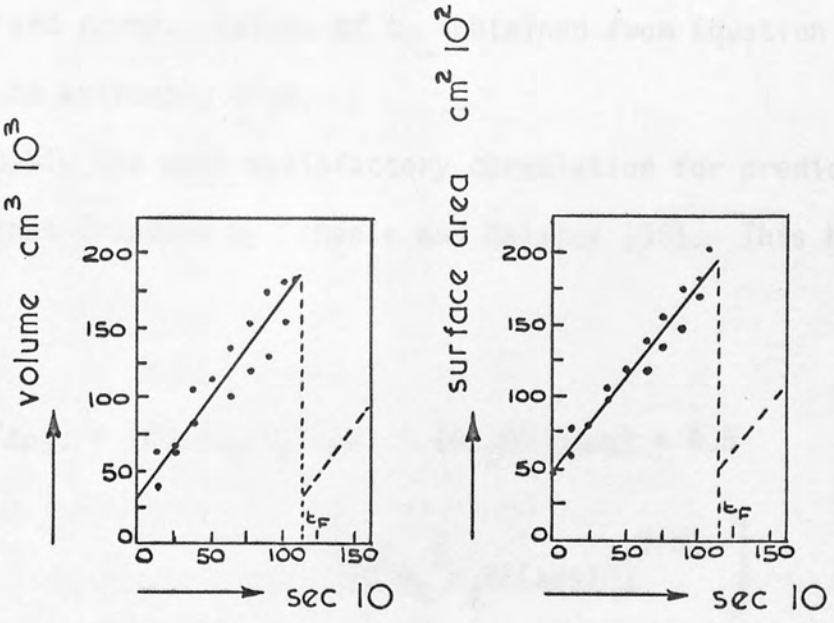

Fig. 3.12 Volume - time relation and surface area - time relation for drop formation

where P and q were dependant upon the system. For isobutanol drops in water, P = 5.74 and q = 0.0658.

For a highly viscous continuous phase, Narasinga RaO et al (94) proposed the following expression for t_{RL}, on the assumption that the mass of the rising drop remained constant,

$$t_{RL} = \left[\frac{6 \pi d_n \mu_c d_m}{\phi_v (\rho_c - \rho_d) g} \right]^{1/2} \qquad (3.13)$$

where d_n = capillary diameter, d_m = diameter of drop of volume V_{min}. For a continuous phase with low viscosity t_{RL} was found from Equation 3.11 by trial and error. Values of t_{RL} obtained from Equation 3.12 were found to be extremely high.

Probably the most satisfactory correlation for predicting drop size is that proposed by Scheele and Meister (95). This has the form,

$$V_D = F \left[(\pi \theta D_N / \Delta\rho g) + (20 \mu Q D_N / D_F{}^2 \Delta\rho g) - (4 \rho_D Q U / 3 \Delta\rho g) + 4.5 \right.$$
$$\left. [Q^2 D_N{}^2 \rho_d \theta / (\Delta\rho g)^2]^{0.33} \right] \qquad (3.14)$$

where F is the Harkins-Brown (96) correction factor, which can be estimated from a plot of F vs. $D/(FV)^{0.33}$ given in the literature (88, 96). Little work has been published regarding Region (III), in which jetting from the nozzle, becomes apparent (95). In region (IV) jetting is fully developed and drop formation takes place at the end of a Rayleigh jet (93).

Once the drop volume has been estimated the surface area can be obtained from the shape of the drop. The surface-area and the volume of a drop have in fact been shown to have a linear relationship (93,97). Heertjes and de Nie (98) using the system isobutanol-water proposed the following expression for the total surface-area A, during the time of formation,

$$A = A_t + A_R = BV + A_R \qquad (3.15)$$

where A_t = the area of the releasing drop

A_R = the area of the rest drop

B = a proportionality factor

V = the volume of the growing drop

Finally, the drop volume-time and surface area-time relations for system isopar-H*-water, have been determined by Angelo et al (99). Their results are shown in Fig.3.12.

3.3.2 Break-up Mechanisms

Break-up of a droplet occurs if it undergoes sufficient deformation, and the local flow pattern persists for a sufficient length of time. The forces causing deformation are a viscous stress and/or dynamic pressure in the surrounding continuous phase.

Hinze (100) identified the various local flow patterns and the forces causing different types of deformation. Deformation is counteracted by a surface force of the magnitude $(\sigma/_d)$ arising from the interfacial tension σ. Therefore, the forces controlling droplet break-up are, dynamic pressure, P, surface force $(\sigma/_d)$ and a viscous stress of the magnitude $\frac{\mu_D}{d} (P/_{\rho_D})^{1/2}$.

From the above expressions Hinze (100) selected the dimensionless groups,

$$N_{vi} = \frac{\mu_{D/d}}{(\rho_D \sigma/d)^{1/2}} \qquad \text{viscosity group}$$

$$N_{we} = \frac{P}{\sigma/d} \qquad \text{Weber number}$$

Deformation increases with increasing N_{we} until, at a critical N_{we}, break-up occurs.

For break-up to result from viscous stresses, the drop must be small compared to the region of local viscous flow (100). Break-up due to dynamic pressure fluctuation has been considered by Hinze (100). Under this regime changes in velocity over a distance equal to the drop diameter, cause dynamic pressure to develop; this pressure determines the size of the largest drops present. An expression for the maximum drop size may be derived,

$$(N_{we})_{crit.} = \frac{\rho u^2 d_{max}}{\sigma} \qquad (3.16)$$

After Kolomogoroff (101), Hinze (100) considered the case of isotropic turbulence and suggested the following expression.

$$d_{max} \left(\frac{\rho_c}{\sigma}\right)^{3/5} E^{2/5} = C_1 \qquad (3.17)$$

where C_1 is a coefficient in the power number, $E = \frac{4}{\pi} C_2 \frac{N^3 R^5}{HD^2}$. This presupposes a high Reynold's number, (Re > 50,000) and the macroscale of turbulence based upon the agitator characteristics,

$L >> y$, where y is the microscale of turbulence.

C_1 was reported to be approximately 0.72, based on an analysis of the rotating cylinder by Clay (102). However in a later study (41), Equation 3.17 was tested and the effect of E was found to be greater than that given by an exponent of 2/5, poorest agreement being found with a viscous dispersed phase.

A similar expression has been proposed by Shinnar and Church (103).

$$\frac{E_K}{\sigma d^2} \propto 0.26 \qquad (3.18)$$

where E_K is the kinetic energy and equivalent to the difference between the surface energy of an oscillating drop and the surface energy of the two smaller ones formed by break-up of the former drop. Here a drop was assumed to be oscillatory if its viscosity and density were near to that of the surrounding oscillating continuous phase.

For conditions of local isotropy, the kinetic energy of an oscillating drop is expressed as

$$E_K \propto \overline{\rho u^2(d)\, d^3} \qquad (3.19)$$

From Equations 3.18 and 3.19, the following expression can be obtained,

$$\frac{\rho u^2(d)\, d}{\sigma} = We \simeq 0.26 \qquad (3.20)$$

From the assumption made in its derivation, Equation 3.20 appears to be limited to systems in which the two phases possess nearly equal viscosities and densities.

For fully baffled conditions Rushton et al (104) derived the following expression,

$$We = \frac{K_1 N^2 R^{4/3} d^{5/3} \rho}{\sigma} \quad \text{for } d >> y \qquad (3.21)$$

A similar correlation was later proposed by Vermeulen (105) whose results were in good agreement with Equation 3.21. Vermeulen's correlation, based upon results for a wide range of liquid systems, has the form,

$$\frac{\rho N^2 R^{4/3} d^{5/3}}{\sigma (f_x)^{5/3}} = 0.016 \qquad (3.22)$$

where f_x is a function of hold-up and coalescence.

For droplet break-up in an R.D.C., Misek (33) identified three different regions of break-up, viz turbulent, transitional and laminar and proposed a different expression for each of these regions.

The approach followed (33,75) was the same as that of Hinze (100) and Shinnar and Church (103), albeit with the addition of the following assumptions for the case of the R.D.C.,

(i) The highest dynamic pressure is exerted near the wall and $\propto V_c^2$ at any point.

(ii) V_c, in the vicinity of the rotor is proportional to the peripherial speed and diminishes exponentially towards the wall, thus

$$V_c = V_o / e^{(K_1 \Delta R)} \qquad (3.23)$$

(iii) The effect of compartment height is a power function of the Weber number, thus,

$$We = K_3 \left(\frac{H}{D} \right)^a \qquad (3.24)$$

the exponents were evaluated experimentally and the following expression proposed for break-up in the turbulent region,

$$\frac{d_h N^2 R^2 \rho_c}{\sigma \, EXP.(0.0887 \, \Delta R)} = 16.3 \left(\frac{H}{D} \right)^{0.46} \qquad (3.25)$$

For the transitive region, i.e., below a critical Reynolds number $(Re)_{crit} \simeq 6 \times 10^4$, the following expression is valid,

$$\frac{d_h N^2 R^2 \rho_c}{\sigma \, EXP.(0.0887 \, \Delta R)} = 1.345 \times 10^{-6} \left[\frac{R^2 N \rho_c}{\mu_c} \right]^{1.42} \qquad (3.26)$$

Further decrease in the mixing intensity into the laminar region ($Re << 10^4$) leads to a different break-up mechanism (33). The vertical velocity of the drops becomes significant and the drops appear to break up by successive impacts on the stators and discs. By analogy with the break-up mechanism in packings, but from very limited experimental work, Misek proposed the expression,

$$d = 0.38 \left(\frac{\sigma}{\Delta\rho \, g} \right)^{0.5} \qquad (3.27)$$

Mumford (35,106) found that below $Re \simeq 1.75 \times 10^4$ the hydraulic mean diameter could be estimated successfully using Equation 3.27 with the

numerical coefficient having a value of 0.55. However droplet break-up by impact on stators or discs was not the predominant mechanism (107). This was confirmed by Thomas and Mumford (108) who showed that direct impact on flat plates did not cause droplet rupture when drops were travelling at their terminal velocities. However, small drops may rupture by impact on the edge of the stators or discs as shown by Thornton (109). Therefore drops would be expected to rupture, only if they impinge vertically within one drop diameter of the disc or stator edge or horizontally on the edge of a stator.

From the work of Kolomogoroff (101) and later Levich (110) the stable drop radius is given by,

$$r_{s.d.} \simeq \sqrt{2}\left[\frac{\sigma}{K_f.\rho}\right]^{3/5} \quad \frac{L^{2/5}}{V^{6/5}} \qquad (3.28)$$

where K_f is a constant and has a value of 0.5 for liquid drops falling in a gaseous medium,

L is a characteristic dimension of the turbulence, and

V is the velocity.

Values of minimum stable drop size obtained from Equation 3.28 and observed maximum drop diameter in a R.D.C. have been plotted against the group $(\sigma/\Delta\rho g)$, as shown in Fig.3.13 (107). Good agreement was obtained with several solvents except trimethylpentane, which may be attributable to its having a lower density than most common solvents and a high surface tension. Below a minimum speed, ≃ 4.5ft/sec., the rotating disc does not affect the size distribution (107). The lower limit is determined by an impact mechanism (109) and the upper limit by the distributor size (88, 107).

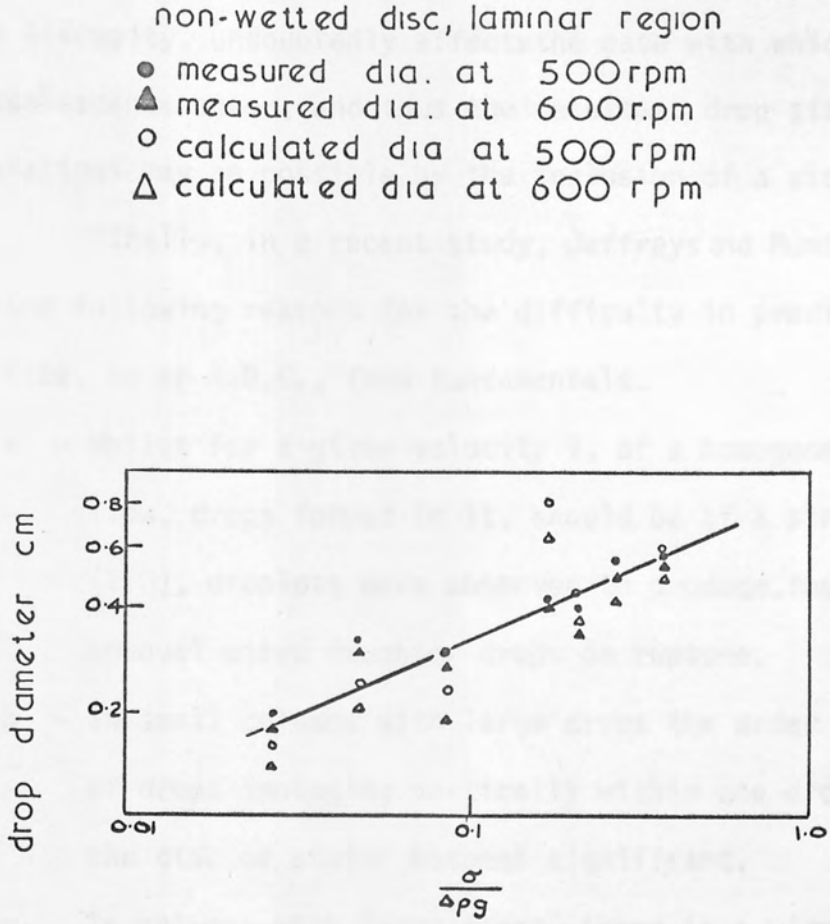

Fig. 3.13 Measured d_m and calculated d_{sd} (107)

It should be noted that none of the above expressions contain a viscosity term. Since viscosity, particularly dispersed phase viscosity, undoubtedly affectsthe ease with which break-up and coalescence occur, and thus the resultant drop size, better correlations may be possible by the inclusion of a viscosity term.

Finally, in a recent study, Jeffreys and Mumford (107) gave the following reasons for the difficulty in predicting the mean drop size, in an R.D.C., from fundamentals.

a - Whilst for a given velocity V, of a homogeneous isotropic flow, drops formed in it, should be of a single size (110), droplets were observed to produce four or more unequal sized daughter drops on rupture.

b - In small columns with large drops the order of proportion of drops impinging vertically within one drop diameter of the disc or stator becomes significant.

c - In columns with large discs, there is a wide variation of V, in the unstable region and hence a spectrum of drop sizes.

3.3.3 Drop Size Distribution

In all practical liquid-liquid contacting devices, the dispersed phase exists predominantly as discrete drops. In order to analyse extraction data the assumption commonly made is that these drops are spherical and of uniform size. This permits the definition of an interfacial area a, contact time t, and transfer coefficient k, based on the average drop. From this,is obtained the characteristic number of transfer units,

$$T = k\,a\,t$$

at a certain plane in the contactor and for the drop population as a whole. However, this is an idealized picture, since it is well established, that in most contactors, particularly if they are agitated, there are competing effects, viz., the generation of new drops due to shear or local turbulence in the bulk flow, and of droplet coalescence due to drop interaction effects (111,112). These result in a wide range of drop sizes. This size distribution is bounded by an upper limit or maximum stable drop size (100,113), which in the absence of coalescence will be determined by the size of the nozzles, and a lower limit or minimum size, dependant upon the prevailing break-up processes. This minimum size, may be dictated by the size that is just entrained by the continuous phase (114).

Olney (114) and Stainthorpe and Suddal (115) reported that there was a distribution of mean drop size along the column length. Hence the assumption of uniform drop size may lead to serious errors, when interpreting mass transfer data. If there is a large range of drop sizes existing in a column the drop size distribution f(d) must, therefore, be included in the analysis.

For the R.D.C. Mumford (35) found that, in the region of $Re \simeq 10^4$, the mean drop sizes were independent of hold-up and in agreement with the correlation proposed by Misek (77), Equation 3.27. At increased speed, the overall tendency was for drop sizes to increase over the whole spectrum with hold-up, which confirmed the earlier findings of Olney (114).

The effect of hold-up on the mean drop size has been correlated by Vermeulen (105), for agitated dispersions, within the hold-up range 10%-40%, by the Equation,

$$\frac{d}{D\phi} = C_1 N_{we}^{-0.6} \tag{3.29}$$

A similar expression has been proposed by Calderbank (116) who varied the hold-up from almost zero to 20%, and obtained,

$$\frac{d}{D} = C_2 (1 + 9\phi) N_{we}^{-0.6} \tag{3.30}$$

Shinnar and Church (103) developed correlations for the mean drop size of drops in agitated dispersions using Kolomogoroff's theory of isotropic turbulence. For dilute dispersions, in which hold-up or coalescence effects were insignificant,

$$\frac{d}{D} = C_3 N_{we}^{-0.6} \tag{3.31}$$

At high hold-up where coalescence was important, the mean drop size was correlated by,

$$\frac{d}{D} = C_4 N_{we}^{-0.375} \left[\frac{A(h)}{\gamma L} \right]^{0.375} \tag{3.32}$$

where A(h), was a function of the energy of adhesion between two drops, each of unit diameter and separated by a distance h.

It is of interest to note that since, for high and moderate hold-ups, $d \propto \phi$ the variation of the mean drop size with the column height would be expected to be similar to that for hold-up, as described in para (3.2.1.1).

In the presence of mass transfer the mean drop size normally varies dependent upon the direction of transfer. For transfer from the dispersed to continuous phase mean drop sizes are generally larger. This is mainly attributable to the increased rate of coalescence. Transfer in the opposite direction giving rise to a reduction in coalescence rate results in smaller drop sizes. Hence for the case of mass transfer from droplets to the continuous phase, capacity measurements were higher than those obtained from binary systems studies; conversely lower capacity values than for binary systems were obtained when mass transfer was in the opposite direction (72).

However the effect of varying amounts of undistributed solute in the dispersed phase on the droplet diameter is uncertain although with solutes such as acetone and acetic acid Logsdail et al (72) observed that the diameter increased rapidly with solute concentrations up to 1-2%, and beyond this point the increase became less pronounced.

3.3.4 Coalescence

The efficiency of liquid-liquid extraction columns is greatly influenced by the ease or otherwise with which coalescence occurs in,

a - the settling zone, ultimately in the form of drop-plane interface coalescence; and

b - the mixing section, normally in the form of drop-drop coalescence.

However, even, in the mixing section droplets may coalesce with any available liquid interface or solid surfaces, e.g., on column wall, packing or agitators. It is of interest to note that drop coalescence with a solid surface (essentially wetted) is one case of a deformable drop at a non-deformable interface.

Coalescence occurs in two basic stages:-

i - Drainage of the continuous phase from between the dispersed elements until a critical film thickness is attained.

ii - Rupture of this film.

The factors most affecting drainage and film rupture, and which hence control the process of coalescence, are summarised in Table 3.1 (117).

TABLE 3.1

	Variable (increasing)	Effect on coalescence time	Explanation in terms of effect on phase-2 film drainage rate
1.	Drop size	Longer	More phase 2 in film
2.	Length of fall	Longer	Drop 'bounces' and film is replaced
3.	Curvature of interface towards drop (a) Concave	Longer	More phase 2 in film
	(b) Convex	Shorter	Less phase 2 in film
4.	Interfacial tension	Shorter	Less phase 2 in film (More rigid drop)

TABLE 3.1 continued

	Variable (increasing)	Effect on coalescence time	Explanation in terms of effect on phase-2 film drainage rate
5.	Phase μ ratio $(\frac{\mu \text{ drop}}{\mu \text{ continuous}})$	Shorter	Either less phase 2 film or increase in drainage rate
6.	Phase $\Delta\rho$	Longer	More deformation of drop more phase 2 film
7.	Temperature	Shorter	Increases phase μ ratio
8.	Temperature gradients	Shorter	Thermal gradients 'weaken' film
9.	Vibrational effects	Shorter	Assist drainage rupture
10.	Electrostatic effects	Shorter	Increase effective gravitational force
11.	Applied electric field	Shorter	Increases effective gravitational force
12.	Presence of a third component		
	(a) stabiliser	Longer	(a) Forms 'skin' around drop
	(b) mass transfer into drop	Longer	(b) Sets up interfacial tension gradients which oppose flow of film
	(c) mass transfer out of drop	Shorter	(c) Sets up interfacial tension gradients which assist flow of film

3.3.4.1 Coalescence in the Mixing Section

Little data are available on coalescence in agitated columns. Davies et al (118), using the system Kerosene-water, found that drop-drop coalescence was not significant in a pilot plant R.D.C at hold-ups up to about 10%, whereas Misek (75) claimed that at high hold-ups of the order of 18% drop-drop coalescence occurred. In a later study Mumford (35) found that interdroplet coalescence was only appreciable with very high hold-ups and disc peripheral speeds of the order of 460ft/min. i.e., conditions approaching flooding. This, however, was carried out in an R.D.C. section with only two compartments, permitting a larger influence by end effects.

From a purely theoretical approach, Howarth (119) has developed an equation for the frequency of coalescence of uniformly sized spherical drops in a homogeneous isotropic turbulent flow suspension of infinite extent. The frequency of coalescence is considered to depend on the frequency of collisions and the fraction of collisions which results in coalescence. The coalescence frequency is given by

$$v = \left[\frac{24\ X x\ \overline{V}^2}{d^3}\right]^{1/2} \quad \exp.\ (-3w^{*2}/4\overline{V}^2) \qquad (3.33)$$

where X is the hold-up, x is the distance between the centres of the drops, $\overline{V}^2$ is the mean square Langrangian turbulent velocity fluctuation, w* is the critical approach velocity and d is drop diameter. Although equation (3.33) gave good agreement with Madden and Damerells observation, that $v \propto X^{1/2}$ for water drops dispersed

in toluene in an agitated tank, the assumptions made in the derivation seriously limit its application to real systems (35).

In a later study, Misek (120) assumed that a dispersion can be characterised by a hydraulic mean drop diameter, that these drops exactly followed the turbulent fluctuation in the continuous phase and that every collision of droplets resulted in coalescence. Since drop-drop coalescence may either occur in the bulk of the turbulent liquid or at the column wall, Misek proposed a different expression for each case.

For coalescence in the bulk liquid,

$$\ln \frac{d}{d_o} = K_7 (n^1 d^3) V_o^{1/2} \left(\frac{D}{\gamma}\right)^{1/2} = K_8 X \left(\frac{\sigma}{d_o \rho}\right)^{0.25} \left(\frac{D}{\gamma}\right)^{0.5} = Z_1 X \qquad (3.34)$$

For coalescence at the vessel wall,

$$\ln \frac{d}{d_o} = K_5 (n^1 d^3) V_o \left(\frac{D}{\gamma}\right) = K_6 X \left(\frac{\sigma}{d_o \rho}\right)^{0.5} \left(\frac{D}{\gamma}\right) = Z_2 X \qquad (3.35)$$

Coefficients Z_1 and Z_2 were determined indirectly based on phase flow-rate measurements using Equation 2.1. Drop size d_o was calculated from the terminal falling velocities of solid spheres.

Only a fair agreement was obtained with these equations for a number of binary systems in various column designs, as can be seen from the considerable scatter in Fig.3.14. A constant K_8 of value 1.59×10^{-2} was claimed to be independent of the type of mixer. However it is doubtful whether coalescence characteristics in columns as different in operation as the R.D.C. and Oldshue-Rushton can properly

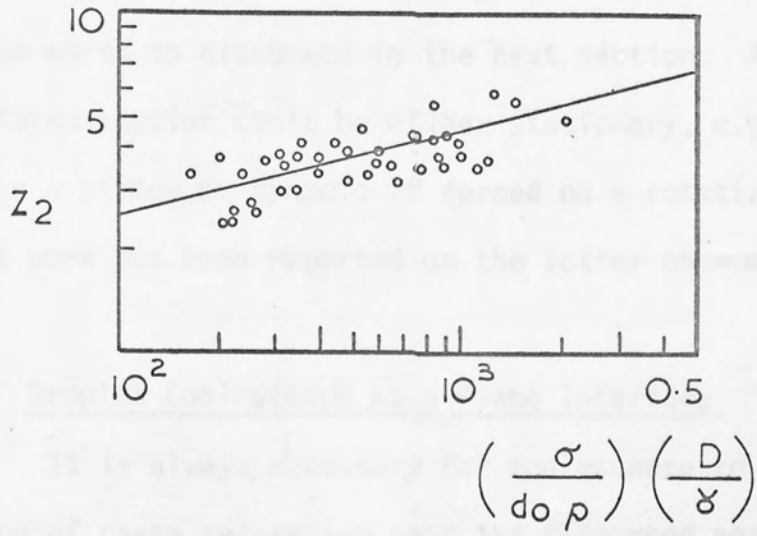

Fig. 3.14. Experimental verification of equation 3.35 (120)

be represented by a single equation (35). Furthermore, the equations make no allowance for the known variation in the ease of coalescence with drop size.

Drop coalescence with solid surfaces is strictly a case of 'wetting' and will, therefore, be considered in Chapter 5. Drop coalescence with an interface in the mixed section may be considered as a special case of drop coalescence with a plain interface which is discussed in the next section. An interface in the agitated section could be either stationary, e.g., if it is formed on a stator or dynamic if formed on a rotating disc. No relevant work has been reported on the latter phenomena.

3.3.4.2 Droplet Coalescence at a Plane Interface

It is always necessary for coalescence to occur at the interface of phase separation near the dispersed phase outlet from a column. If dispersed phase droplets do not coalesce readily at this interface the residence time will be increased and result in reduced capacity.

Whilst, droplet coalescence at a plane interface is not included in this investigation, it has been the subject of many studies, and excellent reviews are available (121,122).

Many correlations for the rest or coalescence time are given in literature (121,122). For swarms of drops, some are of the general form,

$$\log (N/N_o) = Fn(t) \qquad (3.36)$$

where N is the number of drops not coalesced after time, t.

N_o is the total number of drops.

In other expressions, the coalescence time $t_{1/2}$, is correlated with R, the rate of arrival and coalescence of drops of diameter d, thus,

$$R \propto d/t_{1/2} \qquad (3.37)$$

For single drops at a plane interface, few correlations have been proposed for coalescence time as a function of the physical properties of the system, (117,123,124).

3.3.4.3 Effect of Mass Transfer on Coalescence

Coalescence rates may be greatly affected by the presence of mass transfer dependent upon the direction of transfer. Many investigators have found that mass transfer aids coalescence when the solute is transferred from the dispersed to the continuous phase but hinders coalescence when it is in the opposite direction. This is in accordance with the mechanism proposed by Groothuis and Zuiderweg (125) on the basis of the generation of motion in a fluid interface due to variations in surface tension associated with concentration gradients, i.e., the Marangoni effect. This, however is only true if the solute decreases the interfacial tension, since McFerrin and Davison (126), using the system water-diisopropylamine-salt, in which the solute salt increased the interfacial tension, found that transfer into the drop aided coalescence and out of the drop hindered it.

In a study by Jeffreys and Lawson (127), using a ternary system of benzene-acetone-water, coalescence times were shown to change with the direction of transfer in accordance with the theory of Groothuis and Zuiderweg (125). Similar results were reported by Sawistowski (128) employing the system water-diethyl carbonate with propionic or acetic acid as solute. Jeffreys and Lawson's results showed that with transfer from the drop, coalescence times were almost independent of the solute concentration. A progressive increase in stability was reported with increasing rates of mass transfer into the drop.

McCay and Mason (129), who measured both the thickness of the film trapped between the drop and interface and its thinning rate, by an interferometric method, confirmed that mass transfer changed the rate of film thinning but not the film thickness at rupture.

In a recent study of coalescence with mass transfer in both a binary and a ternary system, viz., isobutanol dispersed in water and acetone diffusing from water drops into benzene respectively, Heertjes and de Nie (130) concluded that the effect of mass transfer on the rate of coalescence of drops in binary systems could not be explained entirely by interfacial phenomena. For the ternary system their results were inconclusive.

A theoretical treatment of the Marangoni effect, has been presented by Sternling and Scriven (131). The results explain how it is possible for some systems to be stable with one transfer direction yet unstable with the other, and for other systems to be unstable with either direction of transfer.

Clearly a considerable amount of further work, yielding quantitative data, will be necessary before this phenomena is fully understood and applicable in practice.

3.3.4.4 Coalescing Aids

Various mechanical aids and designs have been employed to assist coalescence at the exit from liquid-liquid extractors. The settler, as in the mixer-settler equipment is most common. However these have mostly been for primary dispersions only , whereas, fine dispersions,are commonly encountered in practice. Apart from baffles, numerous methods have been proposed to assist separation of the latter. These include separating membranes, electrostatic coalescers and various types of packing (1).

Apart from external settlers, for which a wide range of designs are available (1), knitted mesh packings are probably the most convenient coalescing aids. Their use with primary dispersions was studied by Thomas and Mumford (108), who confirmed that for maximum efficiency the coalescer material should be preferentially wetted by the dispersed phase, possess a large surface to volume ratio, have interstices small enough to cover the range of drop sizes encountered, and yet cause as low a pressure drop as possible. The common objection to their use is that even with voidages as high as 98 percent, they may be prone to blockage by any solid present. However, practical results indicate that this objection may be over-ridden by the degree of promotion of coalescence (108). It has been reported that no inter-drop coalescence occurred in the bulk fluid (121).

Hence high separation efficiency is only achieved if droplets can approach and adhere to the packing surface and reside there long enough for interdrop collision to occur. Further design recommendations may be referred to elsewhere (121).

3.4 AXIAL MIXING

Axial mixing plays an important role in the determination of extractor efficiency especially with agitated columns such as the R.D.C. Many investigations have been performed to determine its effects. Which is usually presented in the form of axial mixing coefficients, E_C' for the continuous phase and E_D' for the dispersed one. These are a measure of the respective eddy diffusivities.

In a study by Strand et al (74), employing R.D.C. columns of 6, 25, 42 and 85 inches diameter, E_C' was correlated by the following Equation;

$$\frac{(1-x)}{V_c H} E_C' = 0.5 + 0.09\,(1-x)\,\frac{RN}{V_c}\left(\frac{R}{D}\right)^2\left[\left(\frac{S}{D}\right)^2 - \left(\frac{R}{D}\right)^2\right] \quad (3.38)$$

For the dispersed phase,

$$\frac{xE_D'}{V_D H} = 0.5 + 0.09\ X\ \left(\frac{RN}{V_D}\right)\left(\frac{R}{D}\right)^2\left[\left(\frac{S}{D}\right)^2 - \left(\frac{R}{D}\right)^2\right] \quad (3.39)$$

Equation 3.39 gave only a fair agreement in a 6 inch R.D.C. while Equation 3.38 gave better agreement, as shown in Figs.3.15 and 3.16.

- ○ solid particles 140 - 175 μ
- △ solid particles 420 - 590 μ
- ⊕ kerosene dispersed in water

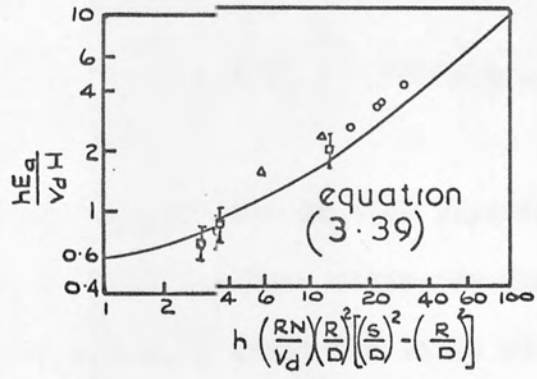

Fig. 3.15. Dispersed-phase axial diffusion 6-in diam. rotating disk contactor (74)

- ○ 6" dia. R.D.C (two units)
- △ 42" dia. R.D.C.

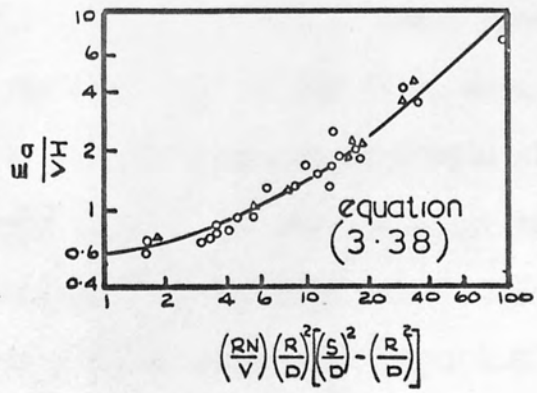

Fig. 3.16 Axial diffusion, single-phase flow RN/V > 30 (74)

In a later work Stemerding et al (132) correlated E_C^1 for R.D.C.s of 3 inch to 7ft. in the following way,

$$E_C^1 = 0.5\ H \cdot V_c + 0.012\ R.N.H\ \left(\frac{S}{D}\right)^2 \qquad (3.40)$$

This equation is only applicable at high Reynolds numbers. No corresponding correlation has been estimated for E_D^1 but this has been reported to vary from 1 to 3 times the value of E_C^1 (133).

Westerterp and Landsman (134) studied axial mixing in two small R.D.C. columns 4.1 and 5.0 cm diameter, using water as the homogenous liquid phase. Their results, as well as those obtained from an earlier study (135) in a 10 cm diameter column, were well correlated by the equation

$$P_c\ B = \frac{E_C L}{E_A} = \frac{2n}{\left[1 + 13 \times 10^{-3} \frac{(NR)}{F_C}\right]} \qquad (3.41)$$

Stainthorp and Sudall (115) determined back mixing in both phases using a 3.5 cm diameter R.D.C. under conditions of mass transfer. They reported that values of E_C were about 15% higher than those predicted by the correlations of Strand et al (74) and values of E_D did not apply at all. It was suggested that E_D values could be assumed to be twice the magnitude of those predicted.

Conversely in an industrial scale R.D.C. 100 cm in diameter, Misek and Rozkos (136) found that values of axial diffusivities were only 27 to 55% of the values predicted by Equations 3.38 and 3.39. Therefore Misek (137) proposed the following equation for the continuous phase,

$$F_B = [-0.00212 + 0.00434 \left(\frac{S}{D}\right)^2 + 0.0264 \left(\frac{R}{D}\right)^2] N.R \quad (3.42)$$

Considerable scatter of data was, however, found and agreement with this Equation was worst in the larger columns, where a considerable tendency for the increased size to reduce longitudinal mixing (137).

Although the above studies were fairly extensive and covered a wide range of column size, little account was taken, experimentally, of the effect of changes in column geometry. This was considered in a study of continuous phase axial mixing carried out by Miyauchi et al (138). They investigated both single-phase and two--phase countercurrent flow in a 15cm diameter R.D.C. Simple two stage columns 10 and 30cm in diameter were also used for non-flow conditions. Water was used as the continuous phase throughout. Flow and non-flow data were in good agreement and could be correlated by,

$$\text{For } \frac{NR^2}{v} > 1.2 \times 10^5 : \frac{f}{NR} = 4.3 \times 10^{-3} \left(\frac{D}{H}\right)^{1/2} \left(\frac{D}{S}\right)^{1/4} \quad (3.43)$$

$$\text{For } \frac{NR^2}{v} < 1.2 \times 10^5 : \frac{f}{NR} = 4.5 \times 10^{-2} \left(\frac{D}{H}\right)^{1/2} \left(\frac{D}{S}\right)^{1/4} \left(\frac{NR^2}{v}\right)^{-1/5} \quad (3.44)$$

where f is the mean actual rate of interstage mixing per unit area of stator opening, and,

v is the kinematic viscosity of the mixed phases, $\frac{\mu_m}{\rho_m}$, with the mean density,

$$\rho_m = \rho_c h_c + \rho_d h_d \quad (3.45)$$

and mean viscosity

$$\mu_m = \frac{\mu_c}{h_c} \left[1 + \left(\frac{\mu_d \, h_d}{\mu_c + \mu_d} \right) \right] \qquad (3.46)$$

In the same study a correlation, based on the concept that the mean rate of energy dissipation in the column determines the turbulent dispersion in the fluid, was given. This correlation which is common for both Rotating Disc and Oldshue-Rushton columns, was tested against the data of various workers (74,132,134,138,139), and was found to provide an excellent basis for predicting the rates of interstage mixing in the continuous phase for various combinations of column geometry and mixer design. The correlation is reproduced in Fig.3.17.

3.5 MASS TRANSFER EFFICIENCY

3.5.1 Summary of Data

Numerous studies have been made of the effect of the different parameters on R.D.C.'s efficiency. Reman and Olney (70) investigated the influence of column geometry and flow rates.

Efficiency was found to increase with,

(i) Decreasing stator opening.

(ii) " compartment height.

(iii) Increasing ratio of dispersed to continuous flow.

(iv) " peripheral speed.

(v) " specific load.

However, under certain conditions, increase in peripheral speed and specific load reduced the efficiency, due to back mixing. This was also observed earlier by Vermijs and Kramer (73).

MIXCO - type colums

△ two stages non-flow exp.

▲ continuous column exp.

rotating disc columns

○ two - stages non - flow exp.

● continuous column exp.

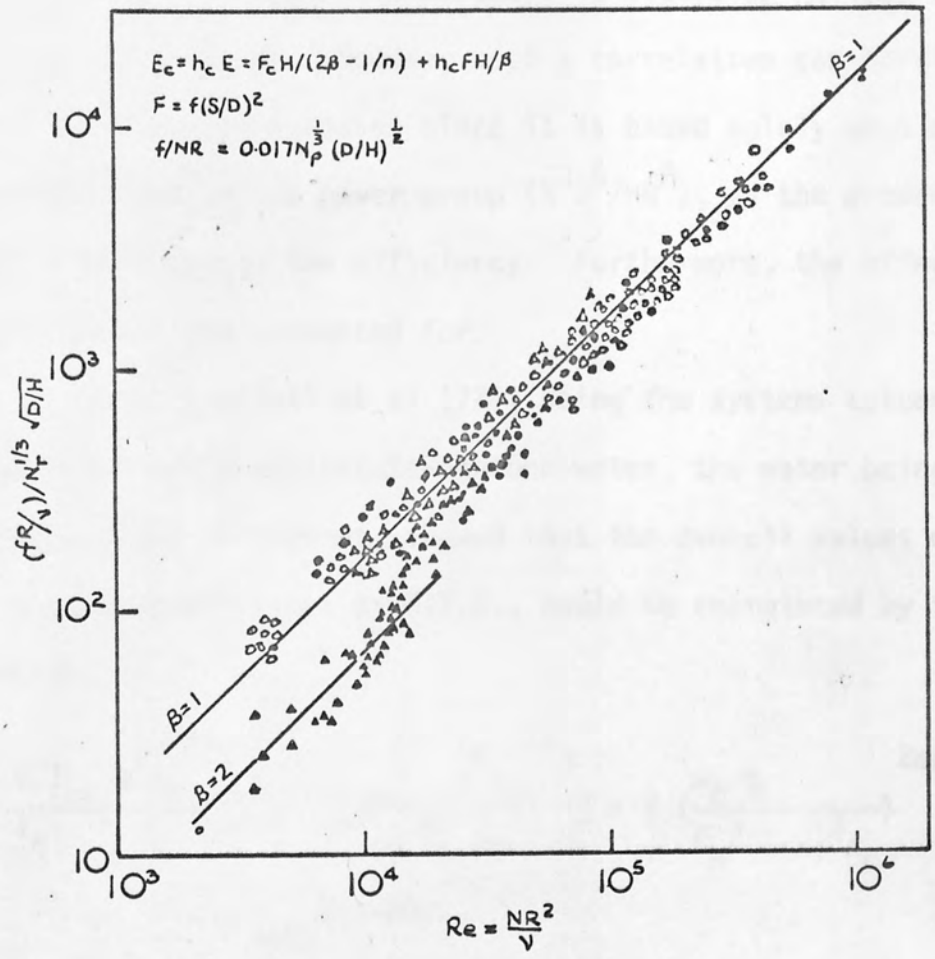

Fig. . 3.17. Unified correlation of continuous phase backmixing for rotating disc and Oldshue-Rushton columns (138)

Reman and Olney interpreted their results by plotting the efficiency, defined as the number of stages per foot column height, versus the energy input per unit volume (N^3R^5/HD^2). Data for two column diameters, 4 inches and 16 inches correlated well, as shown in Fig.3.18. This suggests that there is little or no loss in efficiency on scale-up. However such a correlation can hardly be relied on for design purposes since it is based solely on a drop size, determined by the power group (N^3R^5/HD^2), as the predominant factor in determining the efficiency. Furthermore, the effect of back-mixing was not accounted for.

Later Logsdail et al (72), using the systems toluene-acetone-water and butylacetate-acetone-water, the water being the continuous phase throughout, showed that the overall values of the mass transfer coefficient or H.T.U., could be correlated by the expression,

$$\left[\frac{(H.T.U.)_{oc}}{V_c}\left(\frac{g^2\rho_c}{\mu_c}\right)^{1/3}\right] x = \left[\frac{x}{K_{oc}.a}\left(\frac{g^2\rho_c}{\mu_c}\right)^{1/3}\right] = K\left(\frac{\mu_c\, g}{\overline{V}_N^{\,3}(1-x)^3\rho_c}\right)^{2m/3} \left(\frac{\Delta\rho}{\rho_c}\right)^{2(m-1)/3} \qquad (3.47)$$

Use of this expression for design purposes necessitates evaluation of the constant K, the exponent m, and the characteristic velocity $\overline{V}_N$.

This may be determined from tests with the given system in a small-scale laboratory column. Alternatively for the case of transfer from an aqueous into a solvent phase, i.e., a case of

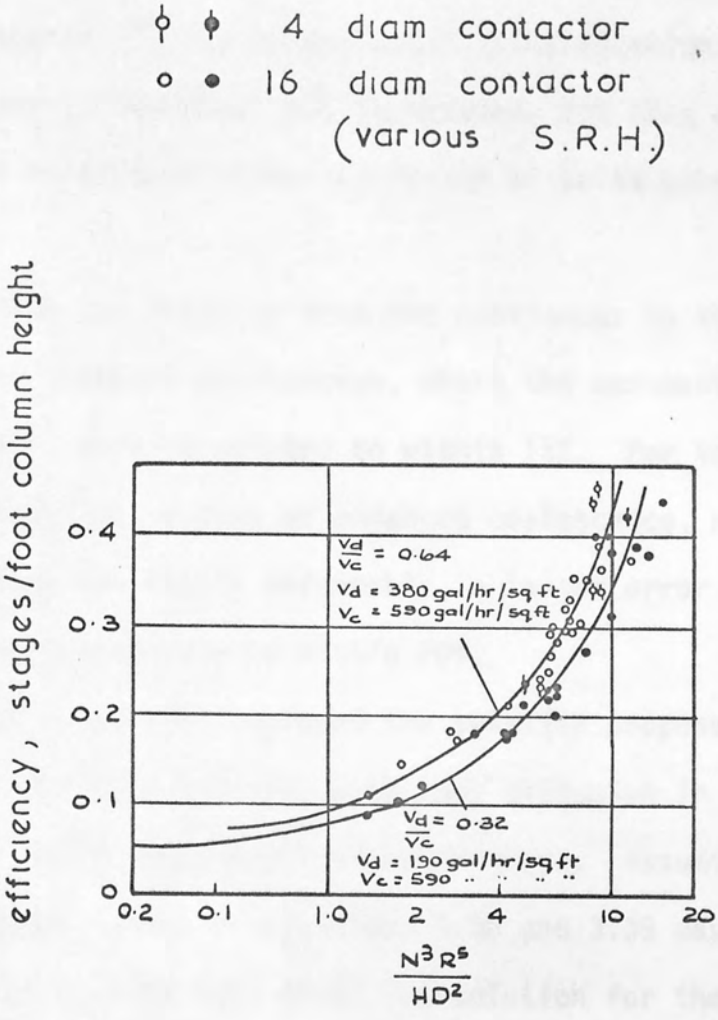

Fig. 3.18 Efficiency for system water - kerosene - butylamine. System water - kerosene - butylamine, water dispersed (70)

hindered coalescence, $\overline{V}_N$ may be evaluated using Equation 3.2.

However in deriving this expression, the drag coefficient–Reynolds number relationship for the region of solid spheres was employed.

The data for transfer from the continuous to the dispersed phase, a case of hindered coalescence, where the assumption would appear reasonable, were correlated to within 15%. For transfer in the opposite direction, a case of enhanced coalescence, resulting in larger drops which are easily deformable, a larger error was incurred and the data correlated only to within 20%.

Strand et al (74) employed the solution proposed by Sleicher (140), for mass transfer with eddy diffusion in both phases, to estimate the "true" mass transfer coefficient. Assuming that the axial diffusivities, given in Equations 3.38 and 3.39 may be used as the eddy diffusivities in this model the solution for the condition $\psi_p = \psi$ is given approximately by,

$$\frac{T}{T_p} = \frac{N_{Pe_f} \; N_{Pe_s}}{N_{Pe_f} N_{pe_s} - T_p[aN_{pe_f} + bN_{pe_s} + c\sqrt{N_{Pe_f} N_{Pe_s}} - d\sqrt{N_{Pe_f} + N_{Pe_s}} + f(N_{Pe_f} - N_{Pe_s})e^{-gT}]} \qquad (3.48)$$

[The meanings of all symbols are given in the nomenclature].

To evaluate the "true" number of overall transfer units, T, T_p may be calculated from the plug-flow equation for mass transfer,

$$T_p = \frac{1}{F-1} \ln \frac{1-\psi_p}{1-F\psi_p} \qquad (3.49)$$

The coefficients, a,b,c,d,e,f and g in Equation 3.48 are given in a tabulated form as functions of the extraction factor F.

The overall Peclet numbers are given by,

$$N_{Pe_f} = \frac{V_d H}{h E_a} \frac{L}{H} \quad , \quad N_{Pe_s} = \frac{V_c H}{(1-h) E_a} \frac{L}{H}$$

for a dispersed feed phase and,

$$N_{Pe_f} = \frac{V_c H}{(1-h) E_a} \frac{L}{H} \quad , \quad N_{Pe_s} = \frac{V_d H}{h E_a} \frac{L}{H}$$

for a dispersed solvent phase.

A trial and error procedure is required in order to determine T, since it also appears in the term e^{-gT}.

For the case where T is known and T_p is required a similar procedure is employed, using an equation analogous to Equation (3.48).

Finally, since by definition,

$$T = \frac{Ka}{V} \cdot L \tag{3.50}$$

and the expression for interfacial area a, assuming spherical drops, is

$$a = \frac{6h}{d} \tag{1.3}$$

the "true" transfer coefficient K can be obtained.

The authors compared the values of K thus obtained with values of the overall transfer coefficients, calculated assuming (i) stagnant drops and (ii) circulating-oscillating drops (74). The results, reproduced in Fig.3.19, indicate that the behaviour of the drops in an R.D.C. lies somewhere between that of stagnant drops and circulating-oscillating drops.

The transfer coefficients for stagnant drops (K_{SD}) were estimated using the Newman (141) relation, Equation 4.15, for the inside coefficient and for the outside coefficient,

$$(k_o)_{SD} = 0.001\ u^* \tag{3.51}$$

where u* is the relative velocity.

For circulating-oscillating drops, K_{CD}, was estimated from the Handlos and Baron (142) relation but for consistency the authors added the stagnant drop coefficient $(k_i)_{SD}$ to the value of k_i. Thus,

$$(k_i)_{CD} = \frac{0.00375\ u^*}{1+\frac{\mu_i}{\mu_o}} + (k_i)_{SD} \tag{3.52}$$

For the outside coefficient, they used the expression,

$$(k_o)_{CD} = \sqrt{\frac{4}{\pi}}\ \sqrt{\frac{D_o\ u^*}{d}} \tag{3.53}$$

Although the equations given by Strand et al (74) and by Olney (114) and referred to below are general and more realistic than earlier correlations, they make no allowance for the different mechanisms of mass transfer associated with the different directions

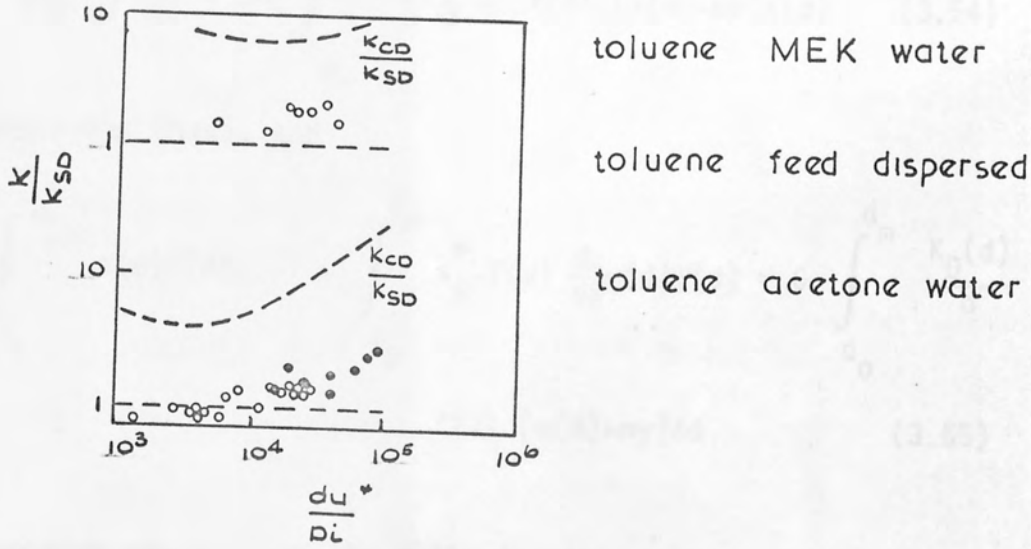

Fig. 3.19. Comparison of the actual mass transfer coefficient, K, to those assuming (i) circulating-oscillating drops, K_{CD}, and (ii) stagnant drops, K_{SD}

of transfer. A better mass transfer estimation should be possible by using two different correlations, one for each transfer direction.

The system of equations proposed by Olney (114), may be expressed as,

$$E_c \frac{d^2y}{dz^2} + \frac{V_c}{1-h} \frac{dy}{dz} = -\frac{6h}{1-h} \int_{d_o}^{d_m} \frac{K_D(d)}{d} f(d) [x(d)-my]\delta(d) \qquad (3.54)$$

for the continuous phase; and

$$E_D \frac{d^2}{dz} \int_{d_o}^{d_m} x(d)f(d)\delta(d) - \int_{d_o}^{d_m} V_s^* f(d) \frac{dx}{dz}(d)\delta(d) = 6 \int_{d_o}^{d_m} \frac{K_D(d)}{d} f(d) [x(d)-my]\delta d \qquad (3.55)$$

for the dispersed phase, with the following boundary conditions at

$z = o$: $\quad dy/dz = 0$

$$-E_D \frac{d}{dz} \int_{d_o}^{d_m} x(d)f(d)\delta(d) + \int_{d_o}^{d_m} V_s^* f(d) [x(d)-x^\circ]\delta(d) = 0$$

at $z = 1$: $\quad E_C \frac{d^2y}{dz^2} + \frac{V_c}{1-h} (y-y_o) = 0$

$$\frac{d}{dz} \int_{d_o}^{d_m} x(d) f(d)\delta(d) = 0$$

where f(d) is a function representing the drop size distribution in the column.

Equations 3.54 and 3.55 have been developed, assuming spherical drops with specific surface area $a = 6/d$.

The values of E_C and E_D, the axial diffusivity coefficients for the dispersed and continuous phase respectively, may be calculated using equations 3.38 and 3.39. However, Olney's model can only be applied by writing a computer programme and solving numerically, provided the type of droplet distribution in the extractor is either known or predictable.

3.5.2 Fundamental Analysis

The performance of a countercurrent extraction column may be analysed by considering the diffusion of the solute species across the interface of the two liquid phases. This is expressed mathematically as (1, 143).

$$N = k_x (x-x_i) \quad (3.56)$$

$$= -k_y (y-y_i) \quad (3.57)$$

N is the number of moles transferred across a unit area per unit time.
x_i, y_i are concentrations at the interphase.
On the generally accepted assumption that x_i and y_i are in equilibrium and that the distribution coefficient,

$$m = (y_i/x_i)^* = \text{a constant} \quad (3.58)$$

it is possible to formulate relations(3.56)and (3.57) as,

$$N = +K_x (x-x^*) \quad (3.59)$$

The overall coefficient K_x may be expressed as the sum of the individual resistances of both phases, thus

$$\frac{1}{K_x} = \frac{1}{k_x} + \frac{1}{mk_y} \qquad (1.2)$$

and

$$x^* = y/_m \qquad (3.60)$$

Relation 1.2 is often applied even under conditions when m is not constant and when relation 3.60 is not completely valid.

The simplest mass transfer model is that which neglects longitudinal mixing and assumes piston flow of the phases through the column. This situation is shown diagramatically in Fig.3.20.

If R and E are the flow rates of the raffinate and extract phases,

a is the interfacial area and

H is the height of the extractor

the final relationship is, (1)

$$N_{toR} = \int_{x_{R2}}^{x_{R1}} \frac{dx_R}{(1-x_R)\,]_n \frac{(1-x_R^*)}{(1-x_R)}} = \frac{H}{H_{toR}} \qquad (3.61)$$

$$H_{toR} = \frac{R}{K_R a (1-x_R)_{om} C_{Rav}} \qquad (3.62)$$

The integral in Equation 3.61 is defined as the number of overall transfer units based on the raffinate phase, N_{toR}; H_{toR} is the height of overall transfer unit. Similar expressions may be derived for the extract phase.

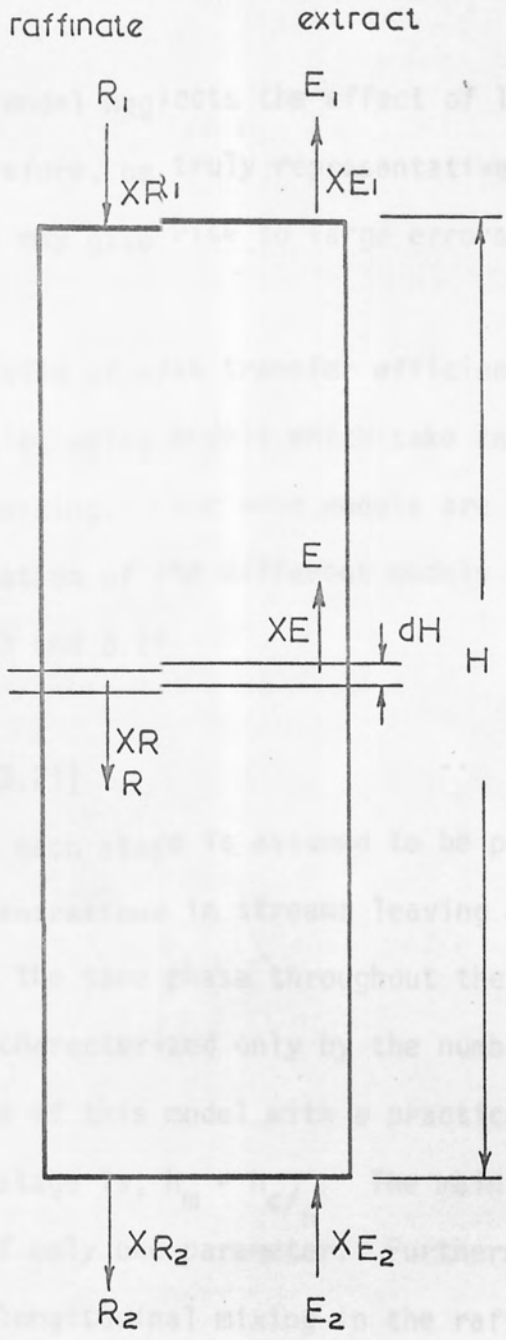

Fig. 3.20. Piston flow condition in a countercurrent extractor

However this model neglects the effect of longitudinal mixing and cannot, therefore, be truly representative of conditions in the extractor. This may give rise to large errors in the predicted efficiencies.

Better prediction of mass transfer efficiency has recently been shown to be possible, using models which take into account the effect of longitudinal mixing. Four such models are discussed below; A diagramatic representation of the different models is reproduced in Figs.3.21, 3.22, 3.23 and 3.24.

(i) Stage Model, (Fig.3.21)

In this model each stage is assumed to be perfectly mixed, so that the solute concentrations in streams leaving any stage are identical with those in the same phase throughout the stage. Longitudinal mixing is characterized only by the number of stages required. By comparison of this model with a practical column the height equivalent of a stage is, $h_m = h_{c/n}$. The main limitation of this model is the use of only one parameter. Furthermore it is not possible to distinguish between longitudinal mixing in the raffinate and solvent phases, and the concentration profile is only approximate. Therefore this model is only useful for those cases where longitudinal mixing in both phases is of similar magnitude and where its influence on mass transfer is not high ($h_{m/H_x} < 1$).

A material balance on the ith stage is described by (1,143):

$$U_x \ (x_i - x_{i-1}) = U_y \ (y_{i+1} - y_i) \qquad (3.63)$$

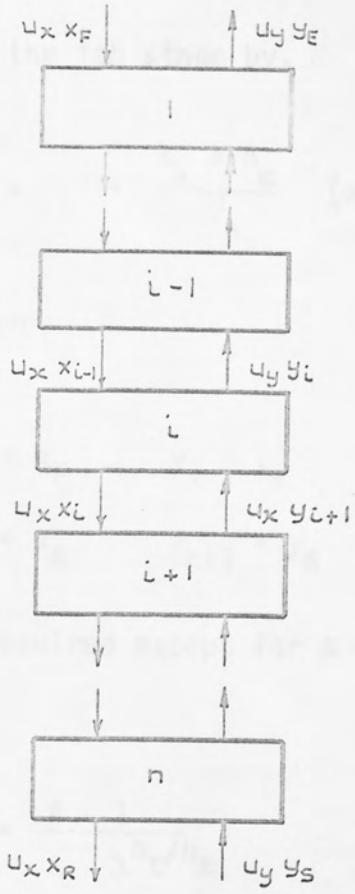

Fig. 3.21. Stage model

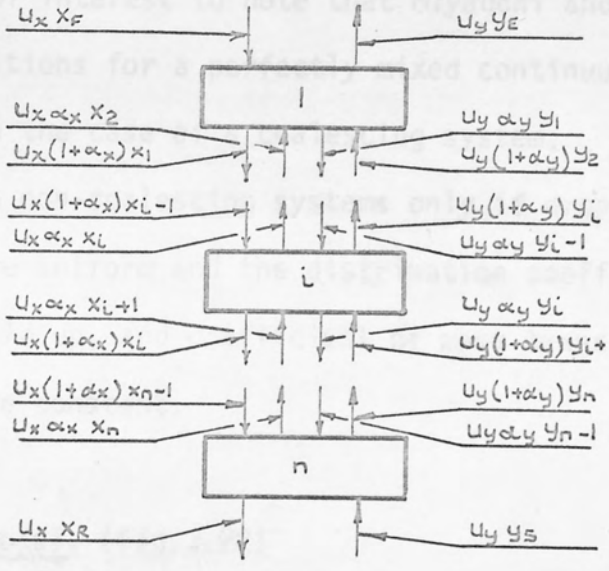

Fig. 3.22 Backflow model

and the mass transfer in the ith stage by,

$$x_i - x_{i-1} = \frac{K_x a h_m}{U_x} (x_i - x_i^*) \qquad (3.64)$$

The boundary conditions are,

$$x_o = x_F \qquad y_1 = y_E$$

$$x_n = x_R \qquad y_{n+1} = y_S$$

A graphical solution is required except for a linear case (140).

$$\zeta = \frac{A - 1}{A - \lambda h_c/h_m} \qquad (3.65)$$

where

$$\lambda = \frac{H_x + A h_m}{H_x + h_m} \qquad (3.66)$$

It is of interest to note that Miyauchi and Vermeulen (144) showed that conditions for a perfectly mixed continuum may be satisfied

(a) in the case of a coalescing system;

(b) in non-coalescing systems only if drop-sizes are uniform and the distribution coefficient, hold-up, and coefficient of mass transfer are constant.

(ii) Back Flow Model, (Fig.3.22)

This model may describe flow conditions in a countercurrent extractor, when one phase is entrained in the main flow of the other

in a stagewise system. From Fig.3.22 a material balance on the ith stage is represented by

$$U_x[(1-\alpha_x)X_{i-1}-(1+2\alpha_x)X_i+\alpha_x X_{i+1}]= -U_y[-\alpha_y Y_{i-1}+(1-2\alpha_y)Y_i-(1+\alpha_y)Y_{i+1}] =$$

$$= \quad N.\ h_m.a \qquad (3.67)$$

and the mass transfer described by the well known relation, Equation 3.56.

The governing finite difference equation is obtained by combination of Equations 3.67 and 3.56. The boundary conditions result from balances around the end stages:

for $i = 1$: $\quad U_x(x_F-x_1) + U_x\alpha_x(x_2-x_1) = K_x a(x_1-x_1^*)\ h_m$

$$y_1 = y_E$$

for $i = n$: $\quad U_x(x_{n-1}-x_n)+ U_x\alpha_x(x_{n-1}-x_n) = K_x a(x_n-x_n^*)\ h_m$

$$x_n = x_R$$

An analytical solution for the linear case is given in reference (145). For the general case a graphico-numerical procedure is required (146).

(iii) Diffusion Model, (Fig.3.23)

This model describes solute transfer, within the phase from loci of higher concentration to those of lower concentration,

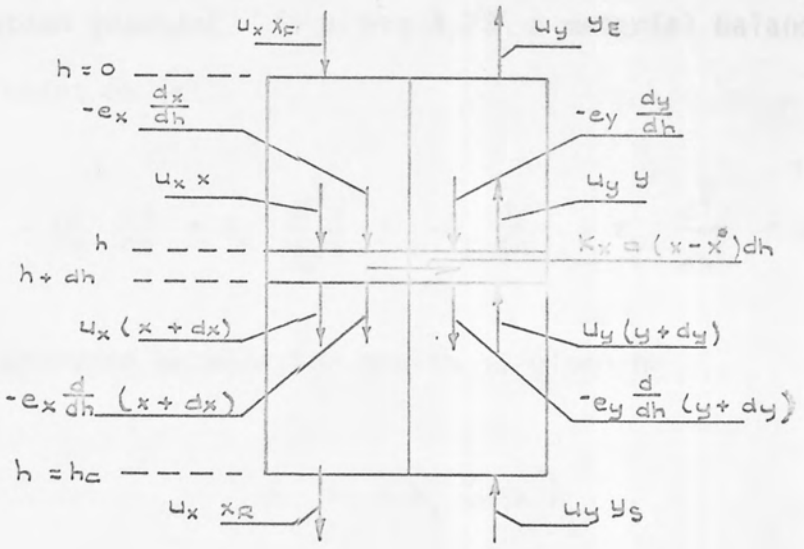

Fig. 3.23. Diffusion model

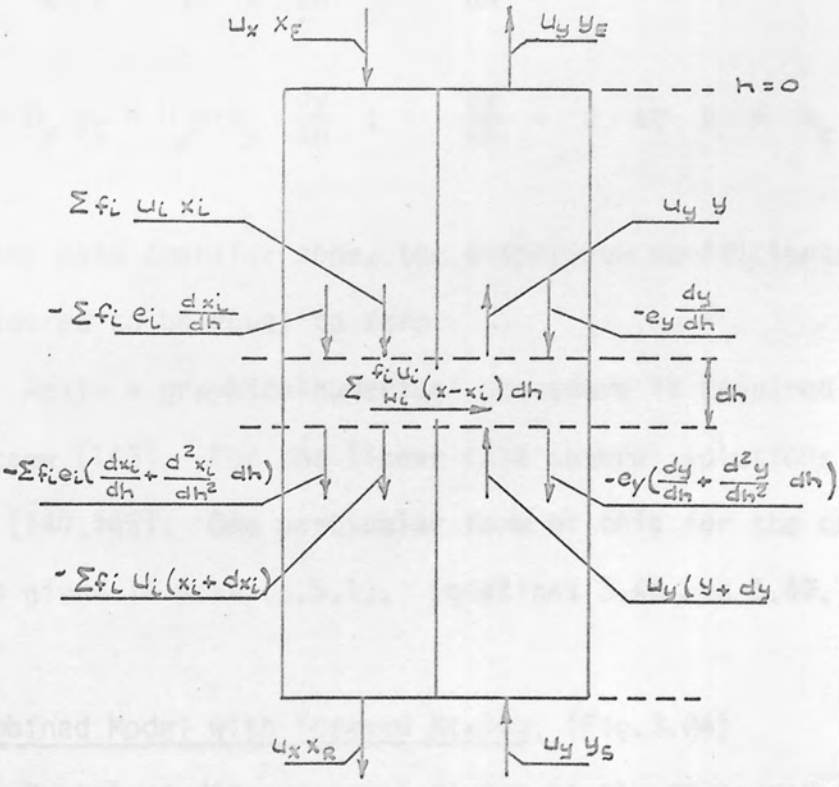

Fig. 3.24. Combined model

as a diffusional process, i.e., the mass flux is proportional to concentration gradient. From Fig.3.23 a material balance over height element dh is:

$$- U_x \frac{dx}{dh} + e_x \frac{d^2x}{dh^2} = -U_y \frac{dy}{dh} - e_y \frac{d^2y}{dh^2} = N.a \qquad (3.68)$$

The mass transfer between the phases is given by

$$N = + K_x (x-x^*) \qquad (3.56)$$

The boundary conditions are obtained by performing material balances for both ends of the column thus, (147)

$$U_x x_F = U_x x - e_x \frac{dx}{dh} \; ; \qquad \frac{dy}{dh} = 0 \text{ at } h = o$$

$$U_y y_S = U_y y + e_y \frac{dy}{dh} \; ; \qquad \frac{dx}{dh} = 0 \text{ at } h = h_c$$

Outside the mass transfer zone, the dispersion coefficients e_x and e_y are considered to be equal to zero.

Again a graphico-numerical procedure is required for the general case (143). For the linear case several solutions have been obtained (140,145). One particular form of this for the case of an R.D.C. is given in para (3.5.1). Equations 3.48 and 3.49.

(iv) Combined Model with Forward Mixing, (Fig.3.24)

Recent studies on axial mixing in the dispersed phase (114) have shown that neither the diffusion or the backflow models describe

the mixing of the dispersed phase with sufficient accuracy for those cases where the dispersed phase has a significant polydisperse character and coalescence and redispersion does not take place. This is especially true for agitated columns operating with low hold-ups. Under these conditions, since drops of differing sizes have different velocities which, influence the residence time distribution, another mechanism of axial mixing occurs. This has been called forward mixing to distinguish it from back-mixing (148). Thus the combined model takes account of both mechanisms of longitudinal mixing. One such model describing mass transfer in an R.D.C. has been proposed by Olney (114) and is given in para.3.5.1 Equations 3.54 and 3.55.

Whilst no analytical solution has been proposed for this model due to the complexity involved, a calculation procedure similar to that for the diffusion model has been adopted to solve the general case (143).

In the present work it is thought that simpler, and possibly more accurate, methods for estimating the mass transfer efficiency may be possible by considering models obtained from single drop studies. This is discussed in the following chapter.

4. MASS TRANSFER BETWEEN DROPLETS AND THE CONTINUOUS PHASE

4.1 MASS TRANSFER DURING DROP FORMATION

The rate of mass transfer in liquid-liquid systems is affected by:

a. the rate of formation of the droplets,

b. the rate of their passage through the equipment and finally,

c. their rate of coalescence.

Many workers have, therefore, determined the extent of mass transfer taking place during drop formation. Sherwood (149) stated that 40% of the extraction occurred during this period, and West (150) claimed only 14%, but Licht and Pansing (151) could not detect any special effect. More recent workers (99,152,153) have shown that about 10% of the extraction occurs during the formation periods. However the researches of Sawistowski (153) show that the prediction of precise extraction rates during drop formation is difficult because of the rapid changes which take place in interfacial tension during this period. Nevertheless many mathematical expressions have been proposed to predict dispersed phase mass transfer rates during drop formation. These are summarised in Table 4.1. The drop is assumed to grow as a sphere and K_{df} is based upon the time of formation t_f and the surface area at the point of detachment. All the expressions describe diffusion mass transfer and are based on one of the following theoretical models,

1. The model of an ageing rigid boundary layer which increases in surface area.

TABLE 4.1

Models for Drop Formation Mass Transfer

Eqn.No.	Authors	Model
4.1	Licht and Pansing (151)	$K_{df} = \frac{6}{7} (D_d/\pi t_f)^{1/2}$
4.2	Heertjes et al (152)	$K_{df} = \frac{24}{7}(D_d/\pi t_f)^{1/2}$
4.3	Groothuis and Kramer (157)	$K_{df} = \frac{4}{3} (D_d/\pi t_f)^{1/2}$
4.4	Coulson and Skinner (160)	$K_{df} = 2\sqrt{3/5} (D_d/\pi t_f)^{1/2}$
4.5	Heertjes and de Nie (98)	$K_{df} = 2(a_o/a_r + 2/3)(D_d/\pi t_f)^{1/2}$
4.6	Heertjes and de Nie (98)	$K_{df} = 2(7/3)(a_o/a_r + 1/3)(D_d/\pi t_f)^{1/2}$
4.7	Ilkovic (154)	$K_{df} = 1.31 (D_d/\pi t_f)^{1/2}$
4.8	Angelo et al (99)	$K_{df} = \frac{2}{\tau}\sqrt{\tau} (D_d/\pi t_f)^{1/2}$

TABLE 4.2

Model	F $d/_6$
1	.86
2	1.31
3	1.48
4	1.78 front
	1.31 equator
	0.50 rear

2. In the ageing boundary layer, the concentration gradient increases because of the increase of surface area by stretching; the 'balloon model'.
3. The boundary layer ages as with a rigid layer. Surface is increased by addition of fresh surface elements; the 'fresh surface model'.
4. For the boundary layer a flow pattern has been developed in which a varying rate of stretching occurs.

Various modifications of these models are possible.

In deriving the mathematical expressions for mass transfer the following conditions have been assumed in all cases:

(i) The interfacial concentration is that at saturation.

(ii) Mass is transported by diffusion perpendicular to the interface.

(iii) The process of diffusion is slow as compared with the process of drop growth.

(iv) Variations in the diffusion coefficient in the direction of flow are neglected.

The theoretical models discussed above may be reduced to a common form,

$$E_F = F \left(\frac{D\, t_F}{\pi}\right)^{1/2} \qquad (4.9)$$

in which E_F = the efficiency during drop formation,

D = diffusion coefficient,

t_F = time of drop formation,

F = a proportionality constant, dependent upon the model used and the surface area-volume relation of the growing drop.

Values of the factor F for the four models are given in Table 4.2, for the simplified case of a spherical drop of diameter d.

Model 1 was proposed by Licht and Pansing (151), but although it has been recommended by various workers, it has not been verified experimentally. However, it represents a limiting case, giving the lowest value of F.

Model 2 was introduced by Ilkovic (154), and has been applied for the case of uniform stretching. This model has been studied extensively, and has given a deviation of < 20% from experimental results (155).

This model may be used for cases where the continuous phase film is controlling, although Baird (155) applied the model for a case where the dispersed film was controlling.

The theory of surface stretch has been further studied by Beek and Kramers (156) and by Angelo et al (99) and a mathematical expression proposed by the latter is given in Table 4.1.

In Model 3, the surface elements may have a time of contact with the continuous phase ranging from t = o to t = t_F. Groothuis and Kramers (157) have applied this model to mass transfer from a gas to growing liquid drops.

Model 4, was introduced and verified by Michels (158) for gas bubbles growing in a liquid, but has yet to be explored for liquid-liquid systems.

As to which model should be used in a particular case poses some difficulty. Apart from model 1, which is unlikely, models 2, 3 and 4 differ by very little. However Heertjes and de Nie (98)

developed a method to distinguish more clearly between models 2 and 3. This involved the formation of drops with constant volume at different times of formation, using a varying time of rest between the formation at constant frequency of drop formation. The mass transfer to the drop at rest, which is not normally accounted for, was also included in the calculation. Under these conditions models 2 and 3, yielded two different types of correlation, as shown in Fig.4.1, in which the total efficiency (E) for the column and end effects is given as function of $(t_F)^{0.5}$. The forms of plot obtained for both models were then compared to those obtained from experimental results. As shown in Fig.4.1, the fresh surface model, but not the stretching surface model plot, was similar to that obtained experimentally. Heertjes and de Nie (98), therefore, concluded that for the system studied (isobutanol-water), model 3 was more suitable. However, this method has yet to be verified for other systems.

The contribution of the resting drop to the surface area, and hence mass transfer, may be demonstrated by considering the change in values of factor F for models 2 and 3 for different surface area-volume relations. For isobutanol drops in water formed at a 1mm capillary with t_f = 2 secs. The data are reproduced in Table (4.3) (13).

TABLE 4.3

	Linear A-V relation			Sphere
	rest drop	drop	total	
Model 2	19.7	31.8	51.5	43.8
Model 3	12.9	41.6	54.5	49.0

20 drops per minute d_c = 0·195cm

△ experimental

– – – stretching surface

—— fresh surface

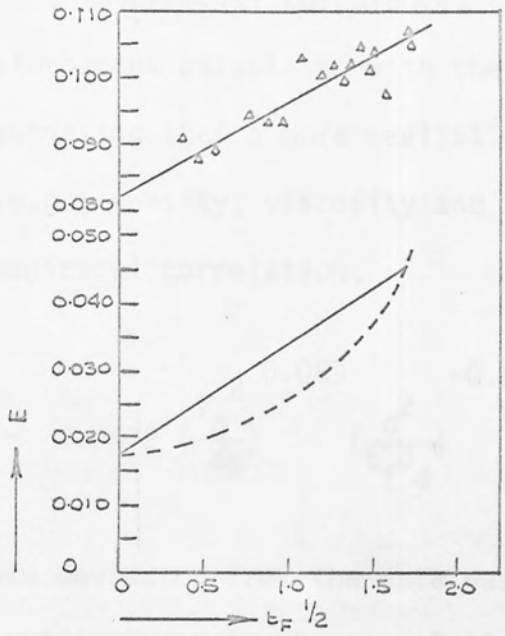

Fig. 4.1 Experimental and theoretical relations between efficiency and the square root of the time of drop formation (93)

The mathematical expressions given in Equations 2,3,4,7 in Table 4.1, were tested by Skelland and Minhas (159) and found to predict considerably lower mass transfer rates than the observed values. This was due to the lack of allowance in the models of internal circulation, caused by the impinging jet while the drop grows, the effect of, interfacial turbulence, the influence of the rest drop, and disturbances associated with the drop detachment. They, therefore, suggested that a more realistic model should include other parameters, e.g., density, viscosity and interfacial tension, and proposed the empirical correlation,

$$\frac{K_{df}\, t_f}{d} = 0.0432 \left(\frac{V_n^2}{dg}\right)^{0.089} \left(\frac{d^2}{t_f D_d}\right)^{-0.334} \left(\frac{\mu_d}{\sqrt{\rho_d d \sigma}}\right)^{-0.601} \qquad (4.10)$$

The average absolute deviation from the data was 26%. Solute concentration was not included in the correlation since the experiments were only conducted for dilute concentrations.

Equation (4.10) covers the following range of variables:

$$0.521 \times 10^{-2} \leqslant \left(\frac{Kd_f\, t_f}{d}\right) \leqslant 8.140 \times 10^{-2} \qquad (4.10a)$$

$$1.286 \times 10^{4} \leqslant \left(\frac{d^2}{t_f D_d}\right) \leqslant 12.31 \times 10^{4} \qquad (4.10b)$$

$$0.165 \times 10^{-2} \leqslant \left(\frac{\mu_d}{\sqrt{\rho_d d \sigma}}\right) \leqslant 0.961 \times 10^{-2} \qquad (4.10c)$$

$$0.163 \times 10^{-2} \leqslant \left(\frac{V_n^2}{dg}\right) \leqslant 0.3955 \qquad (4.10d)$$

This correlation represents the overall mass transfer occurring during drop formation, which includes mass transfer during drop growth, during the detachment of the drop and the influence of the rest drop.

A theoretical expression for k_{df} was also given,

$$k_{df} = \frac{V_d}{a_f t_f} \left(\frac{2I_f}{4V_d - I_f} \right) \qquad (4.11)$$

The symbols are defined in the nomenclature.

A plot of predicted versus observed k_{df} is given in Fig.4.2.

4.1.1 Mass Transfer at Different Rates of Formation

Much of the published work on mass transfer during drop formation has been confined to very large formation times of between 2 and 50 seconds and does not, therefore, reflect the high transfer rates associated with circulation in growing drops being formed at higher frequencies, i.e., $t_f < 1.5$ secs. Heertjes et al (93) observed that isobutanol drops formed in water in < 1.3 sec. exhibited a very marked circulation, whereas no circulation occurred for formation times larger than 1.5 sec.

Furthermore Coulson and Skinner (160) stated that, for formation times of less than 4.0 sec. the rate of mass transfer was proportional to $t_f^{0.7}$, whereas above 4.0 sec. the rate of mass transfer was independent of the time of formation.

Generally, mass transfer at low rates of formation region I, as shown in Fig.3.11, is always accompanied by local changes in density. This promotes free convection if the speed of formation is low. In these cases, therefore, mass transfer is comparable to that

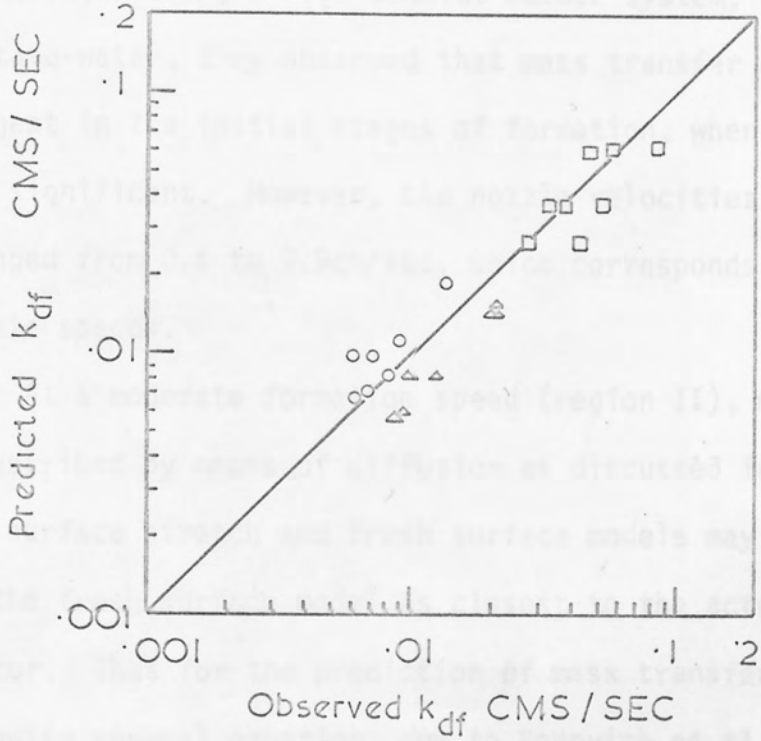

○ ethyl acetate system
□ chlorobenzene system
△ nujol & CCl_4 system

Fig. 4.2. Correlation : mass transfer during drop formation. (159).

with drops formed at moderate speed on which is superimposed the contribution of free convection. The effect of convection during drop formation has been demonstrated in a study by Rajan and Heideger (161). Using a high Schmidt number system, viz., ethyl acetoacetate-water, they observed that mass transfer coefficients were largest in the initial stages of formation, when convection was most significant. However, the nozzle velocities used in this study ranged from 0.6 to 9.9cm/sec. which corresponds to formation at moderate speeds.

At a moderate formation speed (region II), mass transfer can be described by means of diffusion as discussed in para 4.1. Both the surface stretch and fresh surface models may be used here. However the fresh surface model is closest to the actual phenomena which occur. Thus for the prediction of mass transfer in this region the following general equation, due to Popovich et al (162) may be used,

$$E_F . V_{dr} = \frac{4n}{2n+1} \int_0^1 \left\{ (1-y^2)dy . (C^* - C^\circ) \left(\frac{D}{\pi} \right)^{1/2} B_p t^{(2n+1)/2} \right\} \quad (4.12)$$

where n and B_p are defined by: the surface area $A = B_p t^n$ and $y = (1-t/t_1)^{1/2}$; t is the time at which a fresh surface element is formed and t_1 that when the mass transfer is considered. For the special case of a spherical drop the equation reduces to

$$E_F = \left(\frac{A_R}{2V_{dr}} + \frac{4}{3} B \right) \left(\frac{Dt_F}{\pi} \right)^{1/2} \quad (4.13)$$

The surface area-volume relation used in the derivation of this equation was given in Equation 3.15. In a study by Heertjes and de Nie (130,164) two modified forms of Equation 4.13 were proposed to fit their data.

In the case of formation at high speed (region IV), large contributions to mass transfer are caused by strong circulation in the drop. For circulating drops Johnson (152,153) showed that the amount of transfer taking place during formation could be estimated by the correlation,

$$E_F = \left(\frac{20.6}{d}\right) \cdot \left(\frac{\pi}{Dt_f}\right)^{1/2} \qquad (4.14)$$

Groothuis and Kramers (157) have observed a jet action in the drop at Re > 40 to 50, Re being based on the inside diameter of the capillary. This is in agreement with the results of Dixon and Russel (97) who introduced a degree of turbulence. The increase of mass transfer at high speeds of formation has also been reported by Ueyama et al (163). Heertjes and de Nie (98) reported that deviations from the diffusion model occur at Re > 15. The work of Angelo et al (99) should also lie in this region since the Reynold's number was between 200-300. They reported that their surface-stretch penetration model gave a value of $\overline{K}$, a dimensionless mass transfer coefficient for the formation period, = 5.35. The corresponding value obtained for the simple penetration model with no account of stretching of the surface, gave a value of $\overline{K} = 2$. However, values of $\overline{K}$ obtained using the surface-stretch model were generally lower than those obtained using the fresh surface model proposed by Groothuis and Kramers (157).

The two results differed from their average by only 6%.

No data seem to exist for region III.

4.2 MASS TRANSFER DURING DROPLET RELEASE

During the period of release drops are caused to oscillate. This is accompanied by interfacial changes as a result of deformation. The length of the period of drop release depends upon the system and on the conditions applied. Values of the order of 0.1 sec. have been reported for isobutanol in water (98, 164).

The amount of mass transfer during release was reported by Licht and Conway (165) to be of the same magnitude as that for the period of drop formation, whereas Popovich, Jervis and Trass (162) concluded that drop release had no effect at all. The different conclusions may be attributed to the fact that in the later work, the main resistance to mass transfer was in the continuous phase. Marsh and Heideger (166) deduced that a high contribution to mass transfer occurred during release and the first second of rise. In a recent contribution Heertjes and de Nie (98,169) showed that, for isobutanol drops in water, the mass transfer coefficient during release was six times greater than the value for the preceding period. However, confirmation of this awaits further work with other liquid-liquid systems.

4.3 MASS TRANSFER TO AND FROM FORMED DROPS

This section will be divided into two main parts, viz.,

mass transfer in the dispersed phase and that in the continuous phase. The situations for rigid drops and non-rigid drops will be considered separately.

4.3.1 Mass Transfer in the Dispersed Phase

4.3.1.1 The rigid drop

This is the limiting case which will only hold for small drops. The process involved is one of non-stationary diffusion, and is adequately represented by the Newman (141) relation,

$$E = \frac{C_o - C_f}{C_o - C^*} = 1 - \frac{6}{\pi^2} \sum_{n=1}^{\infty} \frac{1}{n^2} \exp. \left[-n^2 \pi^2 \frac{D_D t}{a^2}\right] \qquad (4.15)$$

Recently, Skelland and Minhas (159) proposed an expression for the mass transfer coefficient of a drop during free fall,

$$K_{dr} = \frac{S_{drc}}{t_{cr}\, a_r [1/2(C_{di} + C_{df}) - C_d^*]} \qquad (4.16)$$

where S_{drc} is the solute transferred per drop, t_{cr} is the contact time, C_{di}, C_{df} and C_d^* are the initial, final and equilibrium concentrations, and a_r is the surface area, taken as that of an oblate spheroid having the same volume as that of the falling drop. The validity of this equation remains to be proven.

4.3.1.2 The non-rigid drop

This description covers circulating and oscillating drops. Circulation within the drop may be laminar, Re < 1, or turbulent Re > 1.

As a result of these phenomena, the drop may be completely mixed.

For the case where the circulation has completely developed, mass transfer rates, are known to be 1.5 times that for a rigid sphere. Higher rates can be expected for oscillating drops.

For the regime of laminar circulation, which can be described by the Hadamard (167) streamlines, the Kroing and Brink (168) relation can be applied for the case when resistance to mass transfer in the continuous phase is zero,

$$E = 1 - {}^{3}/_{8} \sum_{n=1}^{\infty} A_n^2 \exp. \left[- \lambda_n \frac{16 D_D t}{a^2} \right] \qquad (4.17)$$

Equation 4.17 is restricted to regimes for which Re < 1. However, Johnson and Hamielec (169) have found that in some cases it can be used for higher values of Re. Furthermore it has been shown that up to Re = 10 the flow patterns resemble those at lower Reynolds numbers.

For the case of turbulent circulation, Handlos and Baron (142) proposed a model, based on a Turbulent flow; due to random radial motion, superimposed upon a circulatory pattern. For zero resistance in the continuous phase their expression is,

$$E = 1 - 2 \sum_{n=1}^{\infty} (A_n')^2 \exp. \left[- \frac{\lambda_n' U_t}{128 (1 + \frac{\mu_D}{\mu_c}) d} \right] \qquad (4.18)$$

Equation 4.18 has been verified experimentally by Skelland and Wellek (170) and Johnson and Hamielec (169). The former authors also recommended the use of the empirical relation of Garner and Tayeban (171), Equation 4.30, to calculate k_c for use with the

above equation. It should be noted however that, as discussed later, relation 4.30 has been derived for oscillating drops.

Olander (172) reported some discrepancies when using Handlos and Baron's model for cases involving short times of contact. This was attributed to the fact that in developing the model only one term has been used, of the series, which appears in the mathematical expression. This is permissible for long contact times only. Thus Olander proposed a correction for the calculated mass transfer coefficient,

$$K_d = 0.972 \; K_{HB} + 0.075 \frac{d}{t} \qquad (4.19)$$

where K_d is the actual transfer coefficient and K_{HB} is that calculated by means of Handlos and Baron's model.

Equation 4.19 is for cases where the resistance in the continuous phase is zero.

Oscillating drops: For systems with a low continuous phase viscosity, drops begins to oscillate at Re = 200. A good agreement has often been found between the rates of mass transfer for oscillating drops and those with rapid internal circulation. However, in many instances (88,99) the rates of mass transfer are considered to be much higher, for oscillating drops.

Rose and Kintner (173) have proposed a model of an interfacial stretch applied to an oblate ellipsoid combined with internal mixing of the drop. This yielded,

$$E=1-\exp\left[- \frac{2\pi D_E}{V} \int_{t_o}^{t_f} \frac{1}{f_1(t)} \left\{ \left(\frac{3V}{4\pi (a_o + a_p |\sin w' t|)^2} \right)^2 \frac{1}{2\alpha} \ln \frac{1+\alpha}{1-\alpha} + (a_o + a_p |\sin w' t|)^2 \right\} dt \right] \qquad (4.20)$$

Definition of the symbols is given in the nomenclature.

When tested for different systems, the deviation from experimental results was reported to be approximately 15%. The reasons for this discrepancy, may be (i) end effects, (ii) the degree of oscillation and (iii) the possible presence of impurities and surfactants.

Another model based upon surface-stretch and internal mixing concepts is that of Angelo et al (99). This does not take any account of the different rates of stretching as does the previous one. The empirical relation for k_d is,

$$k_d = \left(\frac{4D_d\, w\, (1+\varepsilon_o)}{\pi}\right)^{1/2} \qquad (4.21)$$

in which w is the frequency and ε_o is a dimensionless factor for the amplitude, which is given by,

$$\varepsilon_o = \varepsilon + {}^{3}/_{8}\, \varepsilon^2 \qquad (4.22)$$

The surface-time relation is

$$S = S_o\, (1+\varepsilon \sin \tau) \qquad (4.23)$$

where τ is a dimensionless time and ε is the amplitude of surface-stretch calculated from a knowledge of the maximum and minimum surface area per cycle.

Strictly speaking the model is only valid for a whole number of oscillations, i.e., for a fractional number it gives too low a result. Furthermore, values predicted by this model do not differ significantly from those obtained using the Rose and Kintner's model or even, for that matter, from those predicted by the Handlos and Baron model. The later model was proposed for drops with very rapid circulation.

Very little study has been made of mass transfer during the period of development of movement of the drop. However it is difficult to distinguish between mass transfer occurring in this period and that during release. Mass transfer rates have been reported to be very high, during the first seconds of drop life (171).

The contribution made to mass transfer by any satellite drops is considered to be negligible, since most of these drops have a volume of only about 1% of that of the mother droplet. However, if calculations are necessary, for these, rigid drop relations may be used.

From the above discussion, the use of an overall mass transfer coefficient to describe the various contributions can be justified. The overall coefficient also includes the contribution during release.

4.3.2 Mass Transfer in the Continuous Phase

One of the main difficulties in predicting continuous phase mass transfer rates is the estimation of any contribution due to the wake of the drop. Thus the process has often been described as an overall process for the whole drop, using a partial coefficient of mass transfer k_c. This coefficient is then correlated via a Sherwood number to the variables of the process. Many such correlations have been proposed in the past, some of which are given in Table 4.4.

4.3.2.1 From and to rigid drops

For this case, Equation 4.25 in Table 4.4. has been proposed by Linton and Sutherland (175) and recommended by Griffith (176). However in a study by Rowe et al (177), it was suggested that a different type of correlation, should be used. The latter correlation included a term accounting for the diffusion process, Equation 4.26. Both Equations 4.25 and 4.26 make no allowance for the effect of the wake, and therefore, Kinard et al proposed Equation 4.27 which includes the wake effect as well as other effects. In Equation 4.27 the figure 2.0 represents the contribution by diffusion, whilst $(Sh)_n$, accounts for the natural convection effect; since $(Sh)_n = f(Gr),(Sc)$; the third term is the contribution at the top, and the last term for the wake effect at the rear of the drop.

Since the concentration in the wake is larger than in the bulk of the continuous phase, the contribution of mass transfer by the wake is therefore not very large, particularly when a mean k_c is used as in Equations 4.25 and 4.26. Thus, it cannot be said that Equation 4.27, whilst based on a sound approach, fits the results better than the other two. Baird and Hamielec (178) reported that the contribution made by the wake was only 10% of the total mass transfer. It is worth mentioning that the type of wake can be described by the angle of separation θ_s, as shown in Fig.4.3. For rigid spheres Linton and Sutherland (175) recommended the following equation for θ_s,

$$\theta_s = 83 + 191\ Re^{-1/3} \qquad (4.24)$$

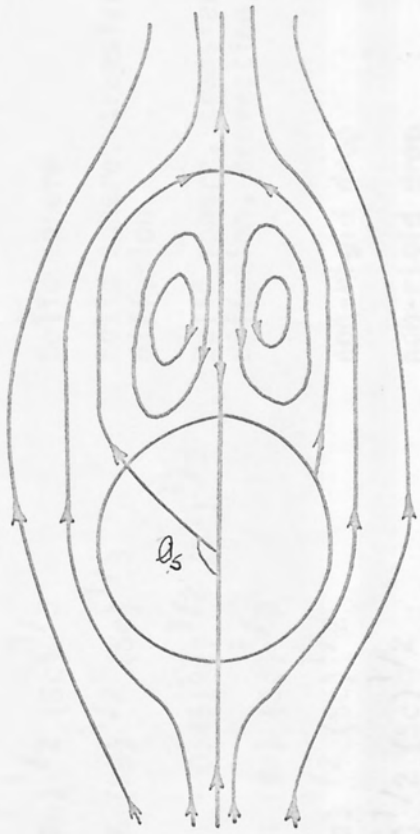

Fig. 4.3

TABLE 4.4

Empirical Models for Continuous Phase Mass Transfer Coefficient

	Eqn. No.	Author	Equation	Comment
1.	4.25	Linton and Sutherland (175)	$Sh = 0.582\ (Re)^{1/2}\ (Sc)^{1/3}$	Solid sphere
2.	4.26	Rowe et al. (177)	$Sh = 2 \div 0.76\ (Re)^{1/2}\ (Sc)^{1/3}$	Solid sphere, transfer by diffusion
3.	4.27	Kinard et al (174)	$Sh = 2 + (Sh)_n + 0.45(Re)^{1/2}\ (Sc)^{1/3} + 0.0484\ (Re)\ (Sc)^{1/3}$	Solid sphere, transfer by diffusion, convection, etc.
4.	4.28	Boussinesq (cited in Ref.93)	$Sh = 1.13\ (Re)^{1/2}\ (Sc)^{1/2}$	non-rigid drop
5.	4.29	Garner and Tayeban (171)	$Sh = 0.6\ (Re)^{1/2}\ (Sc)^{1/2}$	non-rigid drop
6.	4.30	Garner and Tayeban (171)	$Sh = 50 + 0.0085(Re)\ (Sc)^{0.7}$	oscillating drop
7.	4.31	Hughmark (179)	$Sh = 2 + 0.084\ [Re^{0.484}\ Sc^{0.0339}\ (d\ g^{1/3}/D^{2/3})^{0.072}]^{3/2}$	oscillating drop

Finally from the findings of Hughmark (179) it can be observed that the exponent of the Schmidt's number increases with Re, and that the exponent of the Reynold's number indicates an eddy contribution from the wake at Re > 450.

4.3.2.2 From and to non-rigid drops

The correlations proposed to describe the mass transfer in this case are similar to those given for rigid drops, i.e., k_c found via a Sherwood number relation. These expressions are given in Table 4.4. In Equation 4.28, the proportionality constant may be lower than 1.13 due to the existence of a wake under practical conditions. Thus Garner and Tayeban (171) proposed Equation 4.29 with a constant of 0.6. Thorsen (180) proposed, for cases of high Reynold's numbers, the use of a correction factor for the constant 1.13, as given by:

$$\left[1 - \frac{4(3\sqrt{3} - 2)}{5\sqrt{\pi}} \cdot \frac{1}{Re^{1/2}} \cdot \frac{1 + 4\ \mu_d/\mu_c}{1 + (\rho_d/\rho_c \cdot \mu_d/\mu_c)^{1/2}} \right]^{1/2} \qquad (4.32)$$

However, it should be noted that Equation 4.28, as it stands, was claimed to be valid for many cases.

Again, in none of these equations has any attempt been made to separate out the influence of the wake. A clear presentation of the flow pattern in the wake has been given by Garner and Tayeban (171), as shown in Fig.4.3. The angle of separation θ_s is much larger than for rigid drops and in the order of 135°-150°. An expression for the volume of the wake has been given by Hendrix, Dave and Johnson (181). This has the form,

$$\frac{Q}{V_{dr}} = 1.86 \times 10^{-5} \quad (Re)^{1.90} \quad \left(\frac{\Delta\rho}{\rho_c}\right)^{-0.06} \quad \left(\frac{\mu_c}{\mu_d}\right)^{1.94} \qquad (4.33)$$

It should be noted that although the effects of the wake appear to be important in single drop studies, they may be less significant in real cases involving swarms of drops, particularly in agitated systems. Interaction and turbulence caused in the latter cases may result in the destruction of the wake.

The influence of oscillation of the drops on mass transfer has been described by Elzinga and Banchero (182) who reported an increase of up to 45% in mass transfer, due to oscillations. For oscillating drops, k_c may be calculated from Equation 4.30, proposed by Garner and Tayeben (171). Equation 4.30 has been used and recommended by various authors. Recently, Hughmark (179) derived an empirical relation based on measurements of five systems this correlation is given in Table 4.4, Equation 4.31.

The influence of the wake in this case is even more difficult to separate. Hendrix et al (181) observed that oscillation of drops resulted in irregular oscillation of the wake, and that the wake diminished rapidly with the distance travelled by the drop and did not follow the drop closely.

Finally, reference must be made to two recent contributions by Treybal and his co-workers (183,184). In both studies, the results for agitated vessels were correlated by the equation,

$$k_c = k_s + 3.9 \left(D_A/\theta_c\right)^{0.5} \qquad (4.34)$$

where k_s, is a steady state coefficient estimated from the data for suspended solid particles identical in size to the drops (185), and θ_c represents the time between coalescence and redispersion. The latter was estimated from observation of the change in mean drop size from the level in the vessel just opposite the impeller to that at top and bottom.

$$\frac{1}{\theta_c} = 2 \left[\frac{(d_{pT}^3 + d_{pB}^3)/2 - d_{pM}^3}{d_{pM}^3} \right] \frac{1}{t_c} \qquad (4.35)$$

The circulation time, t_c, was estimated for the baffled vessels from the work of Holmes et al (186). The second term on the right of Equation 4.34 represents the enhancement of the mass transfer rate resulting from the relatively violent coalescence phenomenon. The constant 3.9 is an empirical one chosen to provide the best fit of the data.

Equation 4.34 was developed for transfer direction, continuous → dispersed, i.e., a coalescence aided environment, at hold-ups of 0.5 to 9.9%. Most experimental results were correlated to within 20%, by this Equation.

4.4 MASS TRANSFER DURING COALESCENCE

Considerable literature have dealt with the mechanism of coalescence of drops, at a liquid interface, and the effect of mass transfer on coalescence was discussed in para 3.3.4.3. By contrast little information is available on mass transfer during coalescence.

Johnson and Hamielec (169) derived an expression for k_{dc} for the highly simplified case of a drop coalescing immediately upon

reaching the boundary between the phases. The drop contents were assumed to spread out over the entire coalescence surface in a uniform layer. Mass transfer was regarded as occurring according to the pentration theory and the time of exposure of the layer was taken to be the same as the time of formation of the drop. Thus,

$$k_{dc} = (D_d/\pi t_f)^{1/2} \qquad (4.36)$$

Similar results were reported by Licht and Conway (165) and Coulson and Skinner (160). However, these results were, later, criticised by Licht and Pansing (151) and Skelland and Minhas (159). The later authors reported that mass transfer during formation was many times greater than that for coalescence and the contribution due to the later could be ignored. Indeed, this was corroborated by the findings of Angelo and Lightfoot (99), who successfully correlated their results for formation + rise + coalescence by neglecting transfer due to coalescence in their high interfacial tension systems. It may be noted, here, that coalescence referred to is that of a drop on a plain interface, which occurs at the end of the column, after most of the mass transfer has already taken place in previous sections. Thus an inherently low driving force at this point will give rise to small mass transfer rates.

However, Skelland and Minhas (159) derived an expression for the mass transfer coefficient at coalescence k_{dc}. This is given by:

$$k_{dc} = \frac{2V_d}{a_c t_f}\left[\frac{2\,I_{f,c} + (k_{df}/V_d)\,a_f t_f\,(I_{f,c} - 4V_d)}{8\,V_d - 2I_{f,c} - (k_{df}/V_d)\,a_f t_f I_{f,c}}\right] \qquad (4.37)$$

Definition of the symbols is given in the nomenclature. Furthermore the authors correlated their experimental results by an expression similar to that proposed, in the same study, for drop formation; Equation 4.10. The correlation for drop coalescence is:

$$\frac{k_{dc}\, t_f}{d} = 0.1727 \left(\frac{\mu_d}{\rho_d D_d}\right)^{-1.115} \left(\frac{\Delta\rho g d^2}{\sigma}\right)^{1.302} \left(\frac{V_t^2\, f_t}{D_d}\right)^{0.146} \qquad (4.38)$$

The average absolute deviation from the data was approximately 25%.

Recently, Heertjes and de Nie (93,164) concluded that mass transfer during the actual process of coalescence (E_{ec}) can be neglected for two reasons. Firstly the mechanism of coalescence shows that drainage of a drop into the homophase does not permit entrainment of continuous phase in the homophase and secondly coalescence is so rapid (about 3×10^{-2} sec) that no substantial mass transfer is to be expected.

So far only the case of droplet coalescence with a liquid interface has been considered and the effect of interdroplet coalescenceon mass transfer remains to be investigated. However, mention has been made in the literature (35,93) that coalescence of drops in swarms caused an increase in oscillation and hence the creation of a fresh interface albeit of a small magnitude. These are counteracted by the reduction in the surface area. The nett result may in fact cause an overall decrease in mass transfer. However, in study by Mok and Treyball (183), in agitated vessels, k_c was found to be approximately twice as large and $k_c a$, approximately five times as large, for the unbaffled vessel as for the baffled

vessel at the same impeller power. This was attributed to the greater coalescence frequency in the unbaffled vessel.

Higher mass transfer rates may be possible in columns, where a coalescene-redispersion mechanism exists, rather than only discrete drops. It is worth mentioning here that drop-interface coalescence may occur in the mixing section of the column, e.g., in the case of dispersed phase wetted internals as discussed in para 3.3.4.1.

4.5 OVERALL COEFFICIENT OF MASS TRANSFER

The overall mass transfer coefficient may be calculated from the principle of additive resistance, i.e., the overall resistance to mass transfer will be the sum of the individual resistance inside and outside the drop, at the different stages of mass transfer, plus the resistance at the interface. In practical cases the latter is usually attributed to the presence of surface active agents. However, the interfacial resistance may be neglected for design purposes in all but a few cases, such as when solute transfer is accompanied by slow chemical reaction at the interface (10).

In some cases, the resistance of one phase may predominate, and design can then be based on that phase. A criterion, as to which phase is controlling may be referred to here. This requires the knowledge of the times for a droplet to attain 60% or 90% solute concentration. The phase requiring the larger time is controlling. The time θ, may be estimated from the following Equations (35). For the dispersed phase,

$$\frac{Q_\theta}{Q_o} = 1 - \exp\left[-2.25\left(\frac{4D_d'\pi^2\theta}{d^2}\right)\right] \qquad (4.39)$$

and for the continuous phase.

$$\frac{Q_\theta}{Q_o} = 1 - \text{erf}\left(\frac{x}{\sqrt{4D_c'\theta}}\right) \qquad (4.40)$$

4.6 MISCELLANEOUS PHENOMENA

4.6.1 Mass Transfer and Interfacial Instability

It is well known that the interface becomes unstable in cases of high concentration mass transfer. In such cases mass transfer can be increased considerably by local currents. Sawistowski and Goltz (153), have measured mass transfer during drop formation, showing an increase in the transfer coefficient of some factor by this effect. Golden (187) claimed that about 35% of the transfer occurring in forming and collapsing drops, could be attributed to interfacial activity. Instabilities can also be caused by temperature differences. Under conditions of instability drops formed on a nozzle may be erupting, circulating or stagnant. Criteria for stability of the interface have been presented by Sawistowski and Austin (188).

4.6.2 Influence of Surface-active Agents

This phenomenon is outside the scope of this study. However, in general it can be said that the primary effect of surfactants is to suppress the physical characteristics which distinguish non-rigid from rigid drops; e.g., oscillations, deformation, circulation and instabilities at the interface (93).

5. WETTING EFFECTS

In this Chapter the effect of wetting on the performance of extraction equipment will be discussed, with particular reference to the R.D.C.

5.1 BASIC CONCEPT OF WETTING

The terms 'wetting' and 'non-wetting' are generally used to describe whether or not a given liquid spreads on a particular solid surface. This will occur if the total free energy of the system is thereby reduced; the reduction in the surface free energy so obtained is defined as the spreading coefficient. For a solid adsorbed surface film the spreading coefficient is given by,

$$S_{C(S)} = \gamma_S - \gamma_{SL} - \gamma_{LV} \qquad (5.1)$$

If, however, the solid is covered with an adsorbed surface film then,

$$S_{C(SV)} = \gamma_{SV} - \gamma_{SL} - \gamma_{LV} \qquad (5.2)$$

γ_{SV}, γ_{SL} and γ_{LV} denote the solid-gas, solid-liquid and liquid-gas interfacial tensions respectively.

In many instances when a liquid is placed upon a surface it will not completely wet it, but rather will remain as a drop exhibiting a definite angle of contact between the liquid and the solid; this is

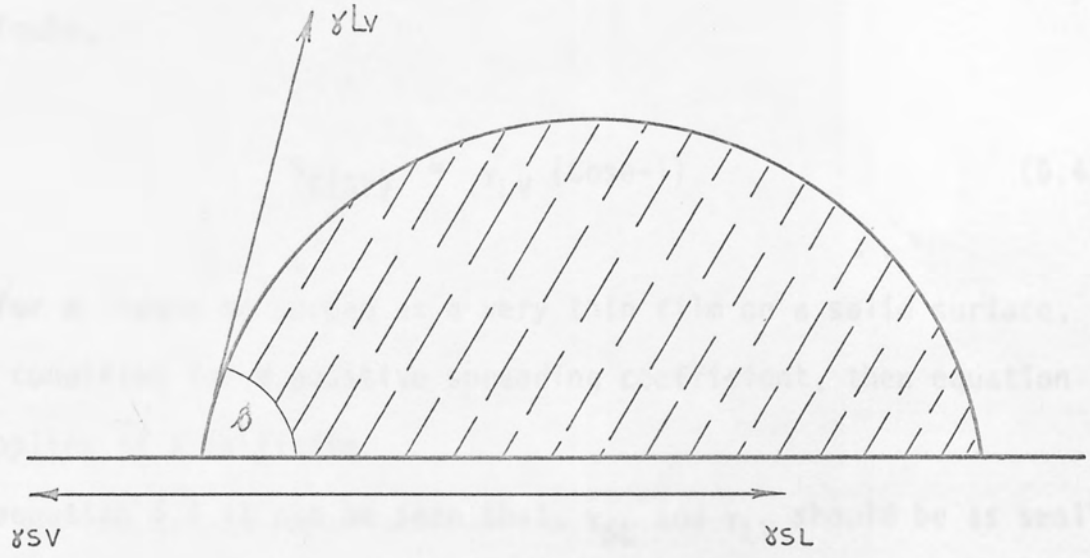

Fig. 5.1. A sessile drop at equilibrium

referred to as the 'contact angle'. From a consideration of the conditions for static equilibrium of a sessile drop, shown in Fig.5.1, the Young and Dupre (189,190) equation, is obtained,

$$\gamma_{SV} - \gamma_{SL} = \gamma_{LV} \cos\theta \qquad (5.3)$$

Substitution of equation 5.3 into equation 5.2, yields the spreading coefficient in terms of the contact angle and the surface tension of the liquid,

$$S_{C(SV)} = \gamma_{LV} (\cos\theta - 1) \qquad (5.4)$$

Thus for a liquid to spread as a very thin film on a solid surface, i.e., condition for a positive spreading coefficient, then equation 5.4 applies if θ is finite.

From equation 5.4 it can be seen that, γ_{SL} and γ_{LV} should be as small as possible in order to achieve good spreading. This may be promoted by the addition of a surfactant to the liquid (118). Alternatively the liquid and solid may be chosen such that spreading will occur.

In contact angle measurements, a difference has been observed between the advancing and receding contact angles. Many proposals have been made as to the factors involved, e.g., contamination of either the liquid or solid, frictional forces and surface roughness. These studies have been reviewed elsewhere (189). The effect of surface roughness on the contact angle is represented in Fig.5.2. Case A shows the liquid front resting at a point down the slope and the apparent angle of contact ($\theta_{app.}$) is greater than the real one.

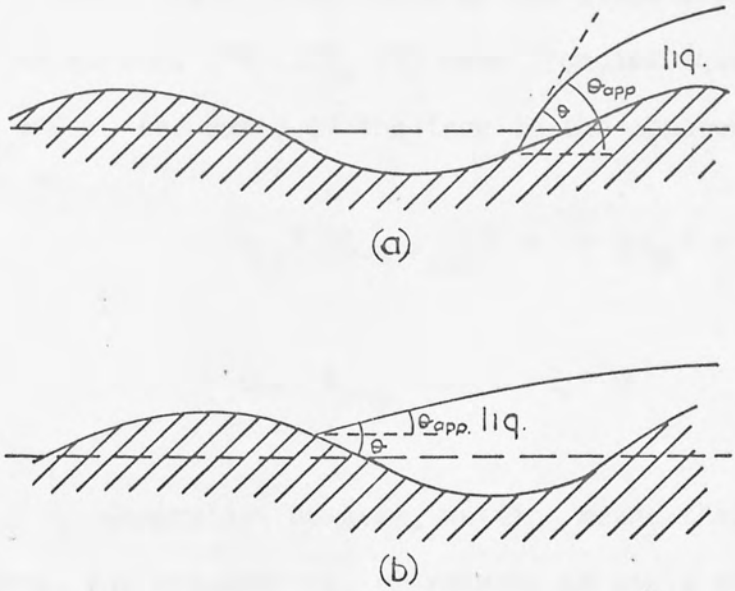

Fig 5.2 Effect of surface roughness on apparent contact angle (189)

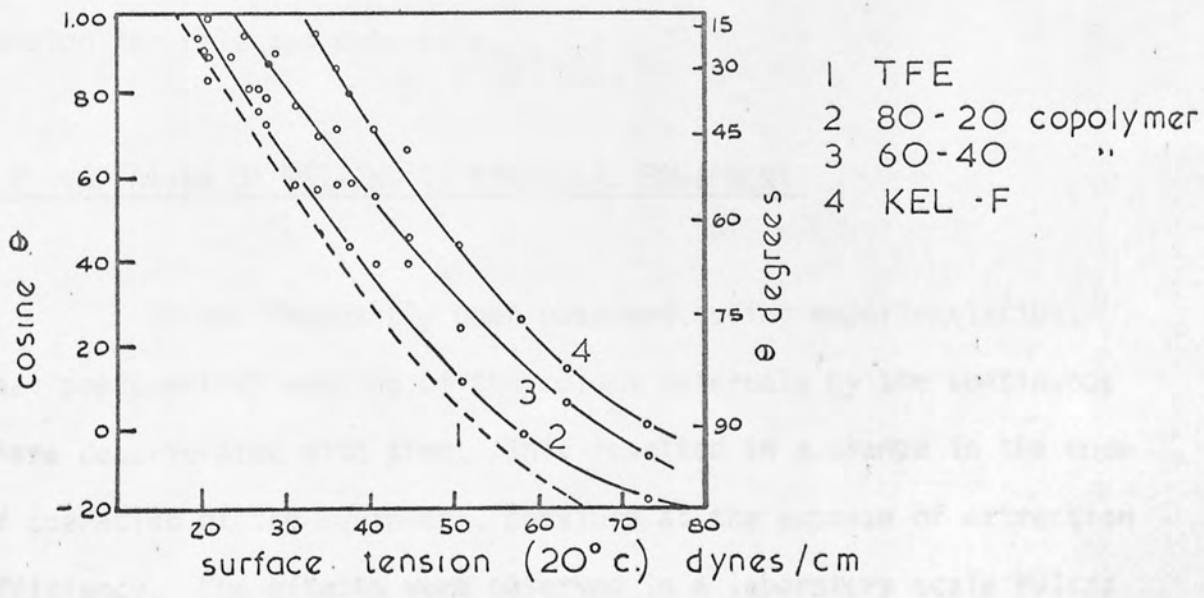

Fig. 5.3. Surface tension versus the contact angle of various liquids on fluorinated polymers (190)

Case B shows the resting point up the slope and hence $\theta_{app} < \theta$. Earlier workers (191,192,193) have proposed equations relating $\theta_{app.}$ and r, the ratio of the true to the apparent surface area, by

$$\gamma_{LV}^{\circ} \text{ Cos } \theta_{app.} = r\,(\gamma_{SV}^{\circ} - \gamma_{SL}) \qquad (5.5)$$

$$\text{Cos } \theta_{app.} = r \text{ Cos } \theta \qquad (5.6)$$

Generally, however, wetting means that the contact angle in zero, and non-wetting, represents an angle greater than 90°. High surface energy materials, e.g., most metals and glass, are wetted by liquids with high surface tension such as water or glycerine whilst low surface energy materials, e.g., plastics, are wetted by liquids with low surface tension including most organic liquids. Figure 5.3 shows the relation between the contact angle and surface tension for selected materials.

5.2 VARIATION OF WETTING IN PRACTICAL EQUIPMENT

It has frequently been observed,during experimentation, that preferential wetting of the column internals by the continuous phase deteriorated with time. This resulted in a change in the mode of operation of the equipment, possibly at the expense of extraction efficiency. The effects were observed in a laboratory scale Pulsed Plate column by Coggan (26), who observed different types of dispersions at different times. These are reproduced in Fig.5.4. Type IV, being the normal operating regime and the other types

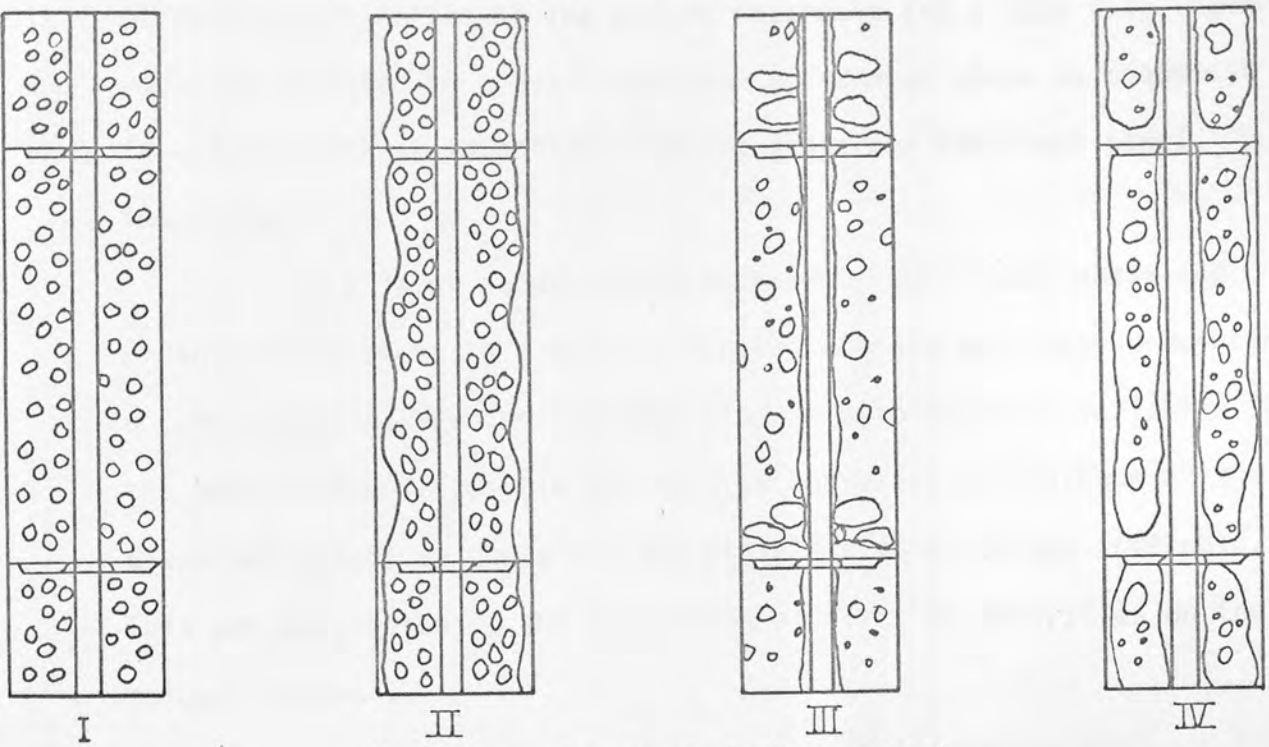

(columns shown in half section)

TYPE I NON-COALESCING DISPERSION. THE DISCONTINUOUS PHASE WETS NONE OF THE SURFACES IN THE COLUMN AND DOES NOT COALESCE.

TYPE II WALL-COALESCING DISPERSION. THE DISCONTINUOUS PHASE WETS THE COLUMN WALL AND FORMS A CONTINUOUS MOVING LAYER.

TYPE III PLATE-COALESCING DISPERSION. THE DISCONTINUOUS PHASE WETS THE PLATE CARTRIDGE BUT NOT THE WALL. DROPLETS ARE LARGE.

TYPE IV PLATE AND WALL COALESCING. THE DISCONTINUOUS PHASE WETS ALL THE SURFACES WITHIN THE COLUMN AND COALESCES RAPIDLY ON CONTACT. IT RUNS DOWN (OR UP) THE COLUMN WALL AND THE CARTRIDGE TIE ROD.

Fig . 5.4 Effect of wetting on the type of dispersions (26)

transitory. This, however, was not strictly a case of deterioration of wetting properties of the column internals and a type (IV) regime would be expected to prevail whenever an aqueous phase is dispersed in columns with preferentially wetted glass and stainless steel internals.

In a later study, using an aqueous continuous phase and organic dispersions in a R.D.C., Scheibel column and Oldshue-Rushton column sections, Mumford (35) was also able to detect a variation in the wetting properties (in the form of increased coalescence of the dispersed phase) on the glass and stainless steel column internals. This was attributed to the deposition of dirt or impurities on the column internals.

It is generally accepted that such conditions are not favourable to extractor operation and that columns should be preferentially wetted by the continuous phase in order to achieve non-coalescing dispersions (1,17,135,118). However it has been suggested that columns with dispersed phase wetted internals might prove more efficient with systems for which dispersed phase film resistance is controlling (35).

The nature of the wettability of the column internal also has a profound effect upon the efficiency and capacity of extraction equipment as described in the subsequent paragraphs. Therefore some knowledge of the performance of dispersed phase wetted columns would be useful, such that changes in the column mode of operation can be anticipated, and steps taken to counteract them, e.g., by variation in throughput, phase ratio or rotor speed.

5.3 THE EFFECT OF WETTING ON THE PERFORMANCE OF EXTRACTION EQUIPMENT

5.3.1 Hydrodynamics

Little work has been reported on the effect of wettability on the hydrodynamics of extraction equipment , although some work has been carried out to investigate its effect on the mass transfer efficiencies.

However, a reduction in the volumetric capacity of a R.D.C. with wetted discs have been reported (35,49). Mumford (35) using toluene dispersed in water and p.t.f.e. discs demonstrated that a circular element of dispersed phase was attached to the tip of the disc and observed that flooding commenced in the plane of the disc. The reduced capacity was roughly correlated in terms of the increasing constriction factor (114) given by,

$$C_R' = \frac{D^2 - (R+2W)^2}{D^2} \qquad (5.7)$$

where W is the element width.

This result is contrary to what would be expected at low disc speeds since the increased coalescence promoted by the wetting effect resulted in bigger drops having higher settling velocities. Hence higher capacities should be possible as was reported by Coggan (26) in the pulsed plate column. However the R.D.C. section investigated by (35,49) had a low geometric constriction factor ($C_R = \frac{D^2-R^2}{D^2}$) and it may be that designs with higher constriction factors could produce different results, i.e., higher capacity. When the stators were made 'wetted' gross coalescence of the dispersed phase occurred giving rise to large globules leaving the stators by drip point formation.

In the same study (35) it was found that, in the Scheibel and Oldshue-Rushton column sections, the wettability of the turbine agitator was not important. The use of wetted mesh packing in the Scheibel column, produced a pool of the dispersed phase over the packing and very small drops in the agitated compartment at conditions prior to flooding. At lower hold-ups, drop phenomena, were similar to those for non-wetted packings.

The variation of hold-up along the length and diameter of the column has not been reported for wetted columns. Mumford (35) however, reported that erratic results were obtained for "point" hold-up measurements, due to the unequal distribution of the dispersed phase within each compartment.

In a pulsed packed column, an unglazed ceramic packing wetted by an aqueous dispersed phase gave higher flooding limits than a polyethylene packing wetted by a continuous toluene phase (194). Sege and Woodfield (195) obtained higher capacities with stainless steel plates than with fluorothene ones, using an organic dispersion in an aqueous continuous phase, in a pulsed plate column.

5.3.2 Droplet Phenomena

5.3.2.1 Formation at Orifices

As described in para (4.3.1), any distributor plate should, preferentially, be wetted by the continuous phase to produce a continuous stream of drops at fairly constant size. In a study of the formation of droplets from a circular orifice at varying contact

angles, Haynes et al (19) found that as the contact angle was increased, i.e., the dispersed phase wetted the plate, the dispersed phase tended to spread along the plate surface and form relatively large droplets before breaking away under the action of gravity. Conversely liquids with small contact angles formed from the orifice without spreading. Thus for organic droplets formed from an orifice, an increase in size up to 10 fold has been reported for p.t.f.e. compared with metal plates (19).

5.3.2.2 Drop size distribution

There is no published data on the effect of wettability of the column internals on the drop size distribution, although it has been generally observed that large globules formed by drip point mechanism, from static wetted internals (26,35). However in a rotary agitated contactor such as the R.D.C., at low flow rates of the dispersed phase extremely small droplets may be formed from the tip of the wetted disc in a manner similar to that described for disc atomizers (196) and rotating cups (197).

5.3.2.3 Break-up mechanisms

The mechanism of droplet break-up in a column with wetted internals is dependent upon the column geometry. The mechanism of break-up in a Scheibel column with wetted packing is described in para (5.3). For R.D.C. and Oldshue-Rushton columns with wetted stators, the mechanism was reported to be drip point formation from the stator (35). However, a more interesting situation occurs in an R.D.C. with dispersed phase wetted discs, since drop formation

from the disc then resembles atomization from centrifugal discs in oil burners. In the latter the liquid is discharged as a flat sheet and the manner in which this sheet disintegrates depends on the operating conditions. Three regimes have been identified viz. (198),

i Rim distintegration

ii Perforated sheet disintegration

iii Wavy sheet disintegration

and these are fully discussed in Chapter 6.

Regime (iii) shown in Fig.5.5, may involve a sinuous wave which occurs at high velocities giving rise to complete atomisation, or a symmetrical wave which occurs at lower speeds. The latter is the predominant mechanism during normal operating conditions of a wetted disc R.D.C. (35).

For wave disintegration of a liquid sheet attenuating according to $h = F/\theta$ in a stationary gas the ligament diameter was given by (199).

$$d_L = \left(\frac{4h}{n''}\right)^{1/2} \qquad (5.8)$$

To evaluate this, h the sheet thickness at break-down and n", the wave number, were expressed in terms of f, the total growth of the wave. This analysis yielded the following equation (199).

$$d_L = 0.9614 \left[\frac{B^2 \sigma^2}{\rho_c \rho_D U^4}\right]^{1/6} \left[1 + 2.6 \sqrt[3]{\mu \frac{B \rho_c^4 U^7}{72 \rho_D^2 \sigma^5}}\right]^{1/5} \qquad (5.9)$$

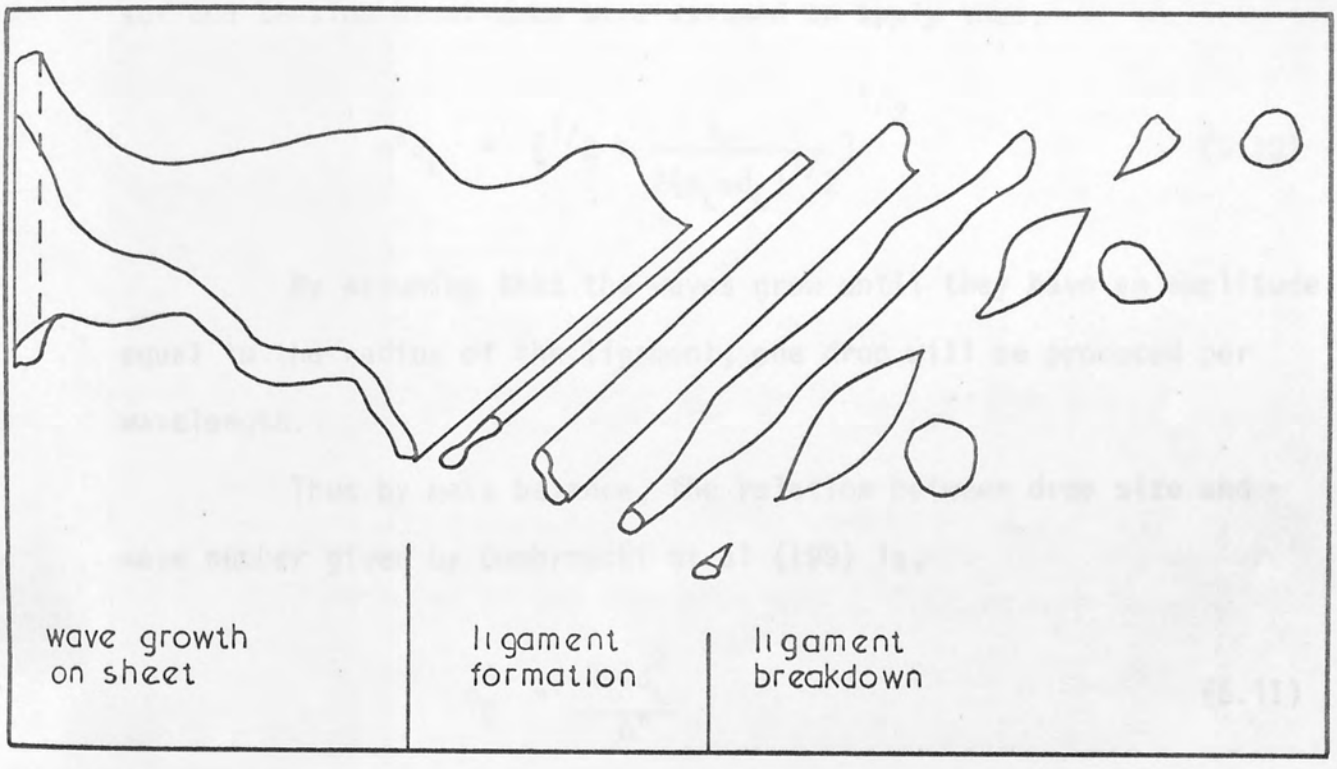

Fig. 5.5. Wavy sheet disintergration and ligament breakdown (199)

In an earlier work (200) it was observed that the ligaments were produced from a liquid sheet break-down through symmetrical waves. Weber (201) has analysed the properties of these waves, where surface tension forces predominate. For ligaments moving transversely through the continuous phase, Weber's results for surface tension break-down were assumed to apply thus,

$$n''d_L = \left[{}^{1}/_{2} + \frac{3\mu}{2(\rho_L \sigma d_L)^{1/2}} \right]^{1/2} \qquad (5.10)$$

By assuming that the waves grow until they have an amplitude equal to the radius of the ligament, one drop will be produced per wavelength.

Thus by mass balance, the relation between drop size and wave number given by Dombrowski et al (199) is,

$$d_D^3 = \frac{2\pi\, d_L^2}{n''} \qquad (5.11)$$

Combining this equation with equation 5.10 leads to,

$$d_D = \left[\frac{3\pi}{\sqrt{3}} \right]^{1/3} d_L \left[1 + \frac{3\mu}{(\rho_L \sigma d_L)^{1/2}} \right]^{-1/6} \qquad (5.12)$$

where d_L is given by Equation (5.9) .

In a 3" R.D.C. section, using a dispersion of toluene in water, Mumford (35) observed drop sizes comparable to those predicted from equation (5.12) particularly at rotor speeds > 800 r.p.m.

5.3.2.4 Coalescence

As mentioned earlier drops tend to coalesce with static wetted internals giving rise to large globules. However, initially the drops spread on the surface, forming a film whose thickness depends on the operating conditions; subsequently drops coalesce with this film. With thin liquid films this is analogous to coalescence with a non-deformable interface. Whilst for films with appreciable thickness, the situation would resemble coalescence with a deformable interface. In rotary agitated columns, however, conditions are different and rather more complex than coalescence on a plane interface, since moving interfaces are involved.

5.3.3 Mass Transfer Efficiency

In studies of the effect of wettability on mass transfer efficiency in various extractor designs, it has generally been concluded that the best efficiency was obtained when the continuous phase wetted the internals. Under such conditions a uniform dispersion of small droplets is obtainable, rather than the films and globules produced by coalescence of the dispersed phase on the wetted internals. However wettability is influenced by the direction of solute transfer and therefore this factor has to be considered when assessing possible effects of wetting on the column efficiency.

In a 4 inch perforated plate column, with the system toluene-diethylamine-water, Garner et al (17) found that, when the transfer was from the dispersed water to the continuous toluene; continuous phase "wetted" polyethylene plates gave a continuous stream of droplets and higher efficiency. When the transfer was in the opposite direction; higher efficiency was obtained using metal plates.

Sobotic and Himmelblau (18) studied the effect of plate wetting characteristics in a pulsed, sieve-plate column. Either stainless steel or polyethylene plates resulted in smaller rates when acetic acid was transferred from an aqueous dispersion to a continuous ketone phase. Substantially higher rates were observed for acid transfer from the continuous ketone phase to water using polyethylene plates in the column. An alternating plate arrangement gave results intermediate between the performance of all polyethylene or all stainless steel plate columns. Other investigators (26,195) reported higher HTU values for pulsed plate columns with dispersed phase wetted internals. For aqueous dispersions, Sege and Woodfield (195) reported that capacities as high as those of stainless steel plates and HTU values as low as those obtained with fluorothene plates may often be attained by the use of "dual plates", i.e., plates with one plastic (organic wetted) and one stainless steel (aqueous wetted) face. The plates were orientated with the plastic face towards the organic phase inlet end of the column.

For packed columns many investigators (202,203,204) reported higher mass transfer coefficients when the dispersed phase did not wet the packing. However, Berg, Manders and Switzer (205) found higher efficiencies with water dispersed regardless of the wetting properties of the packing. Whilst Osmon and Himmelblau (206) found that plastic packing was best for the transfer of acetic acid from M.I.B.K. to water. When the transfer was in the opposite direction ceramic packing gave better results irrespective of whether the aqueous phase was dispersed or continuous.

Furthermore in a pulsed packed column Jackson et al (194) found that polyethylene packing gave substantially higher transfer rates than unglazed ceramic packing, for the transfer of benzoic acid from dispersed toluene to a continuous water phase. The use of the two types of packing in alternating bands resulted in a performance intermediate between that of each packing employed separately.

Finally in a rotating disc contactor with dispersed phase wetted internals, Davies et al (118) showed that the transfer rate of phenol from dispersed water to kerosine phase was less than that achieved using a conventional R.D.C., i.e., one with continuous phase wetted internals. However this was with phase ratios of 12 to 16:1 compared with the more usual practical range of 0.5 to 4:1. In addition to the discs and stators the column wall was also wetted by the dispersed phase and this caused a large proportion of the dispersed phase to flow along the wall, resulting in a considerable reduction in interfacial area. The results of this work are summarised in Figures 5.6 and 5.7 and show the greater efficiencies achieved with continuous phase wetted internals.

This resumé provides some indication of the effect of wetting phenomena on extractor capacities and efficiencies. However in some cases other factors, e.g., mass transfer direction, may supersede this effect. This is referred to later in Chapter 10.

Further investigation is needed to determine the magnitudes of wetting effect for various degree of wettability of materials.

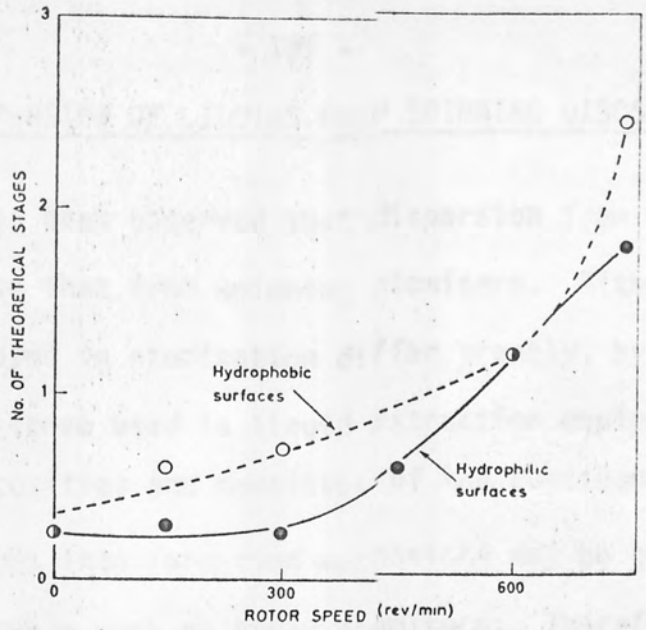

Phase ratio 1 : 12

Fig. 5.6.

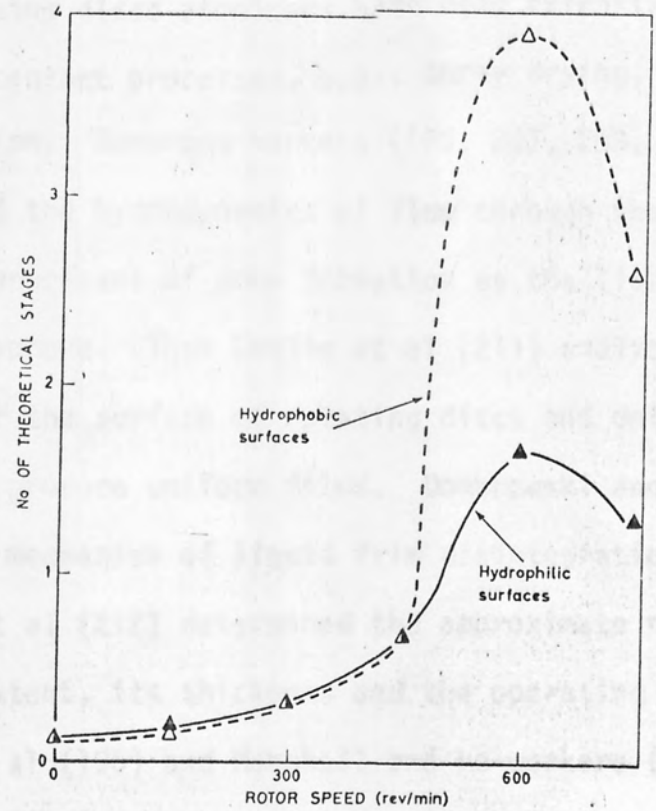

Phase ratio 1 : 16

Fig. 5.7.

Effect of Wetting on Number of Theoretical Stages in an RDC.

6. THE DISPERSION OF LIQUIDS FROM SPINNING DISCS

It has been observed that dispersion from wetted discs is not unlike that from spinning atomisers. Although the rotor speeds employed in atomisation differ greatly, by as much as 10 times, from those used in liquid extraction equipment, e.g., the R.D.C., and the viscosities and densities of the continuous phase also differ, useful insight into formation mechanisms may be gained, from the considerable work on spray atomisers. Therefore, this is reviewed below.

6.1 SPINNING DISC ATOMISERS

Spinning discs atomizers have been extensively used for gas-liquid contact processes, e.g., spray drying, humidifcation and combustion. Numerous workers (196, 207, 208, 209, 210) have investigated the hydrodynamics of flow through these devices and the subsequent processes of drop formation as the liquid disintegrates in the atmosphere. Thus Emslie et al (211) analysed the flow of viscous liquids over the surface of rotating discs and determined the conditions required to produce uniform films. Dombrowski and Frazer (200) studied the mechanism of liquid film disintegration by rotating discs and Dixon et al (212) determined the approximate relation between the sheet extent, its thickness and the operating conditions. Friedman et al (196) and Marshall and co-workers (207, 209) have analysed the flow over vertically vaned discs and proposed correlations for the drop size. Hinze and Milborn (213) have studied the flow

within rotating cups, which are used as atomizers and operate on the same principle as the discs. They have also investigated the mechanism of drop formation. Finally Frazer et al (197) have investigated the flow characteristics of sheets produced from spinning discs.

The operation of all these devices, is dependent upon feeding liquid through a stationary tube to the rotating element, so that the high velocity of the liquid leaving the rotor plus the fact that it is diverging promotes disintegration of the liquid into small drops by the action of the centrifugal force, the liquid is thrown outwards in a radial direction.

Three different mechanisms of drop formation, at tip speeds between 3 and 15 m/sec., have been distinguished for cups (213) and discs (200), viz.,

(i) Direct drop formation. At very low flow rates, i.e., 2.5 lb/hr., the liquid spreads out towards the rim, where it forms a ring. As liquid continues to flow into the ring, its inertia increases and overcomes the restraining surface tension. Disturbances, then, occur on the outer edge. These grow in size until liquid is centrifuged off as discrete drops from the rim. In the process liquid is drawn into a spherical globule but remains attached to the rim by a fine attenuating thread. Upon drop detachment this retaining thread breaks down into a chain of small satellite drops. Since the satellite drops constitute only a small proportion of the total liquid flow rate, for most practical purposes, an almost homogeneous spray is produced.

(ii) Breakdown of threads produced from the lip. When the liquid flow rate, Q is increased, i.e., 2.5 lb/hr. < Q < 28 lb/hr., the retaining threads grow in thickness and form long jets. These jets extend into the atmosphere, are stretched, and finally break down into strings of drops, the diameter of which are smaller than those formed by mechanism (i).

(iii) Sheet disintegration. With further increase of flow rate, the jets are unable to remove all the liquid, the ring is forced away and a thin sheet extends around the lip. The mechanism by which this sheet breaks down, dependent upon rotational speed and viscosity, is discussed later in para. 6.1.1. The drop size spectrum is wide due to the varied behaviour in this region of disintegration.

The transition from thread formation to sheet formation has been studied by Hinze and Milborn (213) and Frazer et al (197). In the former study it was postulated that a sheet is formed when the liquid throughput exceeds the rate of liquid removed by the threads. The transition to sheet formation is then given by:

$$\left(\frac{\rho_L Q^2}{\gamma d_L^3}\right) \left(\frac{\rho_L w^2 d_L^3}{\gamma}\right)^{0.437(1-m)} \left(\frac{\eta^2}{\rho_L \gamma d_L}\right)^{(8m-1)/[8(1-m)]} > \text{const.} \quad (6.1)$$

The theoretical significance of this equation was later confirmed by Frazer et al (197), from a theoretical consideration of the conditions for transition from sheet to thread formation. Thus transition occurs when,

$$\left(\frac{\rho_L n^2 d_L^3}{\gamma}\right) \left(\frac{Q}{n d_L^3}\right)^{4/3} \left(\frac{v d_L}{Q}\right)^{(b-1/3)} > 14.4\ K_o \quad (6.2)$$

Either of these expressions may be used. Since the indicies and the constants have nearly equal values (197).

In an earlier study, on centrifugal discs, Bär (214) failed to distinguish between sheet and thread formation and reported only two mechanisms. In one mechanism, at low flow rates, drops disengaged from the periphery of the disc in a similar manner to mechanism (i), described above. The theoretical equation for this case was,

$$D_{max} = \frac{0.525}{n} \left(\frac{\sigma}{r\rho}\right)^{0.5} \qquad (6.3)$$

where D_{max} is the maximum diameter a drop could attain before disengaging from the disc. This equation was found to be satisfactory with materials having low viscosity but yielded low values with viscous materials (196).

In the second mechanism, predominating at high flow rates, liquid disintegrated after leaving the disc. For this case D_{max} was given theoretically by,

$$D_{max} = \frac{0.102\sigma}{n^2 r^2 \rho_c} \qquad (6.4)$$

Measured drop sizes were two to five times greater than those predicted by this equation, with materials of highest viscosity giving the largest drop sizes (196).

Mechanisms (i) and (ii) as proposed by Hinze and Milborn (213), are not particularly relevant to the present study, since they only occur at low flow rates. The moderate and large flow rates, normally employed in extraction equipment, should result in sheet

formation. Thus, only the later mechanism is considered in later paragraphs. Strictly speaking sheet formation may only occur under conditions of enhanced coalescence in a R.D.C. e.g., the case of wetted discs and or the appropriate direction of mass transfer.

6.1.1 Mechanisms of Sheet Disintegration

The manner in which liquid sheets disintegrate into drops depends on the operating conditions and the physical properties of the system. Three mechanisms of disintegration have been identified (199).

(1) "Rim disintegration", in which the liquid rims of the sheet continually contract due to surface tension effects. Liquid threads which are pulled out from the rim during contraction break up to give large drops.

(2) "Perforated sheet disintegration", in which the free edge disintegrates through a network of threads. Above the free edge point disturbances puncture the attenuated sheet in thin regions and the resulting holes expand until they meet and the thin ligaments joining them disintegrate.

(3) "Wavy sheet disintegration", in which the wave on the sheet caused by the air disturbance results in disintegration by tearing surfaces of liquid off the main sheet.

Regime (1) occurs at low ejection pressures and regime (2) only occurs for a very limited range of conditions. Hence, the third regime is the most common cause of break-up. The wave may be sinuous, which occurs at high velocities giving rise to complete atomization, or dilational which occurs at lower ejection velocities. In the latter case the jet swells and contracts symmetrically. Sinuous

waves are usually the more unstable (199). Sheet break-down may occur through a combination of both mechanisms, under certain conditions. Fig.6.1 show the two different waves. The mechanism of disintegration was primarily determined by the peripheral speed. And viscosity was found to have very little effect. While an increase in flow rate resulted in the sheet becoming much more disturbed and the region of disintegration covered a wider range (197).

6.1.1.1 The extent of the liquid sheet

The effect of the physical properties and operating conditions on the sheet extent a, has been investigated by various workers. Dombrowski and Frazer (200) found that the sheet extent decreased with increasing surface tension. They also observed a small increase with increasing density and a larger increase for an increase in viscosity. The influence of viscosity was later confirmed by Frazer et al (197) who also observed that the extent of the sheet increased with liquid flow rate and diminished with rotary speed. In the same study, expressions were given for the extent of the sheet. For wave disintegration (peripheral speed > 26 ft/sec), the sheet extent a_w, was given by:

$$a_w = \left[31.5 \times 10^4 \left(\frac{v}{r}\right)^{0.25} \frac{(\gamma Qm)^{2/3}}{(nd_L)^2} + \frac{d_L^2}{4} + 0.6\right]^{1/2} - \frac{d_L}{2} \quad (6.5)$$

For combined wave and rim disintegration (peripheral speed < 26 ft/sec).

$$a_{rw} = \left[15.6 \times 10^4 \left(\frac{v}{r}\right)^{0.185} \frac{(\gamma Qm)^{2/3}}{(nd_L)^2} + \frac{d_L^2}{4}\right]^{1/2} - \frac{d_L}{2} \quad (6.6)$$

Both equations were claimed to correlate well with measured data.

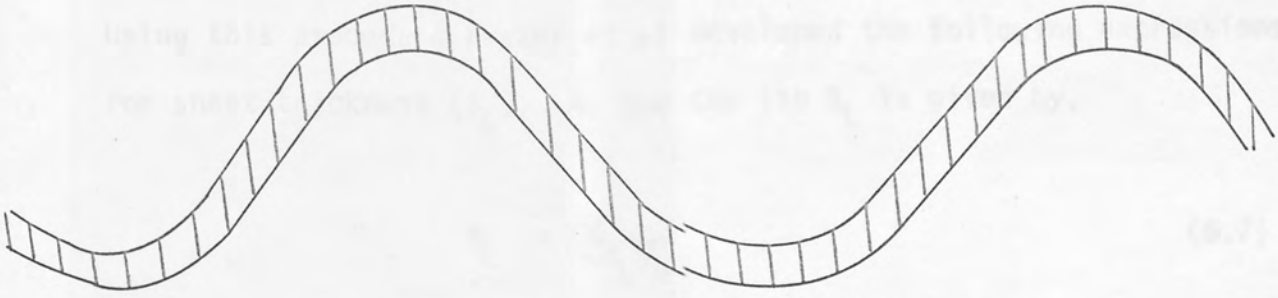

a. Sinuons wave

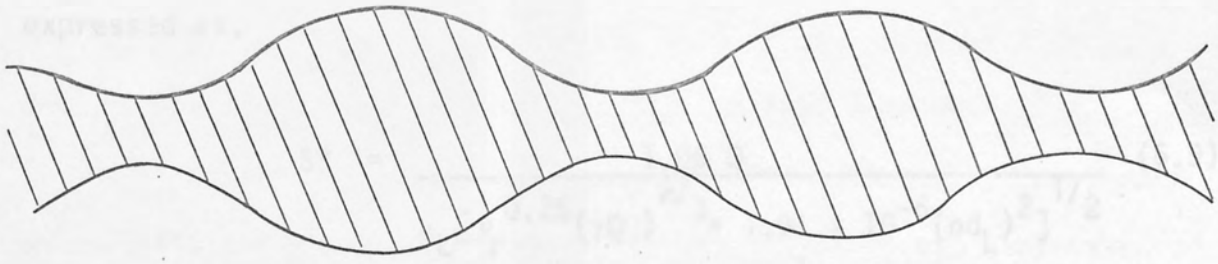

b. Dilational wave

Fig. 6.1. Sinuons and Dilational waves (199)

6.1.1.2 Variation of the sheet thickness

There are three forces acting upon the thinning of liquid sheet: viz friction of the surroundings at the free surfaces, and surface tension and viscous forces opposing the expansion of the sheet. However, their effect can be neglected (215) and the sheet dimensions may be analysed by geometrical considerations (197). Using this procedure Frazer et al developed the following expressions for sheet thickness (S_L). At the cup lip S_L is given by,

$$S_L = \frac{Q}{\pi d_L U_m} \tag{6.7}$$

At a distance a, from the lip,

$$S_L = \frac{Q}{2\pi V\left[\frac{d_L^2 U_m^2}{4V^2} + a\, d_L + a^2\right]^{1/2}} \tag{6.8}$$

The sheet thickness at point of free disintegration S* may be expressed as,

$$S^* = \frac{1.06\, Q}{\rho_L\left[\nu_r^{0.25}(\gamma Q)^{2/3} + 1.91 \times 10^{-6}(nd_L)^2\right]^{1/2}} \tag{6.9}$$

In Equation 6.9,(a) was replaced by Equation 6.5, and Q is in lb/hr.

In general the sheet thickness was found to increase with increasing flow rate and viscosity. The influence of the viscosity, however, was only significant at the lip. Beyond that little or no change in the thickness occurred. The reason for this can be detected from Equation 6.8. As $a \to o$ S_L is controlled by viscosity through its effect on U_m. By increasing the cup diameter, rotor speed or sheet

extent resulted in reduction in the thickness.

6.2 DROP-SIZES PRODUCED BY ATOMIZATION

The numerous expressions proposed to predict the sizes of drops produced by sheet disintegration, fall into two main categories, dependent upon the methods employed in the derivation, viz theoretical or empirical.

6.2.1 Theoretical Approach

The theoretical prediction of drop sizes, is based on an assumed break-up mechanism. For inviscid liquids disintegration is by sinuous waves. This situation is very complex, but can be idealized by considering the waves on the sheet to continue growing until crests are blown out and the sheet breaks into half wave lengths which contract into ligaments. The ligaments are then assumed to disintegrate,by varicose break-up, into drops. However, the present work involves break-up of sheets of real liquids having finite viscosity. For this case Dombrowski and Johns (199) presented an analysis for break-down of an attenuating flat sheet. They assumed that ligaments break-down was by dilational waves, and the proposed expression for drop size together with its derivation is discussed in Chapter 5.

Theoretical equations predict that only one size of drop will be formed whereas in practice a spectrum of drop sizes is obtained and the spray is usually characterised by some average diameter. However it seems reasonably certain that the theoretically predicted diameter will bear some constant relation to the actual average diameter and this is the usual assumption made in testing theories

against experimental results. The drop sizes predicted by the Dombrowski and Johns relation were compared with measured values of the surface-volume mean drop diameter, d_m for wax-sprays obtained by Hasson and Mizrahi (216) and it was found that the points lay satisfactory around the straight line.

$$d_m = 0.676\ d_D \qquad (6.10)$$

The drops measured by Hasson and Mizrahi included those issuing from the rims of the spray sheet, and initial experiments showed that these were 5-10% coarser than those produced from the leading edge. Since in their analysis Dombrowski and Johns (199) were only concerned with drops produced from the leading edge, the constant in Equation 6.10 should be reduced by some 7 1/2% to give a value of 0.63 (199).

6.2.2 Empirical Expressions For Drop Sizes

The various empirical expressions, proposed for mean drop sizes produced from swirl atomisers are summarised in Table 6.1. These correlations are highly specific for the type of atomiser used and cover only a narrow range of liquid properties. However some general conclusions may be drawn from them, viz.,

1. Drop size is approximately proportional to $(\Delta P)^{-1/3}$ for both flat and conical sheets of liquid.
2. Drop size increases with viscosity, the exponent on the viscosity term being ca. 0.2.
3. The effect of surface tension follows a relation of the type $d_D \propto \sigma^{1/3}$ for fan-spray nozzles; the evidence for swirl atomisers is inconclusive.

4. Air density is a very important factor determining the aerodynamic waves causing sheet disintegration. This phenomena has only been fully investigated for flat sheets (217).

TABLE 6.1

Eqn.No.	Equation	Comments	Ref.
1	$d_{32} = 220 \left(\frac{K\sigma}{C_Q^2 \Delta P}\right)^{1/3} \left(\frac{\rho_L}{\rho}\right)^{1/6}$	$\rho < 0.002$ g/cm^3, σ = 24-73 dyn/cm	(217)
2	$d_{32} = 137 \left(\frac{\sigma^{0.2}}{C_Q^{0.8} \Delta P^{0.4}}\right) K^{1/2} \left(\frac{\rho}{\rho_L}\right)$	$\rho > 0.006$ g/cm^3	(217)
3	$d_{32} = 1{,}172.5 \left(\frac{K}{C_Q \Delta P}\right)^{1/3}$		(218)
4	$d_{32} = 4.4 \left(\frac{Q}{\theta}\right)^{1/3} \sigma^{1/3} \rho_L^{1/6} \Delta P^{-1/2}$		(219)
5	$d_{32} = C \left(\frac{\sigma K}{C_Q^2 \Delta P}\right)^{1/3} (\rho_L)^{1/6}$	C = 915±36, for liquid sprays	(216)

6.3 FLOW IN THE NEIGHBOURHOOD OF A ROTATING DISC

The theories and mechanisms of droplet formation from spinning discs atomizers have been considered since they have some similarity with drop formation from a disc wetted by the dispersed

phase. In order to complete the picture it is important to understand the nature of flow around a rotating disc. The flow in the neighbourhood of a flat disc rotating about an axis perpendicular to its plane with a uniform angular velocity ω in a fluid otherwise at rest, can be adequately represented by a system of equations proposed by Navier and later modified by Stokes (220). These are commonly referred to as the Navier-Stokes equation and are given below. The layer near the disc is carried by it through friction and is thrown outwards owing to the action of centrifugal forces. This is compensated by particles which flow in an axial direction towards the disc to be in turn carried and ejected centrifugally. Thus the case is seen to be one of fully three- dimensional flow, i.e., three velocity components exist viz w, in the axial direction z, u in the radial direction r, and v in the circumferential direction ϕ. The three-dimensional flow field is shown in Fig.6.2. (220).

The Navier-Stokes equations are,

$$u\frac{\partial u}{\partial r} - \frac{v^2}{r} + w\frac{\partial u}{\partial z} = -\frac{1}{\rho}\frac{\partial p}{\partial r} + \nu\left[\frac{\partial^2 u}{\partial r^2} + \frac{\partial}{\partial r}\left(\frac{u}{r}\right) + \frac{\partial^2 u}{\partial z^2}\right] \qquad (6.11a)$$

$$u\frac{\partial v}{\partial r} + \frac{uv}{r} + w\frac{\partial v}{\partial z} = \nu\left[\frac{\partial^2 v}{\partial r^2} + \frac{\partial}{\partial r}\left(\frac{v}{r}\right) + \frac{\partial^2 v}{\partial z^2}\right] \qquad (6.11b)$$

$$u\frac{\partial w}{\partial r} + w\frac{\partial w}{\partial z} = -\frac{1}{\rho}\frac{\partial P}{\partial z} + \nu\left[\frac{\partial^2 w}{\partial r^2} + \frac{1}{r}\frac{\partial w}{\partial r} + \frac{\partial^2 w}{\partial z^2}\right] \qquad (6.11c)$$

$$\frac{\partial u}{\partial r} + \frac{u}{r} + \frac{\partial w}{\partial z} = 0 \qquad (6.11d)$$

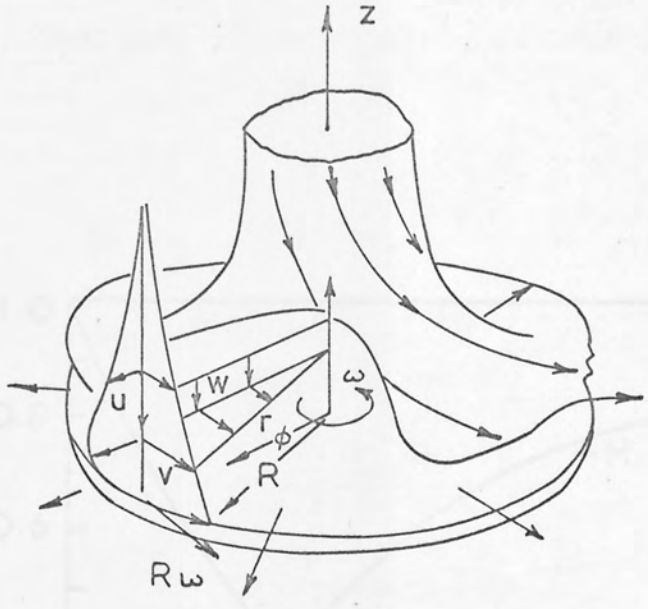

Fig. 6.2. Flow in the neighbourhood of a rotating disc. (after 220, 221) (components of velocity are w - axial, u - radial and v - circumferential).

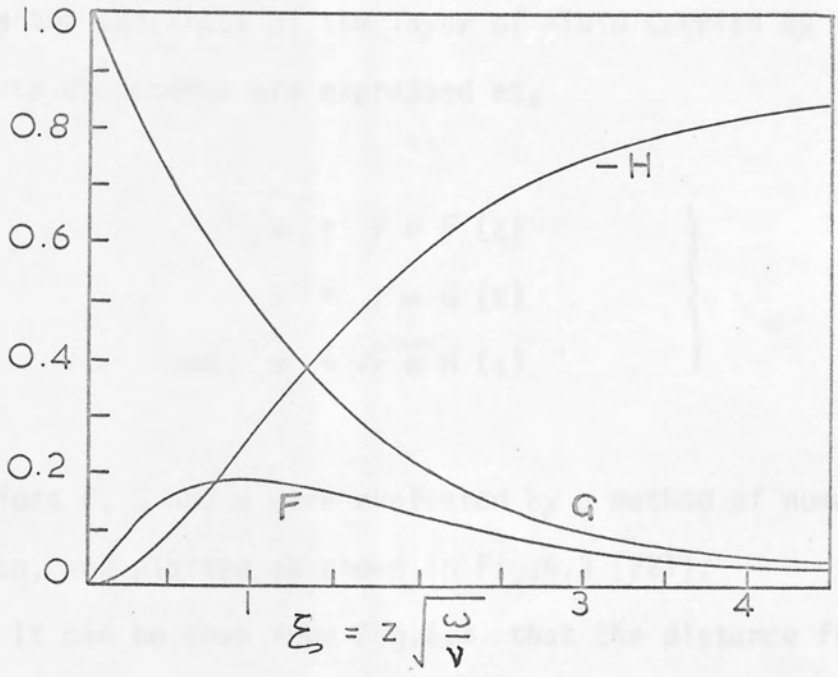

Fig. 6.3. Velocity distribution near a rotating disc; values of functions F, G and H for use in equation 6.13 (221)

The exact solution of this system of equations for the case of a rotating disc as described above has been evaluated by Cochran (221). By introducing a dimensionless distance from the wall,

$$\xi = \frac{z}{\delta} \tag{6.12}$$

where δ is the thickness of the layer of fluid carried by the disc. The velocity components are expressed as,

$$\left.\begin{aligned} u &= r\,\omega\,F(\xi) \\ v &= r\,\omega\,G(\xi) \\ \text{and}\quad w &= \sqrt{r\,\omega}\,H(\xi) \end{aligned}\right\} \tag{6.13}$$

The functions F, G and H were evaluated by a method of numerical integration, and plotted as shown in Fig.6.3 (221).

It can be seen from Fig.6.3 that the distance from the wall over which the peripheral velocity is reduced to half the disc velocity is $\delta_{0.5} \simeq \sqrt{\nu/\omega}$. It should be noted that when $\delta \simeq \sqrt{\nu/\omega}$ is small, the velocity components u and v have appreciable values only in a thin layer of thickness $\sqrt{\nu/\omega}$. The velocity component w, normal to the disc, is small, of the order $\sqrt{\nu\,\omega}$ and can therefore be neglected.

By means of Equations 6.13 and Fig.6.3, the value of the resultant velocity difference across a drop, at any location near the disc, can be found. Mumford (35) used the velocity values thus calculated to predict the stable drop size, at different locations beneath the disc, from Equation 3.28. The results of this study are given in Fig.6.4.

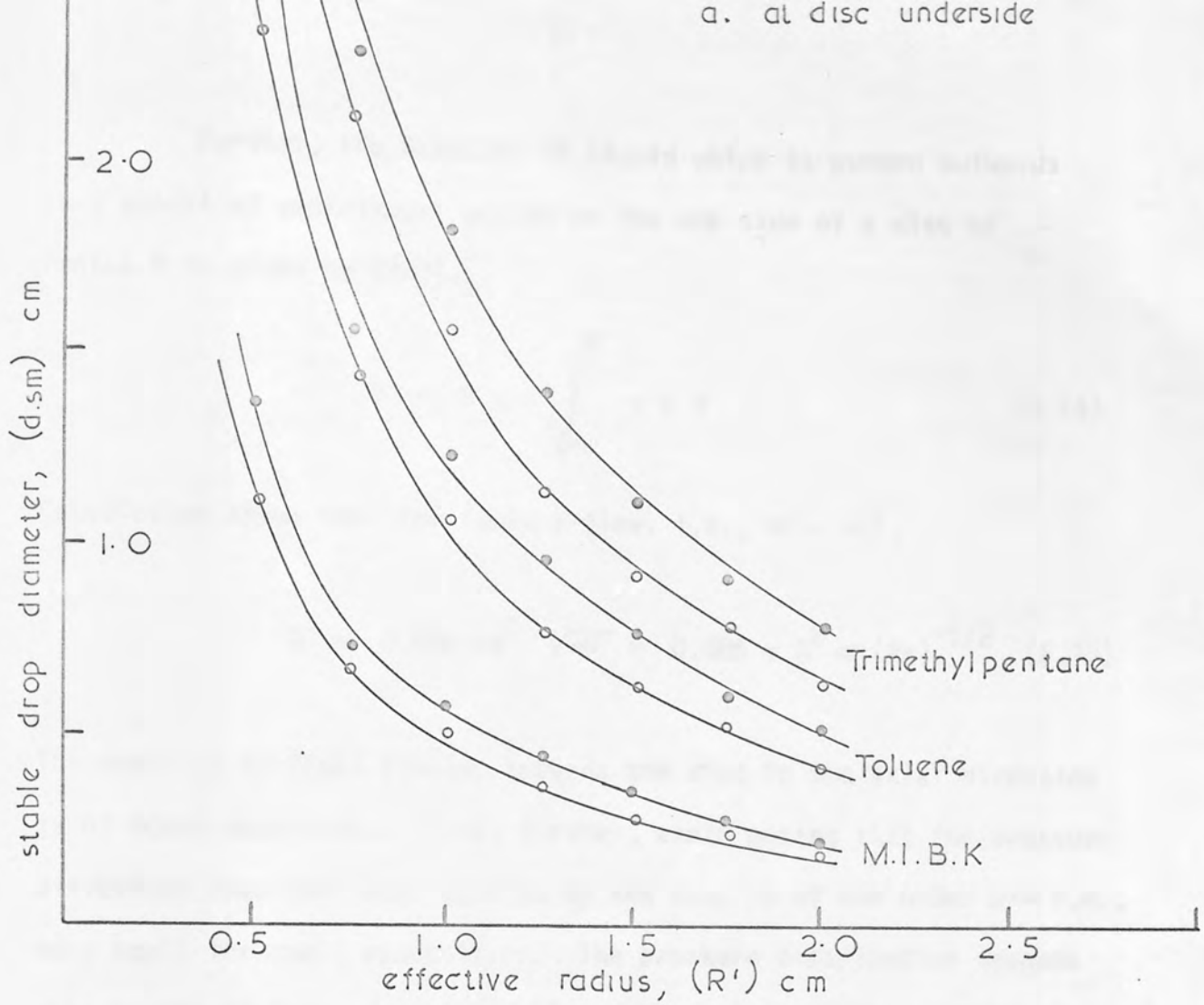

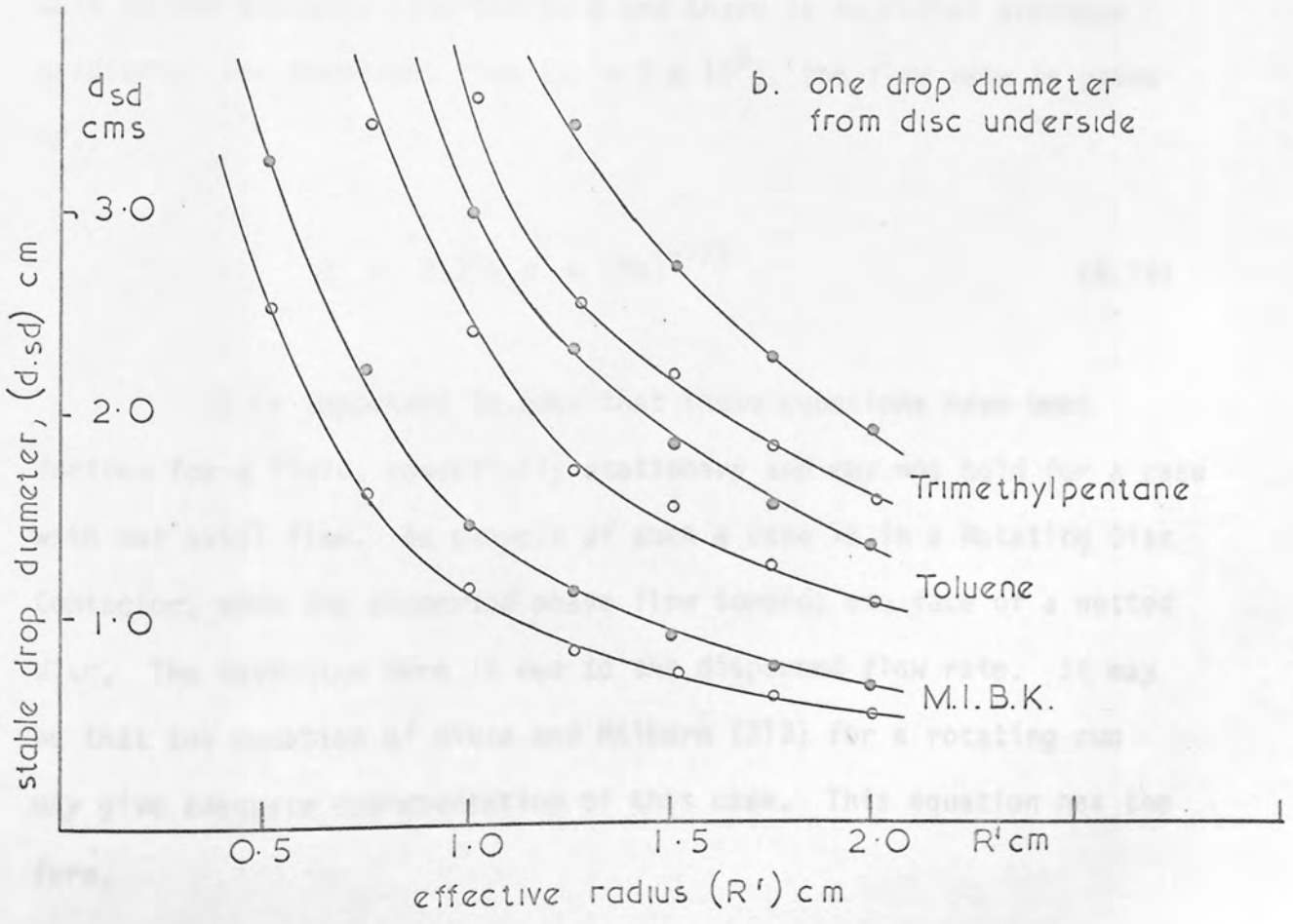

Note :— • 500 r.p.m. ○ 600 r.p.m.

Fig. 6.4. Calculated stable drop diameters (35)

Further, the quantity of liquid which is pumped outwards as a result of centrifugal action on the one side of a disc of radius R is given by (220),

$$Q = 2 \pi R \int_{z=o}^{\infty} u \, d \, z \qquad (6.14)$$

Calculation shows that for laminar flow, i.e., $Re < 10^5$,

$$Q = 0.886 \, \pi R^2 \sqrt{\nu \omega} = 0.886 \, \pi \, R^2 \, \omega \, (Re)^{-1/2} \qquad (6.15)$$

The quantity of fluid flowing towards the disc in the axial direction is of equal magnitude. It is, further, worth noting that the pressure difference over the layer carried by the disc is of the order $\rho \nu \omega$ i.e., very small for small viscosities. The pressure distribution depends only on the distance from the wall and there is no radial pressure gradient. For turbulent flow ($Re > 3 \times 10^5$), the flow rate is given by,

$$Q = 0.219 \, R^3 \, \omega \, (Re)^{-1/5} \qquad (6.16)$$

It is important to note that these equations have been derived for a fluid, essentially stationary and may not hold for a case with net axial flow. An example of such a case is in a Rotating Disc Contactor, when the dispersed phase flow towards one face of a wetted disc. The deviation here is due to the dispersed flow rate. It may be that the equation of Hinze and Milborn (213) for a rotating cup may give adequate representation of this case. This equation has the form,

$$U_m = \left[\frac{2Q^2 n^2 \sin\theta}{3 d \nu}\right]^{1/3} \qquad (6.17)$$

where θ is the half angle of divergence of the cup. For the disc this may be taken as the half angle of the direction of the issuing sheet caused by the countercurrent flow of the continuous phase. U_m is the mean radial velocity, n the rotational speed, d the diameter of the disc and ν the kinematic viscosity.

7. DESIGN OF EXPERIMENTS

7.1 PURPOSE OF INVESTIGATION

On the basis of the literature reviewed in Chapter 5, the behaviour of an R.D.C. in which the discs were wetted by the dispersed phase appeared to be of practical significance. For example it has been suggested (35) that the creation of a new surface in the layer of the dispersed phase wetting the underside of the disc may result in a significant contribution to mass transfer, particularly for those systems in which the dispersed phase mass transfer coefficient is controlling. This study set out to investigate the magnitude of this phenomena together with its effect on hydrodynamics in a pilot scale R.D.C. Furthermore, it appeared that mass transfer models based on the concept of single discrete mean droplets did not adequately represent the operation of agitated contactors, where a coalescence-redispersion mechanism prevails, and may predominate. An attempt has, therefore, been made to develop a more reliable model, by considering this mechanism and the life history of the drop in the contactor.

7.2 MATERIALS OF CONSTRUCTION

Three main materials of construction were employed, viz.,

(1) Glass, for the column sections, pipe connections and storage vessels.

(2) Stainless steel, for stators, discs, rotor shaft, column end plates, pipe connections, sampling rings and pumps.

(3) Polytetrafluoroethylene, (Teflon), for pipe connections, gaskets and alternative discs.

P.t.f.e. was used for the dispersed phase wetted discs, and stainless steel for the non-wetted ones. The liquids used as the dispersed phase were of low surface tension, i.e., < 35 dyne/cm and thus exhibited small contact angles and wetted the low surface energy, p.t.f.e. With stainless steel, a high surface energy material, the dispersed liquids exhibited large contact angles, i.e., a case of non-wetting. Water, with a surface tension of 72 dyne/cm., was used as the continuous phase throughout, this wetted the stainless steel but not p.t.f.e.

Other Materials Used

(i) Brass valves were used in the sampling point arrangements along the column. Valves in the transfer lines were of the Q.V.F. type, constructed of glass and p.t.f.e.

(ii) Polypropylene was used for the cones. This is wetted by organic liquids and was used for the same reason as p.t.f.e.

7.3 SELECTION OF LIQUID-LIQUID SYSTEMS

The range of liquid-liquid systems employed is summarised in Table (7.1).

Their selection was based, in general, on the following considerations.

a. Availability at low cost to a fixed specification;

b. Low or no known toxicity (222).

c. Some results of other workers were available for comparison (35,71,72).

d. To cover a reasonably wide range of physical properties.

The choice of systems 8 and 9 was dictated by the simplicity of the single disc experiment design, as discussed in para. 7.4.2. Both solvents were heavier than water and could be introduced, by means of a simple burette arrangement, to impinge onto the upper side of the disc; simpler lighting and camera arrangements were necessary to photograph this side.

Further both liquids are in common use and are readily available . For system 10 the requirement was for a drop with a density approximately equal to that of water. The reason for this is given in para. 10.3. The physical properties of the liquids used are given in Appendix 2.

TABLE 7.1

	System			
1.	Toluene-Water	4" Pilot Plant R.D.C.	Hydro-dynamics	Wetted and non-wetted discs
2.	Liquid Paraffin-Water	"	"	"
3.	Toluene-(60% Glycerine)Water	"	"	"
4.	(25% Toluene)Liquid Paraffin-Water	"	"	"
5.	(37% Toluene)Liquid Paraffin-Water	"	"	"
6.	Toluene-Acetone-Water	"	Hydro-dynamics and Mass Transfer	" and Cones
7.	Liquid Paraffin-M.E.K.-Water	"	"	W. and N.W. discsonly
8.	CCl_4-Water	12"(Single disc)column	Break-up Mech-anism	W. and N.W. discs
9.	Di n-Butyl Phthalate-Water	"	"	"
10.	Di n-Butyl Phthalate-M.E.K.-Water	4" Q.V.F. Section	Single drops Mass transfer	

7.4 DESIGN AND DESCRIPTION OF EQUIPMENT

7.4.1 4 inch R.D.C. Column

The major part of this work was performed in a 4 inch diameter pilot scale R.D.C. The column consisted of 19 compartments each 2 inches high. The diameter of the discs was 2 inches and that of the stator openings was 3 inches. These dimensions were determined from the design specifications recommended by (70,71,72,73,74,75), and discussed earlier in para.3. For design purposes a phase ratio of 0.5-4.0 to 1, was assumed. Five sampling points were provided at 9 inch intervals along the column; additional sampling points were provided at each of the respective inlets and outlets of the two phases. The stator rings were of stainless steel, and were precision machined to obtain a close fit at the column walls, since the uncharacteristic performance of many laboratory columns may be attributable to phase flows between the column wall and the edge of the stator rings (35). The stators were supported by means of 3 equi-spaced pieces of $^{1}/_{24}$ inch stainless steel wire; this was found to be rigid enough to support the stators, without introducing extraneous baffling effects. The thickness of discs and stators was $^{1}/_{16}$ inch. The discs were fabricated from stainless steel or alternatively from p.t.f.e. In either case the discs were supported by means of a grub screw through the collar of the disc; this was countersunk into the collar so as to eliminate any effect on the pattern of agitation.

In any event, the neighbourhood of the collar is effectively a dead zone and disturbances caused by protruding screws may be very small (35). The discs had straight edges, since discs with sharp or

tapered peripheries would have increased the axial mixing effects (223). The rotor shaft, was supported by bearings at four points in the column, and was fabricated from a $^{3}/_{8}$ inches stainless steel rod.

The heavy phase, which was also the continuous phase in this case, was introduced into the column at a point just above the top compartment, and left via a bottom outlet. The dispersed phase entered the column via a brass or stainless steel distributor plate, and left via a pipe above the coalescence zone, at the top of the column.

Initial dispersion of the lighter phase by the distributor plate was designed to reduce the total hold-up of the dispersed phase in the equipment and to facilitate a rapid approach to equilibrium hydrodynamic conditions in the contactor by simulating the initial break-up stages which would otherwise occupy useful column height.

The disperser was designed to the recommendations of Treybal (1), and comprised $^{1}/_{16}$th inch holes arranged on $^{3}/_{16}$th inch triangular pitch inside a 4 inch diameter circle. The holes were drilled undersize ($^{3}/_{64}$th inch) and then counterpunched to the correct size. This provided a small upward projection around the periphery of each hole and hence more uniform droplets. The disperser was located within a 6 inch to 4 inch Q.V.F. glass pipe reducer to minimise the effects of continuous phase flow on droplet formation. The distributor plate was located 4 inches below the mixing section so that initial droplet formation was substantially unaffected by agitation.

The rotors were driven by a $^{1}/_{4}$ H.P. (0-3000 r.p.m.) A.C. Voss motor. The drive shaft of the motor was coupled to the column

shaft via a flexible rubber joint. The other end was attached via a flexible drive to a permanent 0-3000 r.p.m. tachometer mounted on the control panel. The agitator speed was controlled by means of a Cressall voltage regulator.

Four 50 litres Q.V.F. glass spherical vessels, were used as storage reservoirs and were mounted on a special vessel support. Transfer of the liquids was by means of two Stuart-Turner centrifugal pumps, type No.10 and No.12 capable of handling, 120-140 and 720-150 g.p.h. against 5-20 and 10-45 ft head of water respectively. The pumps were of stainless steel and the pump glands were specially adapted for use with solvents. The speed of each pump was controlled by a Cressall voltage regulator.

Flowrates were measured by independently calibrated rotameters with stainless steel floats. Different sizes of rotameter, viz., 14, 18 and 24, were used dependent upon the flowrates to be measured and the physical properties of the liquids.

$^{5}/_{8}$ inch Q.V.F. stopcocks were used as valves for all applications excepting fine control of flowrates. For this purpose $^{5}/_{8}$ inch Q.V.F. needle valves were installed. 3-way Q.V.F. stopcocks were used at different points in the plant, particularly at the outlets of the vessels, to facilitate drainage. Another drainage point was situated at the bottom of the column.

The liquids could be circulated within one vessel or between two vessels containing the same liquid by by-passes on the pumps. This was found useful when making-up the feed, i.e., when admixing solute in the raffinate phase.

To overcome difficulties in sealing off the agitator stuffing box, the dispersed phase was drawn out at a point just above the coalescence zone thus leaving a "dead space". The dispersed phase

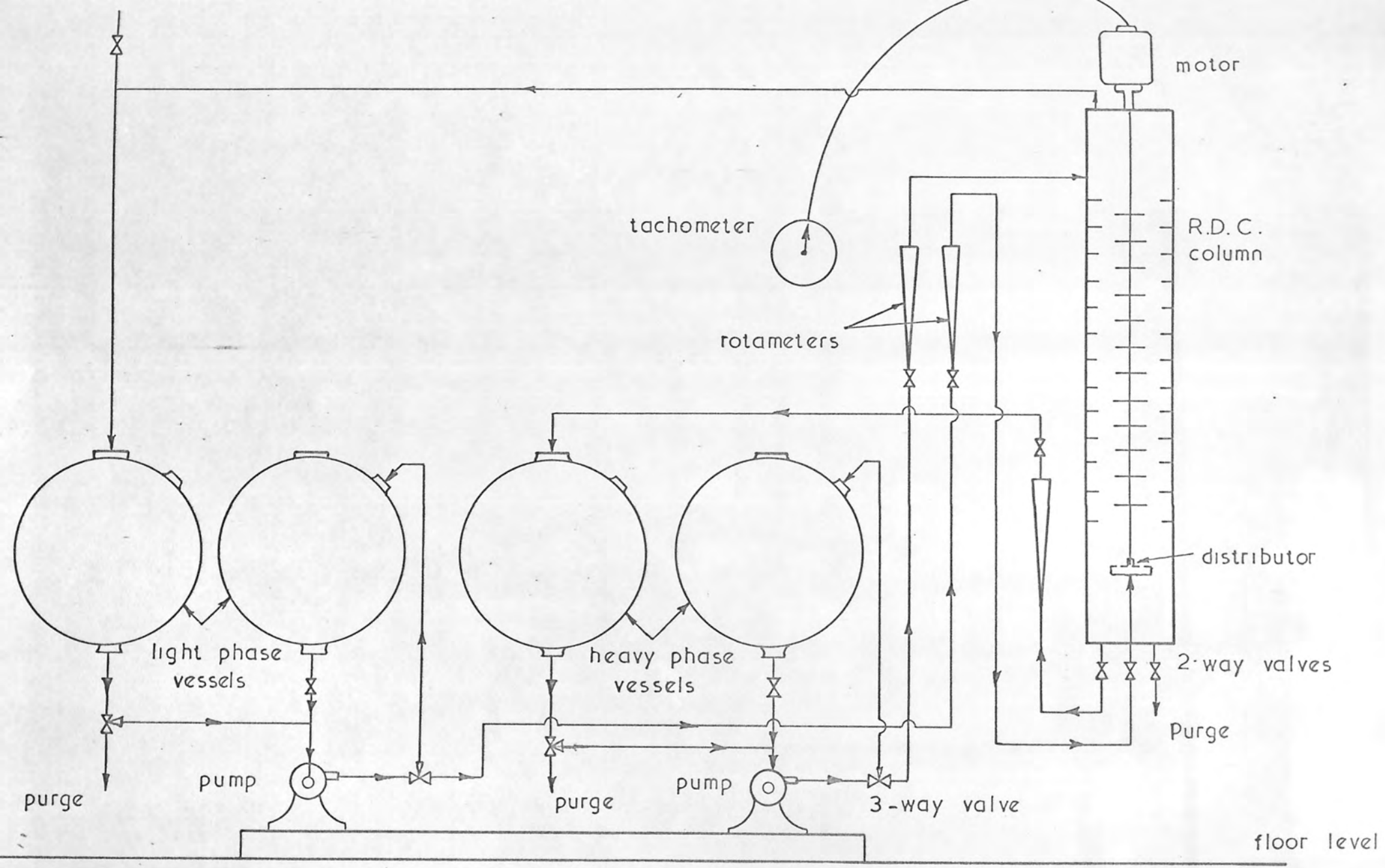

Fig. 7.1. Flow diagram

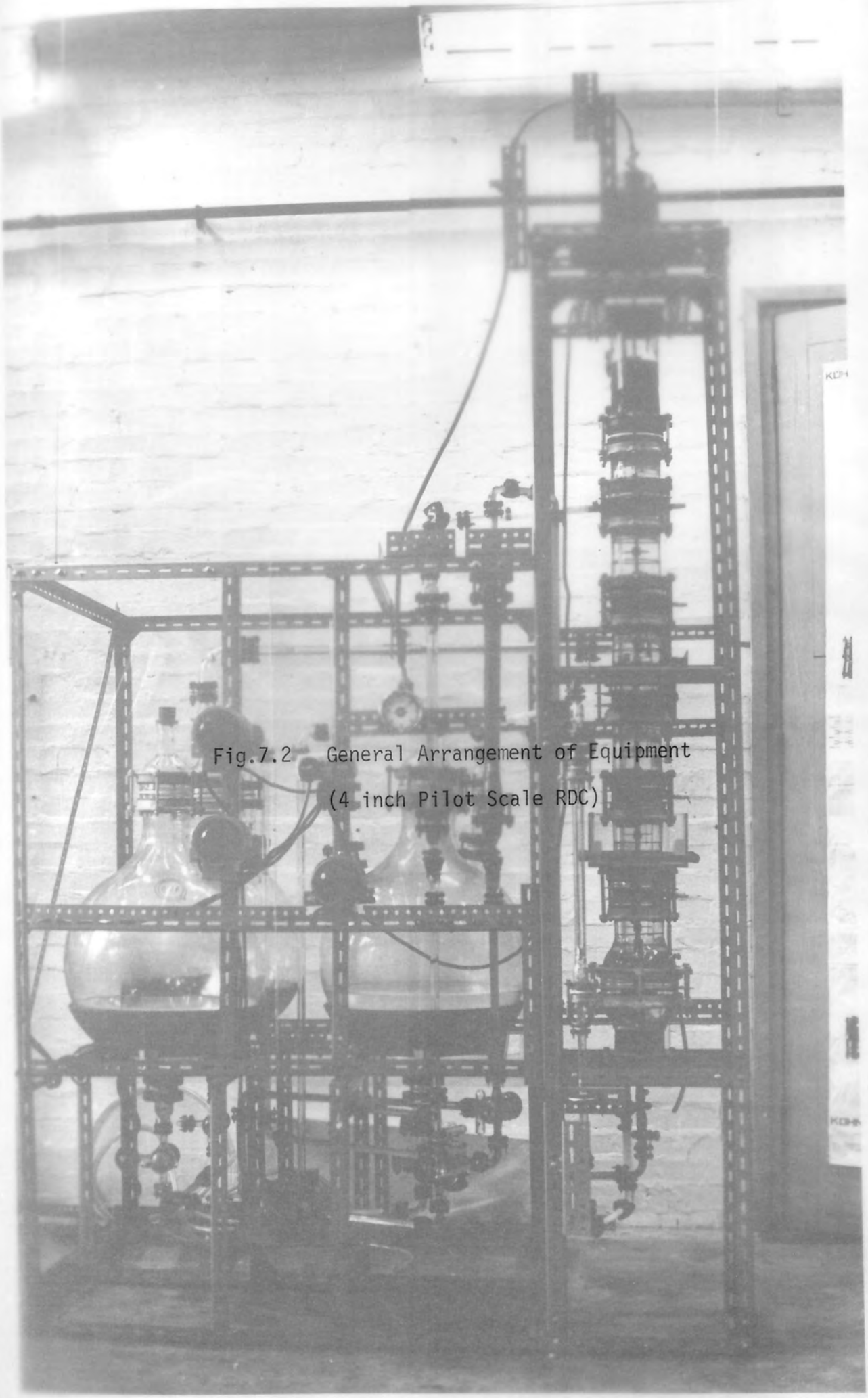

Fig.7.2 General Arrangement of Equipment

(4 inch Pilot Scale RDC)

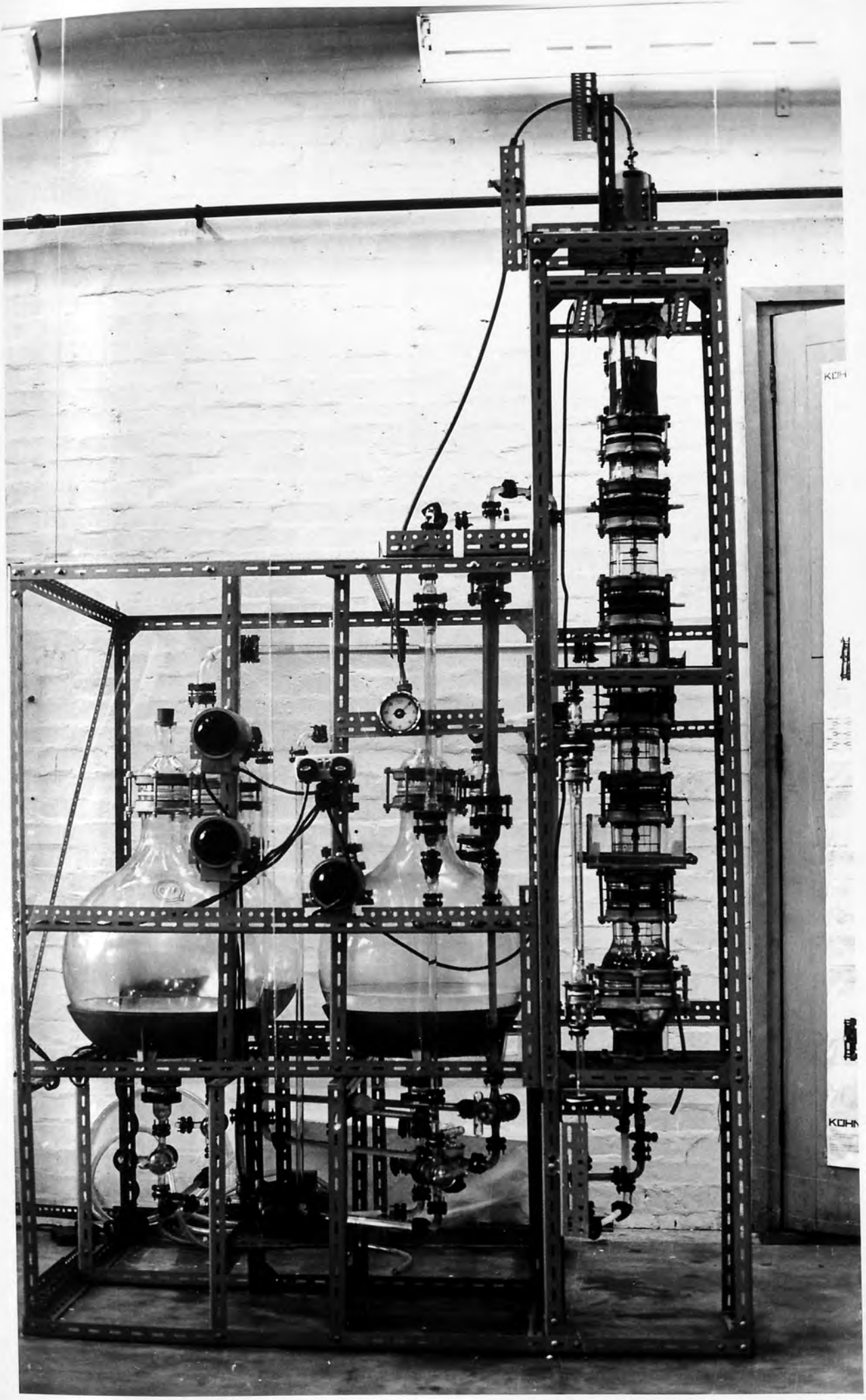

outlet was 1.0 inch in diameter to avoid any restriction upon the liquid.

Adjustment of the liquid-liquid interface was achieved by means of a valve and a rotameter installed on the dense phase return line. This provided a good control of the interface level.

A flow diagram of the equipment is shown in Fig.7.1, and the general arrangement in Fig.7.2.

A section of the column is illustrated in Fig.7.3 and the column details shown in Fig.7.4.

The column was constructed from 4 inch Q.V.F. glass pipe sections. This diameter was selected since smaller sizes may introduce excessive wall effects. However in an earlier study (35) a 3.0 inch diameter column was considered to have only slight wall effects, albeit in the absence of mass transfer. Clearly a column of greater diameter would have required larger storage vessels and more space, and involved higher costs. The contactor section consisted of four 8.0 inch long, 4.0 inch nominal diameter Q.V.F. glass sections. A 1.0 inch stainless steel ring was inserted between each section, through which, sampling tubes were introduced. Each ring provided independent support for the set of stator rings in the section below. Two of these rings were also steady bearings for the shaft. The arrangement of stators and the sampling tube connections to the ring is shown in Fig.7.5. The lower part of the column contained the disperser, which comprised two 6 to 4 inch pipe reducers each 8 inch long. The coalescence section consisted of a 12 inch long glass section followed by a $1\frac{1}{2}$ inch stainless steel section incorporated the dispersed phase outlet. Finally above this was a 6 inch long

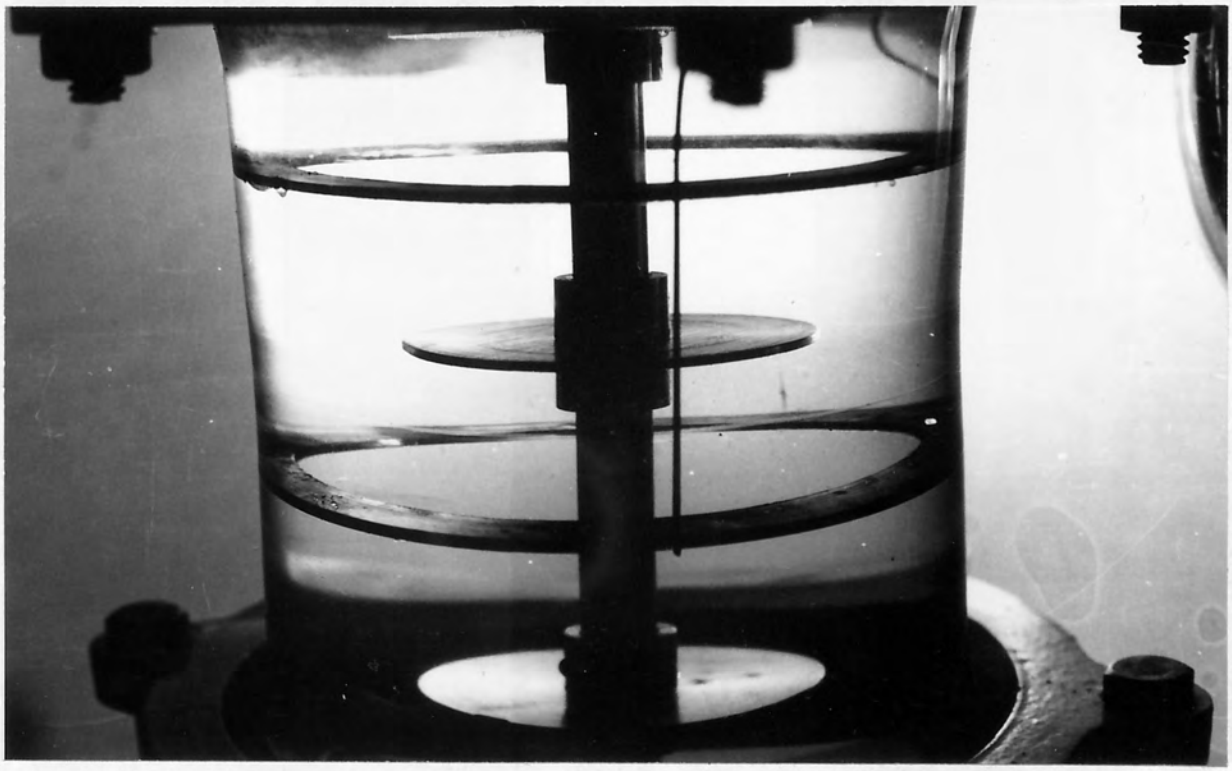

Fig.7.3 Illustration of RDC Column Section

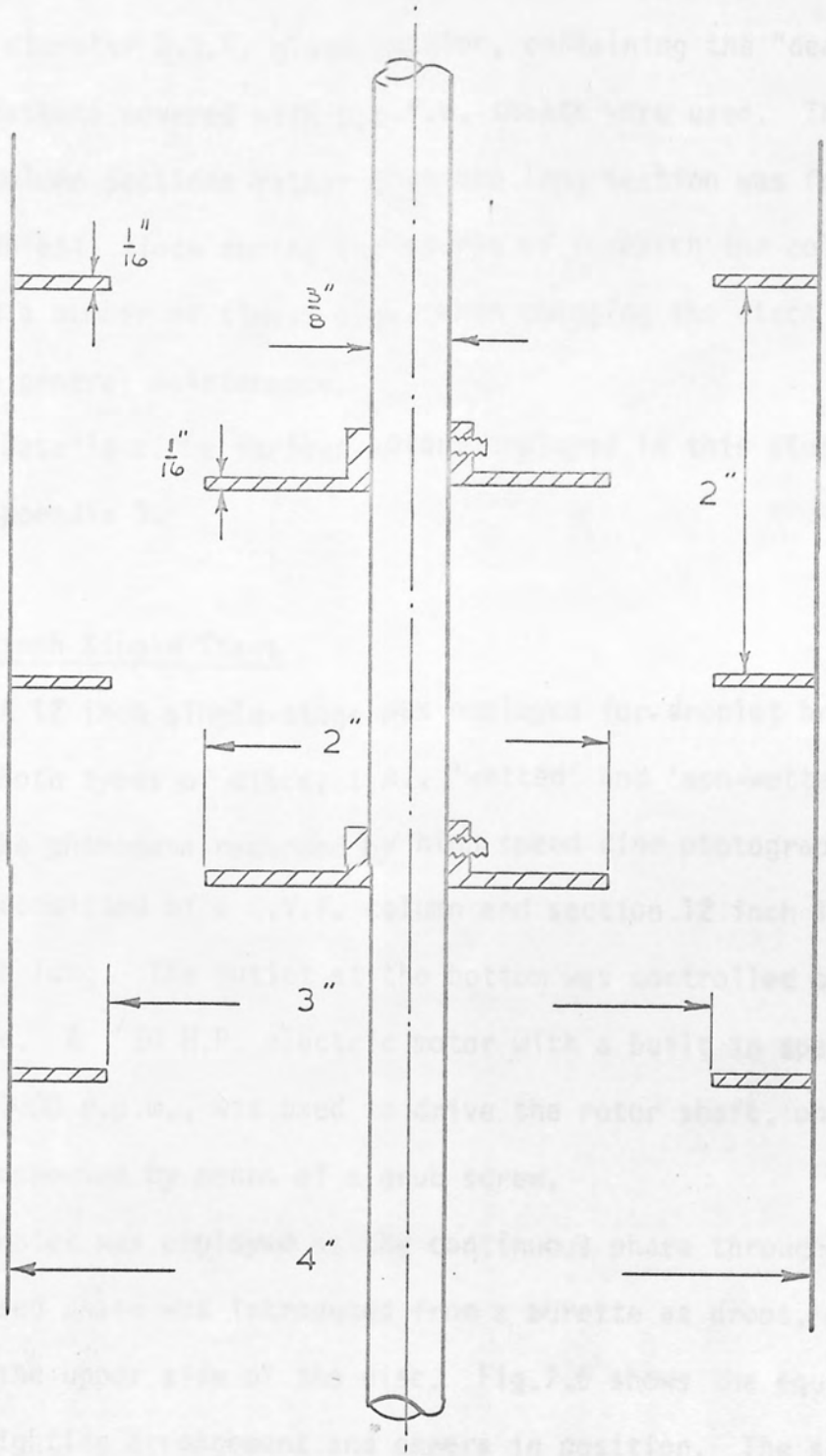

Fig. 7.4 Schematic diagram of a column section

4 inch in diameter Q.V.F. glass section, containing the "dead space". Asbestos gaskets covered with p.t.f.e. sheeth were used. The use of separate column sections rather than one long section was found to be very convenient, since during the course of research the column was dismantled a number of times, e.g., when changing the discs or when performing general maintenance.

Details of the various rotors employed in this study are given in Appendix 3.

7.4.2 12 inch Single Stage

A 12 inch single-stage was employed for droplet break-up studies. Both types of discs, i.e., 'wetted' and 'non-wetted' were used and the phenomena recorded by high speed cine photography. The equipment consisted of a Q.V.F. column end section 12 inch in diameter and 12 inch long. The outlet at the bottom was controlled by a glass drain valve. A $^{1}/_{20}$ H.P. electric motor with a built in speed control, from 0 to 3000 r.p.m., was used to drive the rotor shaft, on which the disc was supported by means of a grub screw.

Water was employed as the continuous phase throughout and the dispersed phase was introduced from a burette as drops, so as to fall onto the upper side of the disc. Fig.7.6 shows the equipment with the lighting arrangement and camera in position. The speed of rotation was measured by a stroboscope. It was found necessary to introduce a single baffle in order to eliminate vortex formation. In addition to 5 inch discs, 2 inch discs, i.e., identical in size to those employed in the 4 inch column, were also studied.

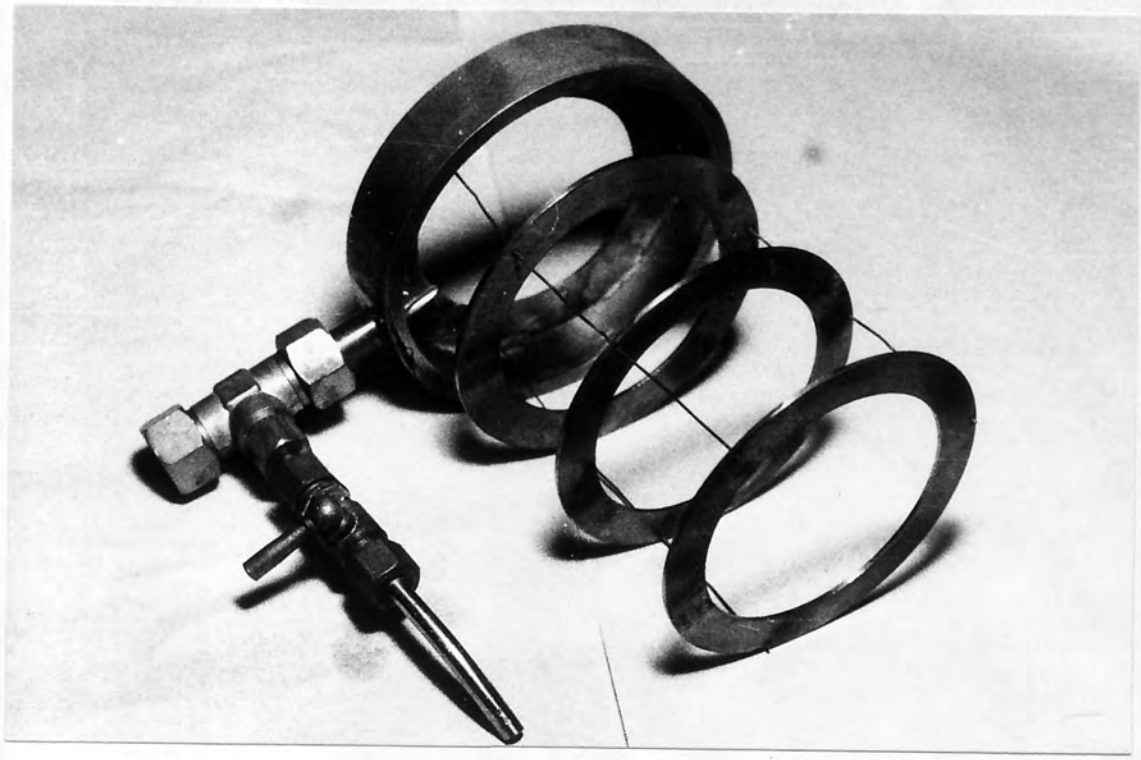

Fig.7.5 Arrangement of Stators and Sampling Point

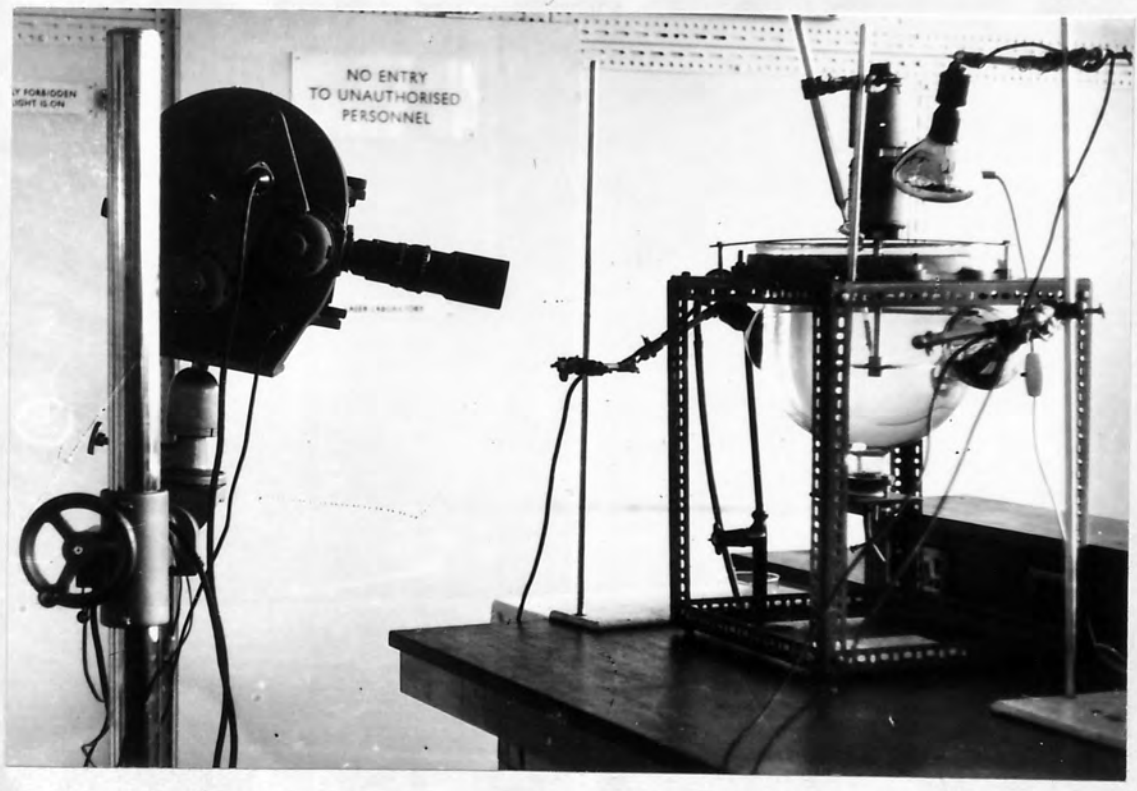

Fig.7.6 12 inch Single Stage Column with Fastax Camera in Position.

7.4.3 4 inch Column Section

The general arrangement of the 4 inch section is as shown in Fig.7.7. It consisted of an 18 inch Q.V.F. glass section, 4 inches in diameter sealed at the bottom by means of a stainless steel plate. The dispersed phase droplets were formed at the nozzle in an aqueous continuous phase.

Only qualitative studies were made. The mechanisms of eruption caused by interfacial turbulence and other droplet behaviour accompanying mass transfer, were recorded by still and ciné photography. A shadowgraphic technique was employed to photograph these phenomena as described in Section 7.6.4.

7.5 EXPERIMENTAL TECHNIQUE

7.5.1 Commissioning Pilot Scale R.D.C.

In commissioning the plant a degree of whip was observed in the rotor shaft, even though the column contained three steady bearings. An additional bearing was therefore installed in the middle section of the column. This was found to have very little effect on the flow regime within the column.

With the dispersion of liquid paraffin in water a lot of axial mixing occurred; this resulted in an appreciable amount of entrainment in the dispersed phase. The use of knitmesh packing, both wetted and non-wetted, to aid coalescence and trap the entrained continuous phase was not successful and resulted in restricting the flow and causing premature flooding in the calming zone. The use of an external settler was found to be more adequate.

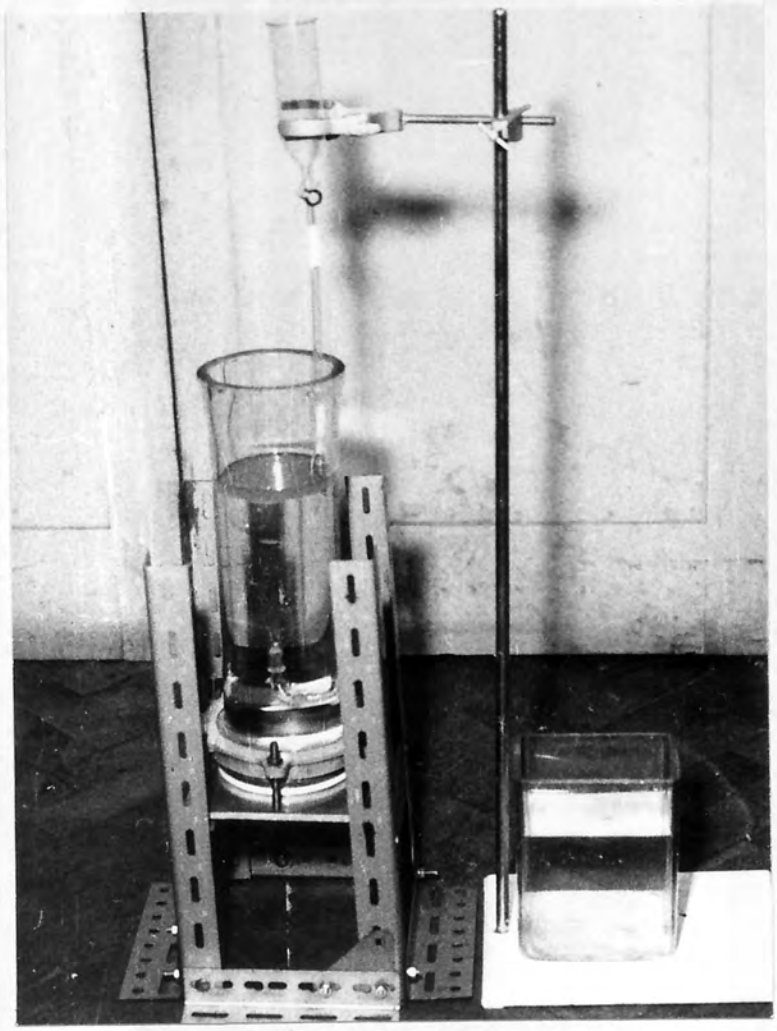

Fig.7.7 4 inch Column Section

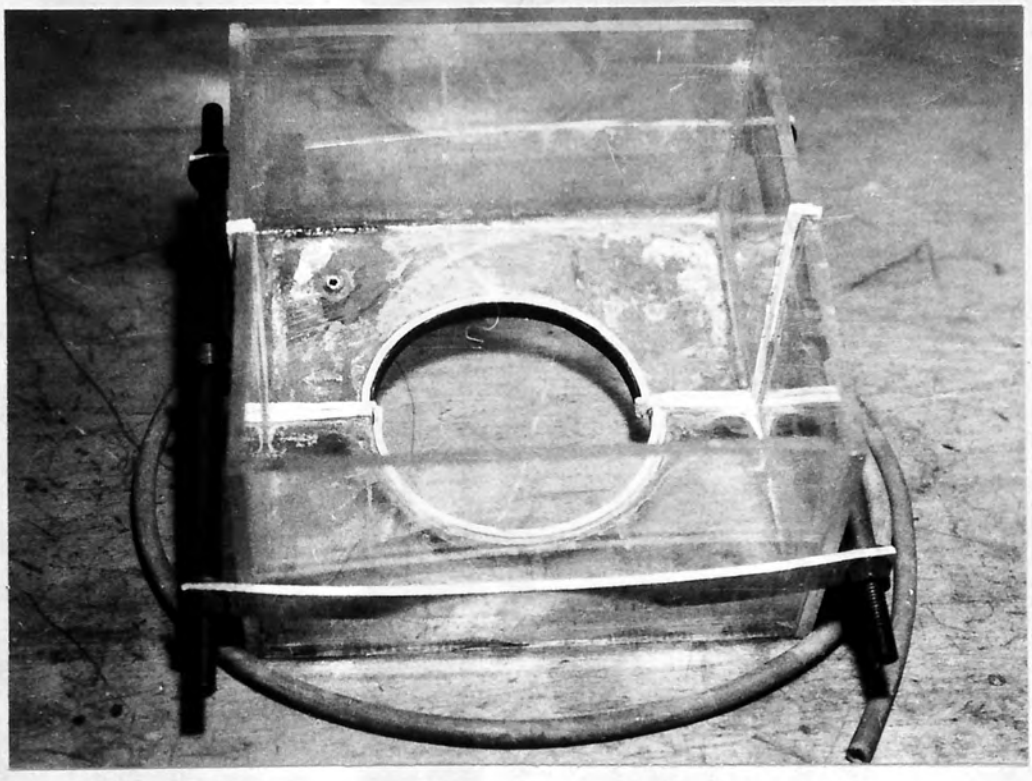

Fig.7.8 Perspex Box Jacket Used To Eliminate Magnification Effects

7.5.2 Cleaning Procedure

An aqueous solution of Decon 90, in the ratio of 1.0-1.5 parts Decon to 10 parts water, was used for cleaning purposes. This was found to be adequate and was safer to use than chromic acid. A similar solution was also used for cleaning sample bottles and measuring cylinders, which were always oven dried before use. Due to the nature of contacting, there was a tendency for dirt and other impurities to be deposited on the column internals in preference to the rest of the equipment. Therefore, close attention was paid to cleaning the column. This was filled with the Decon solution which was allowed to stand for at least 12 hours, followed by agitation for a further $^{1}/_{2}$ to 1 hour. The solution was then circulated through the rest of the system, i.e., pipes and reservoirs, for about $^{1}/_{2}$ hour, and drained away. The whole equipment was then flushed with tap water with the agitation running continuously for 2 to 3 hours. Finally, the equipment was rinsed through with approximately 50 litres of distilled water.

This cleaning procedure was repeated between every series of runs. Before installation of the column and whenever it was subsequently dismantled, e.g., for changing the discs, all internals were cleaned with a solvent, viz. acetone, to remove any grease or oil films resulting from handling.

System Purity Checks

The purity of the system was checked at regular intervals, between each set of runs, by measuring the interfacial tension of the system and the individual surface tensions of the component liquids. Whenever a discrepancy was observed in the values of surface or inter-

facial tension, the liquids were discarded or redistilled.

7.5.3 Measurement of Solute Concentration

Solute concentrations were determined by measurements of the refractive indices. Calibration charts for refractive index vs. solute concentration were prepared by measuring the refractive indicies of solutions made up to known concentrations, and are given in Appendix 4.

Only small quantities of the liquid under test, i.e., 10 mls., were required for this method. Consideration was given to the use of other methods, e.g., titration and conductivity measurement, but these were not applicable to every system. [In the titration method a third component is sometimes added to make the solution titratable. The conductivity method only applies to systems with measureable conductivity changes]. Use was made of an Abbey A60 refractometer, calibrated to five decimal places. This was maintained at a constant temperature of 22.5 ± 0.2 °C by means of a Townson and Mercer temperature control circulating unit.

7.5.4 Determination of Equilibrium Distribution Diagrams

Equilibrium concentrations were determined by making up mixtures on a weight basis, represented by points below the mutual solubility curve (224). The mixtures were contained in stoppered flasks and were then brought to equilibrium by shaking repeatedly and standing for several hours in a thermostat bath at 22.5°C. The layers were then separated, and analysed by the refractive index method.

The equilibrium diagrams for the ternary systems used, viz., toluene-acetone-water and liquid paraffin-M.E.K.-water, are given in Appendix 4.

7.5.5 Miscellaneous Techniques

It was necessary to determine the viscosity and the interfacial tension with water of the solvents employed. Approximate methods of estimating these values from linear weight or volume ratio relationships were found to be invalid for mixtures as shown later in Appendix 4. Nevertheless such methods of approximation have been used elsewhere (123). Cannon-Fensky viscometers and a Cambridge Du Noüy tensiometer were used.

For non-mass transfer runs the system was allowed to reach saturation before any measurements were carried out. This was achieved by recycling both liquids through the column for at least one hour.

7.6 PHOTOGRAPHY AND ASSOCIATED TECHNIQUES

7.6.1 Still Photography

Two different cameras, a Miranda Sensorex and a Pentax Asahi, were employed for still photography. Various extension tubes and telephoto lenses were used dependent upon the nature and position of the object photographed. As later illustrations indicate, both cameras produced photographs of very good quality. In most cases lighting was provided by a single 500 watt photoflood lamp placed directly behind the object. Tracing paper was placed between the lamp and object in order to diffuse and homogenise the light.

Kodak Tri-X, 400 A.S.A. film was used in most cases. Occasionally where a higher definition of the object was required, films of lower speeds, i.e., 125 or 32 A.S.A. were used. The latter types of film required more lighting and thus was provided by an additional one or two 500 watt lamps placed behind the tracing paper.

Aperture opening, shutter speed and focal length were adjusted according to the amount of light provided, the speed of the object and the distance between object and camera. In general a shutter speed of $^{1}/_{1000}$th of a second and f numbers = 5.6, 8 and 11 were found to give best results.

Two to three photographs were taken of each event.

7.6.2 Ciné Photography

Three different ciné cameras were used to the speed range required.

(i) Low (normal) speed, 0-64 f.p.s. At 64 f.p.s. a BeaulieuR16 was used, with various extension tubes and a P3 type, f 0.75 lens.

(ii) Moderate speed, up to 500 f.p.s. - A Milliken DBM-3 camera fitted with the required extension tubes and lenses was used at 70, 100 and 500 f.p.s. The required speed was selected before use and subsequently checked from a spark trace on the edge of the film.

(iii) High Speed, 500-6000 f.p.s. - A Wollensak Fastax type WF 14T camera, was used for ciné photography at 800 and 1000 f.p.s. The camera was fitted with a Fastax-Raptar 50 mm or 152 mm., f2 lens and extension tubes, as required. The speed of the camera was adjusted by means of varying the applied voltage and again checked from a recording on the edge of the film in the form of a spark trace.

In all cases lighting was provided by three 500 watt photo flood lamps placed behind and to the side of the object. Tracing Paper was used to provide light diffusion, and the best position of the camera corresponding to a point of maximum reflective glare and maximum clarity and contrast of the object, was obtained by trial and error.

7.6.3 Elimination of Distortion and Magnification

To obtain meaningful photographs, it was necessary to eliminate distortion and magnification caused by viewing through the curvature of the glass column. For a 3 inch glass column it has been shown that distortion is insignificant excepting for the outer $^1/_8$ inch of the column (35). However, improperly blown glass during fabrication, has points of defect which cause distortion.

It has been suggested that errors due to magnification in a 3 inch diameter glass column would be negligible with an aqueous continuous phase (35,39). This is true provided that the area, photographed, is small compared to the column curvature and the object is very close to the column wall. The magnitude of magnification varies with the distance from the column wall, away from the viewing point.

In this study the problem of distortion and magnification was overcome, by erecting a perspex box jacket around the column section to be photographed, as shown in Fig.7.8. This was in two halves which were pressed against the column and together by means of a clamp. Rubber strips were glued along the edges to prevent leakage. Allowance for drainage was made, as shown in the diagram. The box was filled with a liquid identical with the continuous phase in the column.

7.6.4 Schlieren Technique

In recent years various flow visualization techniques have been used in the qualitative investigation of interfacial convection. One such technique is the Schlieren system shown in Fig.7.9a. It consists of a monochromatic light source (S) focused by a condenser lens (L_1) on a pinhole or slit (P) which then serves as a point or line source of light. A parallel beam of light is subsequently produced by the use of a collimating lens (L_2) focused on a knife edge (K) by a Schlieren lens (L_3) and the image projected onto a screen (I). The use of the knife edge is to cut off unwanted deflected light rays that may be caused by optical inhomogeneity between L_1 and L_2.

Due to the low light intensity of the image produced, which caused difficulty in photography, a modified system was used in this study. As shown in Fig.7.9b, this consisted of a mercury arc as the light source (S) focused by a 16mm microscope objective lens (L_1) (225) on a pinhole (P). A second 16mm microscope objective lens (L_2) was used to colimate the beam which is then passed through the column. Tracing paper was placed on the far side of the column wall and the shadow of the image, rather than the image itself, projected onto it. The shadow was photographically recorded with the camera directly facing the light source as shown in Fig.7.9b. so as to make use of the maximum light intensity.

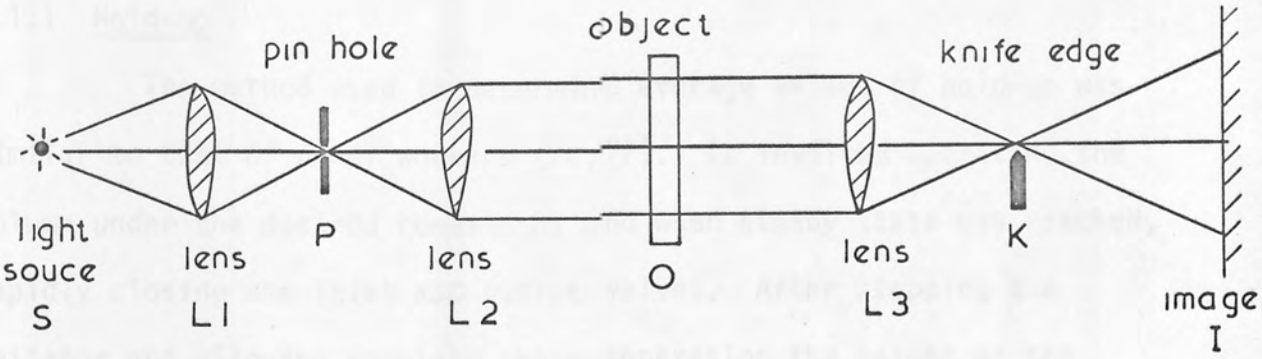

Fig. 7.9.a. Diagrammatic representation of the Schlieren system

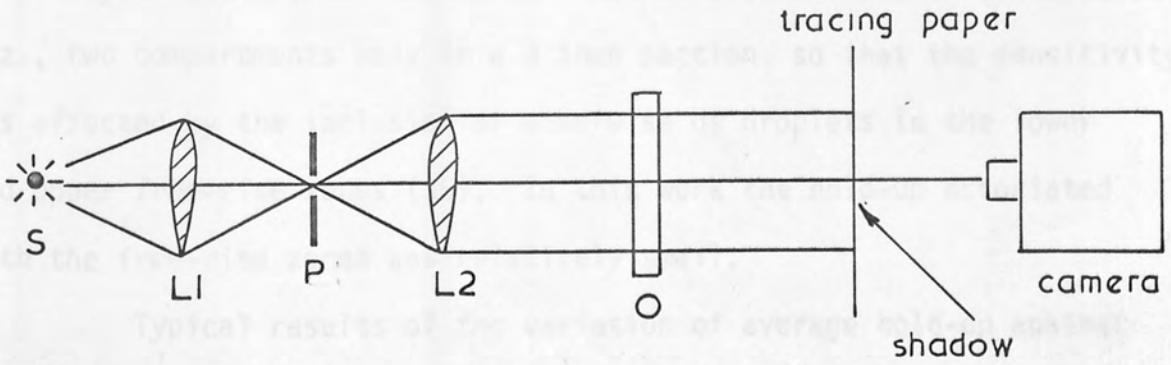

Fig. 7.9.b. Actual optical system used.

8. EXPERIMENTAL PROCEDURES AND RESULTS

8.1 NON-MASS TRANSFER STUDIES

8.1.1 Hold-up

The method used to determine average values of hold-up was similar to that of other workers (72,77). It involved operating the column under the desired conditions and when steady state was reached, rapidly closing the inlet and outlet valves. After stopping the agitator and allowing complete phase separation the height of the dispersed phase below a previously marked interface, and the overall operating height of the column, were measured by reference to a fixed graticule.

This method was found to be satisfactory, although in an earlier work (35) it was reported to give poor accuracy and reproducibility. However, the latter work was done in a small column section, viz., two compartments only in a 3 inch section, so that the sensitivity was affected by the inclusion or otherwise of droplets in the lower and upper free-rise zones (35). In this work the hold-up associated with the free-rise zones was relatively small.

Typical results of the variation of average hold-up against dispersed phase flow rates at various rotor speeds, are reproduced in Figs.8.1, 8.2 and 8.3.

To determine the variation of hold-up along the column axis, point hold-up measurements were made, using a sampling tube positioned as recommended (71) at a point midway between the rotor and upper stator and between S/2 and R/2 from the centre. Apart from the results

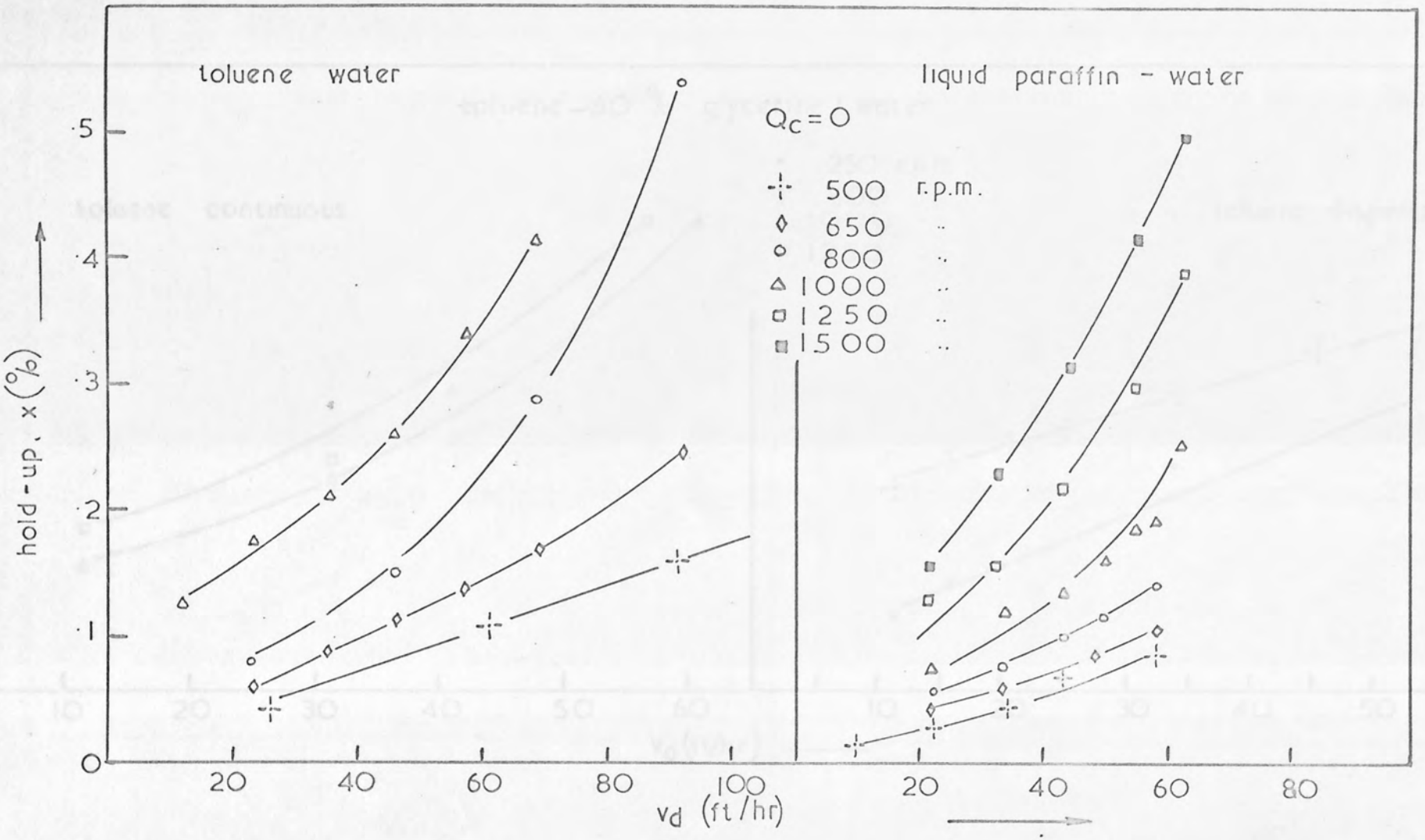

Fig. 8.1. Hold-up vs. dispersed phase flow rate in an rdc with stainless steel discs

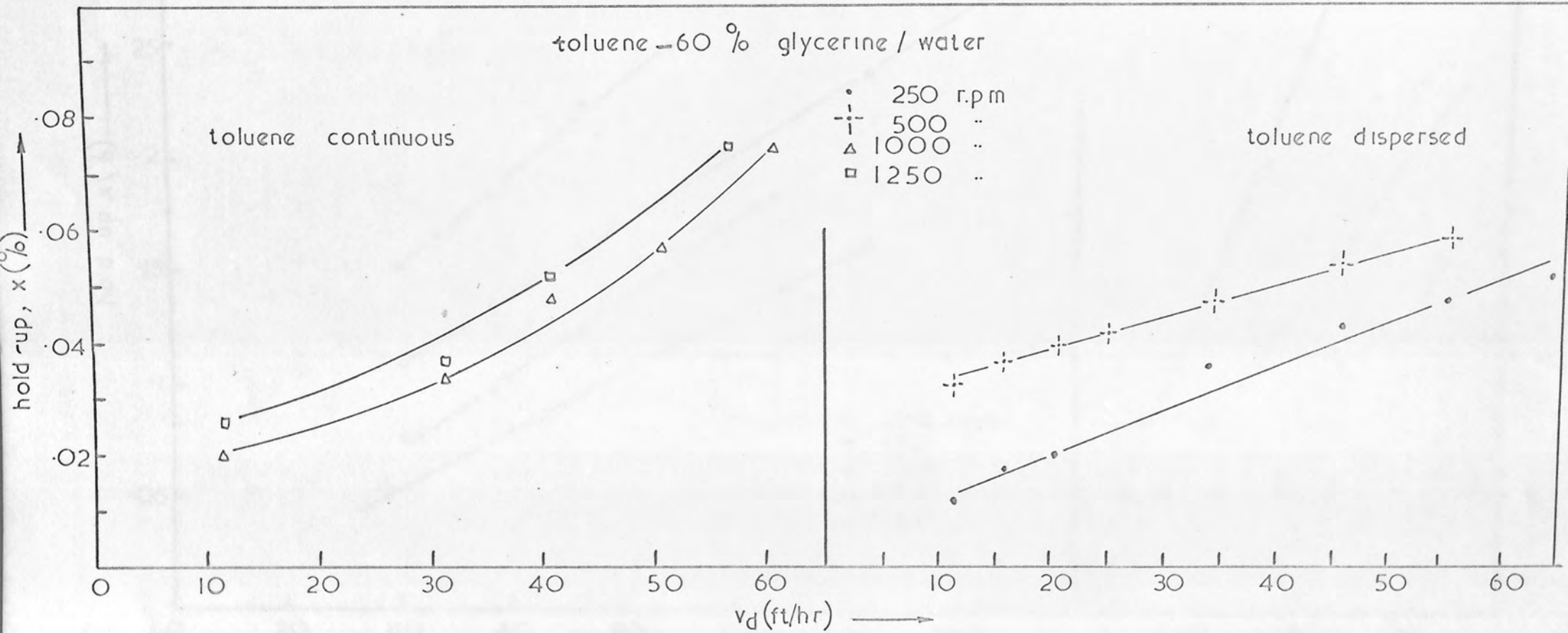

Fig. 8.1 Continued.

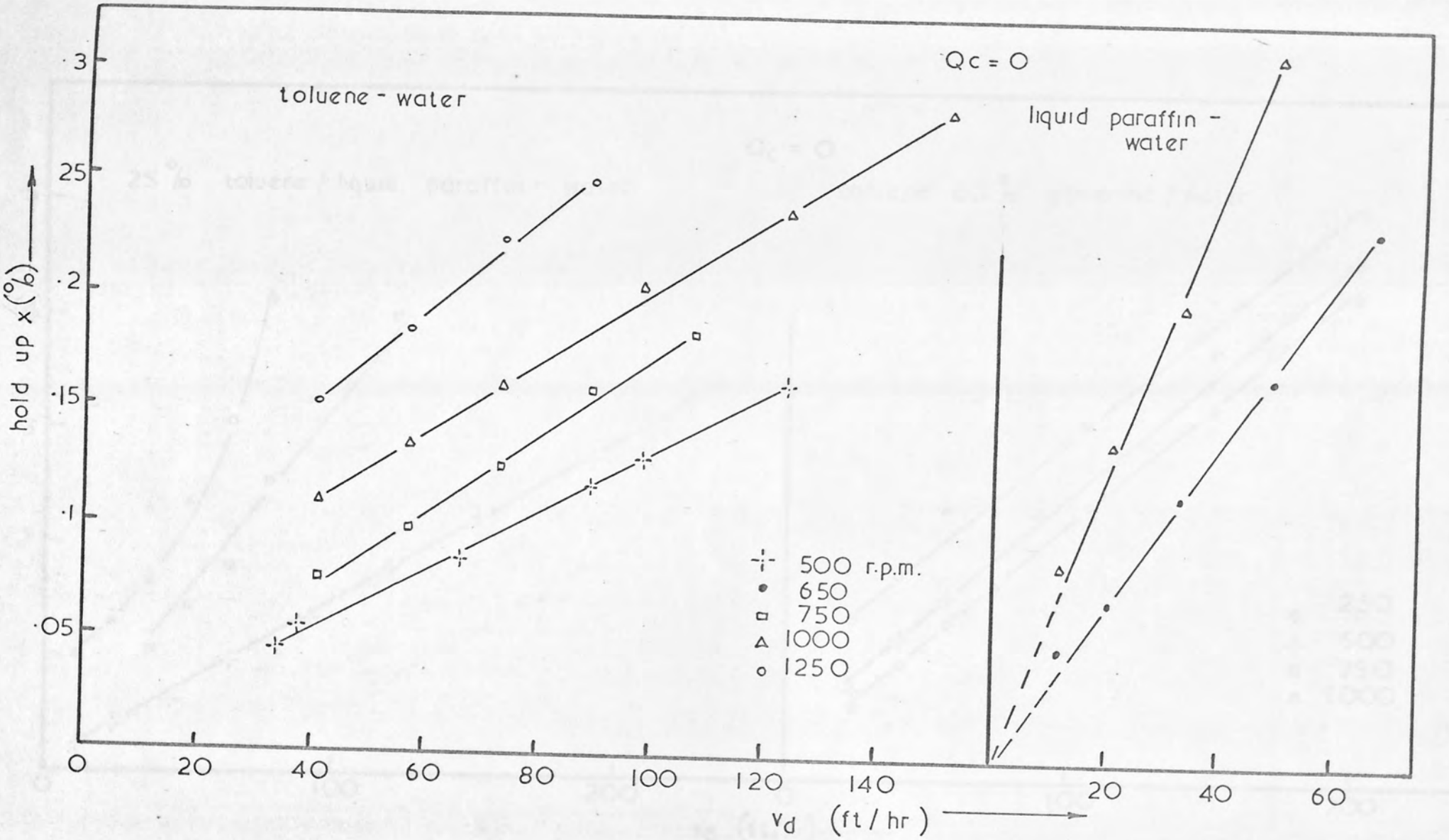

Fig . 8.2 Hold - up vs dispersed phase flow rate for a wetted disc column

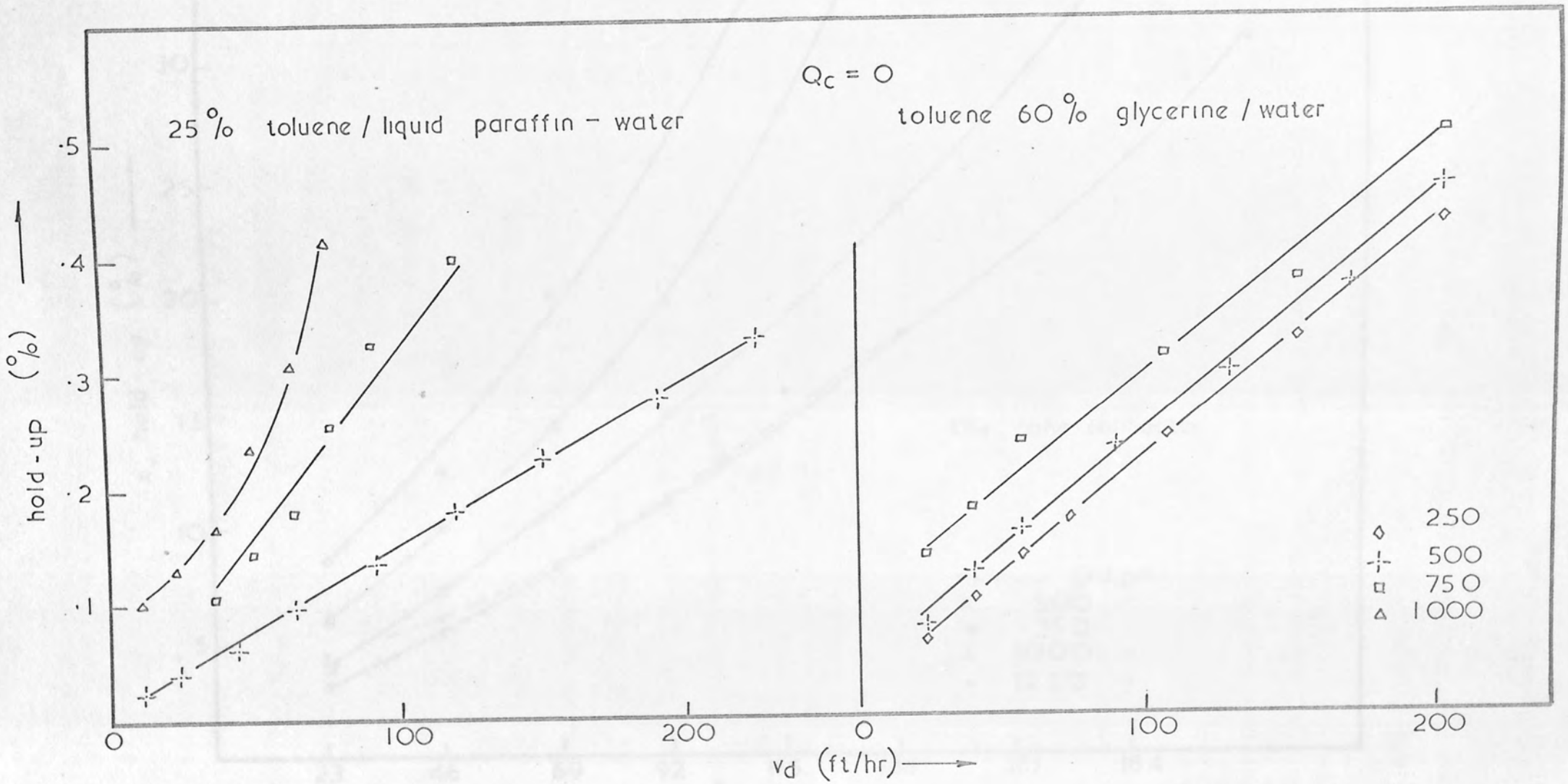

Fig. 8. 2. Continued

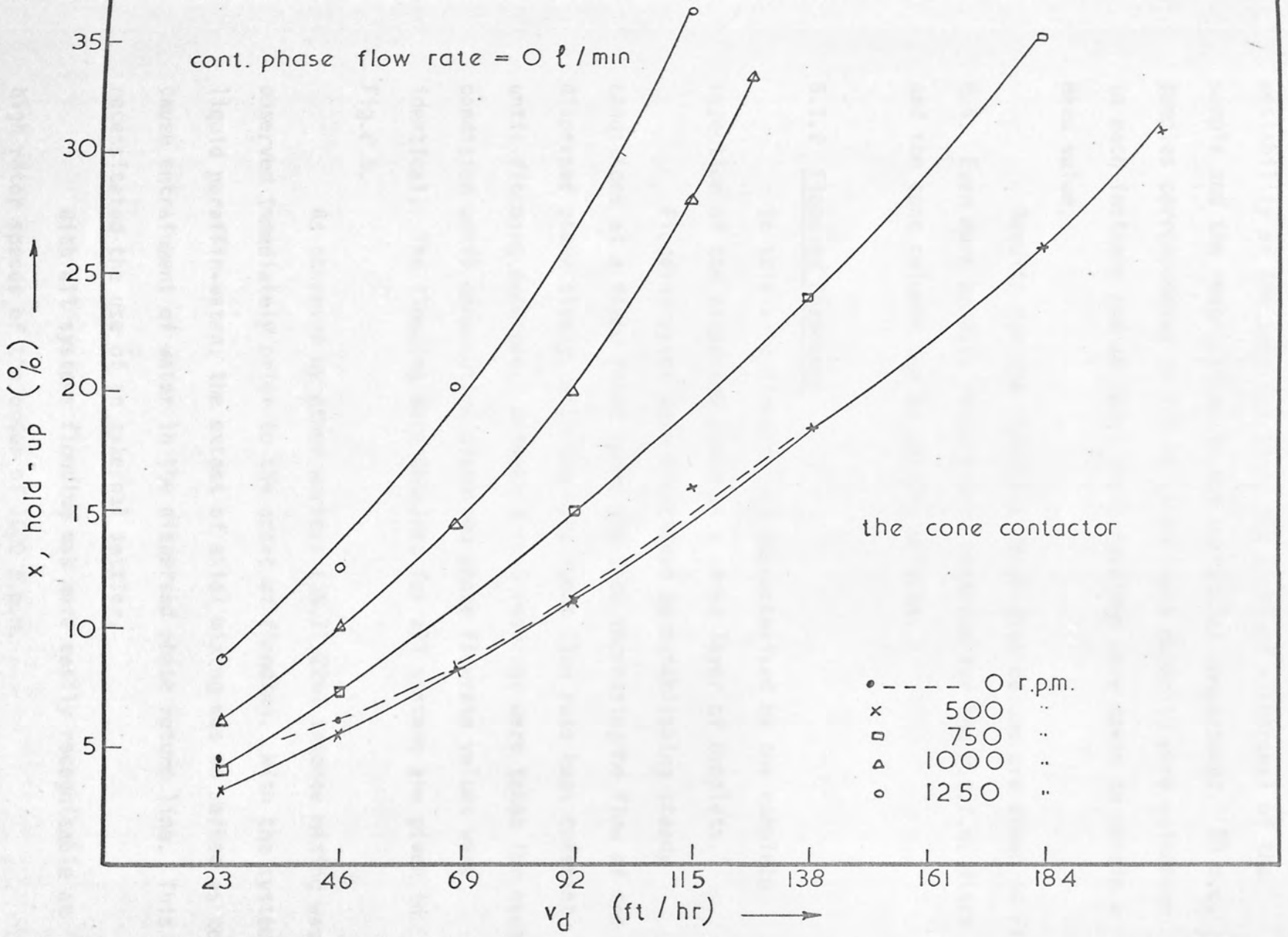

Fig. 8.3. Hold - up vs dispersed phase flow rate

obtained for the system liquid paraffin-(dispersed)-water, the results were rather inconsistent. They were dependent upon the size and wettability of the sampling tube, the speed of withdrawal of the sample and the restrictions in the particular compartment. 50 c.c. samples corresponding to 12% of compartment capacity were withdrawn in each instance and at least three readings were taken to obtain a mean value.

Results for the stainless steel disc column are shown in Fig. 8.4. Even more erratic results were observed for the P.t.f.e. discs and the cone columns due to wetting effects.

8.1.2 Flooding Phenomena

In this work flooding was characterised by the complete rejection of the dispersed phase as a dense layer of droplets.

Flooding rates were determined by establishing steady conditions at a fixed rotor speed and then increasing the flow of the dispersed phase slowly, with the continuous flow rate kept constant, until flooding occurred. Between 3 to 5 readings were taken for each condition until consecutive dispersed phase flowrate values were identical. The flooding data obtained for all systems are given in Fig.8.5.

As observed by other workers (35,71,226) intense mixing was observed immediately prior to the onset of flooding. With the system liquid paraffin-water, the extent of axial mixing was so marked as to cause entrainment of water in the dispersed phase return line. This necessitated the use of an external settler.

With all systems flooding was more easily recognizable at high rotor speeds of the order of 1000 r.p.m.

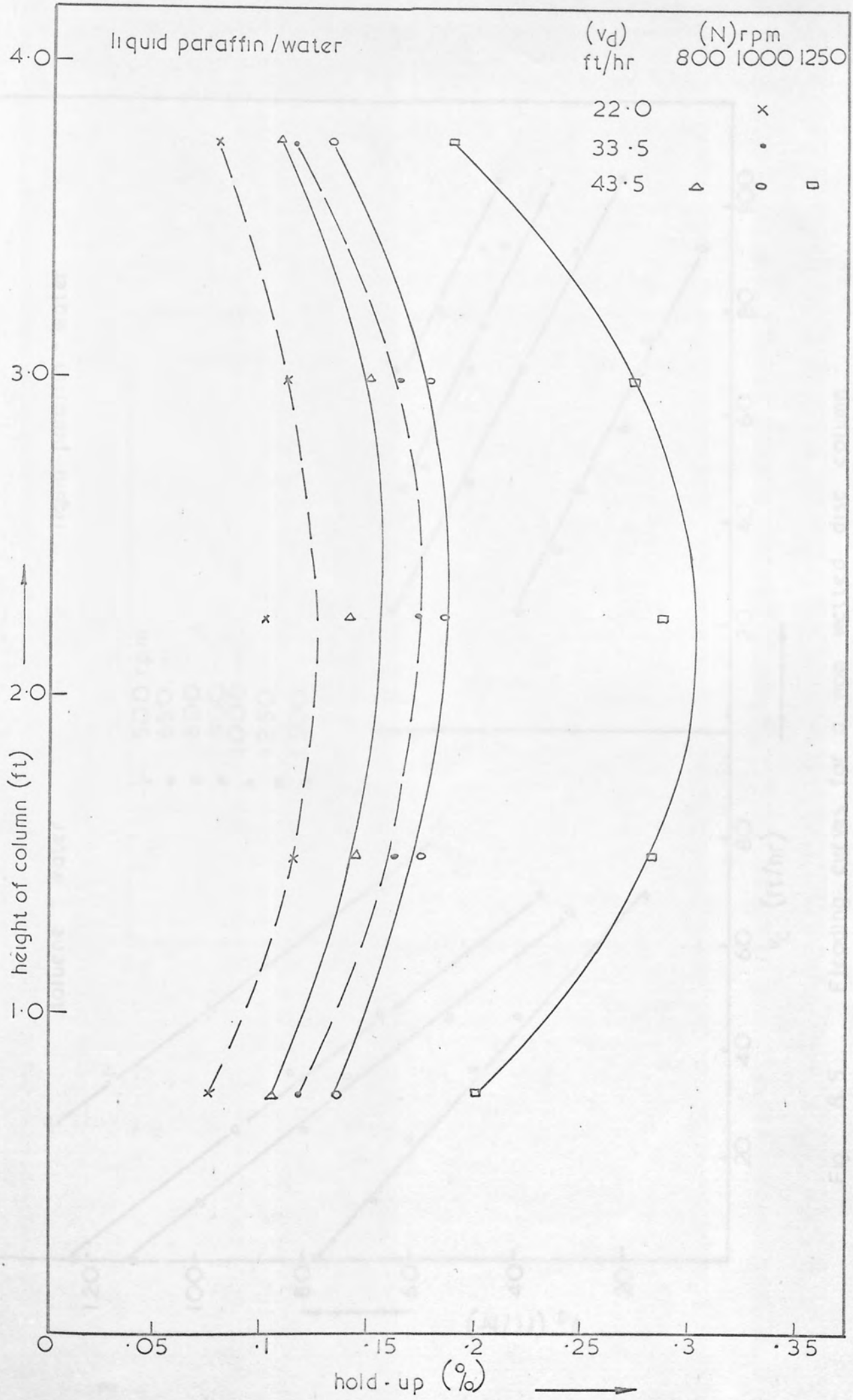

Fig. 8.4 Hold - up profile in an R.D.C.

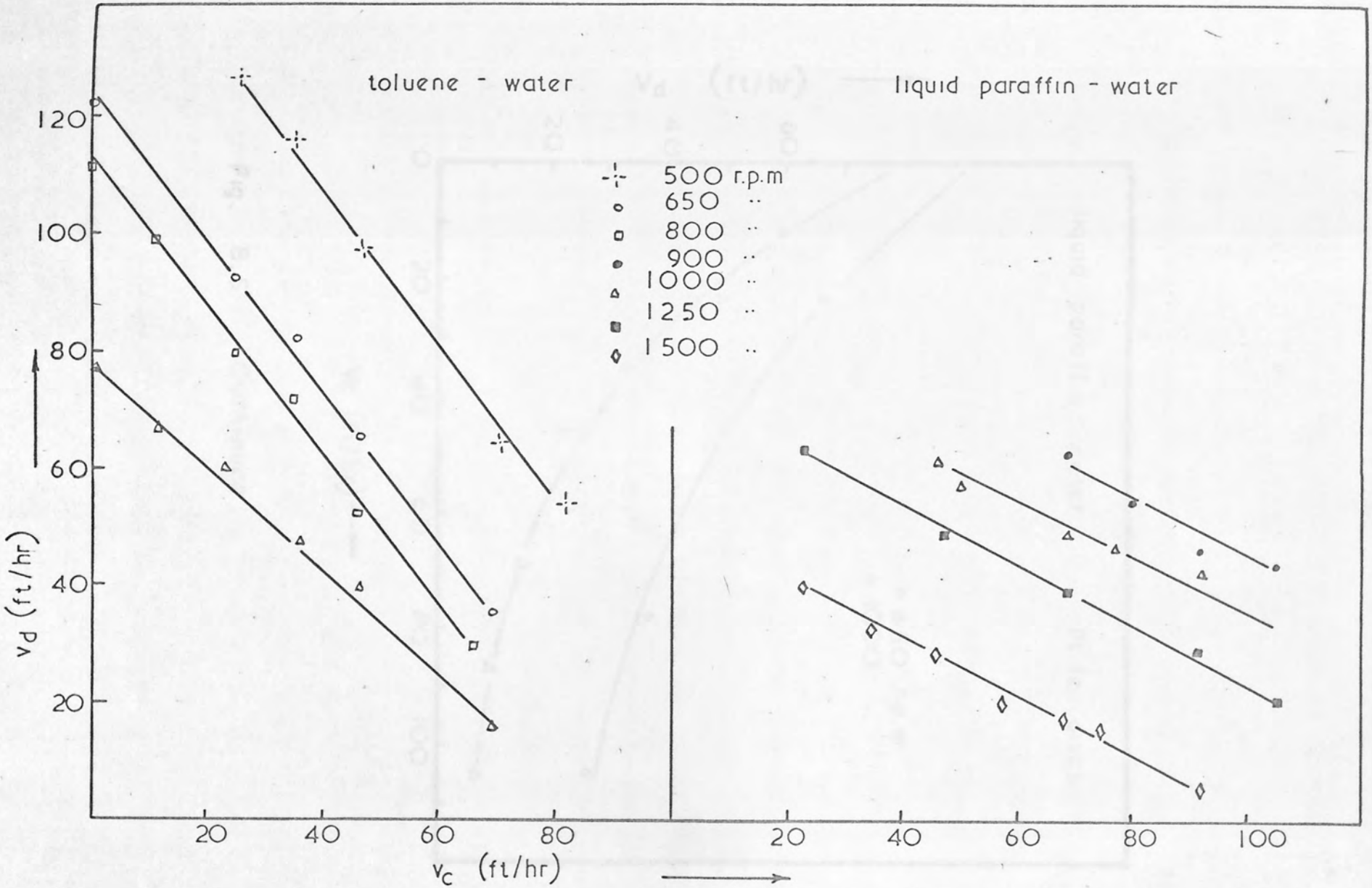

Fig. 8.5. Flooding curves for a non wetted disc column

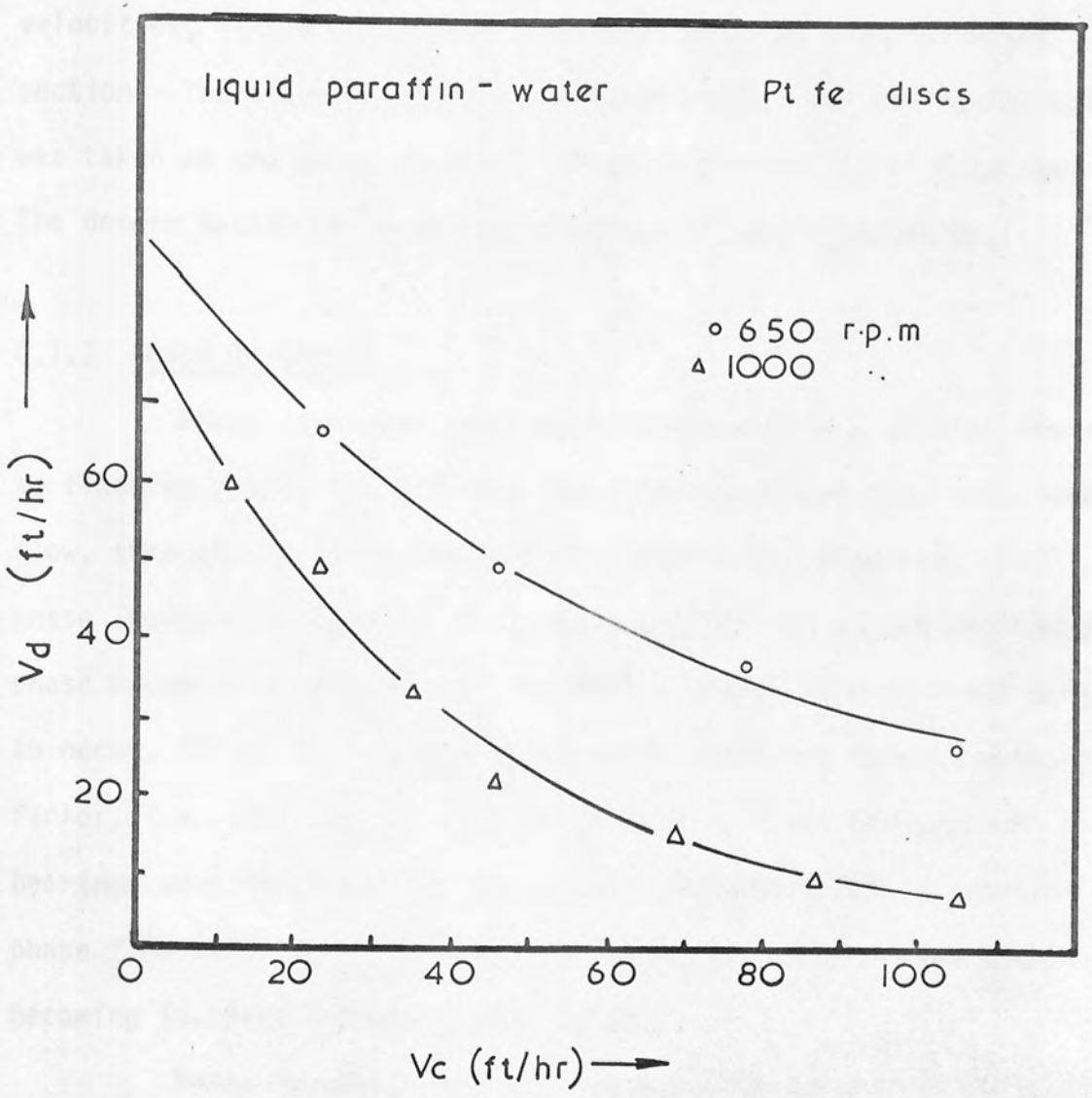

Fig. 8.5. Continued.

The assessment of flooding points presented greatest difficulty in the wetted disc and cone columns. Since dispersed phase was ejected from these rotors as a dense sheet, which in turn disintegrated into large drops possessing high relative velocities, little or no drop rejection occurred from the mixed section. Therefore in these cases the criterion for maximum capacity was taken as the point at which 'phase inversion' first occurred. The determination of phase inversion was as described below.

8.1.3 Phase Inversion

Phase inversion rates were determined in a similar manner to flooding rates, i.e., fixing the rotor speed and continuous phase flow, then slowly increasing the dispersed phase flow rate until phase inversion occurred. This was characterised by the continuous phase becoming dispersed and vice versa. Phase inversion was observed to occur, initially in those compartments with the largest constriction factor, i.e., the 5th and 15th compartments, where the support bearings were situated. A very slight increase in the dispersed phase flow rate, i.e., of the order of 8%, resulted in the phases becoming inverted throughout the column.

Phase inversion was more easily attainable with the p.t.f.e. discs and cone columns, than with the steel discs in the column; this was expected since the former ones were wetted by the dispersed organic phase, thus promoting inversion.

Only the system toluene-water was employed in this study, since with the system liquid-paraffin-water, intense axial mixing occurred well before the start of phase inversion.

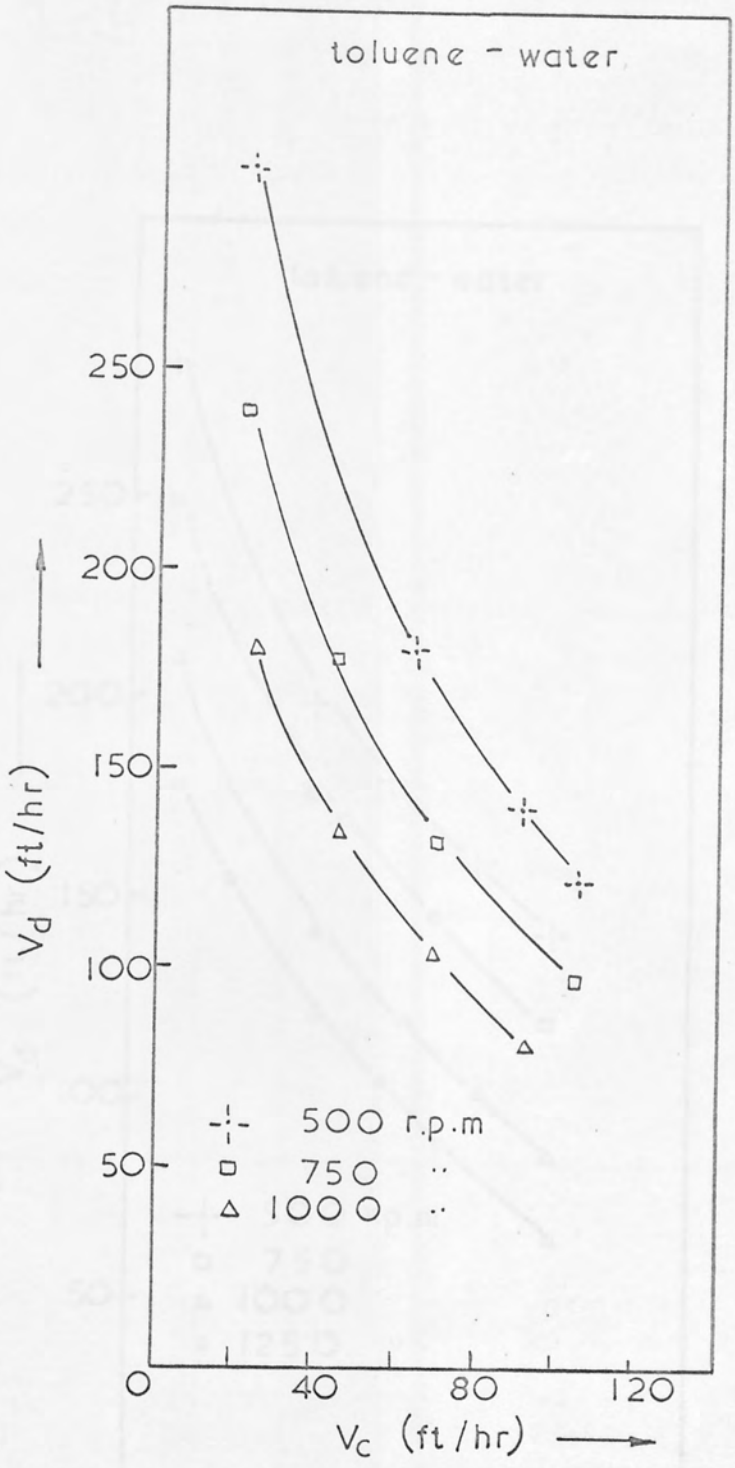

Fig. 8.6 Phase inversion curves for a non-wetted disc column.

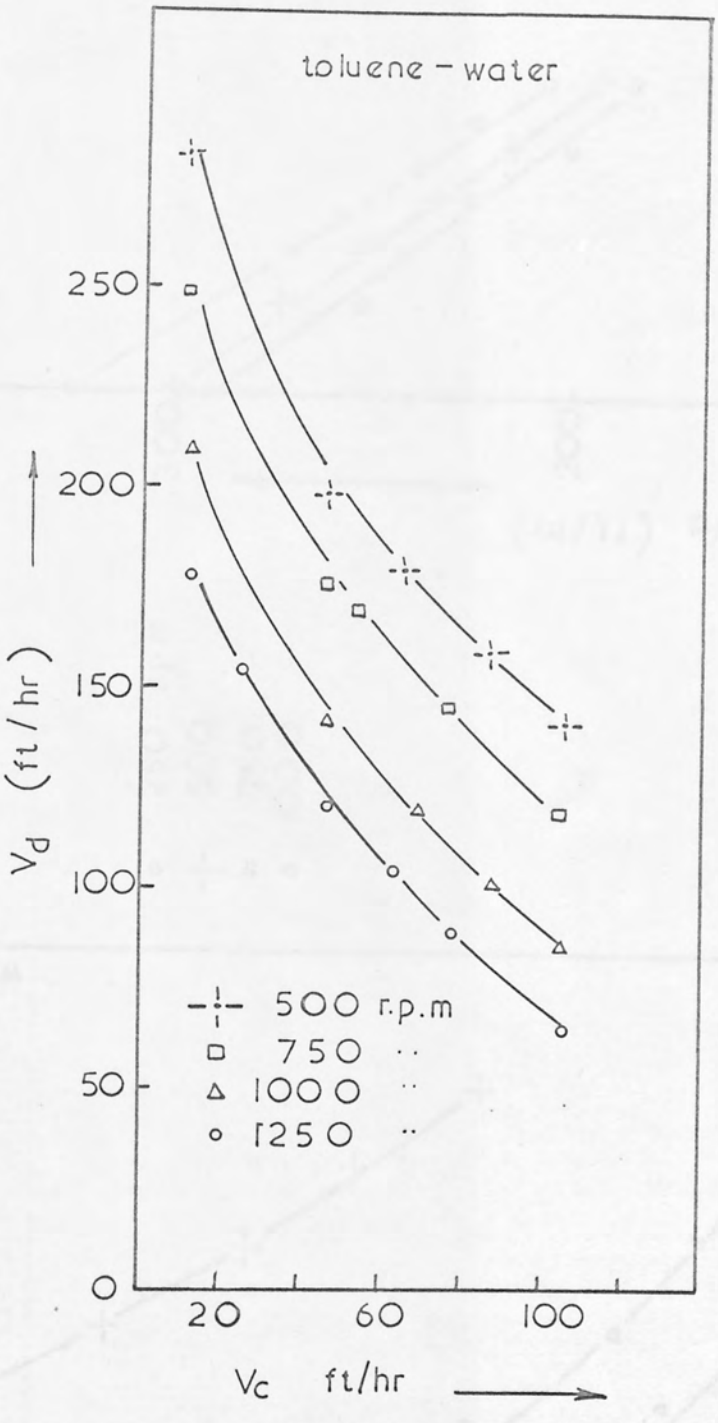

Fig. 8.7. Phase inversion curves for a wetted (ptfe) disc column

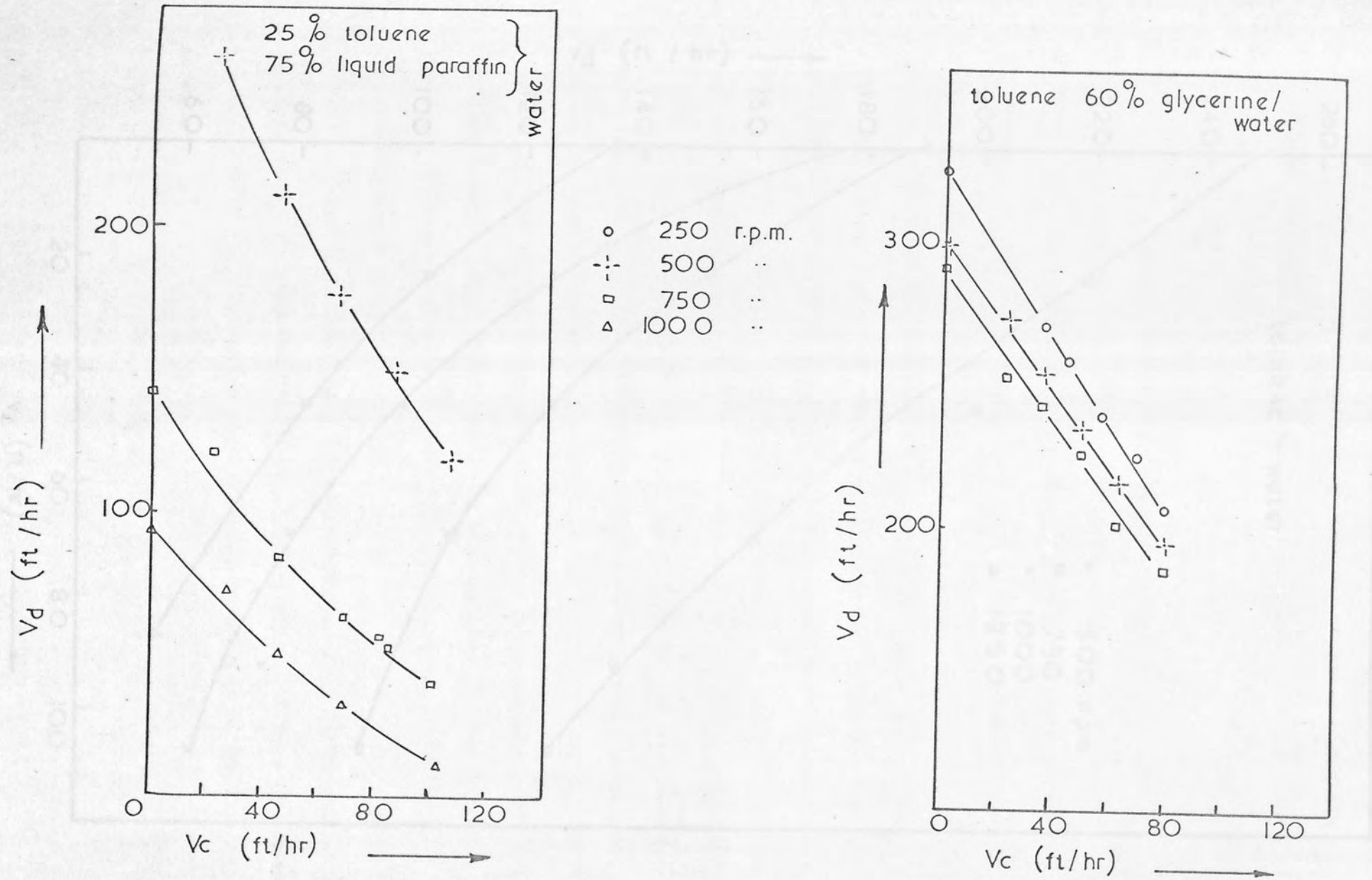

Fig. 8.7. Continued

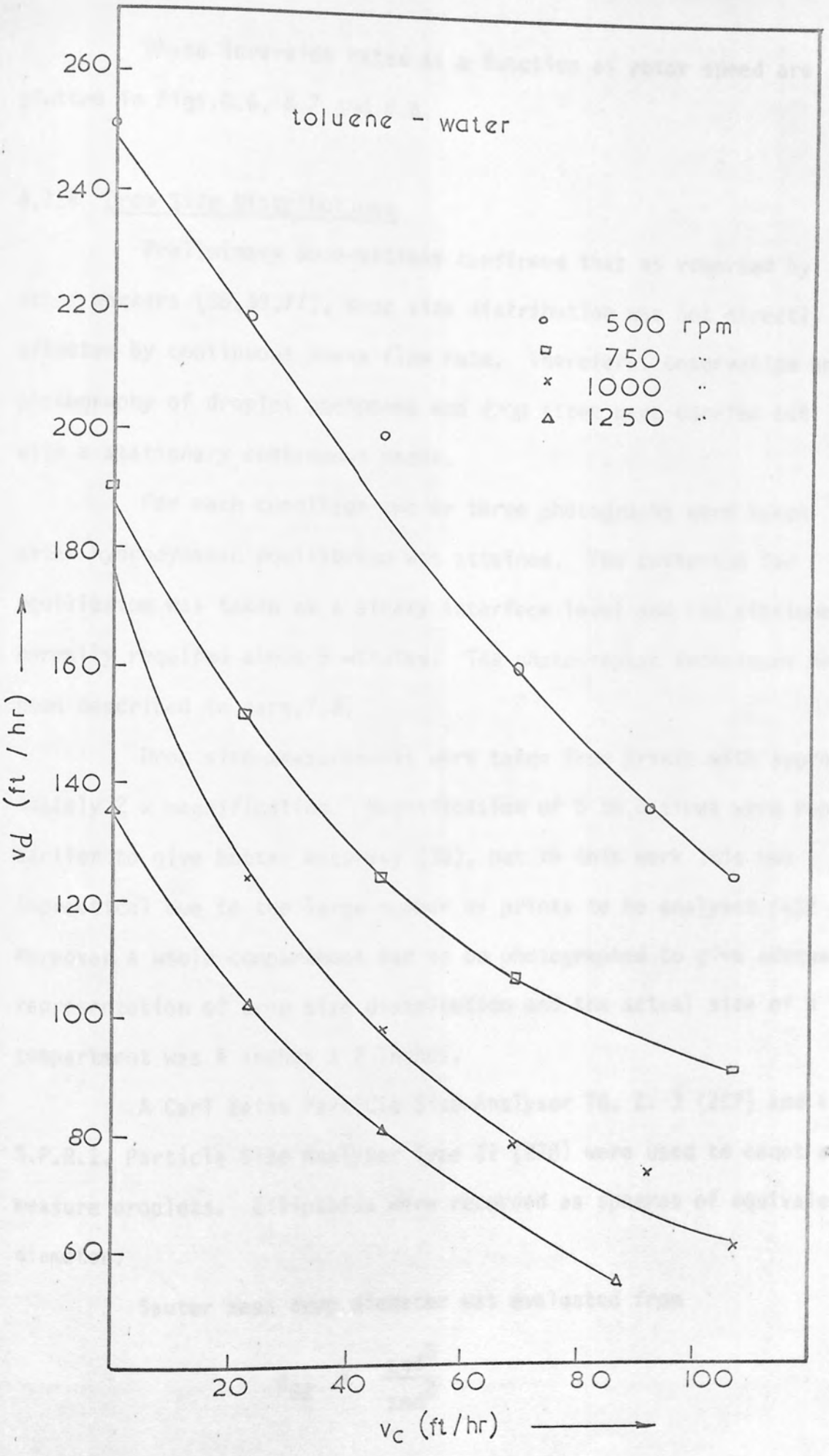

Fig. 8.8. Phase inversion characteristics of the cone column.

Phase inversion rates as a function of rotor speed are plotted in Figs.8.6, 8.7 and 8.8.

8.1.4 Drop Size Distributions

Preliminary observations confirmed that as reported by other workers (35,39,77), drop size distribution was not directly affected by continuous phase flow rate. Therefore, observation and photography of droplet phenomena and drop sizes were carried out with a stationary continuous phase.

For each condition two or three photographs were taken after hydrodynamic equilibrium was attained. The criterion for equilibrium was taken as a steady interface level and its attainment normally required about 5 minutes. The photographic techniques have been described in para.7.6.

Drop size measurements were taken from prints with approximately 2 x magnification. Magnification of 5 to 6 times were reported earlier to give better accuracy (35), but in this work this was impractical due to the large number of prints to be analysed (432 prints). Moreover a whole compartment had to be photographed to give adequate representation of drop size distribution and the actual size of a compartment was 4 inches x 2 inches.

A Carl Zeiss Particle Size Analyser TG. Z. 3 (227) and an S.P.R.I. Particle Size Analyser Type II (228) were used to count and measure droplets. Ellipsoids were recorded as spheres of equivalent diameter.

Sauter mean drop diameter was evaluated from

$$d_{32} = \frac{\Sigma nd^3}{\Sigma nd^2}$$

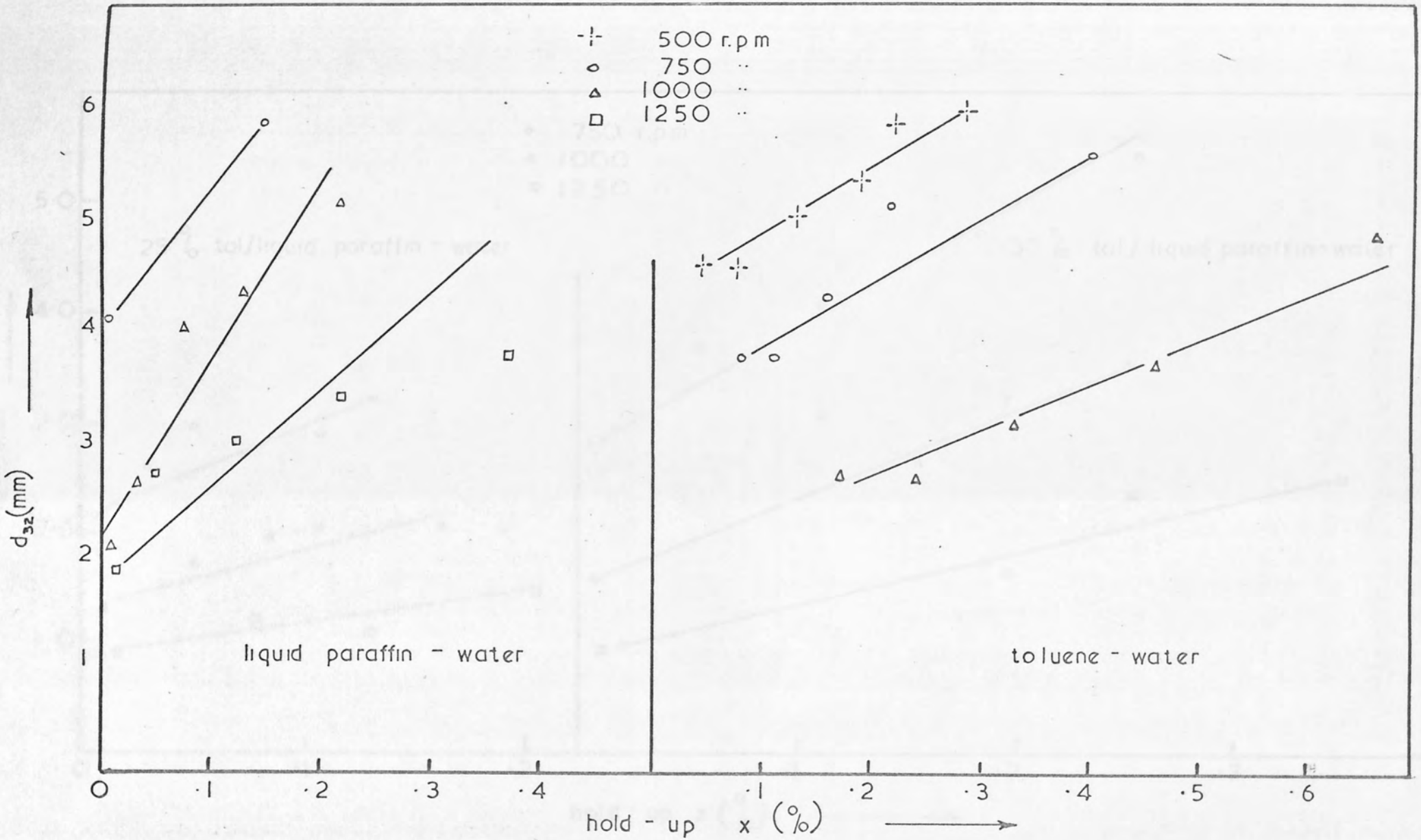

Fig. 8.9. Variation of d_{32} vs. hold-up in a non-wetted disc column

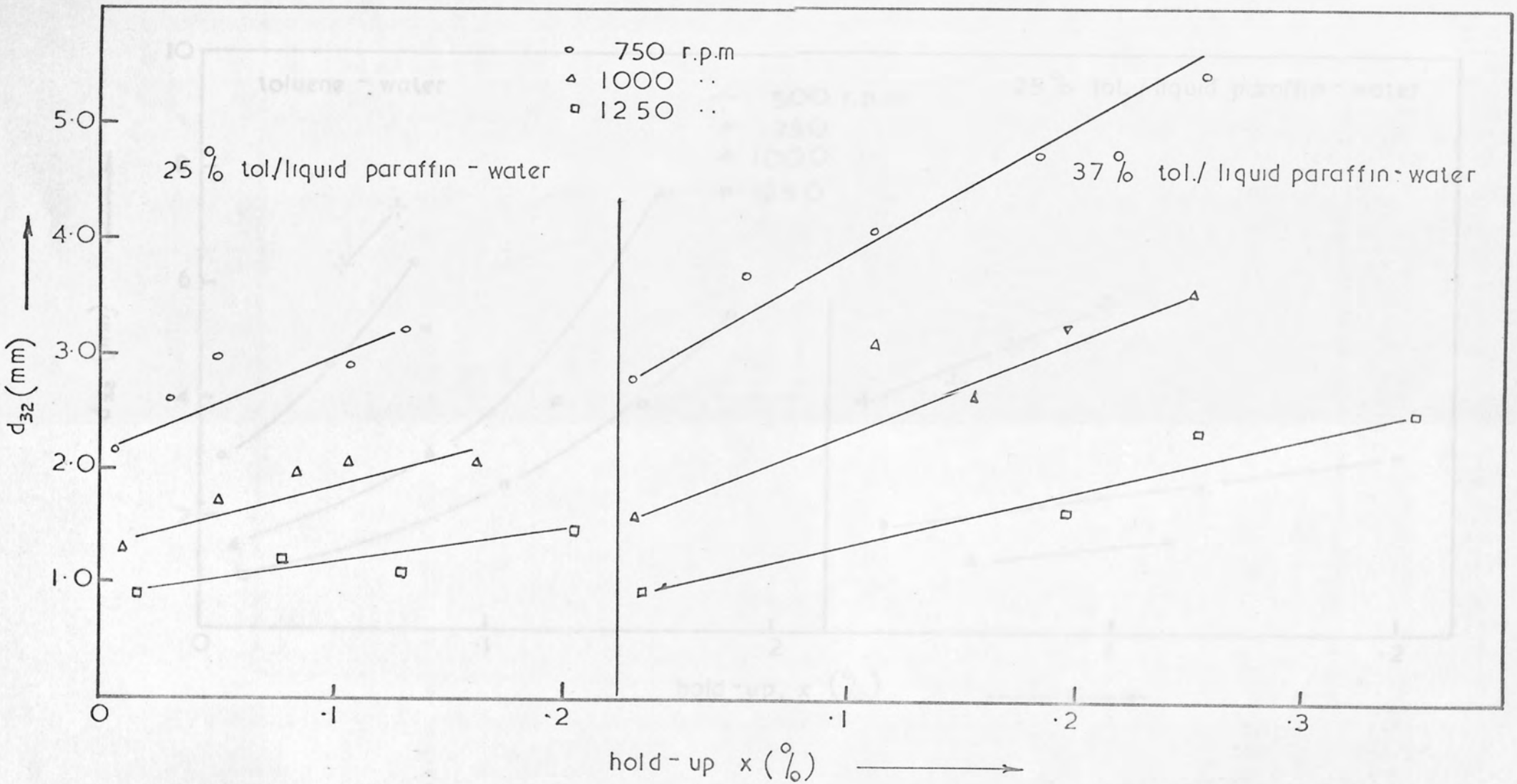

Fig . 8.9 Continued .

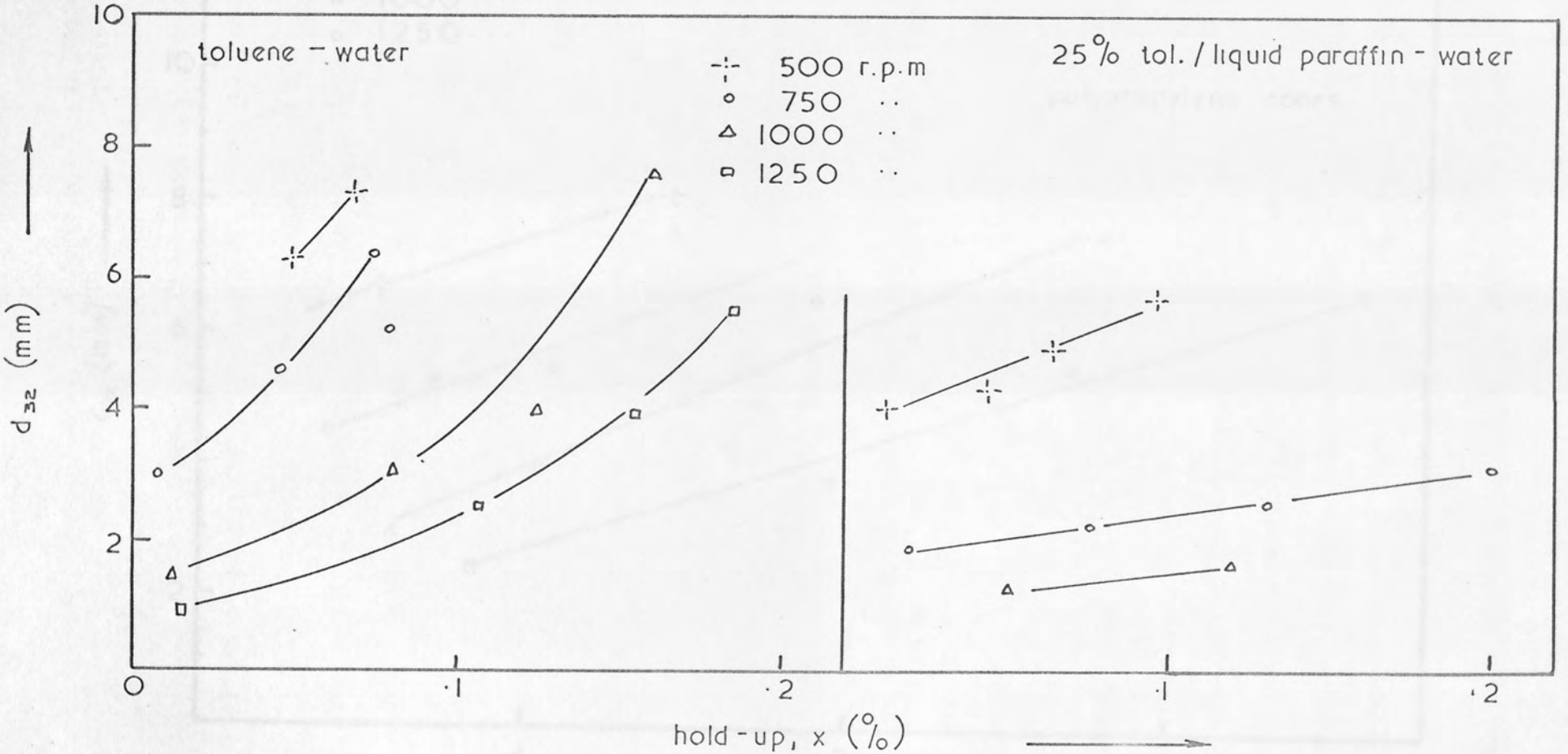

Fig. 8·10 Variation of d_{32} with hold-up in a wetted disc column

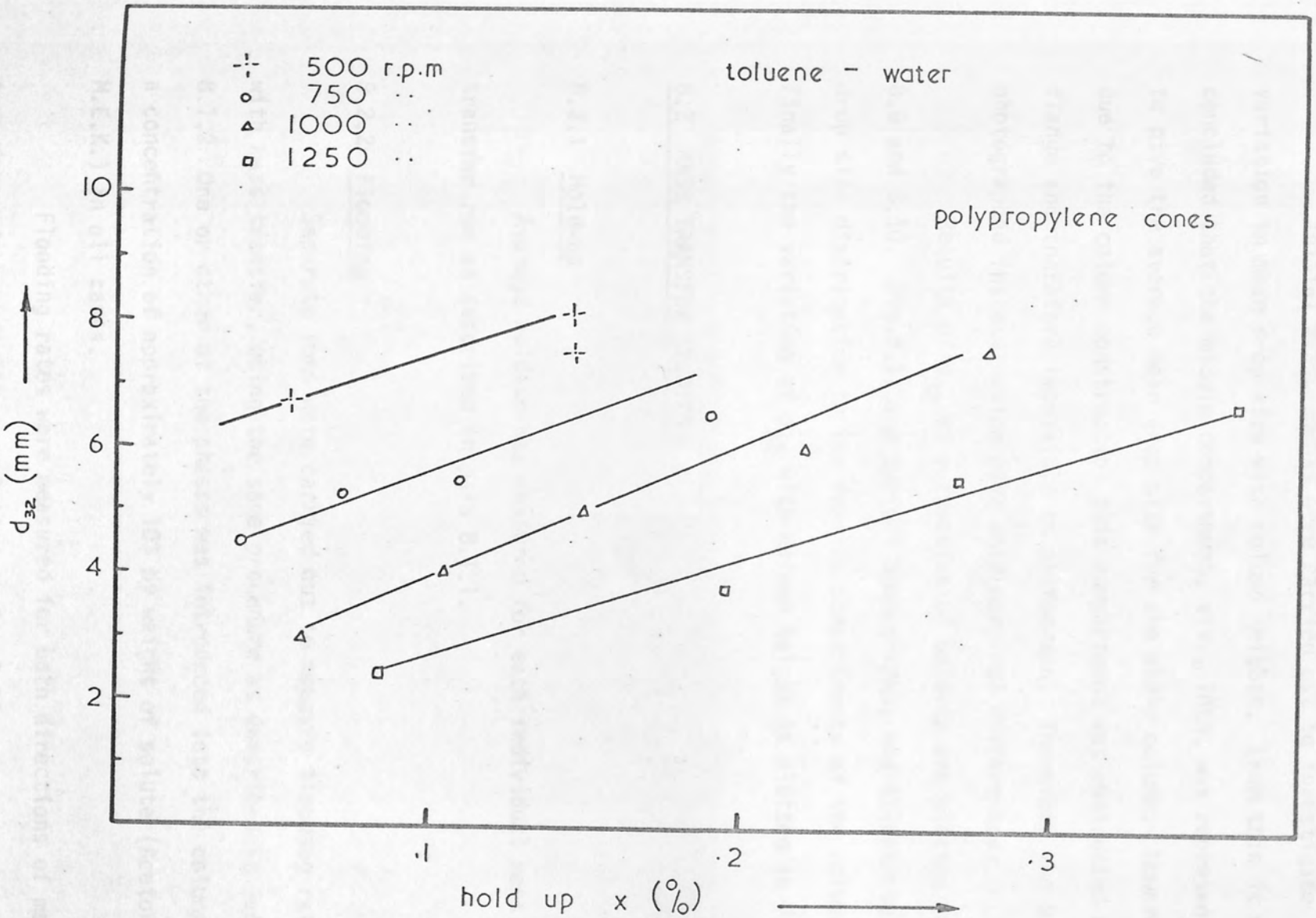

Fig. 8.10 a. Variation of d_{32} with x in the cone column

Typical drop counts and calculations are given in Appendix 8.

Initial measurements were carried out to investigate the variation in mean drop size with column heights. From this it was concluded that the middle compartment, viz., 10th, was representative to give the average mean drop size for the whole column. However, due to the column construction this compartment was obstructed by a flange and therefore impossible to photograph. Therefore the 9th was photographed instead, which gave only marginal differences.

Results of d_{32} as a function of hold-up are plotted in Fig. 8.9 and 8.10. Fig.8.11 are typical photographs, and illustrate the drop size distribution in the various compartments of the column. Finally the variation of d_{32} with column height is plotted in Fig.8.12.

8.2 MASS TRANSFER STUDIES

8.2.1 Hold-up

Average hold-up was measured for each individual mass transfer run as described in para 8.1.1.

8.2.2 Flooding

Separate runs were carried out to measure flooding rates with mass transfer, using the same procedure as described in Section 8.1.2 One or other of the phases was introduced into the column with a concentration of approximately 10% by weight of solute (Acetone or M.E.K.) in all cases.

Flooding rates were measured for both directions of mass transfer and the results are plotted in Fig.8.13.

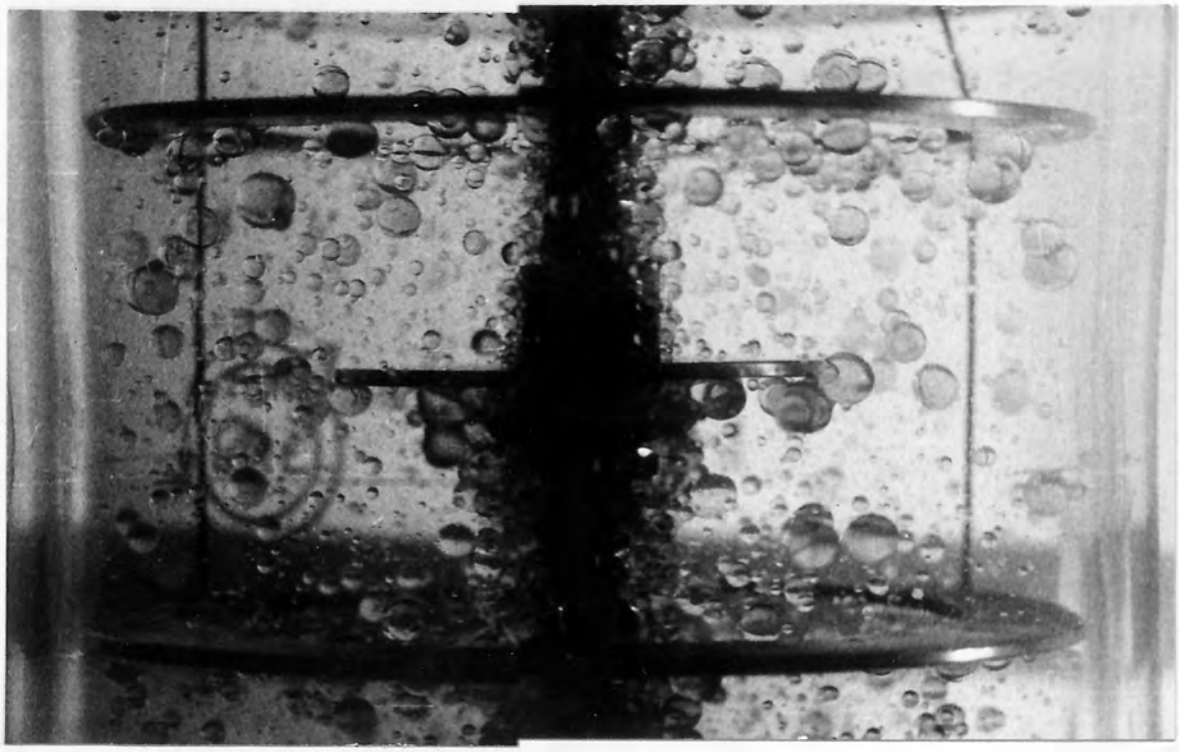

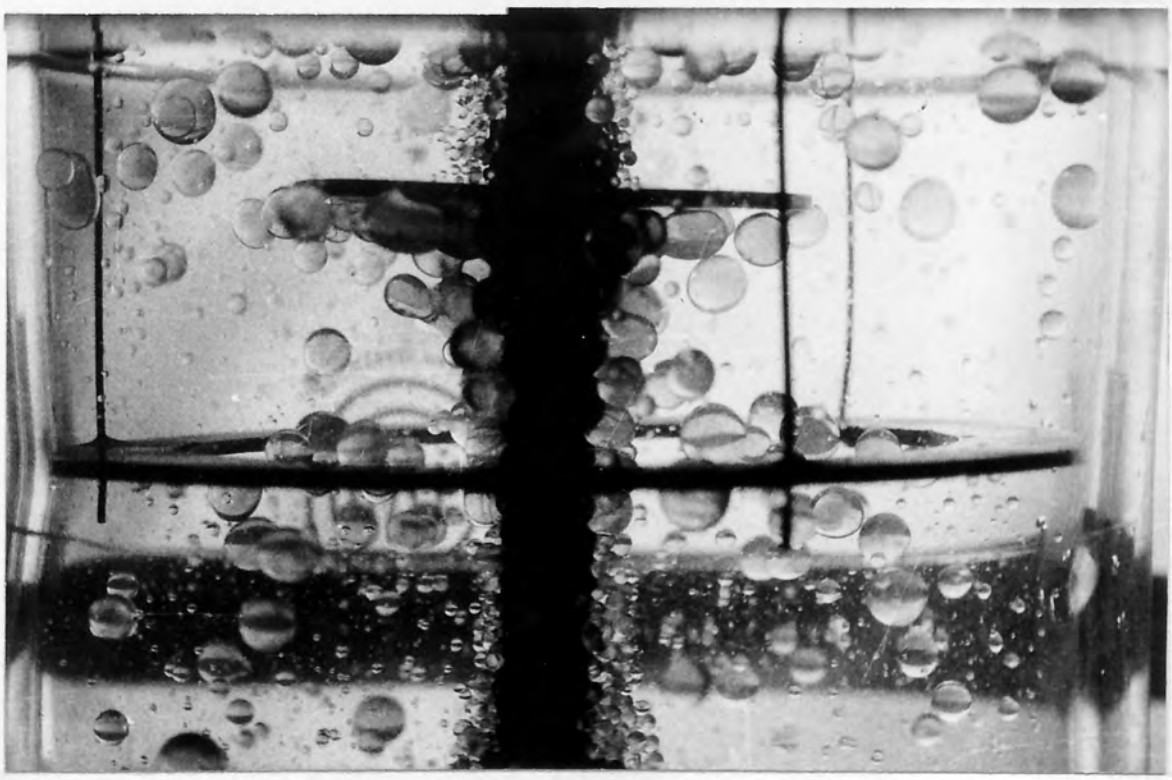

Fig.8.11 Variation of Drop Size with Column Height
(Liquid Paraffin-Water, x = 0.04, 850 rpm)

Top Plate: Compartment Number 18

Bottom Plate: " " 5

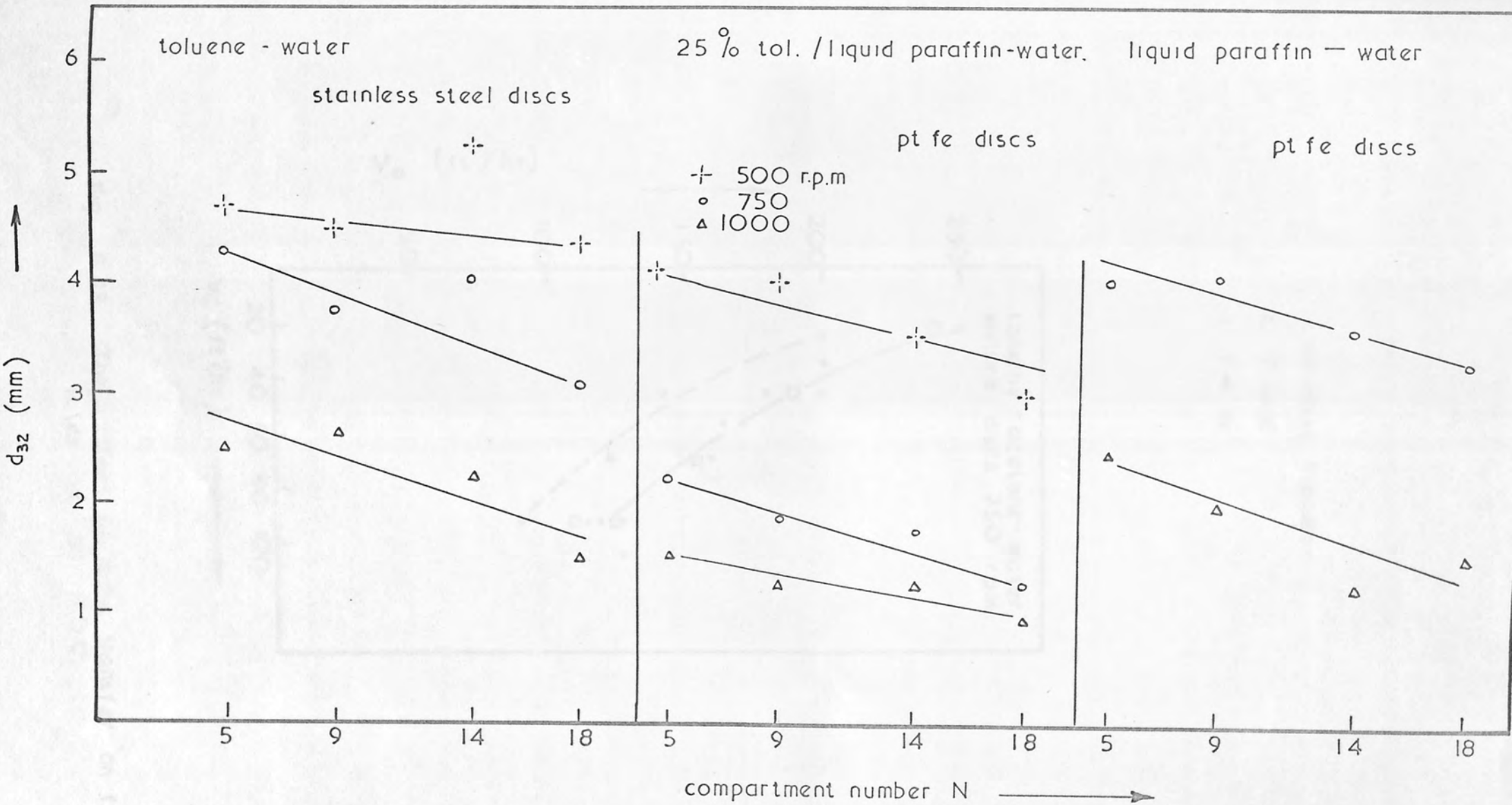

Fig. 8.12. Variation of d_{32} with column height

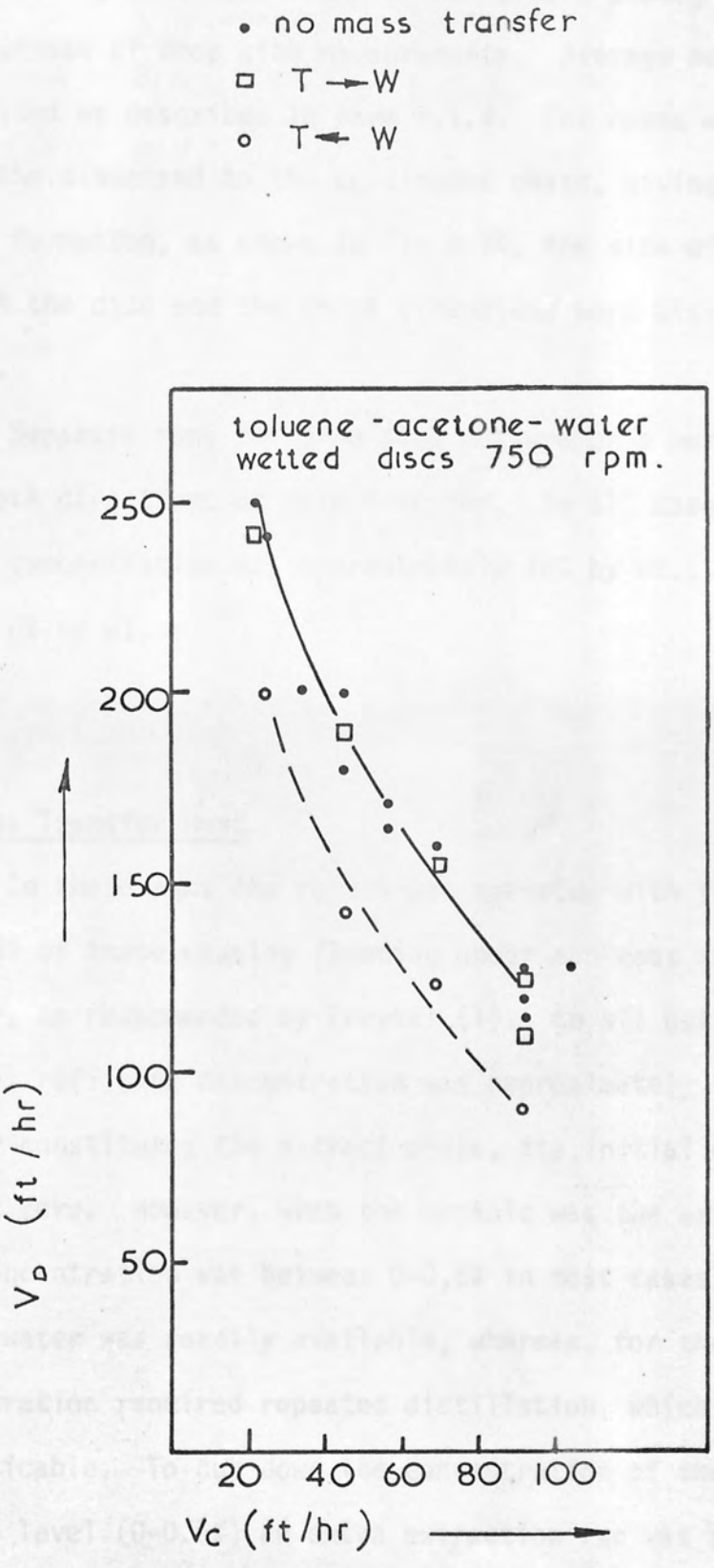

Fig. 8.13 The effect of mass transfer on flooding rates in an R.D.C.

8.2.3 Interfacial Area Estimation

During each mass transfer run 2 to 3 photographs were taken for the purpose of drop size measurements. Average mean drop size was evaluated as described in para 8.1.4. For cases when mass transfer was from the dispersed to the continuous phase, giving rise to cone and sheet formation, as shown in Fig.8.14, the size of the liquid cone underneath the disc and the sheet dimensions were also measured from the print.

Separate runs for drop size measurements were also carried out for both directions of mass transfer. In all cases the initial raffinate concentration was approximately 10% by wt., and that of the extract ≈ 0% by wt.

8.2.4 Mass Transfer Runs

In these runs the column was operated with flow rates between 50% and 60% of those causing flooding under non-mass transfer conditions, as recommended by Treybal (1). In all but a few cases the initial raffinate concentration was approximately 10% by weight, When water constituted the extract phase, its initial concentration was always zero. However, when the organic was the extract phase its initial concentration was between 0-0.5% in most cases, because distilled water was readily available, whereas, for the organic to be 0% concentration required repeated distillation, which was found to be impracticable. To cut down the concentration of the organic to an acceptable level (0-0.5%) an extra extraction run was carried out.

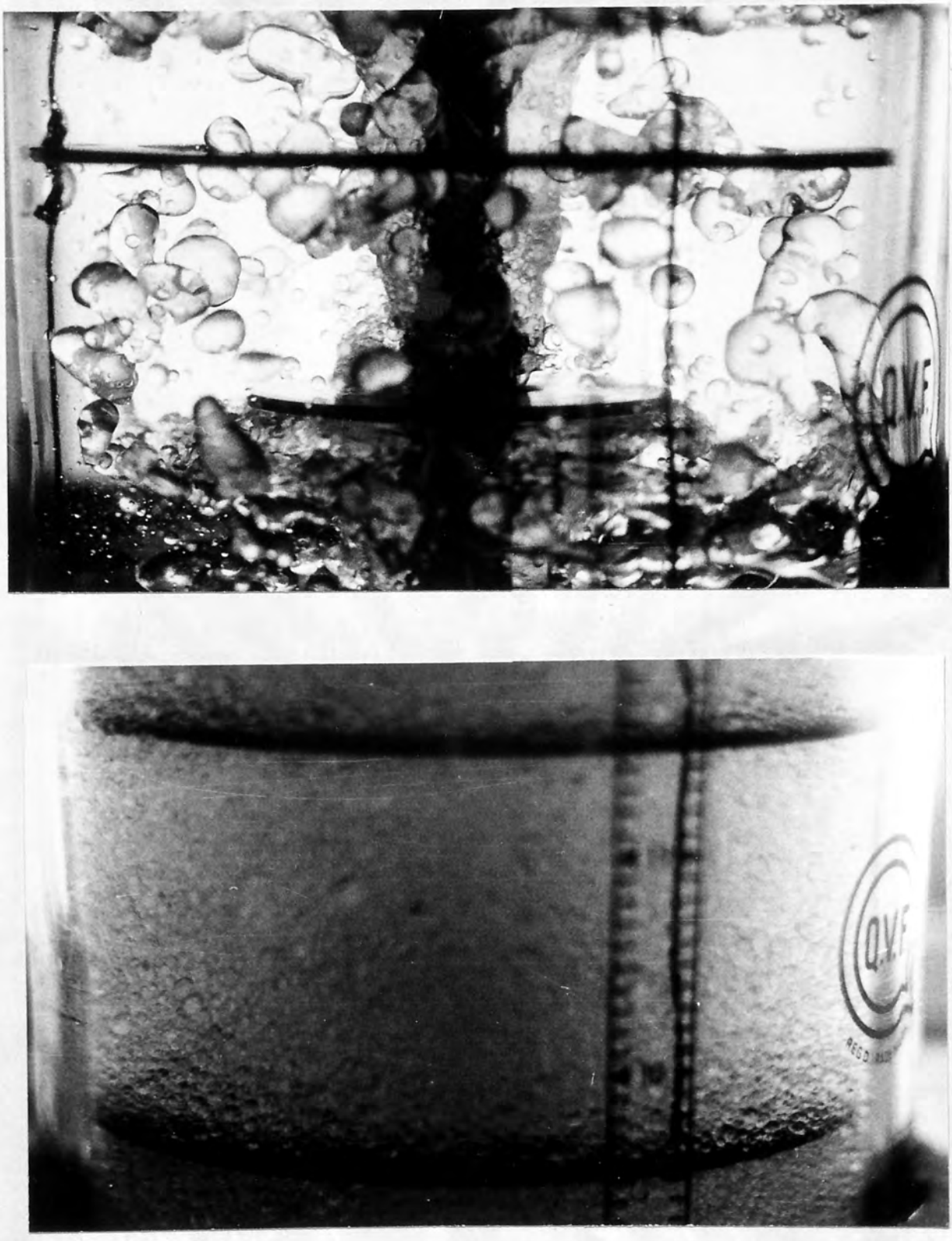

Fig.8.14 Effect of Mass Transfer Direction on Column Behaviour ($Q_c = Q_d = 1.5$ Litre/Min, 1000 rpm)

Top Plate: Toluene (Acetone) → Water

Bottom Plate: Toluene ← Water (Acetone)

The procedure followed during these runs was as follows, First the raffinate solution was made up to the required concentration normally about 10% by weight. The column was then filled with the continuous phase and the agitator adjusted to the required speed. The dispersed phase was introduced into the column and its flow rate adjusted to a set value. When an interface level was attained the continuous phase flow was adjusted to the required value.

After steady conditions were reached, normally after 15 mins., 10 to 20 c.c.s samples were taken from sample ports at the respective phase outlet. Before closing down hold-up and drop size were measured as described earlier.

Initial runs were carried out to determine the time taken for the column to reach steady conditions. This was done by taking 10 to 20 c.c.s samples at 3 minutes time intervals until identical values of solute concentration were obtained for consecutive time intervals. In most cases a minimum value of 6-7 minutes was obtained. For $Q_C=Q_D=2.0\ell/min.$, this would be equivalent to a total flow through the column, of about 2.5 the column volume, significantly different from the value suggested by Coggan of 6 times the column volume (26).

Finally the samples were analyzed by measuring their refractive indicies using an ABBEY A 60 refractometer. From the values, thus, obtained the percentage by weight were then read off from the previously prepared charts given in Appendix 4.

Separate runs were carried out to determine the operating lines. This was done by analysing samples taken from the five sample ports along the column and the inlet and outlet concentrations of the respective phases.

Mass transfer runs were carried out in both directions of transfer. Results of these runs are tabulated in Appendix 6.

Ciné films showing the effects of rotor speeds, flow rates and mass transfer direction on column hydrodynamics, were taken *.

8.3 OTHER STUDIES

8.3.1 Break-up At The Disc Periphery

Droplet break-up from the tip of wetted and non-wetted discs was studied in a 12 inch column section using 5 inch and 2 inch discs. In the case of the smaller discs the 12 inch section was used to minimise wall effects. High speed ciné films, using the Fastax camera at approximately 800 f.p.s., were taken for drops of carbon tetrachloride or dibutylphthalate in water. The range of speeds used was similar to that used for the 4 inch pilot scale R.D.C.*

8.3.2 Interfacial Turbulence

Only qualitative studies were carried out here. Photographic technique, description of equipment and the systems used are given earlier in paras. 7.6, 7.4.3 and 7.3. Still photographs were taken using either the Miranda or the Pentax camera. Low speed, 64 f.p.s. ciné films were also taken to illustrate the different phenomena occurring.* A Milliken DBM-3 camera was used in this instance.

---

* These have been deposited in the Departmental Library.
Their contents are described in Appendix 1.

However, the results are only of limited value due to the large concentration gradient necessary to induce interfacial turbulence a situation which does not normally occur in countercurrent extractors.

9. MATHEMATICAL EXPRESSIONS FOR SELECTED PHENOMENA

9.1 CHARACTERISATION OF PHASE INVERSION

A model has been developed in an attempt to define the phase inversion phenomena reported in Section 3.2.3. The analysis is based on the equation for characteristic velocity discussed in Section 3.2.2 viz.,

$$\frac{V_d}{x} + \frac{V_c}{1-x} = V_N (1-x) \qquad (3.1)$$

Firstly since, V_N is a function of the mean drop size D, it could be expressed as,

$$V_N = KD^n \qquad (9.1)$$

where K is a constant, to account for the physical properties of the system, and agitator speed (3,36).

Considering one phase in the column, substitution of Equation 9.1 into 3.1 and differentiation of D with respect to x yields,

$$\frac{-V_d}{x^2} + \frac{V_c}{(1-x)^2} = K(1-x)\, n\, D^{n-1} \frac{dD}{dx} - K D^n \qquad (9.2)$$

By substitution for KD^n from Equations 9.1 and 3.1 and rearrangement this becomes,

$$\frac{dD}{dx} = \left[V_d \frac{2x-1}{x^2(1-x)} + \frac{2 V_c}{(1-x)^2} \right] \Big/ (K(1-x)n D^{n-1}) \qquad (9.3)$$

Now, at phase inversion,

$D \rightarrow$ a constant maximum value.

Thus $$\frac{dD}{dx} \rightarrow 0$$

Therefore at this condition Equation 9.3 becomes,

$$V_d \frac{2x^*-1}{x^{*2}(1-x^*)} + \frac{2 V_c}{(1-x^*)^2} = 0 \qquad (9.4)$$

where x^* is the value of hold-up at phase inversion.

By rearrangement

$$2 x^{*2} (V_c-V_d) + 3 V_d x^* - V_d = 0 \qquad (9.5)$$

and,

$$x^* = \frac{- 3 V_d \pm \sqrt{(3 V_d)^2 + 8 (V_c-V_d) V_d}}{4 (V_c-V_d)} \qquad (9.6)$$

or

$$\frac{V_c}{V_d} = 1- 3/2 \left(\frac{1}{x^*}\right) + 1/2 \left(\frac{1}{x^{*2}}\right) \qquad (9.7)$$

in which clearly, in practice, x^* must be positive and lie between 0 and 1.0.

Examination of Equation, 9.6 or 9.7, shows that in fact real, positive values of x^* lie between 0 and 0.5 because, $0 < V_c/V_d < \infty$. This represents a condition to maintain countercurrent flow in the column, because for $0.5 < x^* < 1$ small negative values of V_c/V_d are obtained. This suggests that phase inversion should always be

reached at, and persist beyond, this point since the negative sign indicates a reversal of continuous phase flow, i.e., entrainment of small amounts of the continuous phase in the dispersed phase. This situation would obtain until all continuous phase has been purged from the column at x* = 1.0. This is confirmed by reference to the plot of V_c/V_d vs x* given in Fig.9.1.

For the specific case of the R.D.C., two modifications of Equation 3.1 have been proposed. One is due to Kung and Beckmann (71),

$$\frac{V_d}{x} + \frac{K_1 V_c}{1-x} = V_N (1-x) \qquad (3.3)$$

where K_1 is a geometric constant, $K_1 = 1.0$ at $\frac{S-R}{D_K} > 1/24$

$$K_1 = 2.1 \text{ at } \frac{S-R}{D_K} < 1/24$$

Following the same procedure as above, but using Equation 3.3 instead of Equation 3.1, at phase inversion,

$$\frac{V_c}{V_d} = 1/K_1 \left[1-3/2 \left(\frac{1}{x^*}\right) + 1/2 \left(\frac{1}{x^{*2}}\right)\right] \qquad (9.8)$$

When $K_1 = 1.0$ Equation 9.8 is the same as 9.7. However it is doubtful whether a single value of the constant K_1 can account with any accuracy for a range of geometries. A more realistic constant would be one having a different value specific to each geometry.

The second modification of Equation 2.1 proposed by Misek (75) has the form,

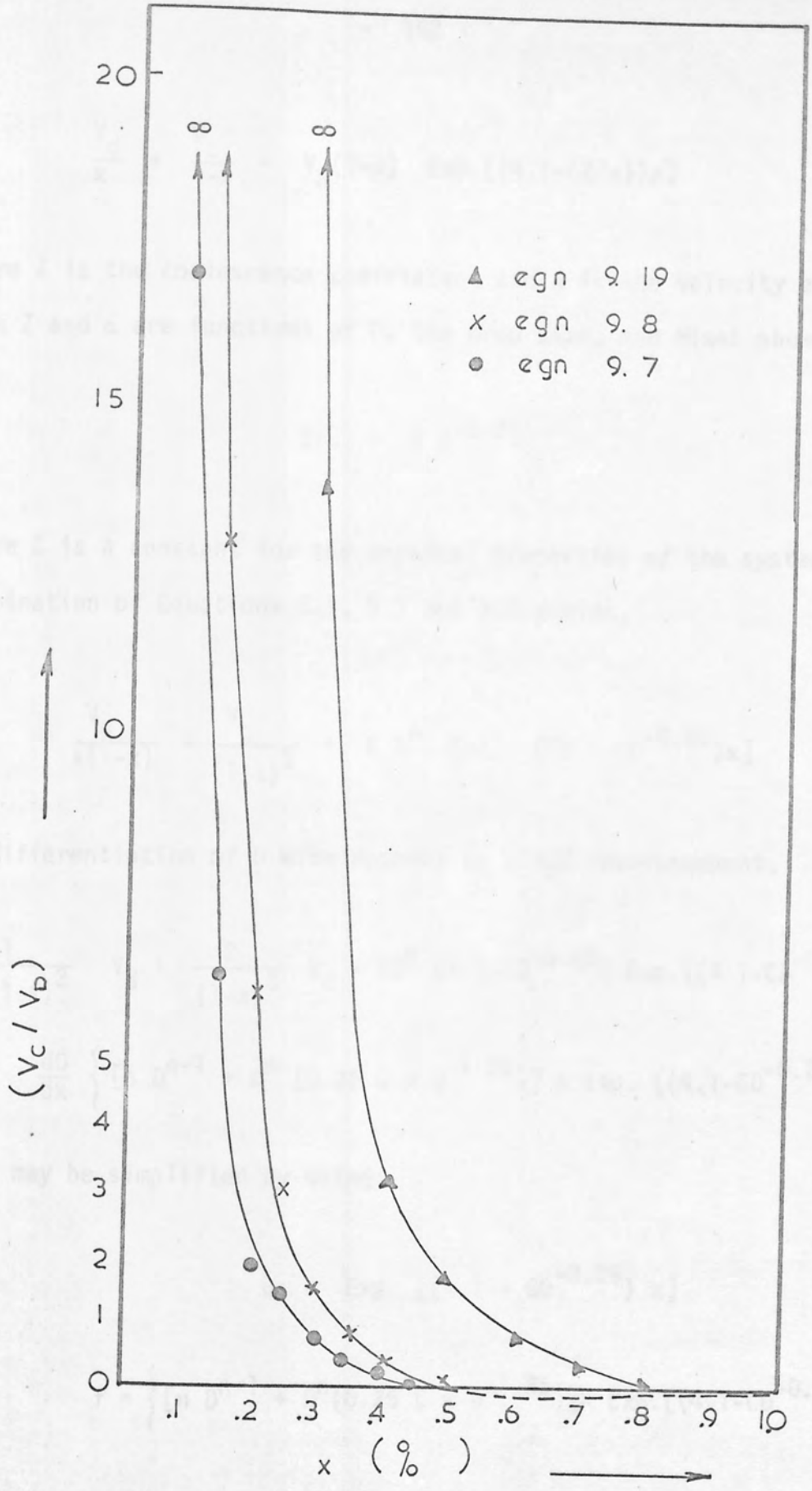

Fig. 9.1 Theoretical hold-up values at phase inversion

$$\frac{V_d}{x} + \frac{V_c}{1-x} = V_N(1-x) \text{ Exp.}[(4.1-(Z/\alpha))x] \qquad (2.1)$$

where Z is the coalescence coefficient and α is the velocity exponent. Both Z and α are functions of D, the drop size, and Misek showed that,

$$Z/\alpha = C\, D^{-0.25} \qquad (9.9)$$

where C is a constant for the physical properties of the system. Combination of Equations 2.1, 9.1 and 9.9 yields,

$$\frac{V_d}{x(1-x)} + \frac{V_c}{(1-x)^2} = K\, D^n \text{ Exp. } [(4.1-CD^{-0.25})x] \qquad (9.10)$$

By differentiation of D with respect to x and rearrangement,

$$\frac{2x-1}{x^2(1-x)^2} V_d + \frac{2}{(1-x)^3} V_c - KD^n (4.1-CD^{-0.25}) \text{ Exp.}[(4.1-CD^{-0.25})x]$$

$$= \frac{dD}{dx} \left\{ [n\, D^{n-1} + D^n (0.25\, C\, x\, D^{-1.25})]\, K \text{ Exp. } [(4.1-CD^{-0.25})x] \right\} \qquad (9.11)$$

This may be simplified by using,

$$u = \text{Exp. } [(4.1 - CD^{-0.25})\, x] \qquad (9.12)$$

and

$$f = \left\{ [n\, D^{n-1} + D^n (0.25\, C\, x\, D^{-1.25})] K \text{ Exp.}[(4.1-CD^{-0.25})x] \right\} \qquad (9.13)$$

to give,

$$\frac{(2x-1)}{x^2(1-x)^2} V_d + \frac{2}{(1-x)^3} V_c - K.D^n.u.(4.1 - \frac{C}{D^{0.25}}) = f.\frac{dD}{dx} \qquad (9.14)$$

Substitution for $KD^n u$ from Equations 2.1 and 9.1, and for $\frac{C}{D^{0.25}}$ from Equation 9.9, then yields,

$$\frac{(2x-1)}{x^2(1-x)^2} V_d + \frac{2}{(1-x)^3} V_c - \left[\frac{V_d}{x(1-x)} + \frac{V_c}{(1-x)^2}\right] (4.1-Z/\alpha) = f.\frac{dD}{dx} \quad (9.15)$$

At phase inversion

$D \rightarrow$ A maximum value

Thus $\frac{dD}{dx} \rightarrow 0$

and $Z/\alpha \rightarrow 0$; since no further coalescence occurs.

Therefore at this condition Equation 9.15 becomes,

$$\frac{(2\,x^*-1)}{x^{*2}(1-x^*)^2} V_d + \frac{2}{(1-x^*)^3} V_c - \frac{4.1}{x^*(1-x^*)} V_d - \frac{4.1}{(1-x^*)^2} V_c = 0 \quad (9.16)$$

By rearrangement,

$$\frac{V_c}{V_d} = \frac{4.1\,x^{*3} - 6.2\,x^{*2} + 1.1\,x^* + 1}{4.1\,x^{*3} - 2.1\,x^{*2}} \quad (9.17)$$

By division Equation 9.17 becomes,

$$\frac{V_c}{V_d} = 1 - \frac{1}{x^*} - \frac{1}{ax^{*2}} + \frac{2}{a^2x^{*3}} + \frac{2b}{a^3x^{*4}} + \frac{2b^2}{a^4x^{*5}} + \frac{2b^3}{a^5x^{*6}} + \text{---} \quad (9.18)$$

where $a = 4.1$

and $b = 2.1$

Equation 9.18 is clearly a power series and can be put in the following form,

$$\frac{V_c}{V_d} = 1 - \frac{1}{x^*} - \frac{1}{ax^{*2}} + 2 \sum_{j=3}^{j} \frac{b^{j-3}}{a^{j-1}\, x^{*j}} \qquad (9.19)$$

where $j = 3,4,5, \ldots j$.

$a = 4.1$

$b = 2.1$

Comparison of Equations 9.19 and 9.7, suggests that the terms in $\sum$ are merely correction factors. The number of factors to be included is dependent upon the column design and system and could be verified experimentally.

It is worth noting that a second approach leads to the same results. This is based on the assumption that

Either $V_N = K V_d^n$ and at phase inversion $dV_d/dx = 0$

or $V_N = K V_c^n$ and at phase inversion $dV_c/dx = 0$

It can be seen that Equation 9.6 is the same as Equation 3.9 given by Logsdail et al (72), for hold-up at "flooding". However the boundary conditions used in the present study, i.e.,

$$D \rightarrow \text{a maximum constant value}, \quad \frac{dD}{dx} \rightarrow 0,$$

are more realistic than those employed by these authors, viz., $\frac{dV_d}{dx} = 0$ and $\frac{dV_c}{dx} = 0$ at flooding, since flooding is a rather ambiguous phenomenon whilst phase inversion is clearly defined. Furthermore, in an accurately designed agitated countercurrent contactor, for the specific case of the R.D.C. within the design limits given in Section 3, phase inversion may set in well before flooding.

However, Equation 9.6 is restrictive and as mentioned earlier, it gives a maximum value of x of 0.5 at $V_c = 0$. This is open to doubt since in practice higher values of x may be possible, before phase inversion occurs; dispersions of up to 97% kerosine in water have been obtained in stirred tanks (229). Thus the more flexible Equation 9.19 may be more representative than Equation 9.6. The flexibility of Equation 9.19 lies in the fact that any number of terms can be taken until the relation fits the data for a given design and or system, since the latter significantly affects phase inversion limits. A trial and error procedure was employed to determine, approximately, the number of terms required in the correlation, this being the minimum number of terms for a value of x between 0 and 1.0 and $V_c/V_d = 0$. A computer programme was developed for this purpose, and the values obtained were, $x = 0.81$, $V_c/V_d < 10^{-37}$ and the number of terms under $\sum = 5$.

It is relevant to note the relation given by Misek (75) for x at flooding,

$$\frac{V_d}{V_c} = \left\{ \frac{2x^2(1-x+[\frac{Z}{\alpha} - 4.1][X-\frac{x^2}{2} - \frac{1}{2}])}{(1-x)^2(1-2x+[\frac{Z}{\alpha} - 4.1][x-x^2])} \right\} \qquad (9.20)$$

This Equation was arrived at using Equation 2.1 and the boundary condition, $\frac{dV_c}{dx} = 0$ and $\frac{dV_d}{dx} = 0$.
Equation 9.20 gave unrealistic values of hold-up, e.g. 0.123 at $\frac{V_c}{V_d} = 1.0$ (75). For the same reasons as those given in connection with Equation 3.9. Equation 9.19 is considered a more realistic

one, furthermore it is more flexible and easier to use due to the absence of the term Z/α, which was assumed to approach zero at phase inversion.

The practical application of the above models is to predict the maximum capacity of an extractor. This is done by calculating x* from either Equation 9.7 or 9.19 for a given flow ratio and rotor speed. This is, then, substituted into one of the corresponding original equations, viz., Equations 3.1 and 2.1. The characteristic velocity, V_N, appearing in the latter Equations may be substituted from an expression of the form given by Logsdail et al (72), Equation 3.3.

Finally, further work is required in this field before the phenomenon of phase inversion may be accurately represented. For example a more representative model may be derived by consideration of the change in surface energy associated with surface area changes at phase inversion.

9.2 AN EXPRESSION FOR MASS TRANSFER IN A COALESCING ENVIRONMENT

As discussed in Section 3.3.4.3, droplet coalescence is promoted by mass transfer from the dispersed to the continuous phase giving rise to larger 'oscillating' drops. These tend in turn to coalesce between themselves, or with any interface available within the column, which is followed by redispersion. In this section a first attempt is made to derive an expression for this case to include the quantitative effects which surface and hydrodynamic phenomena, viz drop formation, coalescence and oscillation, have upon mass transfer.

The analysis utilizes the surface stretch model for mass transfer for single drops (99), represented in terms of the time average mass transfer coefficient $\bar{k}$,

$$\bar{k} = \frac{2}{\tau} \int_0^{\tau} \left[\frac{S(\tau)}{S_o}\right]^2 dt \qquad (9.21)$$

where $S(\tau)$ = area of time-dependent surface

S_o = a characteristic reference area for constant surface.

τ = dimensionless time variable defined by,

$$\tau = t/t_o \qquad (9.22)$$

where t is the time period considered, and t_o is a characteristic constant for any particular system or phenomenon. From this the average dispersed phase mass transfer coefficient k_D is defined as (99),

$$k_D = \bar{k} \sqrt{\frac{D_{AD}}{\pi t_o}} \qquad (9.23)$$

By considering the principle of additive dispersed and continuous phase resistances to mass transfer, the overall mass transfer coefficient, based on the drop phase is (99),

$$K_D = \bar{k}\sqrt{D_{AD}/\pi t_o}\left[\frac{1}{1+m\sqrt{\frac{D_{AD}}{D_{AC}}}}\right] \qquad (9.24)$$

where D_{AD} and D_{AC} are the diffusivities of solute A in the dispersed and continuous phase respectively and m is the partition coefficient.

It will be assumed that, for all oscillating surfaces, the following surface-time relation applies (99),

$$S(\tau) = S_o(1+\varepsilon \sin^2\tau) \qquad (4.23)$$

where ε, the amplitude of stretch can be calculated from a knowledge of the maximum and minimum surface area per cycle.

It will further be assumed that the surface-time relationship for coalescing drops is similar to that for forming drops, which is based on the assumption of linear surface growth rate (97,99),

$$S(\tau) = S_o(1+\beta\tau) \qquad (9.25)$$

where β is a dimensionless surface growth rate constant, which has a negative value for coalescing drops.

In any practical extractor the total mass transfer is the sum of the transfer which occurs,

a) During the initial, and any subsequent, droplet formation periods;

b) During free rise when the drop may be stagnant, circulating or oscillating;

c) During drop coalescence in the settling zone and the mixing section;

and d) From all other transfer surfaces.

For the case in question, i.e., with mass transfer from the dispersed to the continuous phase, the following phenomena were observed, in the R.D.C. at Reynold's numbers below 6.5×10^4 and dispersed phase flow rates > 0.5 l/min.

i) Drops in the vortex beneath the disc, coalesced and formed a liquid cone.

ii) The liquid in the cone flowed upwards (or downwards) due to gravitational forces, and then issued, from the disc's tip in the form of a sheet.

iii)The sheet ultimately disintegrated into drops, i.e., a process of drop formation.

iv) These drops were fairly large in size and oscillated as they travelled up (or down) the column, and finally,

v) Drops coalesced into the liquid cone beneath the disc in the next compartment.

Predictably the drop sizes and cone and sheet dimensions were dependant on the system physical properties, column geometry, flow rates and rotor speed.

The whole cycle was completed between consecutive discs, as illustrated in Figs.9.2 and 8.14.

Therefore the total mass transfer consisted of the sum of the contributions from i- v inclusive.

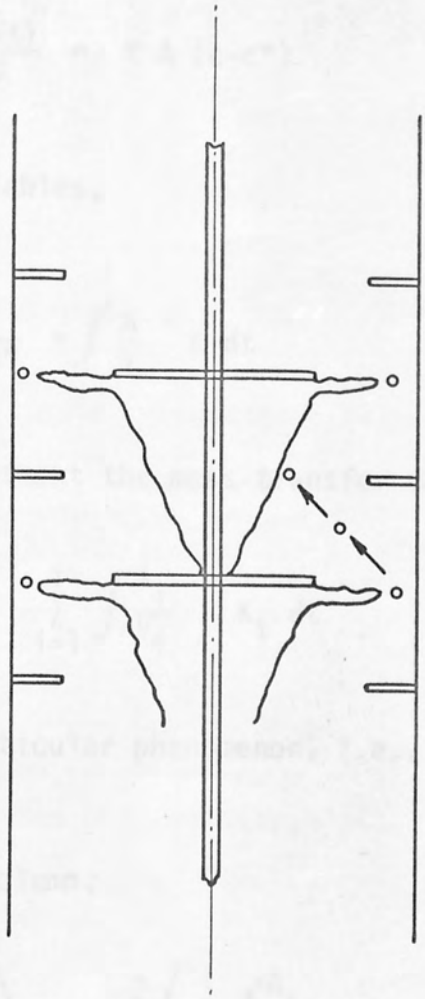

Fig . 9.2. Schematic representation of sheet and vortex formation

The basic equation for mass transfer may be written in the form,

$$\frac{d(Vc)}{dt} = K\,A\,(c-c^*) \qquad (9.26)$$

By separation of the variables,

$$\int \frac{dc}{c-c^*} = \int \frac{A}{V}\,K\,dt \qquad (9.27)$$

So that in any one compartment the mass transfer can be described by,

$$\sum_{i=1}^{i}\left[\int \frac{dc}{c-c^*}\right]_i = \sum_{i=1}^{i}\int \frac{A_i}{V_i}\,K_i\,dt \qquad (9.28)$$

where i refers to any particular phenomenon, i.e., drop formation, drop oscillation, etc.

For the whole column,

$$\sum_{n=1}^{n}\left(\sum_{i=1}^{i}\left[\int \frac{dc}{c-c^*}\right]_i\right)_n = \sum_{n=1}^{n}\left(\sum_{i=1}^{i}\int \frac{A_i}{V_i}\,K_i\,dt\right)_n \qquad (9.29)$$

where n is the total number of compartments. In practice, in using this for calculation, the initial drop formation from the distributor and the final coalescence in the settling zone are assumed to be equivalent to one extra compartment giving a total number of compartments of n+1.

The L.H.S. of Equation (9.29) may be rewritten thus,

$$\text{L.H.S.} = \int_{c_1}^{c_2} \frac{dc}{(c-c^*)} \qquad (9.30)$$

and the R.H.S.

$$\text{R.H.S.} = \sum_{n=1}^{n+1} \left(\int_{t_n}^{t_{fn}} \frac{A_f}{V_f} K_f \, dt + \int_{t_{fn}}^{t_{on}} \frac{A_o}{V_o} K_o \, dt + \int_{t_{on}}^{t_{cn}} \frac{A_c}{V_c} K_c \, dt + \int_{t_{on}}^{t_{con}} \frac{A_{co}}{V_{co}} K_{co} \, dt + \int_{t_{con}}^{t_s} \frac{A_s}{V_s} K_s \, dt \right) \quad (9.31)$$

where the subscripts f, o, c, co, s and n refer to formation, oscillation coalescence, cone, sheet and compartment number respectively.

Equation (9.31) may be simplified with the following assumptions,

1) The volumes of forming and coalescing drops are the same as d_{32} for oscillating drops, since, from experimental observations, little or no break-up or coalescence occurred during drop free travel, i.e., $\frac{V_f}{A_f} = \frac{V_c}{A_c} = \frac{V_o}{A_o} = \frac{V}{A}$

2) The increase in surface areas of the sheet and cone due to waves and ripples is small in magnitude and may be ignored. Hence a constant surface area may be assumed for the sheet and the cone. A specimen calculation showed in fact that an increase of less than 5% occurred in the mass transfer coefficient value, if these were assumed oscillating.

3) Time intervals concerned are of the same magnitude in the different compartments. This was proved by plotting concentrations vs. column height or residence time which gave straight lines.

With these simplifications Equation (9.31) becomes,

$$\int_{c_1}^{c_2} \frac{dc}{(c-c^*)} = n \left\{ \frac{A}{V} \left(K_f \int_0^{t_f} dt + K_o \int_0^{t_o} dt + K_c \int_0^{t_c} dt \right) + \frac{A_{co}}{V_{co}} K_{co} \int_0^{t_{co}} dt + \frac{A_s}{V_s} K_s \int_0^{t_s} dt \right\} \tag{9.32}$$

The individual mass transfer coefficients, K_f, K_o, K_c, K_{co} and K_s can be expressed using Equations 9.24 and 9.33, 9.34 or 9.35, summarised in Table 9.1.

TABLE 9.1

Basic Eqn. for mass transfer coefficient is given by,

$$K_D = \bar{k} \sqrt{\frac{D_{AD}}{\pi t_o}} \left[\frac{1}{1+m\sqrt{\frac{D_{AD}}{D_{AC}}}} \right]$$

$\frac{S(\tau)}{S_o}$	t_o	$\bar{k}$	Eqn.No.	Comments
1	-	$\frac{2}{\tau} \sqrt{\tau}$	9.33	For cone and sheet
$1+\beta\tau$	t_f or t_c	$\frac{2}{\tau} \sqrt{\tau+\beta\tau^2+\beta^2\frac{\tau^3}{3}}$	9.34	For forming or coalescing drops
$1+\varepsilon\sin^2\tau$	$\frac{1}{\pi\omega}$	$\frac{2}{\tau} \sqrt{(1+\varepsilon_o)\tau-\varepsilon_1\sin 2\tau+\varepsilon_2\sin 4\tau}$	9.35	For oscillating drops
		$\varepsilon_o = \varepsilon + {}^3/_8\,\varepsilon^2$	9.36	
		$\varepsilon_1 = {}^\varepsilon/_2 + \frac{\varepsilon^2}{4}$	9.37	
		$\varepsilon_2 = \frac{\varepsilon^2}{32}$	9.38	

The total transfer comprises the net effect of a large number of oscillations and complete cycles of formation and coalescence. Therefore the dimensionless mass transfer coefficients must be evaluated for a whole cycle, thus for formation and coalescence $\tau = 1$, since $t = t_f$ or t_c, and Equation 9.34 becomes

$$\bar{k} = 2\sqrt{1+\beta+\beta^2/3} \tag{9.39}$$

For a complete cycle of oscillation $\tau = \pi$ and Equation 9.35 becomes

$$\bar{k} = \sqrt{\frac{4(1+\varepsilon_o)}{\pi}} \tag{9.40}$$

where ε_o is given by Equation 9.36.

To evaluate ε, the amplitude of surface stretch requires a knowledge of the minimum and maximum surface areas of the drop. These were estimated from an analysis of high speed ciné films. The same technique was used to determine β the surface growth rate, which required the knowledge of size of the formed drop and t_f or t_c. The individual time intervals during which elements of the dispersed liquid were exposed were estimated as follows,

1) Formation time, t_f
2) Coalescence time, t_c

} From high speed ciné films analysis. The results are given in Appendix 6.

3) Exposure time on the sheet, t_s, by measuring the sheet volume V_s from still photographs. Since the total flow of the dispersed phase Q_D forms this sheet at the disc, then

$$t_s = \frac{V_s}{Q_D} = \frac{a}{Q_D}\left(d_L^2 + 2D.d_L \right) \frac{\pi}{4} \qquad (9.41)$$

where a is the sheet thickness

d_L is the sheet extent

D is the disc diameter

4) Exposure time on the cone, t_{co}; similar to t_s thus,

$$t_{co} = \frac{V_{co}}{Q_D} \qquad (9.42)$$

5) For oscillating drops, the exposure time, t_o, will be equal to the mean overall residence time minus the sum of the individual time intervals, mentioned above, in all compartments, i.e.,

$$t_o = \frac{V.x}{Q_D} - n\,(t_f + t_c + t_s + t_{co}) \qquad (9.43)$$

where V is the operating volume of the column,

x is the dispersed phase hold-up, and

n is the number of compartments.

The frequency of oscillation ω, was measured using high speed ciné films analysis.

For the case of hindered coalescence, i.e., involving solute transfer from the continuous to dispersed phase, Equation 9.32 may be used with only the oscillating drop term because of the absence of the other phenomena. Thus,

$$\int_{c_1}^{c_2} \frac{dc}{(c-c^*)} = \frac{A_{oo}}{V_{oo}} \cdot K_o \int_{t_1}^{t_2} dt \qquad (9.44)$$

The validity of the abowe expressions were tested against observed values, as discussed in Chapter 10. Computer programmes developed for these calculations aare given in Appendix 7.

10. DISCUSSION OF RESULTS

10.1 Non-Mass Transfer Studies

10.1.1 Hold-up

In general, hold-up increased with increasing dispersed phase flow rate with all the systems and designs used. The data obtained were lower, in some cases by as much as 50%, than those reported by other workers, e.g. (35). This may be partly attributed to the fact that this design had a different constriction factor, viz., C_R = 0.56 from the one used by the above mentioned author, viz., C_R = 0.49.

"Wetted" disc, viz. p.t.f.e.,and polypropylene cone columns gave lower hold-up values than the "non-wetted" disc columns. This was to be expected since coalescence was enhanced by the "wetted rotors" and thus larger drops with higher terminal velocities, were produced. The effect of rotor wettability on drop size is considered later (Section 10.1.3), but the general effects are shown in Figs. 8.1, 8.2 and 8.3.

The variation of hold-up along the column was as shown in Fig. 8.4, increasing to a maximum value at a point approximately midway up the column and subsequently decreasing. This is in agreement with the earlier findings of Rod (79) and Strand et al. (74). The accuracy of "point" hold-up values obtained in this study, were found to depend upon:-

(i) The position of the sampling tube. Ideally this should be at a point midway between the disc and the stator above it, and at a distance between S/2 and R/2 from the column wall (74).

(ii) Wettability of column internals and the sampling tube. More consistent results were obtained when these were not "wetted" by the

dispersed phase. More accurate results, still, may be possible using a material that is equally "wetted", by both phases, for the sampling tube. Some low surface energy metals exhibit such properties.

(iii) Quality of the dispersion. As anticipated homogeneous dispersions rather than those containing large drops and globules, gave more representative samples. Therefore, more accurate results were obtained with high rotor speeds, e.g., 1000 r.p.m., at conditions well below flooding or phase inversion.

On the basis of the above, and since average hold-up values do not differ greatly from the mean of the "point" hold-up values, it would appear that many practical difficulties can be avoided by considering the average rather than the "point" hold-ups. Contrary to this Strand et al. (74), Rod (79) and later Mumford (35) stressed the importance of "point" hold-up measurements for better mass transfer predictions. However, close examination of the data of the two former authors Figs. 3.6, 3.7 and 3.8 and that obtained in this study tends to support the argument proposed here. The Figures indicate that, excluding the top and bottom points, all points in the column had approximately equal hold-up values. The low values at the two extreme points are due to end effects, viz., the presence of larger drops with higher terminal velocities than that for the characteristic size in the rest of the column. Rod (79) suggested a design modification, as discussed in Section 3.2.1.1, to increase the hold-ups at these points. In any event, as will be shown later, whether "point" or average hold-ups are considered, they should be measured in the presence of mass transfer since in practice the characteristic drop size is dependent upon the mass transfer process. The direction of transfer is also important as discussed in Section 10.2.

Theoretically, hold-up profile would be expected to follow drop size profile. The data suggests, therefore that the characteristic drop size first decreased to a minimum value at a point corresponding to a maximum hold-up value and then increased towards the exit. This however was found not to be the case and the drop size decreased progressively up the column due to the increased number of impacts.

The "point" hold-up results can be reasonably correlated, as shown in Fig.10.1, by Equation 10.1. This expression was arrived at by means of simple extrapolation.

$$x = [0.0013\ N + 0.38\ (V_D - 1) - 1]\ (h - h^2) + 0.076\ (1 - \frac{1}{V_D}) \qquad (10.1)$$

where N, h and V_D are the r.p.m., column height and dispersed phase flow rate.

Finally, the effect of the continuous phase flow rate on hold-up measurements is shown in Fig.10.2. An increase in hold-up values occurred with increasing continuous phase flow rate. Clearly the reason for this was the increase in drop residence times caused by the continuous flow in the opposite direction.

10.1.2 Flooding

For the "non-wetted" discs column capacities were higher, in some cases by as much as 50%, than those obtained by other workers (35,72). This was probably due in part to the difference in design mentioned in Section 10.1.1. However, it may also be to the different criteria taken to characterise flooding.

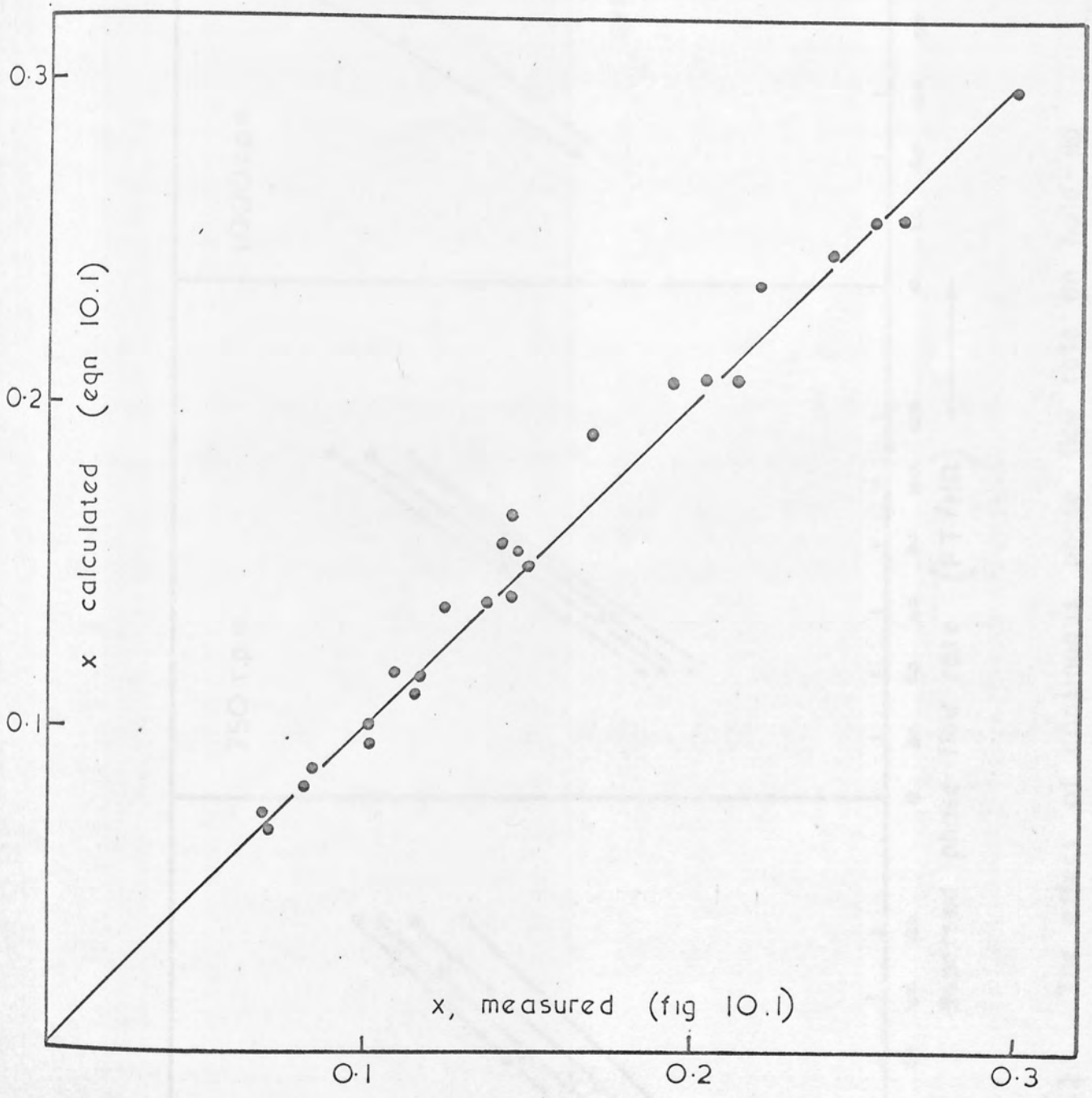

Fig. 10.1 Calculated vs measured point hold-up.

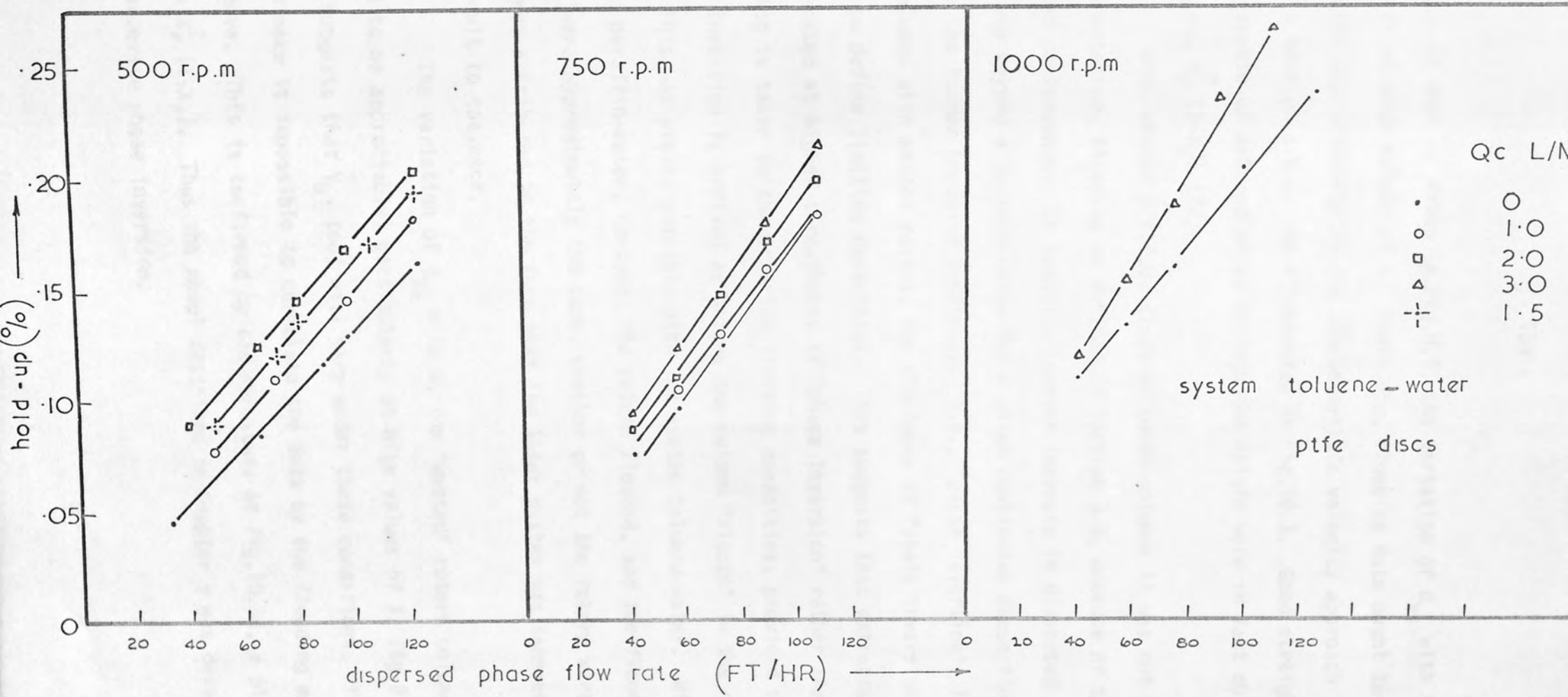

Fig. 10.2. The effect of continuous phase flow rate on hold – up

As was shown in Fig.8.9, the variation of d_{vs} with x was small at high values of x. Therefore, flooding data ought to be correlated approximately by the characteristic velocity approach (72), given in Section 3.2.2. As illustrated in Fig.10.3. Good straight lines capable of extrapolation through the origin were in fact obtained for V_D vs. $X_f^2 (1-X_f)$ (72).

With either p.t.f.e. discs or cones columns it was not possible to characterise, flooding as defined in Section 3.3, because of the enhanced coalescence. In practice however increase in dispersed phase flow rate beyond a certain value for a given continuous phase flow rate led to the former becoming continuous, i.e., "phase inversion". Therefore for columns with wetted rotors, the phenomena of "phase inversion" was taken to define limiting capacities. This suggests that extractors can be operated at higher throughputs if "phase inversion" rather than flooding is taken to characterise limiting capacities, provided of course phase inversion is arrived at before the column "floods" in the normal way. This was proved possible with the system toluene-water. With liquid paraffin-water, however, the column flooded, and the flooding rates were approximately the same, whether or not the rotors were "wetted". This was attributed to the fact that the later system was inherently difficult to coalesce.

The variation of d_{32} with X, for "wetted" rotors columns was found to be appreciable, particularly at high values of X, Fig.8.10. This suggests that $\bar{V}_N$, too, will vary under these conditions. This would make it impossible to correlate the data by the flooding equations as above. This is confirmed by the curvature of Fig.10.3d, a plot of V_D vs $X_f^2 (1-X_f)$. Thus the model described in Chapter 9 was developed to characterise phase inversion.

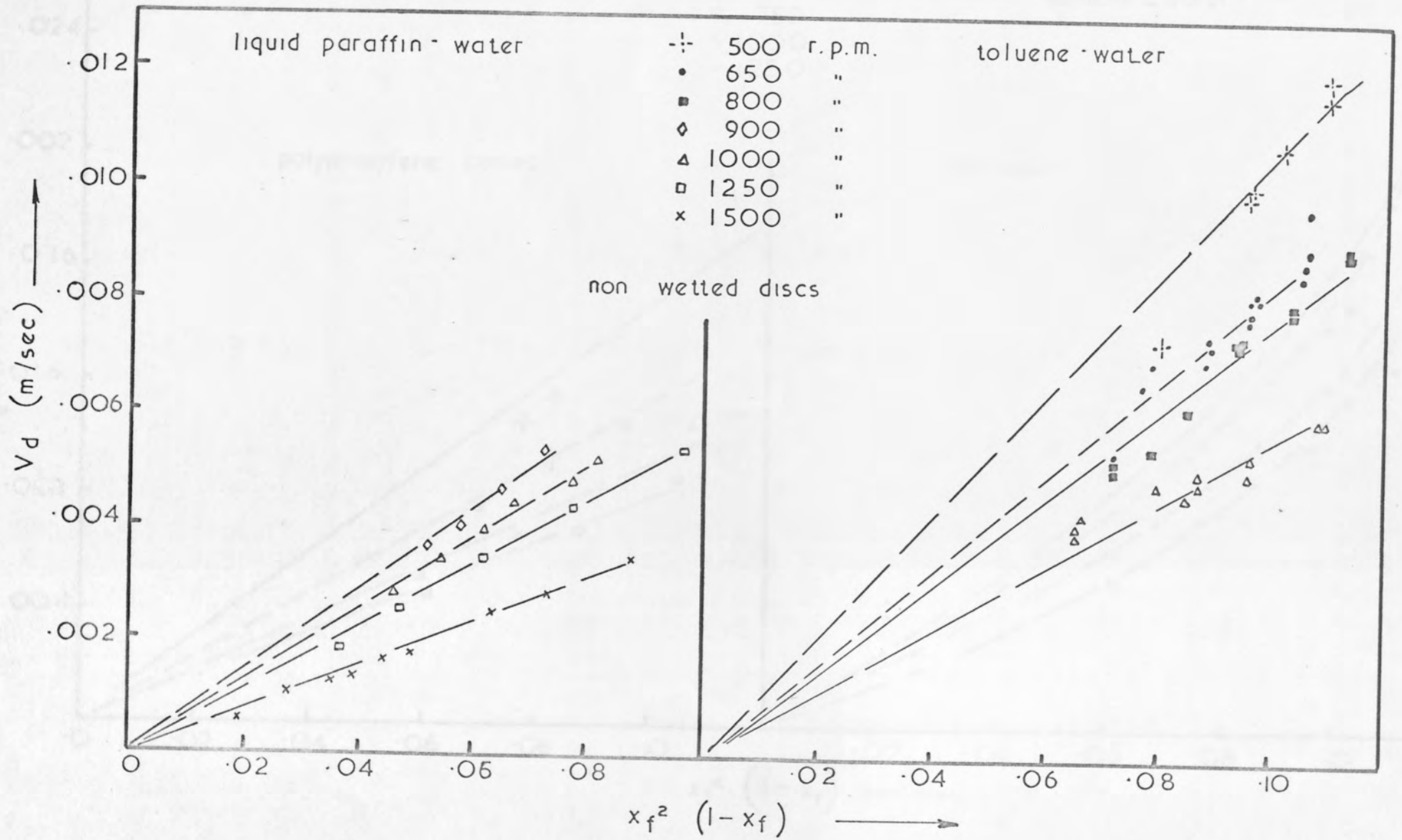

Fig. 10.3 Correlation of flooding data

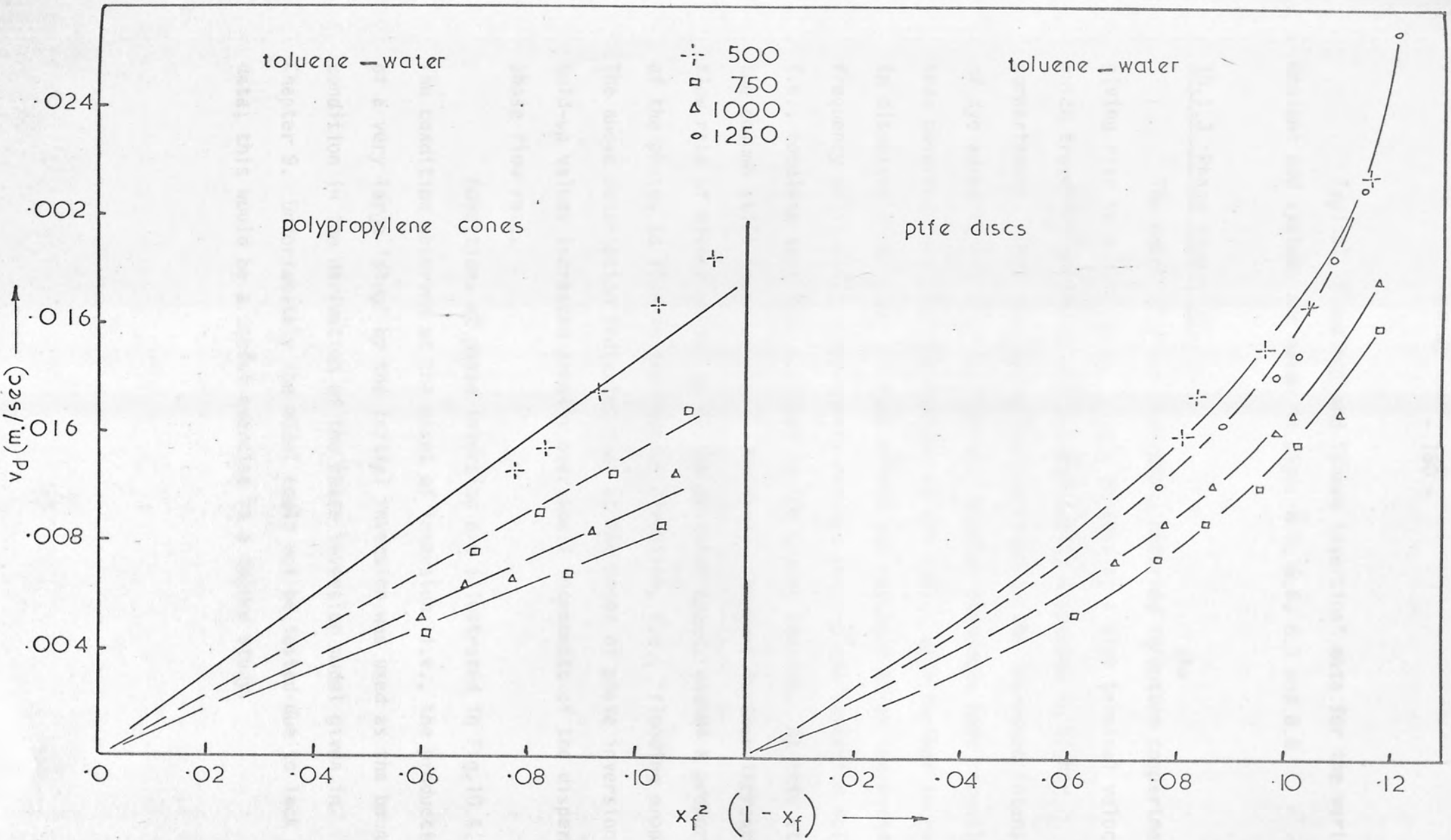

Fig 10·3 continued

Typical "flooding" and "phase inversion" data for the various designs and systems are given in Figs. 8.5, 8.6, 8.7 and 8.8.

10.1.3 Phase inversion

The onset of phase inversion, occurred in the bottom compartment giving rise to a very large 'slug', possessing a high terminal velocity, which travelled up the column and eventually dispersed in higher compartments. This phenomenon was indicated by the increased intensity of dye added to the dispersed phase. Similar phenomena have recently been observed in an Oldshue-Rushton column (37). With further increase in dispersed phase flow the same effect was repeated at an increased frequency until other compartments reached their phase inversion hold-ups, i.e., complete inversion obtained in the mixing section. At this stage the column still operated countercurrently. However further increase in flow rate of either phase, or of the agitator speed, caused a proportion of the phases to flow in the reverse direction, i.e., 'flooding proper'. The above description indicates that at the onset of phase inversion hold-up values increased greatly over small increments of the dispersed phase flow rate.

Conditions at phase inversion are illustrated in Fig.10.4. The condition observed at the onset of inversion, i.e., the production of a very large 'slug' by the initial inversion was used as the boundary condition in the derivation of the phase inversion model given in Chapter 9. Unfortunately the model could not be tested due to lack of data; this would be a useful exercise in a future study.

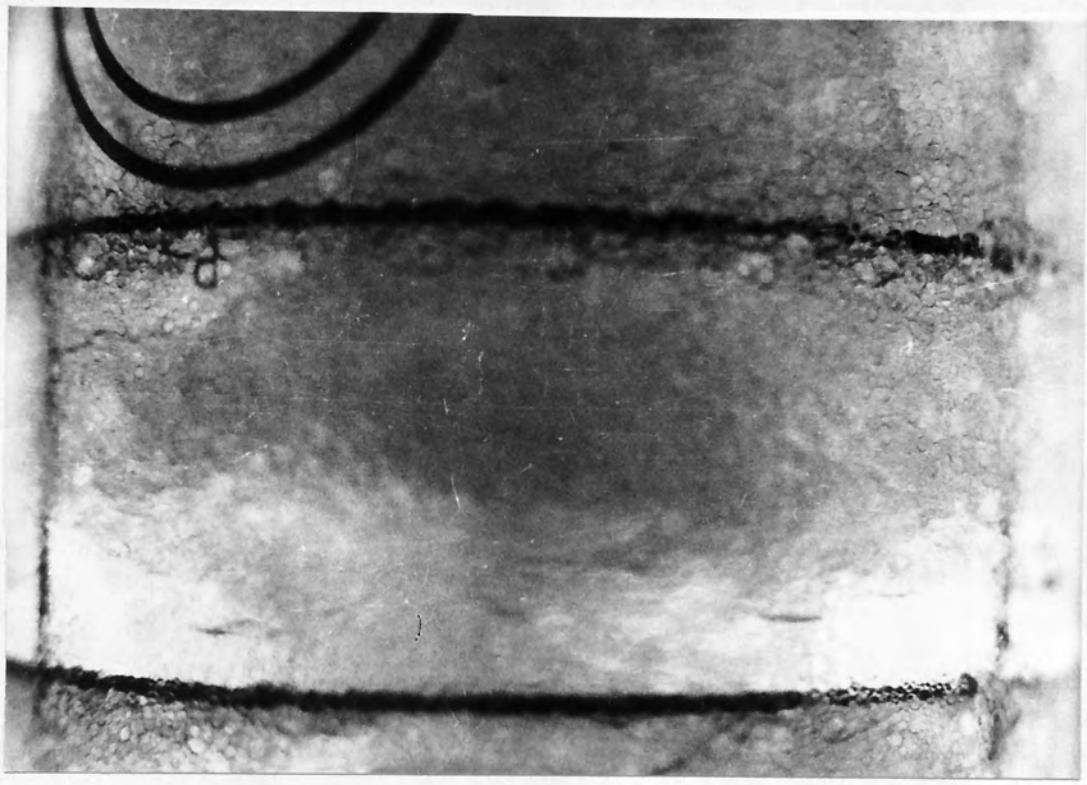

Fig.10.4 Onset of Phase Inversion

(Toluene-Water, 1000 rpm.,

Q_c = 2 Litre/Min, Q_d = 6 Litre/Min).

Toluene was initially dispersed

10.1.4 Mechanisms of Droplet Break-Up and Drop Size Distribution

Generally, droplet break-up on the "non-wetted" disc occurred as described in Section 3.3.2, viz., by a discrete drop undergoing deformations and finally break-up due to velocity gradients at the tip of the disc. At low rotor speeds, e.g., Re < 2.15×10^4, few drops were observed to break-up, by collision with the edge of the stator.

With the "wetted" discs and cones, drops coalesced on the "wetted" rotor surface and redispersion followed by two different mechanisms, similar to those described in Section 5.3.2.3 due to Hinze (100) and Dombrowski et al. (199). These were,

(i) drip point, which occurred at the rotors tip, at dispersed phase flow rates approximately < 0.1 $cm\,s^{-1}$.

(ii) from the periphery of the sheet; this generally occurred at dispersed phase flow rates > 0.1 $cm\,s^{-1}$.

Whilst this was true for the "easy coalescing" system, toluene-water, (σ = 34.1 dynes/cm and μ_d = 0.6 c.p.), discrete drop break-up at the disc's tip was the predominant mechanism with the more "difficult coalescing" system, viz liquid paraffin-water, irrespective of the wetting characteristics of the rotor. However, with p.t.f.e. discs, little of the liquid paraffin coalesced on the disc, particularly at low rotor speeds, viz. Re < 2.5×10^4, so that drip point formation occurred. At higher rotor speeds increased hold-up, prevented visual observation.

Other systems used in this section of the work are listed in Table 7.1.

The variation of drop size with column height is illustrated in Figs.8.11 and 8.12. Contrary to the results for axial hold-up profile,

d_{32} decreased with increasing column height. This discrepancy may be due to end effects. On balance, drop size results are considered to be the more reliable, since as explained in Section 10.1.1, the low hold-up values for the end points were attributed to the sample locations being adjacent to the phase entry and exit positions.

Experimental values of d_{32} shown in Section 8.1.4, were compared with those obtained using the correlations of Misek (33), discussed in Section 3.3.2. Although all experimentation was in the transition region, for which $10^4 < Re < 6 \times 10^4$, all three correlations were considered. None of the correlations gave reasonable agreement with experimental d_{32} values. In general d_{32} values were much greater than the drop size values obtained from Equations 3.25 and 3.26, for the turbulent and transition regions respectively, and much smaller than those obtained by the laminar region correlation, Equation 3.27.

The poor performance of these correlations was not surprising since they take no account of the variation of d_{32} with column height, dispersed phase flow rate and hold-up. Therefore a correlation, for d_{32}, was developed to take account of these factors considering d_{32} as a function of the physical properties of the system, the operating conditions and the column geometry,

$$d_{32} = \phi\ (N, V_d, V_c, X, \mu_d, \mu_c, \rho_d, \rho_c, \sigma, R, S, H, n, D) \quad (10.2)$$

where the notation is given in the nomenclature.

Only the relevant groups described in the literature as governing the drop size in agitated tanks need be considered, and Equation 10.2 arranged in terms of dimensionless groups. It was assumed firstly that the effect of

column height was exponential, i.e., $e^h = 1$, at $h = 0$. For h, to be dimensionless, h/h_{Tot} was considered or n/Z where n, is the compartment number and Z, is the total number of compartments. The expression then has the form

$$d_{32} = k \left(\frac{NR^2\rho_c}{\mu_c}\right)^a \left(\frac{\mu_d}{\mu_c}\right)^b \left(\frac{NR\mu_c}{\sigma_i}\right)^c (x)^d \quad EXP.[e(n/z)] \qquad (10.3)$$

In order to evaluate the numerical constant k and the powers, the dimensionless groups were calculated and fitted by the Least Square Method. The Gauss-Jordan elimination method was used to find the values of k, a, b, c etc., using a digital computer. The various computer programs developed are given in Appendix 7.

Three different correlations were obtained for the various columns,

For the "non-wetted" discs column

$$\frac{d_{32}}{R} = 4.7 \times 10^{17} \left(\frac{NR^2\rho_c}{\mu_c}\right)^{-3.33} \left(\frac{\mu_d}{\mu_c}\right)^{0.23} \left(\frac{NR\mu_c}{\sigma_i}\right)^{2.0} (X)^{0.225}$$

$$EXP\left[0.40\left(\frac{n}{z}\right)\right] \qquad (10.4)$$

The other two correlations for the wetted disc and cone columns are given with the drop size data in Appendix 8.

The best agreement with experimental d_{32} values were obtained by Equation 10.4, probably due to the number of data points used, for this case 92. For the "wetted" discs 50 data points were used and for the cone column only 18 data points were available. Data were correlated to within 20% by Equation 10.4, as shown in Fig.10.5.

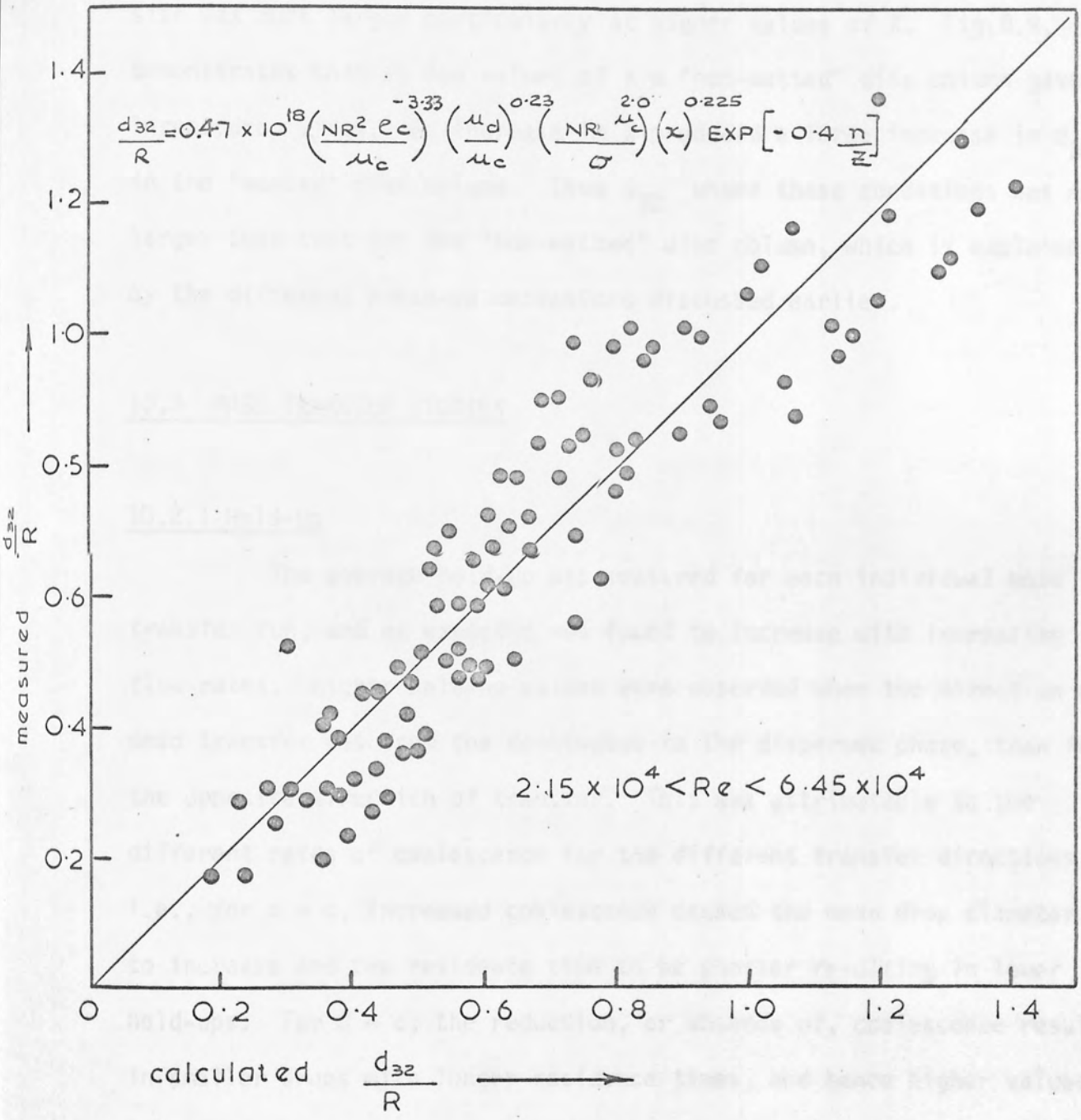

Fig. 10.5 Drop size correlation for a non-wetted disc column.

Typical results for the variation of d_{32} with X are shown in Figs.8.9 and 8.10. For the non-wetted discs column d_{32} increased gradually with X. For "wetted" rotor columns the increase in drop size was much larger particularly at higher values of X. Fig.8.9, demonstrates that at low values of X a "non-wetted" disc column gave larger drop sizes. An increase in X produced a large increase in d_{32} in the "wetted" disc column. Thus d_{32} under these conditions was much larger than that for the "non-wetted" disc column, which is explained by the different break-up mechanisms discussed earlier.

10.2 MASS TRANSFER STUDIES

10.2.1 Hold-Up

The average hold-up was measured for each individual mass transfer run, and as expected was found to increase with increasing flow rates. Higher hold-up values were observed when the direction of mass transfer was from the continuous to the dispersed phase, than for the opposite direction of transfer. This was attributable to the different rates of coalescence for the different transfer directions, i.e., for d → c, increased coalescence caused the mean drop diameter to increase and the residence time to be shorter resulting in lower hold-ups. For d ← c, the reduction, or absence of, coalescence resulted in smaller drops with longer residence times, and hence higher values of hold-up.

Clearly, therefore, hold-up values obtained under non-mass transfer conditions ought not be used to predict practical values during mass transfer. However, for the case d ← c, hold-up values are only

about 10-15% higher than those for non-mass transfer runs. Hold-up values obtained for d → c were in most cases about half those obtained for non-mass transfer runs. The above findings were generally, the same irrespective of the rotor's wetting properties. This suggests that, the different break-up mechanisms and behaviour of droplets resulting from the different directions of mass transfer override the effects of rotor wettability.

10.2.2 Flooding

Flooding rates for the case d → c were higher than or similar to those for non-mass transfer runs. Whilst for d ← c lower flooding rates were obtained. The reasons for this are given in Section 10.2.1.

Typical results are reproduced in Fig.8.13.

10.2.3 Mechanisms of Droplet Break-Up and Drop Size Distribution

From visual and photographic observations, the mechanisms of droplet break-up was, for all practical purposes, independent of the rotor's wetting properties, but strongly dependent upon the direction of mass transfer. Break-up was by sheet or drip point formation for the case d → c and by discrete drop break-up at the tip of the disc for d ← c. This was most obvious with the toluene-Acetone-water system. Though less obvious for liquid paraffin-M.E.K.-water system increased coalescence was detected for the case d → c, by the reduction of axial mixing. Axial mixing was present in non-mass transfer runs and was worsened by transfer in the direction liquid paraffin ← water.

The different mechanisms of droplet break-up are illustrated in Fig.8.14.

Values of d_{32}, for non-mass transfer runs, were, generally, larger than those for the case d ← c, and lower than those for d → c. This was expected and can again be attributed to the reduction, or absence of, coalescence in the former case and its increase in the latter.

10.2.4 Correlation of Mass Transfer Data

The experimental data were interpreted in terms of an overall mass transfer coefficient, K_{EXP}. This was then compared with theoretical values assuming either,

(i) Stagnant drops - K_s,

(ii) Circulating drops - K_c,

(iii)Oscillating drops (surface stretch model) - K_o,

or (iv) The fresh surface model (157).

The diffusivities used in the various models were calculated by the Wilke-Chang (230) correlation. Although this has not been tested for high viscosity liquids, e.g., liquid paraffin it is considered to be the most reliable correlation.

For the case of vortex, sheet and continuous drop formation and coalescence, viz T → W, in the disc column the detailed expression, assuming surface stretch, (Section 9.2) was used. A similar expression using the fresh surface model may be obtained thus:-

For forming and coalescing drops the expression is obtained by substituting the time dependent surface area given by,

$$S(t) = S_o(1+\beta t) \tag{9.25}$$

into the fresh surface expression (157) which may be written, thus,

$$\bar{k} = \frac{2}{\tau} \int_o^\tau \frac{S(t)/S_o}{(\tau-t)^{1/2}}\, dt \tag{10.7}$$

and integrating. The dimensionless mass transfer coefficient is then (99),

$$\bar{k}_f = [\frac{2}{\sqrt{\tau}} + \frac{4}{3}\ \beta\sqrt{\tau}] \tag{10.8}$$

For oscillating drops substitution of the surface-time relation,

$$S(t) = S_o(1 + \varepsilon \sin^2 \tau) \tag{4.23}$$

in Equation (10.7) yields,

$$\bar{k}_o = \frac{2}{\tau}\int_o^\tau \frac{(1+\varepsilon \sin^2 \tau)}{(\tau-t)^{1/2}} \tag{10.9}$$

Evaluation of this expression required graphical integration; the final expression has the form,

$$\bar{k}_o = [\frac{2}{\sqrt{\pi}} + 0.43\ \varepsilon] \tag{10.10}$$

Values of the overall mass transfer coefficient K_d, obtained using the fresh surface model were similar to those obtained using the surface

stretch model, and the deviation between the two values was not more than 5% in all cases. Furthermore, for the system toluene-acetone-water, the circulating drop model gave values similar in magnitude to those obtained assuming surface stretch, i.e., oscillating drops as shown in Figs.10.6 and 10.7. These findings are similar to those obtained earlier by Angelo et al. (99). They are however contrary to the results reported by Strand et al. (74) who used the system toluene-acetone-water, with a dispersed toluene feed, in two RDC columns of 6 and 42 inches diameter and found that the coefficient corresponded to that for stagnant drops. This disagreement is due to the fact that values of d_{32} reported for the latter study were much smaller than those observed here. The range of d_{32} is comparable to the range of d_{max} in Strand's work. Small drops have a tendency to reduced internal mobility; as shown in Fig.IX in Appendix 6 drops cease to oscillate below d = 1.8 mm.

The stagnant drop coefficient in the present study was between 4 and 200 times smaller than K_{exp} for both systems used in all the columns. The oscillating drop coefficient varied between 1.1 and 34 times K_{exp} for the system liquid paraffin-MEK-water irrespective of transfer direction. This wide range may be because the "difficult coalescing" drops of high viscosity, persist as small discrete drops which are more likely to circulate or be stagnant than oscillate; with the second system, viz., toluene-acetone-water larger drops were produced. Thus the oscillating drop coefficient K_o, was in this case closer to K_{exp}.

This is demonstrated in Figs.10.6 and 10.8, which also show that, particularly in the disc columns, the values of K_{exp}/K_o are greater in the case T → W than T ← W. This may be attributable to the surface area estimation by photography, which may not give accurate representation

△ cone column

○ non wetted disc column

□ wetted disc column

empty symbols dispersed → continuous

solid symbols continuous → dispersed

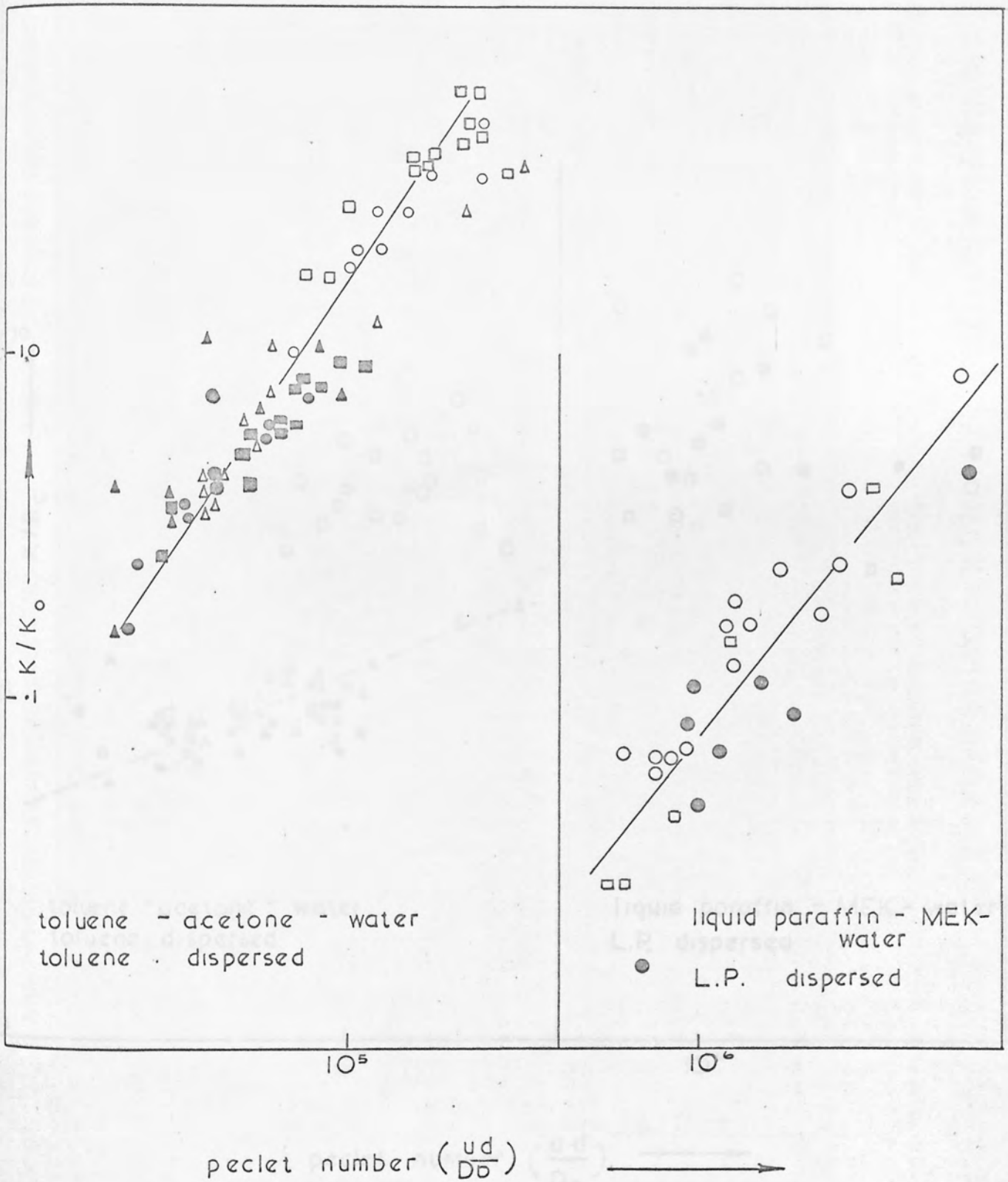

Fig. 10.6 Correlation of oscillating drop mass transfer coefficient

△ cone column
○ non wetted disc column
□ wetted disc column

empty symbols dispersed → continuous
solid symbols continuous → dispersed

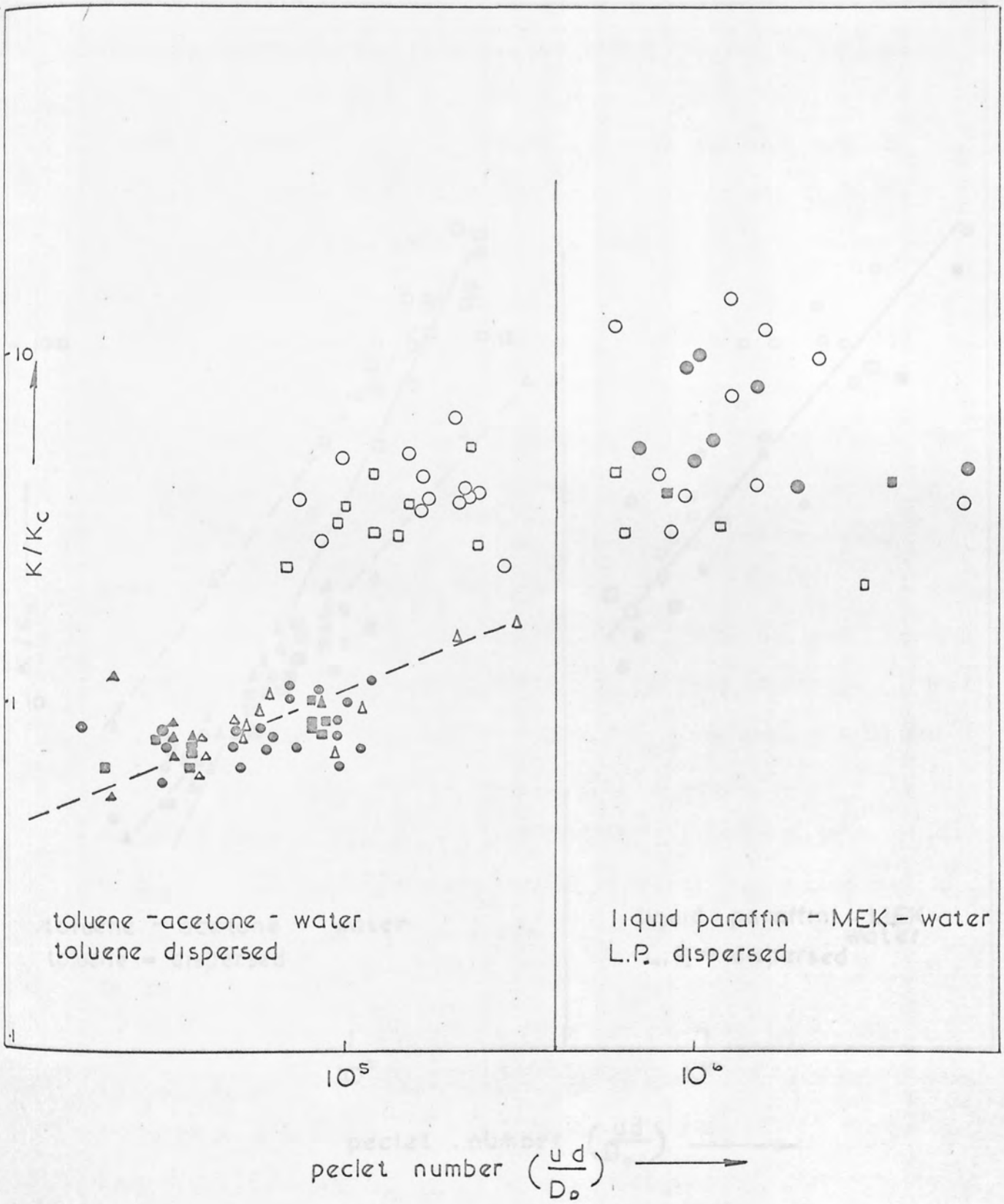

Fig. 10. 7. Correlation of circulating drop mass transfer coefficient

△ cone column

○ non - wetted disc column

□ wetted disc column

empty symbols : dispersed → continuous

solid symbols : continuous → dispersed

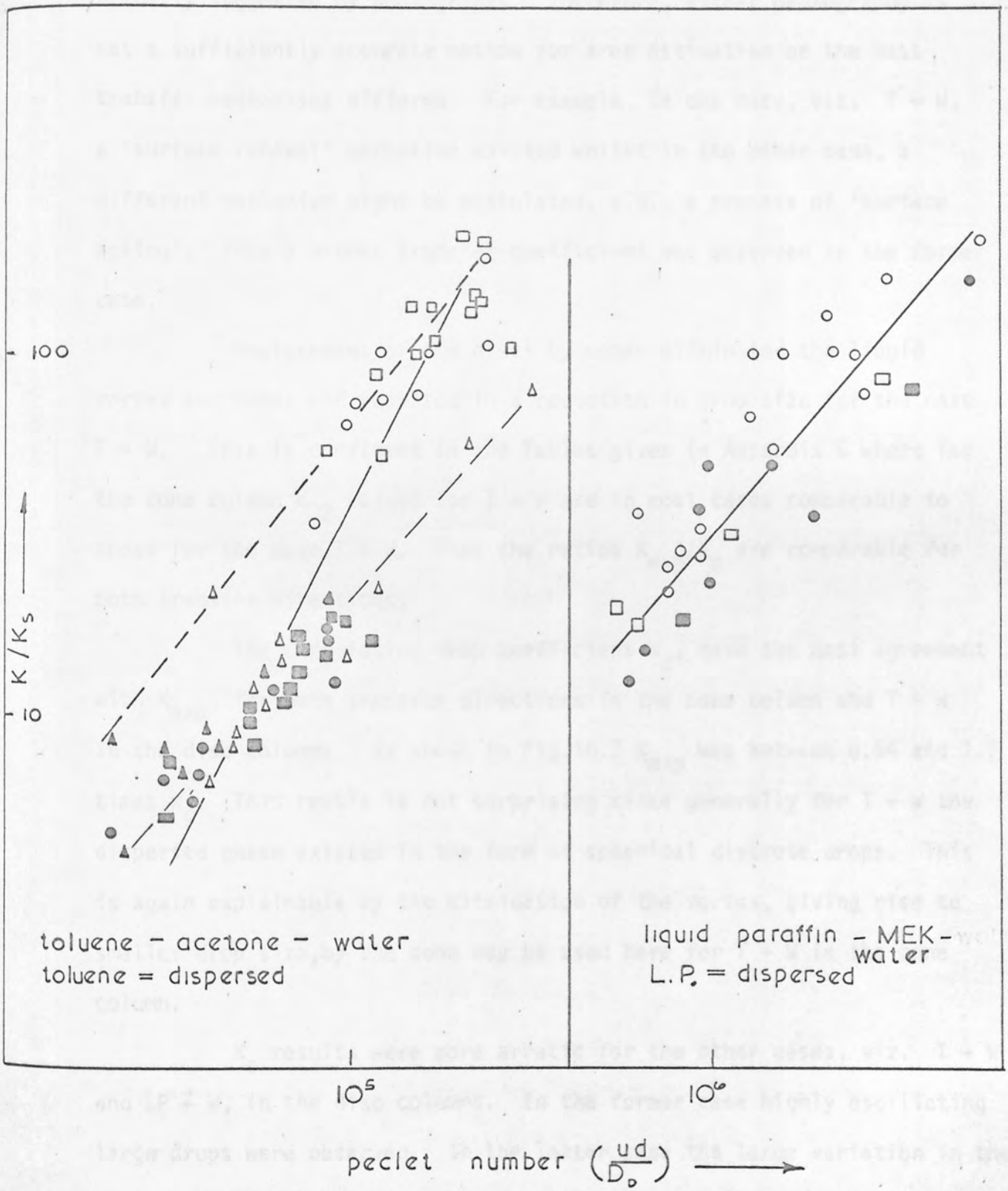

Fig. 10.8. Correlation of stagnant drop mass transfer coefficient

of the effective transfer area. Dependent upon the mechanism of mass transfer the effective interfacial area may be larger or smaller than actually suggested by photographs. Therefore, either photography is not a sufficiently accurate method for area estimation or the mass transfer mechanisms differed. For example, in one case, viz. T → W, a 'surface renewal' mechanism existed whilst in the other case, a different mechanism might be postulated, e.g., a process of 'surface ageing'. Thus a higher transfer coefficient was observed in the former case.

Replacement of the discs by cones eliminated the liquid vortex and sheet and resulted in a reduction in drop size for the case T → W. This is confirmed in the Tables given in Appendix 6 where for the cone column d_{32} values for T → W are in most cases comparable to those for the case T ← W. Thus the ratios K_{exp}/K_o are comparable for both transfer directions.

The circulating drop coefficient K_c, gave the best agreement with K_{exp}, for both transfer directions in the cone column and T ← W in the disc columns. As shown in Fig.10.7 K_{exp} was between 0.54 and 1.7 times K_c. This result is not surprising since generally for T ← W the dispersed phase existed in the form of spherical discrete drops. This is again explainable by the elimination of the vortex, giving rise to smaller drop size, by the cone may be used here for T → W in the cone column.

K_c results were more erratic for the other cases, viz. T → W and LP $\overset{\rightarrow}{\leftarrow}$ W, in the disc columns. In the former case highly oscillating large drops were observed. In the latter case the large variation in the drop viscosity along the column may have influenced K_c, which contains a viscosity term, although particular care was taken to estimate a mean

value of μ_d for each run [The variation of μ_d with MEK concentration in liquid paraffin is given in Fig.VI in Appendix 4, which shows that μ_d varies from 170 to 24 c.p. for a change in concentration from 0 to 10% by weight].

Both the stagnant drop and oscillating drop coefficients varied linearly with the Peclet number as shown in Figs.10.6 and 10.8. Clearly the results obtained will only be valid for similar conditions, viz. systems and the ranges of d_{32} and Peclet number covered.

Finally, the expression developed in Section 9.2, to account for all contributions to mass transfer from forming, coalescing and discrete drops, liquid vortex and sheet, did not show any improvement over the use of the discrete drop assumption. This was rather to be expected since the same models involving surface stretch or fresh surface, were used for all five processes, viz. formation coalescence, etc...., resulting in the calculated mass transfer coefficients for those processes being of similar magnitudes. However, the amount of solute transferred varied. In general Equation 9.29 suggested that in each cycle,

Mass transfer during drop formation was 15-18% of the total
" " " free rise " 46-50% " " "
" " " drop coalescence " 3-4% " " "
" " from the vortex " 6-8% " " "
" " from the sheet " 23-27% " " "

These values correspond to the contact time t, and the specific surface area a. Therefore the high values during free rise and sheet formation are due to these having the highest t and highest a respectively whilst the small values during coalescence and from the vortex correspond to their low t and a values respectively.

Wetting Effect

It is concluded from the above that, under practical conditions, the rotor "wettability" had no significant effect upon mass transfer efficiency. This is confirmed by Figs.10.6, 10.7 and 10.8 above in which the mass transfer coefficients for wetted and non-wetted rotors are of similar magnitude under given conditions. This conclusion is supported by the values of efficiency given in the Tables in Appendix 6. Although for the purpose of performance comparison, the index of effectiveness, I_e

$$I_e = \frac{\text{total throughput}}{\text{volume of one theoretical stage}}$$

is recommended (76), the use of efficiency was justified in this case since the columns were of the same basic design and capable of handling, essentially, similar throughputs.

However at rotor speeds well below the practical range, viz. < 300 rp.m., the drops coalesced with and then broke off the wetted discs. This phenomenon, illustrated in Fig.10.9 may have been the cause of some misleading expectations (35) at higher speeds where the short contact time between the drop and disc does not allow coalescence to take place.

Direction of Mass Transfer

Two different operating mechanisms were observed in the column dependant upon the direction of mass transfer. With transfer dispersed → continuous phase, coalescence was promoted giving rise to vortex and sheet formation and hence conditions of repeated coalescence

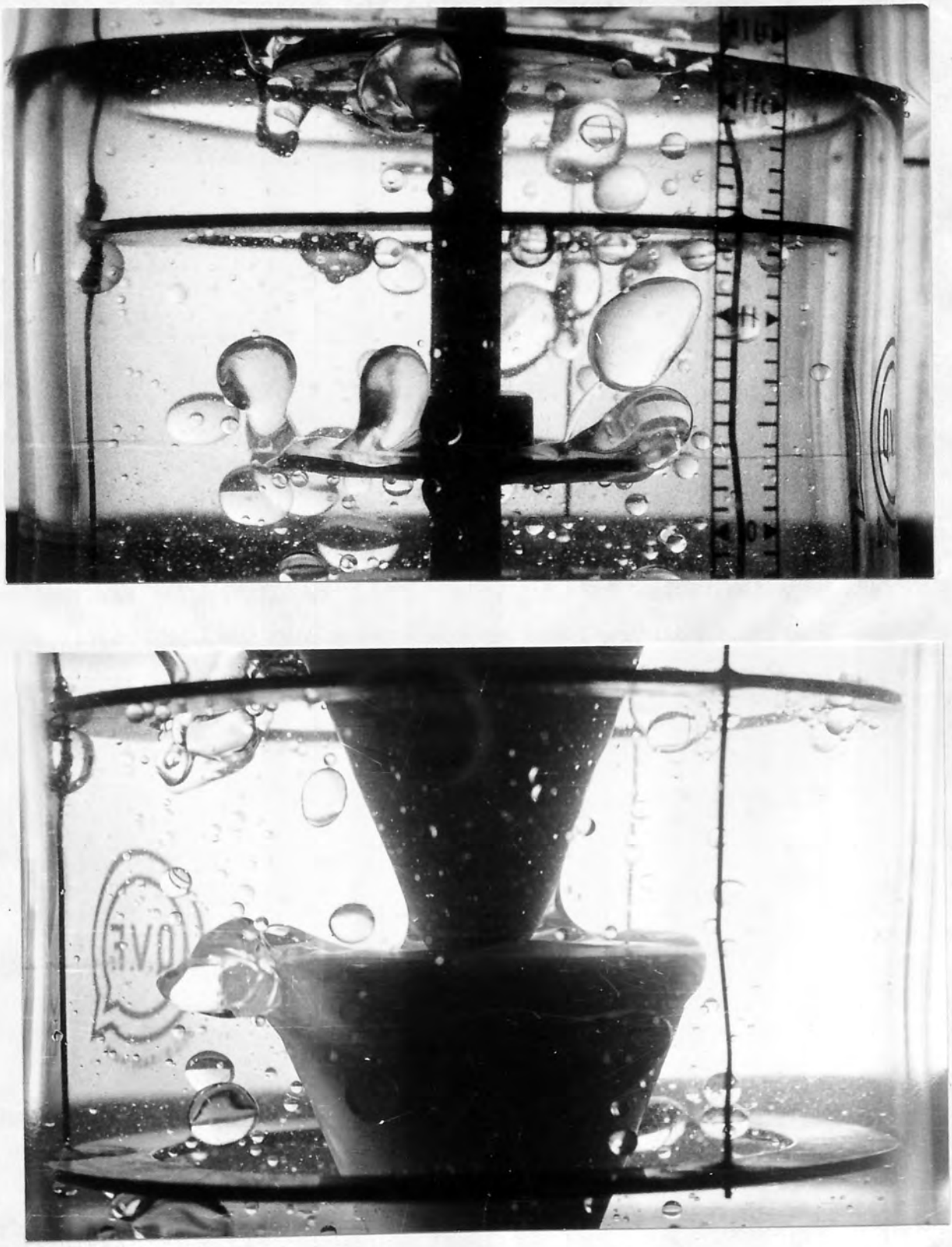

Fig.10.9 Illustration of Wetting Effect on Drop Formation At Low Rotor Speeds (250 rpm).

Top Plate: Ptfe Disc

Bottom Plate: Polypropylene Cone

and redispersion. For the opposite direction of transfer, i.e., continuous → dispersed phase, coalescence was greatly reduced and the column operated as a discrete drop contactor. The two different operating mechanisms are illustrated in Figs.8.14 and 10.10. The effect of transfer direction on coalescence caused by the change in interfacial gradient, i.e., coalescence is reduced or promoted dependent upon whether this gradient is negative or positive (126) was discussed in Section 3.3.4.3. Vortex and sheet formation was only observed in the case of the "easy coalescing" system, toluene-acetone--water. In the case of the "difficult coalescing" system, liquid paraffin-MEK-water, vortex and sheet formation did not occur. However, the increase in coalescence for the case L.P. → W was detected by the substantial reduction in axial mixing and entrainment which occurred under non-mass transfer conditions and with the opposite direction of transfer. The above findings may be of practical significance since axial mixing can be substantially reduced by the appropriate choice of which phase is dispersed, and the direction of mass transfer.

The Effect of Column Height on Efficiency

The column was operated at various effective heights and as expected mass transfer efficiency increased with increasing number of compartments as shown in Fig.10.11.

10.3 Other Studies

10.3.1 Mechanisms of Droplet Break-Up for Wetted and Non-Wetted Discs

With both wetted and non-wetted discs, droplet break-up

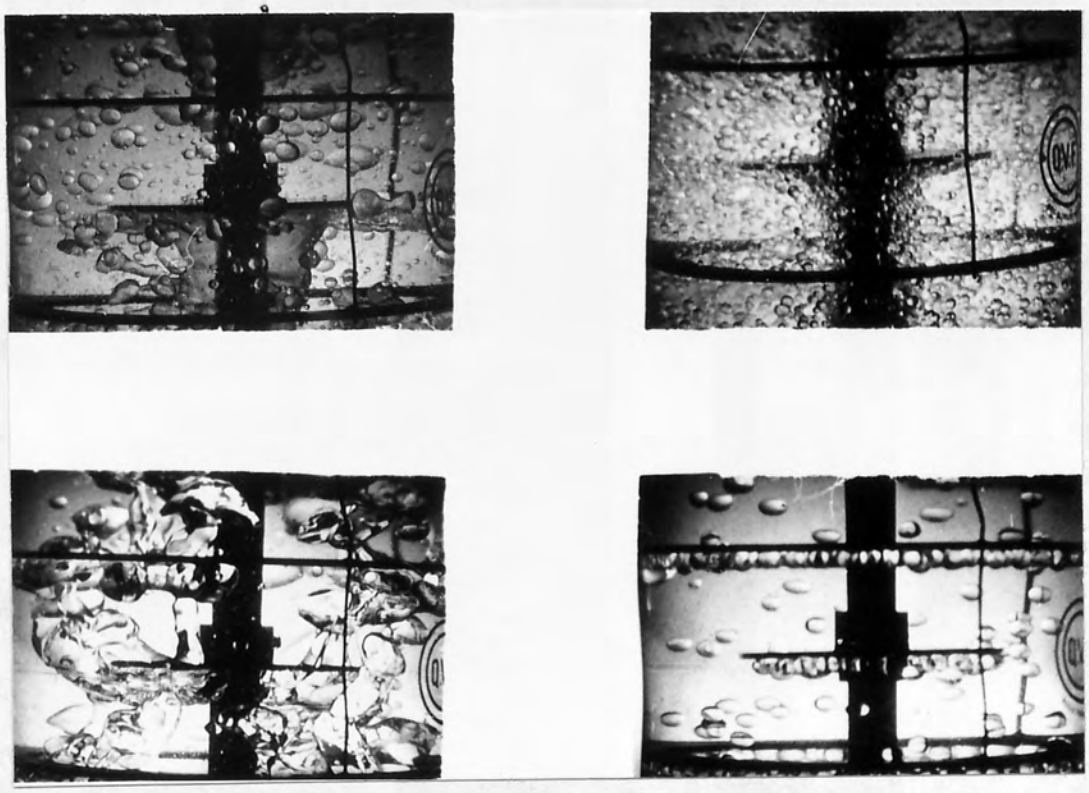

Fig.10.10 Effect of Mass Transfer Direction on Column Behaviour

Top Left: T → W, 1000 rpm. Top Right: T ← W, 1000 rpm.

Bottom Left: T → W, 0 rpm. Bottom Right: T ← W, 0 rpm.

o 1000 r.p.m.

x 750 ..

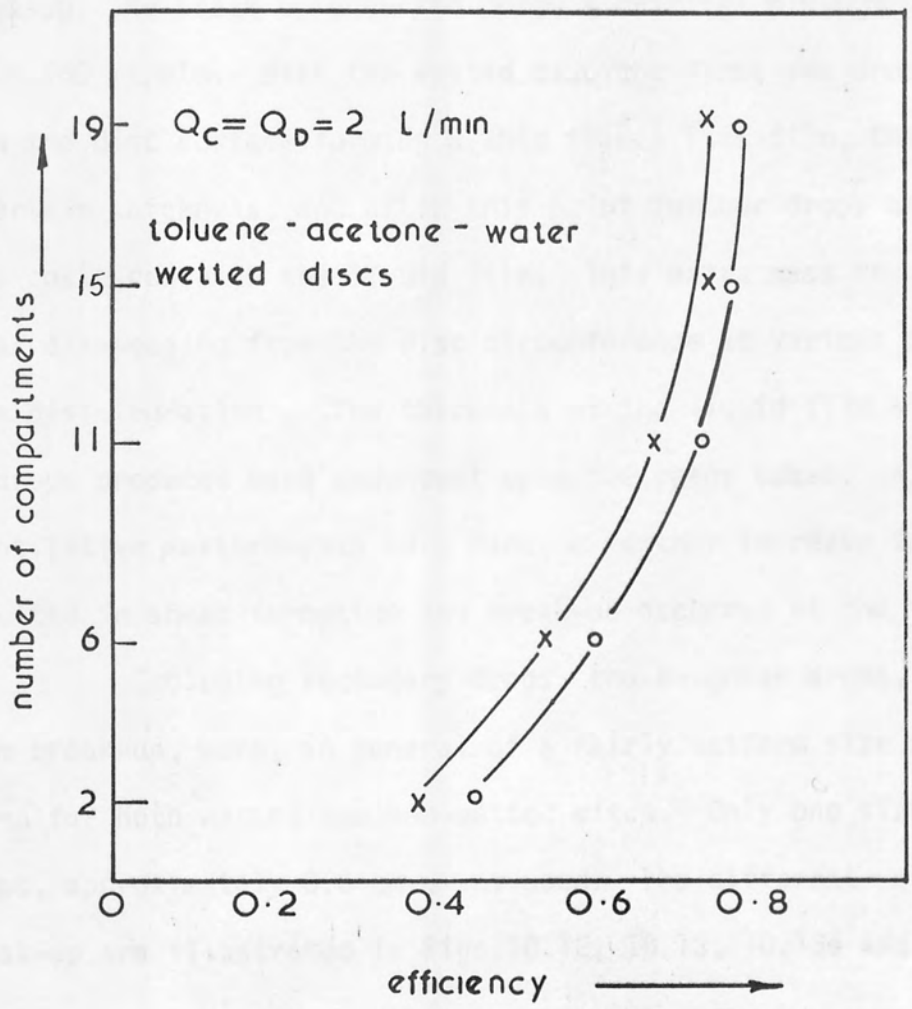

Fig. 10.11 Effect of number of compartments on mass transfer efficiency.

occurred at the disc tip, corresponding with the largest velocity gradients. However, the actual mechanism of break-up differed. With the non-wetted disc the drops of heavy dispersed phase arrived at the disc upper side and bounced along the surface as they travelled towards the disc tip where they underwent first, deformation and then break-up. No break-up occurred below a critical minimum speed, viz. πNR = 260 ft/min. With the wetted disc the first few drops coalesced with the disc surface forming a thin film. This film, then, reached a certain thickness, and after this point further drops arriving at the disc coalesced with the liquid film. This extra mass resulted in small drops disengaging from the disc circumference at various points, i.e., 'rim disintegration'. The thickness of the liquid film and the sizes of drops produced were dependent upon the rotor speed. Although no quantitative measurements were made, a further increase in flow rate resulted in sheet formation and break-up occurred at the free edge.

Excluding secondary drops, the daughter drops, resulting from break-up, were, in general of a fairly uniform size at any given speed for both wetted and non-wetted discs. Only one size of mother drops, approximately 0.6 cm., was used. The different mechanisms of break-up are illustrated in Figs.10.12, 10.13, 10.13a and 10.13b.

10.3.2 Interfacial Turbulence and Single Drop Mass Transfer

The phenomena of mass transfer from forming, discrete and coalescing drops was observed using the optical system described in Section 7.6.4, and the system dibutylphthalate/(MEK)→Water. Although the use of a high concentration driving force, viz. approximately 10% and 0% by volume in the drop and continuous phase respectively, is a

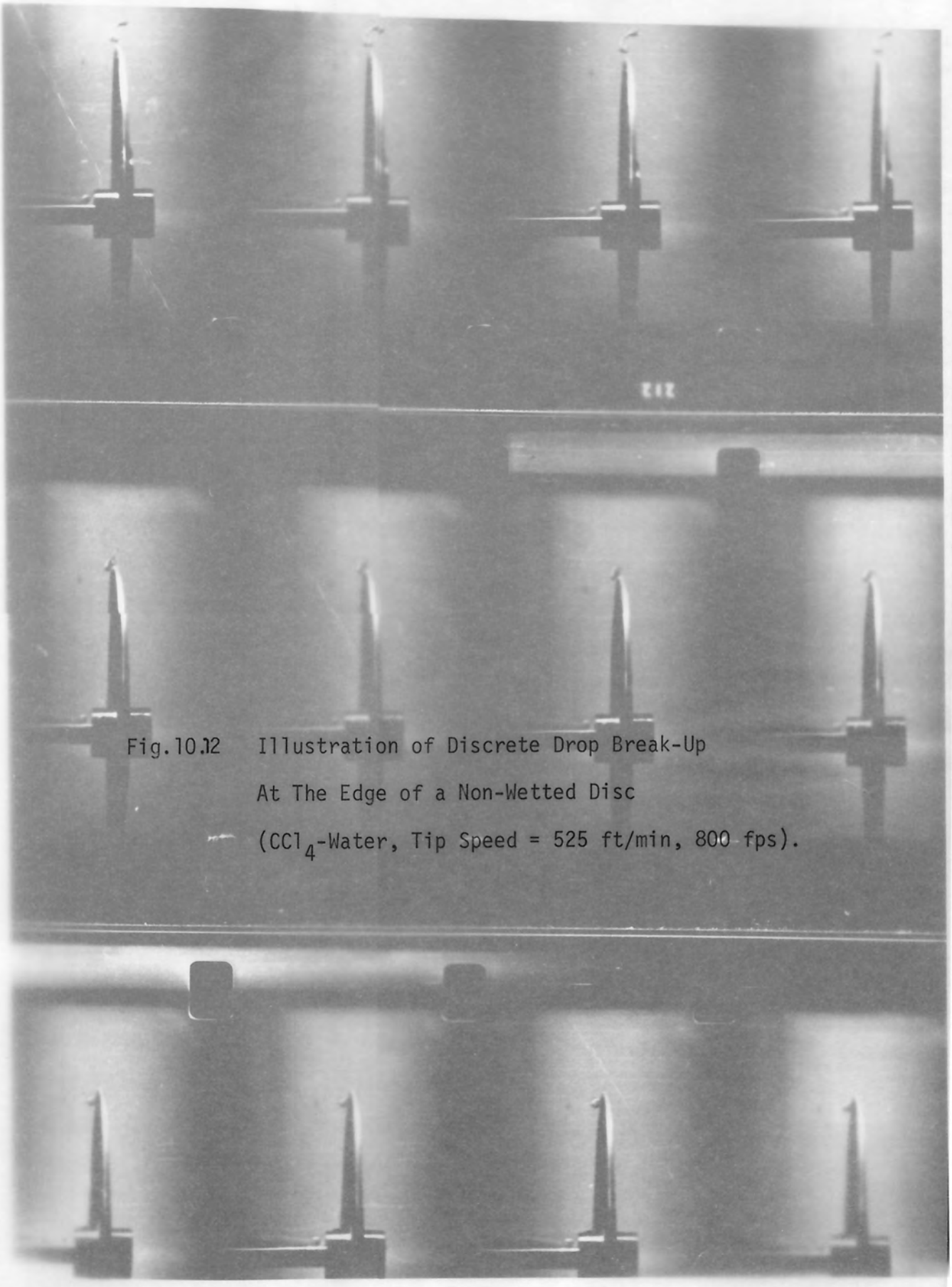

Fig.10.12 Illustration of Discrete Drop Break-Up At The Edge of a Non-Wetted Disc (CCl_4-Water, Tip Speed = 525 ft/min, 800 fps).

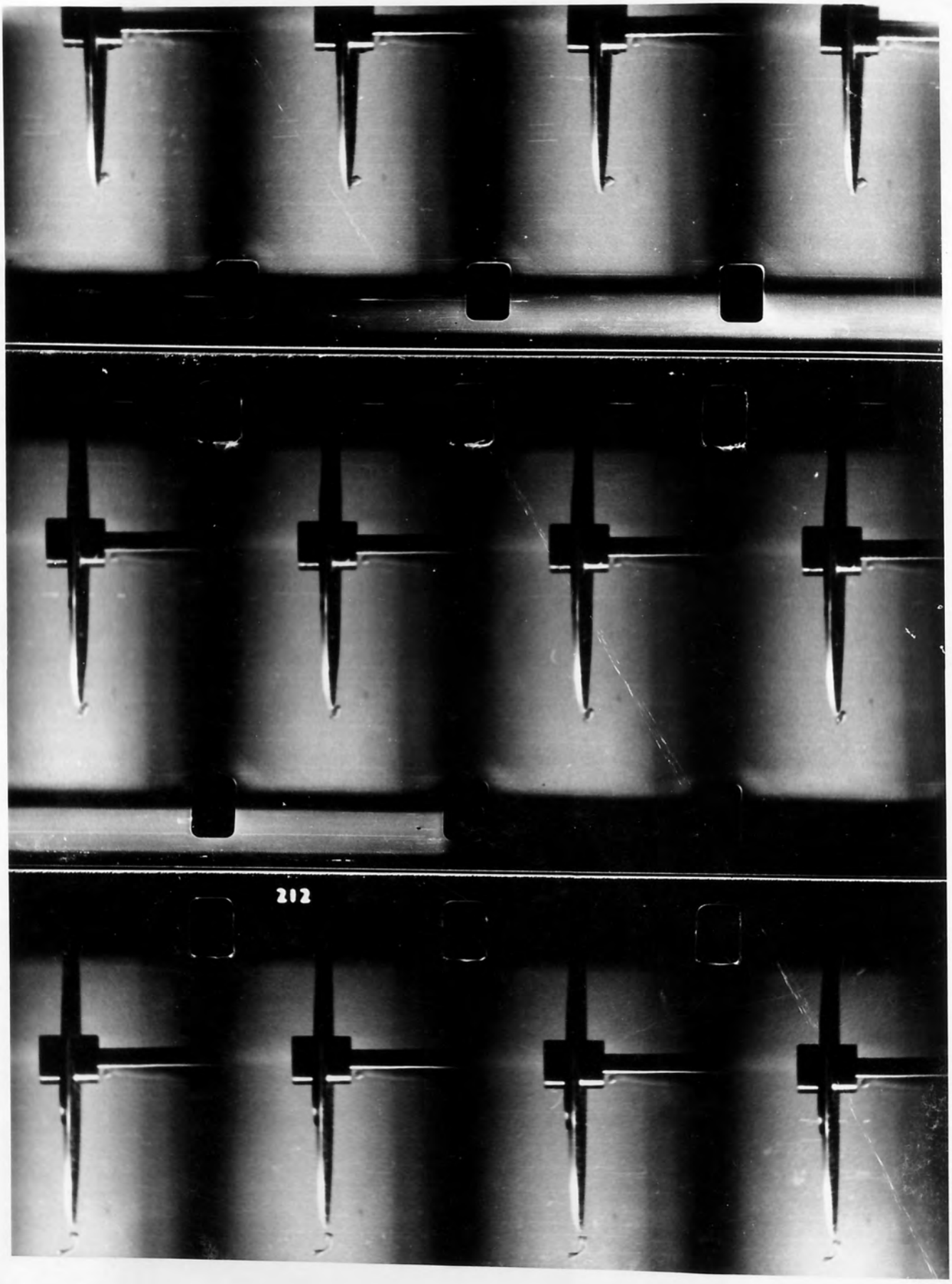
212

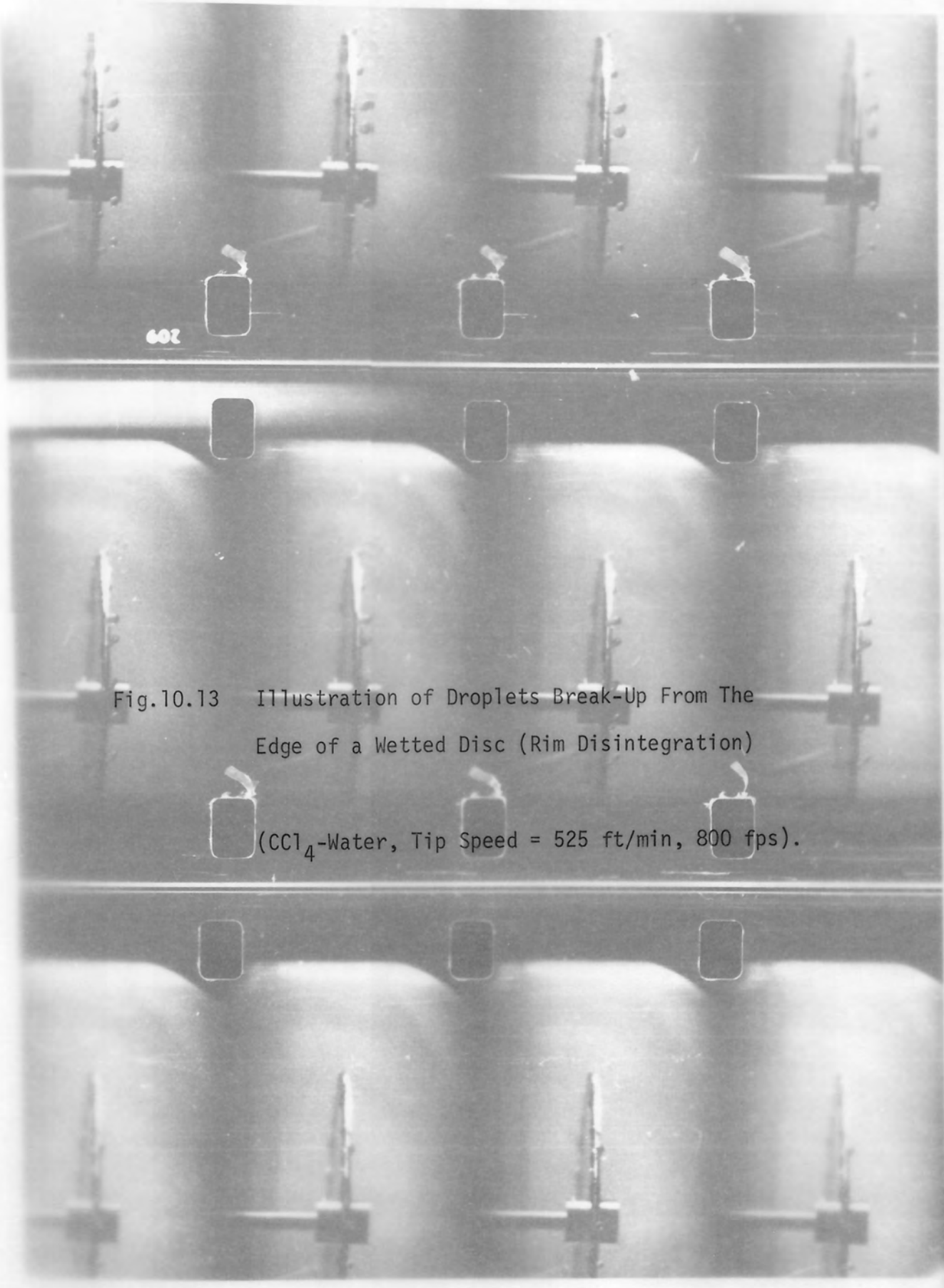

Fig.10.13 Illustration of Droplets Break-Up From The Edge of a Wetted Disc (Rim Disintegration)

(CCl_4-Water, Tip Speed = 525 ft/min, 800 fps).

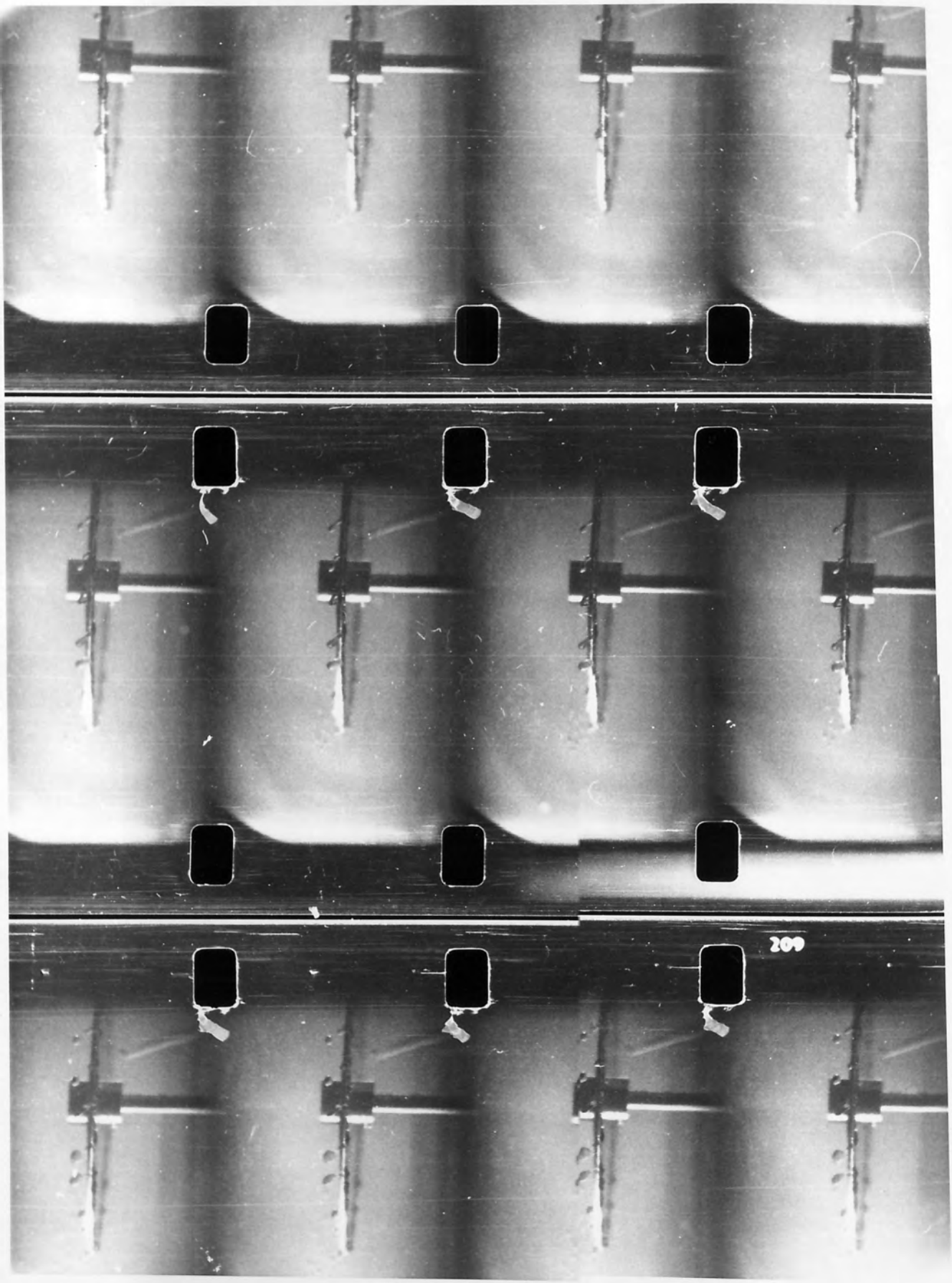

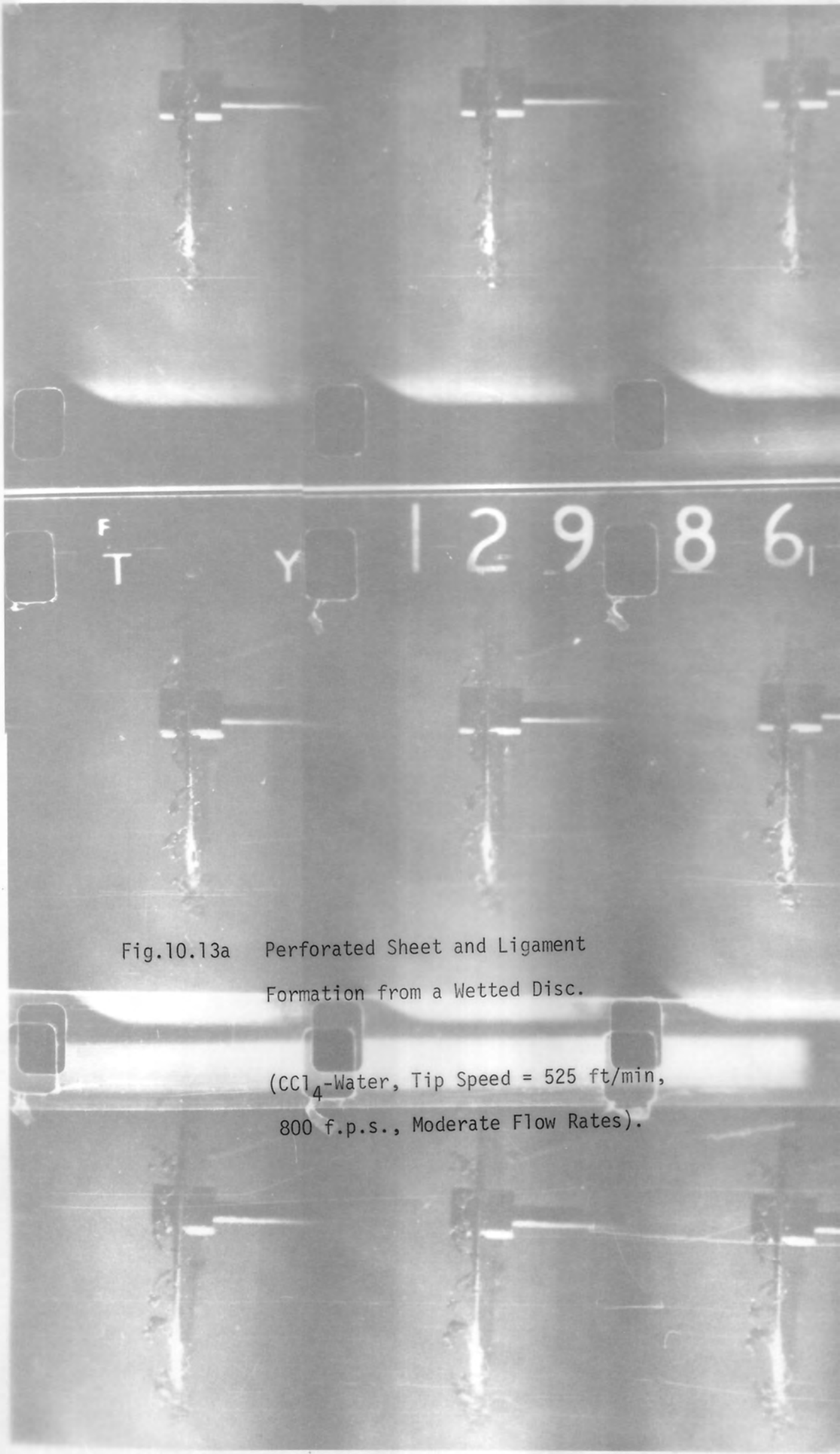

Fig.10.13a Perforated Sheet and Ligament Formation from a Wetted Disc.

(CCl_4-Water, Tip Speed = 525 ft/min, 800 f.p.s., Moderate Flow Rates).

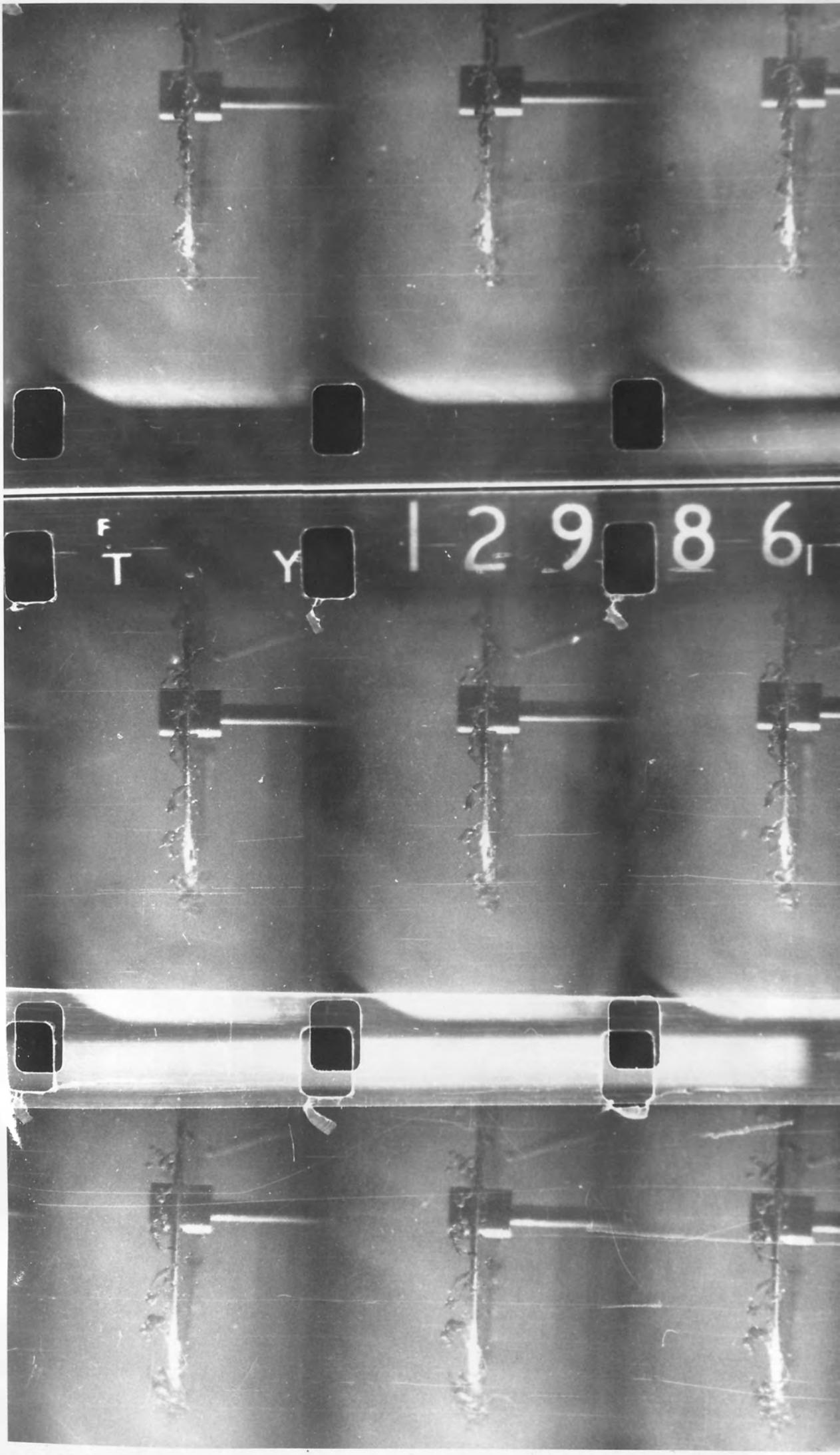
F
T
Y
1 2 9 8 6

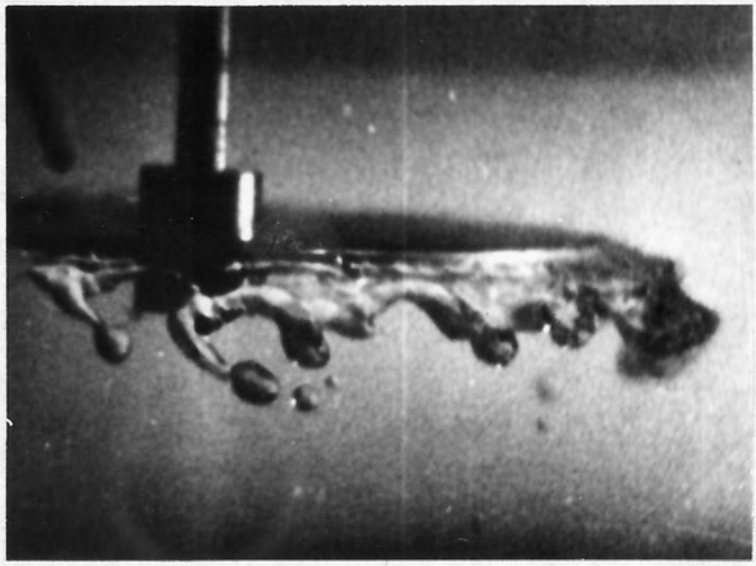

Fig.10.13b Illustration of Mechanism of Sheet Disintegration From a Wetted Disc

(CCl_4-Water, Tip Speed = 525 ft/min).

situation unlikely to be encountered in practice and gives rise to interfacial turbulence, the phenomena observed were considered to be of interest. These are discussed below,

1. Forming Drops - Long formation times (> 1 min) were employed. Although, not a practical condition, this was necessary to allow the various phenomena to develop fully and to facilitate observation.

Three types of forming drops were observed, viz.

i - Pulsating

ii - Circulating

and iii - Stagnant (steady streaming).

The type of drops produced was independent of their size. And may be explained in terms of interfacial activity associated with high concentration mass transfer, and the speed with which the material was supplied, i.e., the jet speed, through the drop. Initially, when the liquid reservoir was full, thus exerting a higher pressure, a fast jet was produced; this resulted in relatively large amounts of solute rich liquid arriving at the top of the drop causing a locality of high concentration on each side of the interface. Possibly elements of a single phase three component mixture existed resulting in easy passage of the arriving material out of the drop. With a very fast jet the drops initially oscillated across the nozzle axis for a few seconds. Then steadied down as the liquid level dropped. Further reduction in the liquid level caused the material to be supplied at a slower rate and a reduction in the high concentration on both sides of the interface. As a result the jet reached the top of the drop and spread down the inside surface in a 'fountain' to gain maximum transfer area. Then

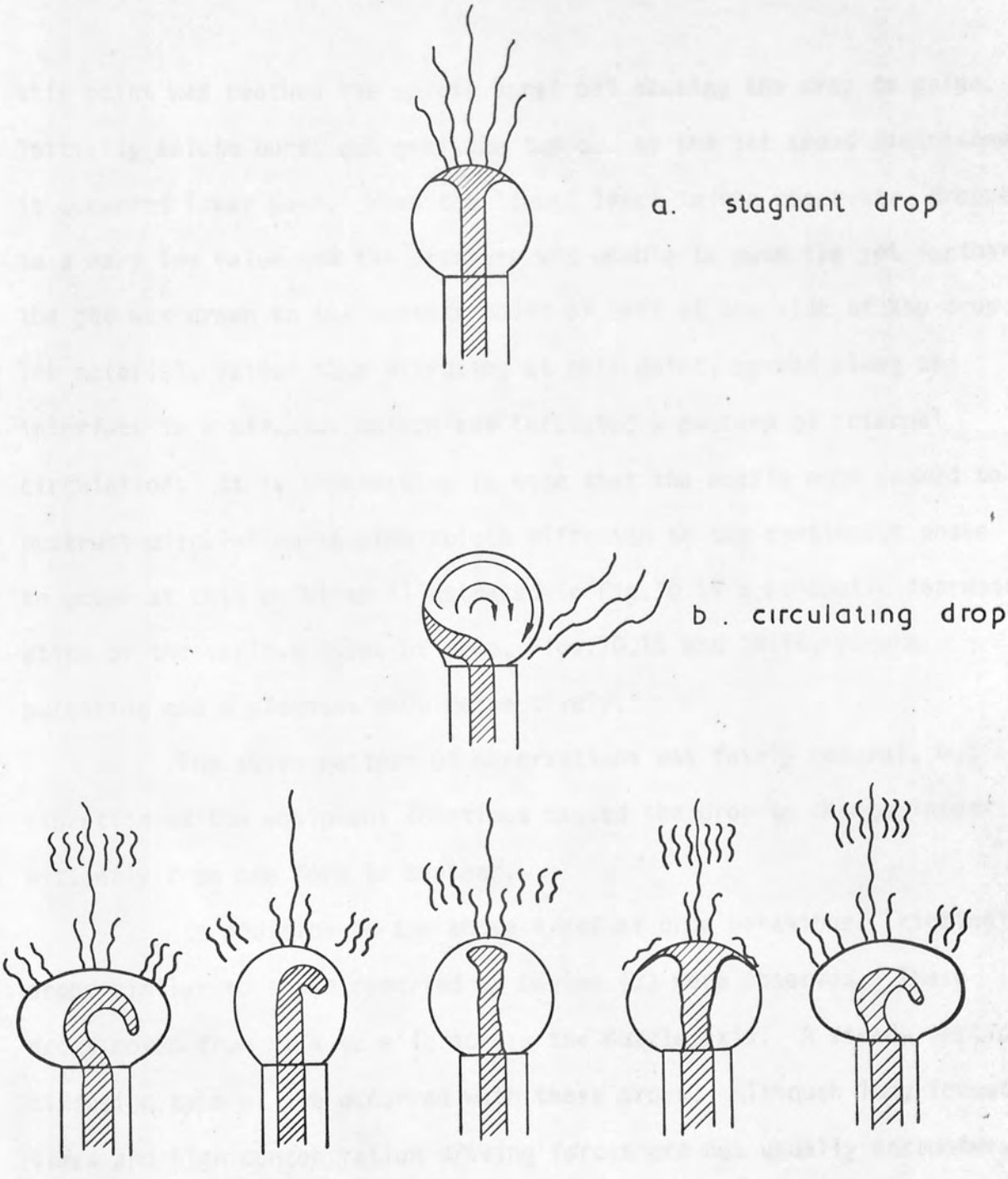

Fig. 10.14. Diffusion mechanisms in forming drops

this point was reached the solute burst out causing the drop to pulse. Initially solute burst out near the top but as the jet speed diminished it occurred lower down. When the liquid level in the reservoir, dropped to a very low value and the pressure was unable to push the jet further, the jet was drawn to the nearest point of exit at one side of the drop. The material, rather than diffusing at this point, spread along the interface in a circular motion and initiated a pattern of internal circulation. It is interesting to note that the nozzle edge seemed to obstruct circulation causing solute diffusion to the continuous phase to occur at this point as illustrated in Fig.10.14 a schematic representation of the various types of drop, Figs.10.15 and 10.16, show a pulsating and a stagnant drop respectively.

The above pattern of observations was fairly general, but vibration of the equipment sometimes caused the drop to change intermittently from one form to another.

In addition to the above types of drop behaviour, 'kicking' drops similar to those reported by Davies (3) were observed. These drops moved from side to side across the nozzle axis. A steady vertical diffusion type of jet occurred with these drops. Although long formation times and high concentration driving forces are not usually encountered in practice, these observations provide some insight in this field on which to base future work.

2. Coalescing Drops - Coalescence times considered here, effectively the time for drainage of the drop contents into the homophase, varied from 0.006 to 0.02 secs. for a range of drop sizes between 3 and 10 mm. This was for the system Toluene(Acetone) → Water. Following complete drainage the resulting drop or interface, depending

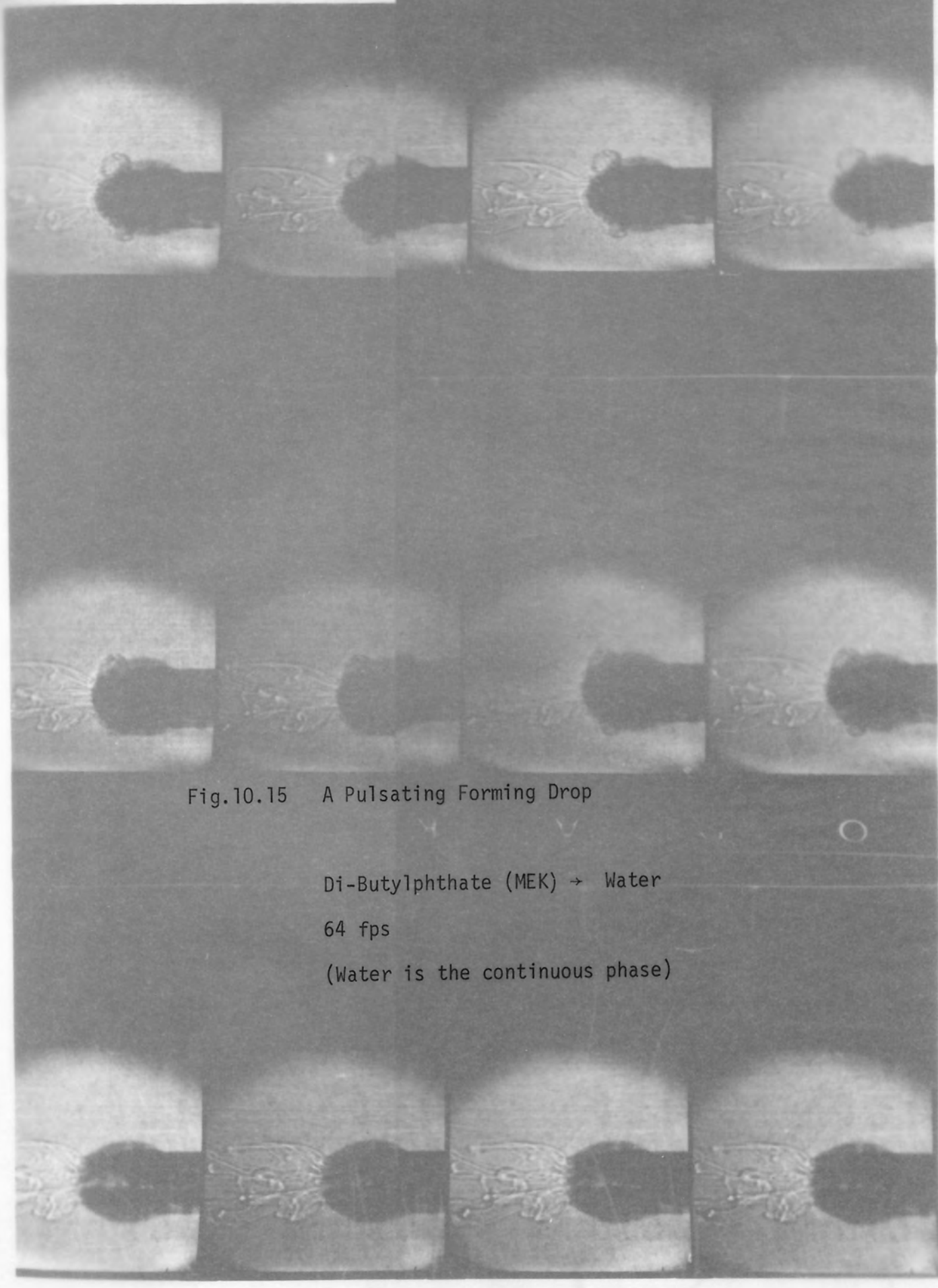

Fig.10.15 A Pulsating Forming Drop

Di-Butylphthate (MEK) → Water

64 fps

(Water is the continuous phase)

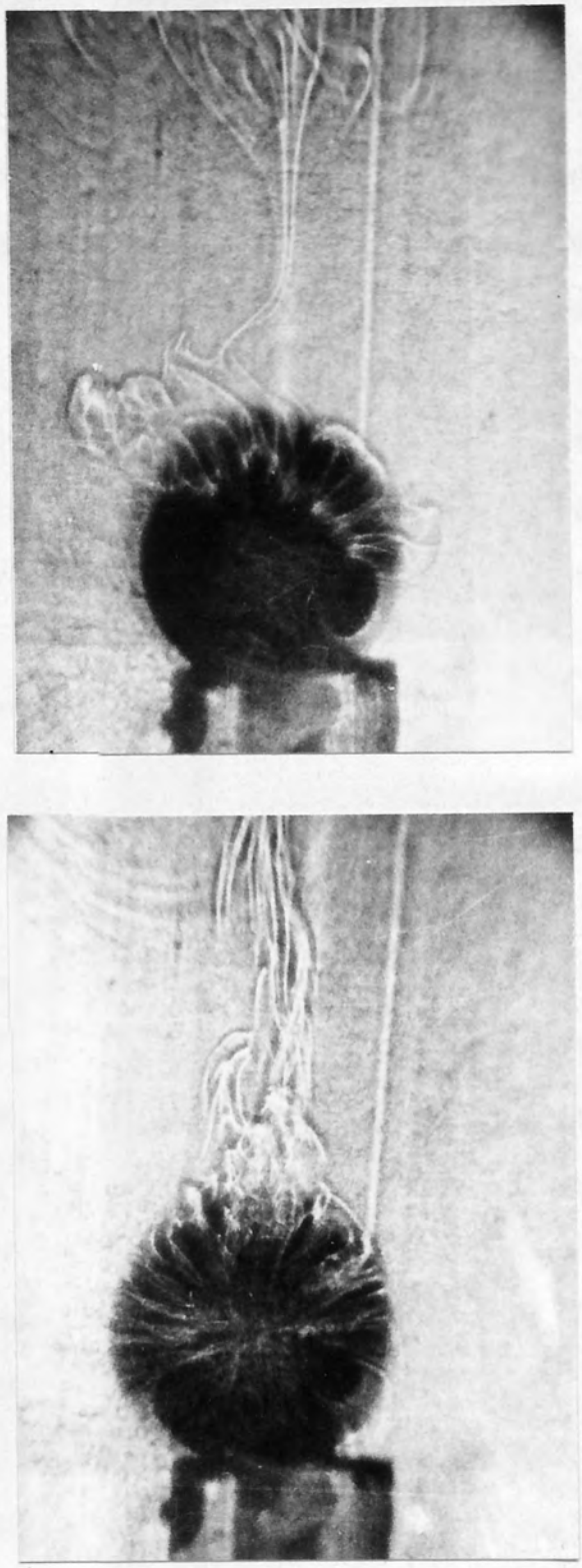

Fig.10.16 Comparison Between A Pulsating (Top) and A Stagnant (Bottom) Forming Drop

DiButylphthalate (MEK) → Water

64 fps.

(Water is the continuous phase)

on whether drop-drop or drop-interface coalescence was being considered, underwent oscillation for a further period of time. Coalescence was accompanied by a sudden burst of solute from the coalescing drop, based upon observation of the lines of diffusing solute it appeared a much larger amount of solute was transferred in this way over a comparable time than in the previous discrete drop stage. This is contrary to earlier findings (93,164). However an increase in mass transfer during this stage could be due to,

i - The violent oscillations that occurred during and after coalescence.

ii - The sudden change in concentration driving force.

This is possibly explained by considering the interface as a third phase, older and having a lower concentration of solute than the arriving drop. As coalescence occurred two fields of concentration gradient were set up, a low one between the drop contents and interface and a much higher one between the drop contents and continuous phase. This may cause a larger amount of solute to diffuse into the continuous phase. To investigate this further elimination of mechanism (i) in order to study (ii) could be effected by introducing a solid interface, e.g.,a surface wetted by the drop phase.

The process of drop-interface coalescence is shown in Fig.10.17. The production of a secondary drop, heavier than the continuous phase, i.e., having a lower solute concentration than the mother drop, is indicative of the magnitude of mass transfer associated with coalescence. A sequence of drop-drop coalescence is shown in Fig.10.18. For this the technique of "density matching"was employed in order to eliminate the visual effects produced by the drop turbulence and the wake. The system

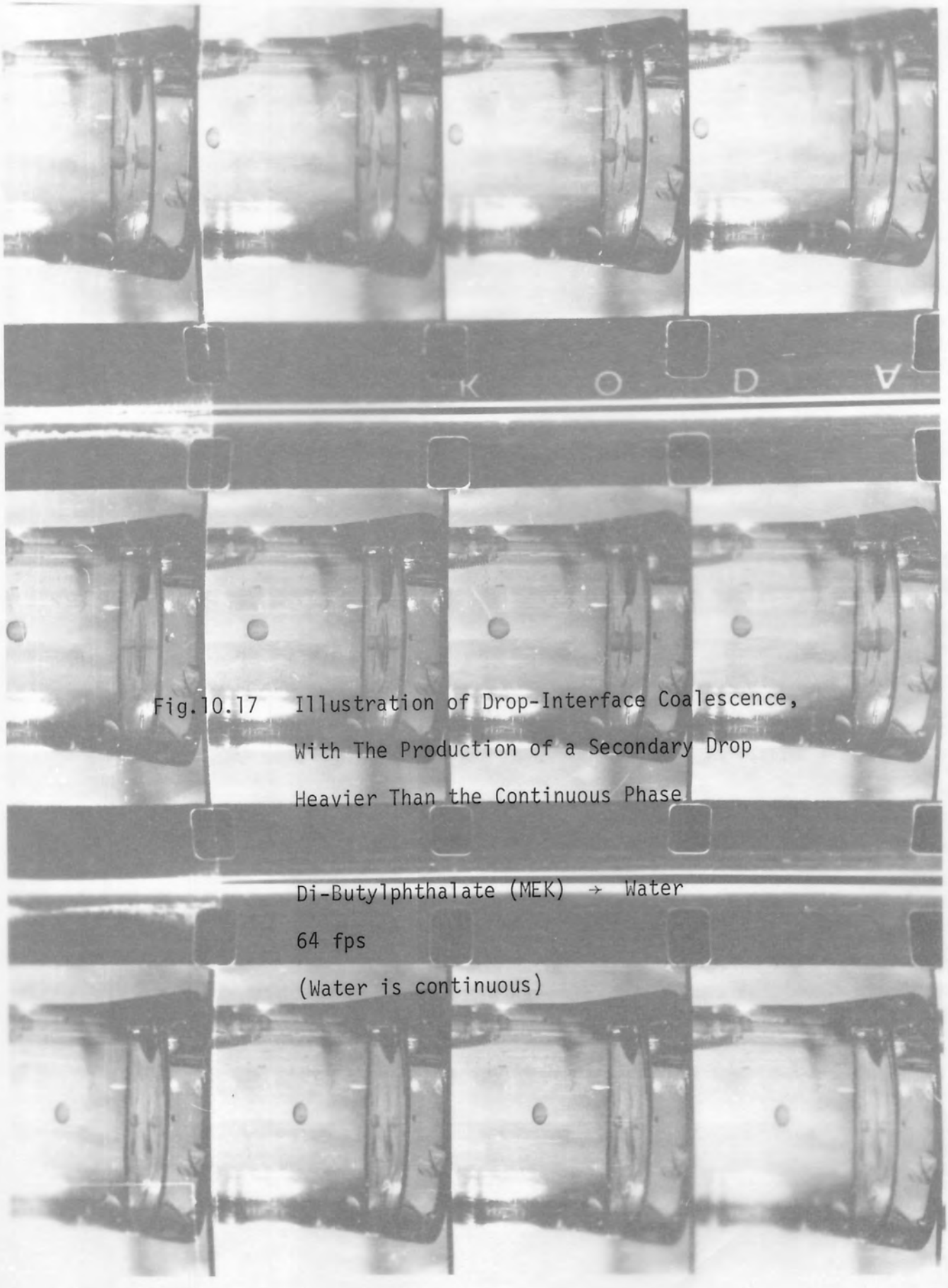

Fig.10.17 Illustration of Drop-Interface Coalescence, With The Production of a Secondary Drop Heavier Than the Continuous Phase.

Di-Butylphthalate (MEK) → Water

64 fps

(Water is continuous)

K O D A

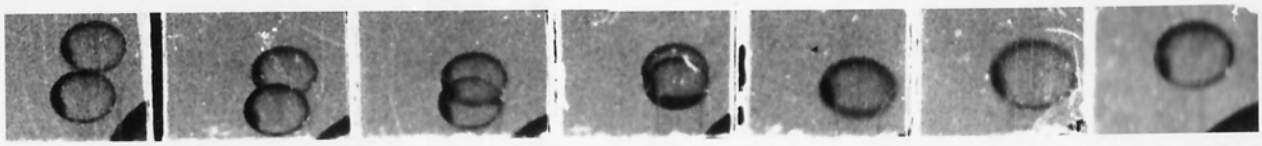

Fig.10.18 Illustration of Drop-Drop Coalescence Using Density Matching Technique

Di-Butylphthate (MEK) → Water

64 fps

(Water is continuous)

used for this purpose was dibutylphthalate-MEK-water; the physical properties of the components are given in Appendix 2. The drop phase was 23% MEK in dibutylphthalate which gave a density slightly lower than that of water to allow the drop to break away from the nozzle. Two drops were produced; these travelled for a distance of a few centimeters and, as their density reached that of water, they remained stationary for a few seconds. Additional solute transfer caused the drops to be heavier than water and to move downwards and to accelerate with further transfer. Although most of the drops which coalesced did so whilst in motion a few coalesced while stationary. One interesting phenomenon observed was the violent oscillations associated with coalescence illustrated in Fig.10.18.

3. Discrete Drops - Only one type of drop was observed, viz. stagnant spheres with the usual wake at the rear as shown in Fig.10.19.

The drops underwent a 'pulse', just after they broke away from the nozzle similar to that described for forming drops. This may have been a continuation of a pulse cycle initiated during formation. However some drops pulsated even after travelling for some time in a stagnant form. This was possibly due to a change in the field of driving force, from a lower to a higher one, causing the drop to jettison some of the solute in order to adjust to the new environment. A sequence showing a pulsating drop is given in Fig.10.19.

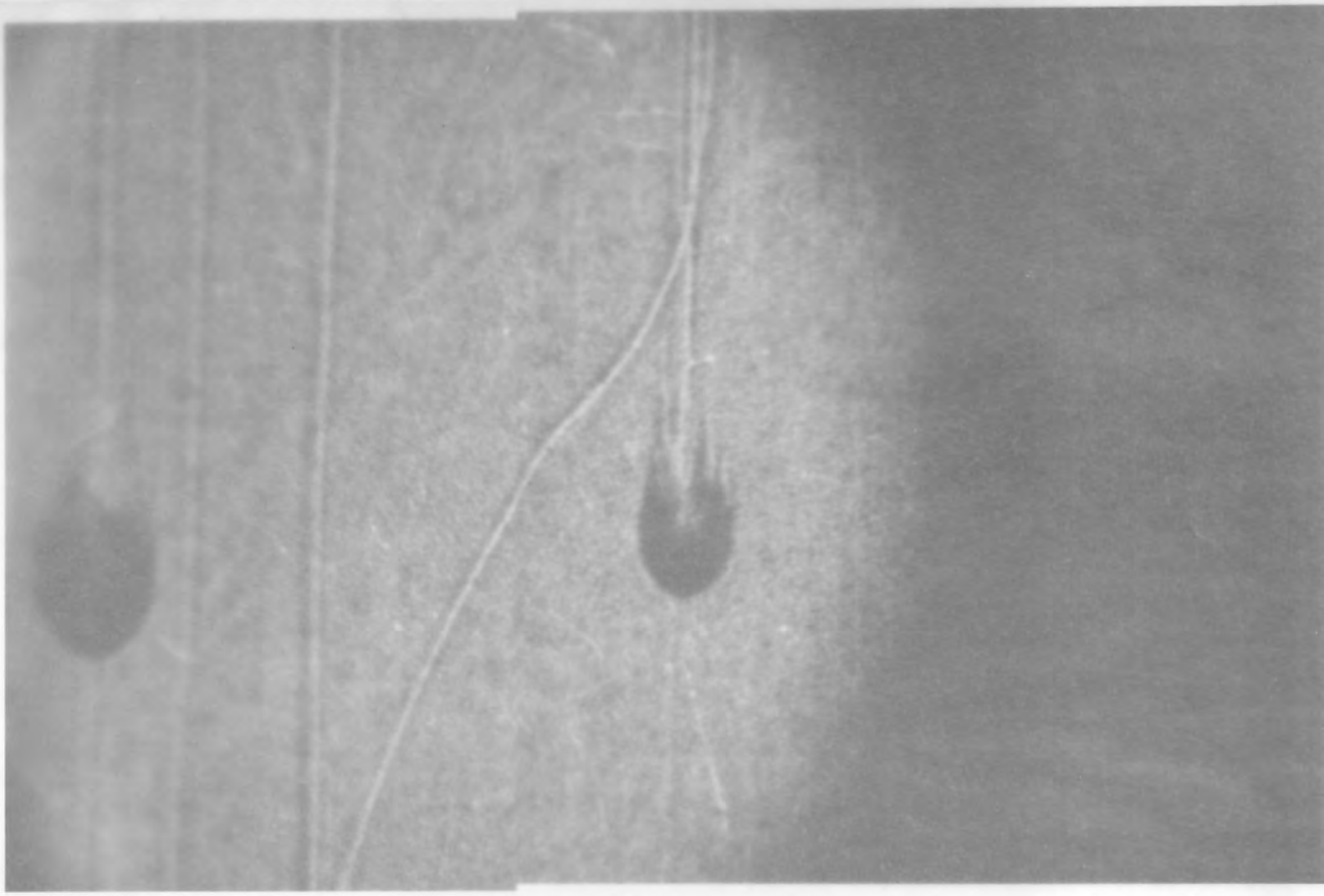

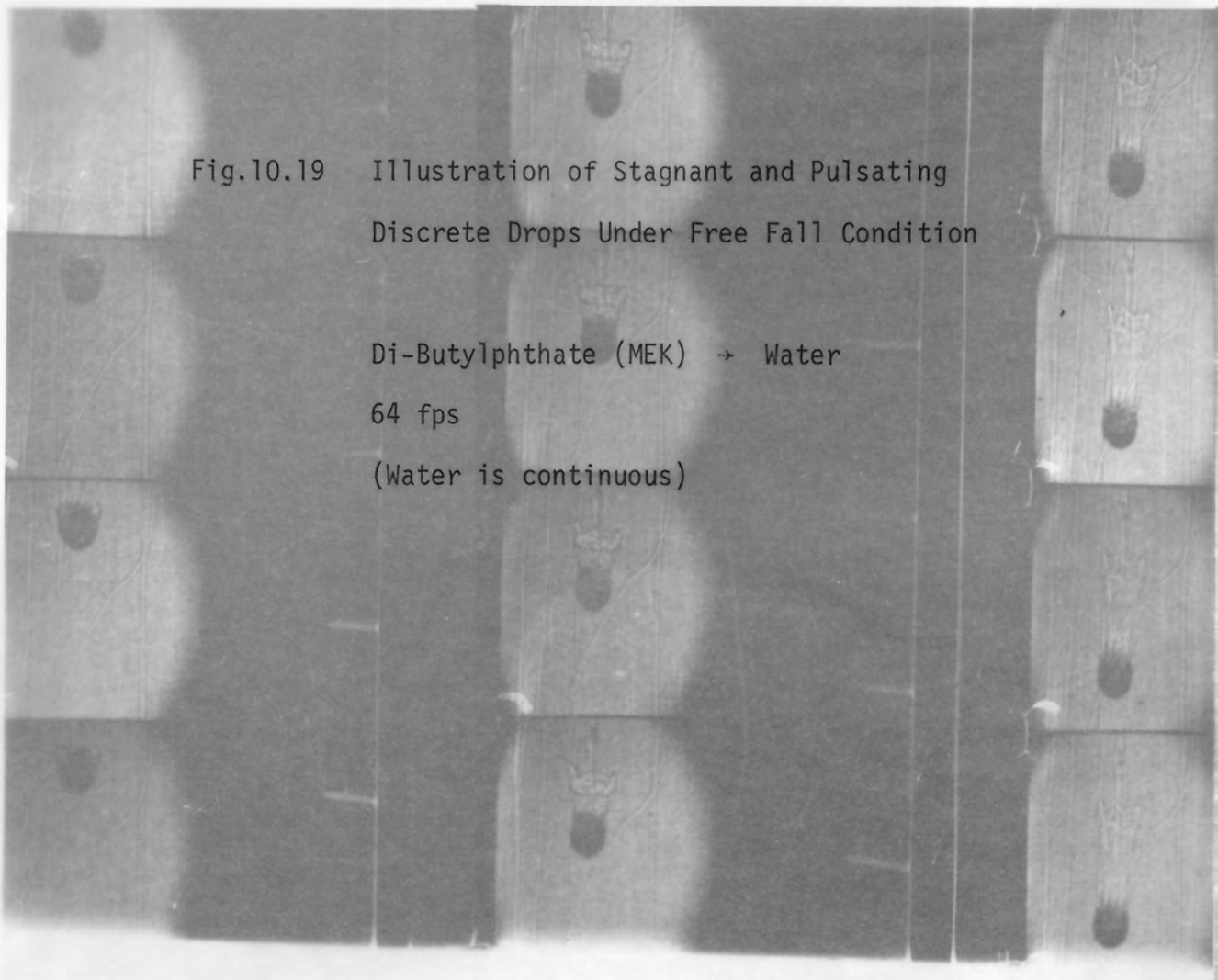

Fig.10.19 Illustration of Stagnant and Pulsating Discrete Drops Under Free Fall Condition

Di-Butylphthate (MEK) → Water

64 fps

(Water is continuous)

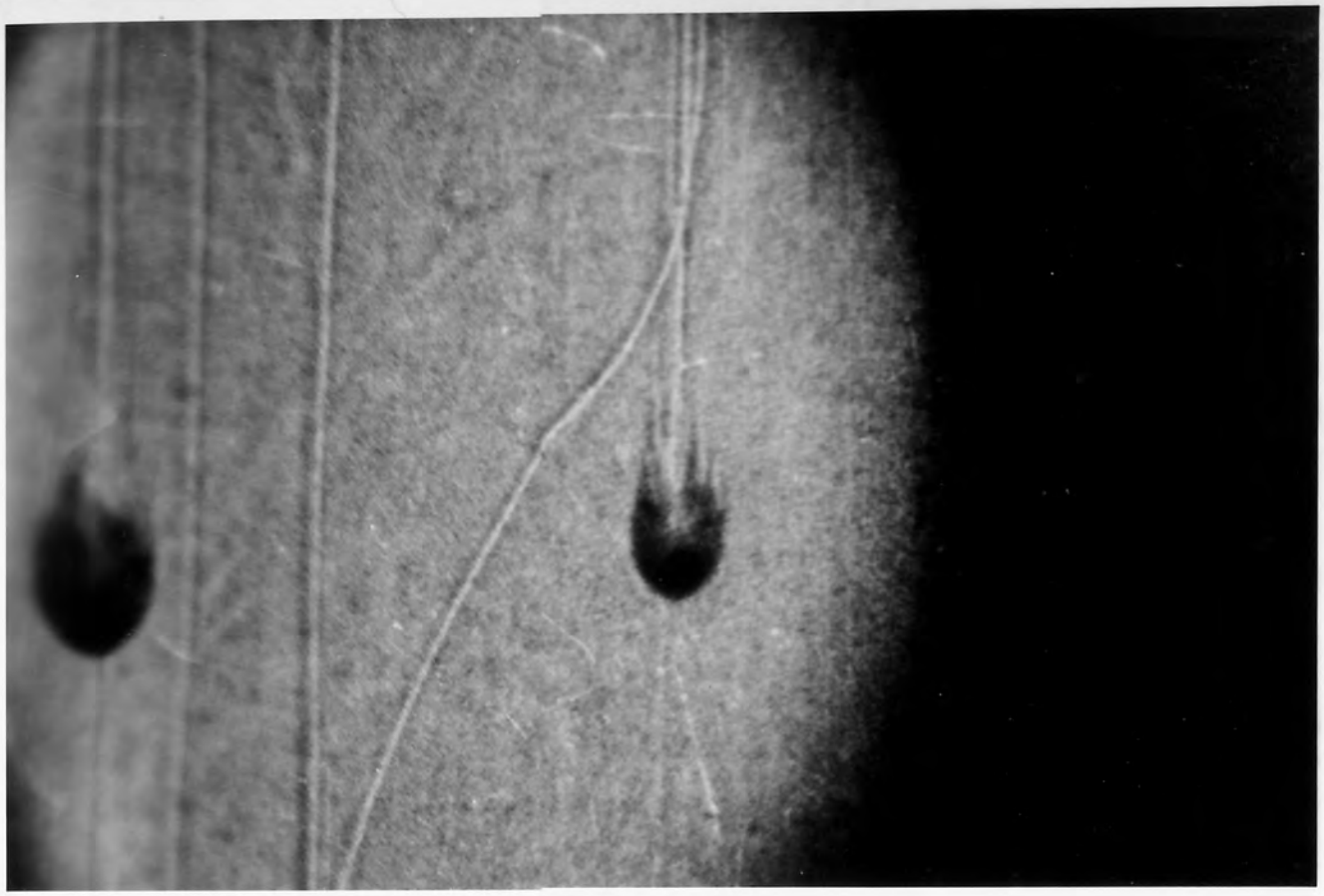

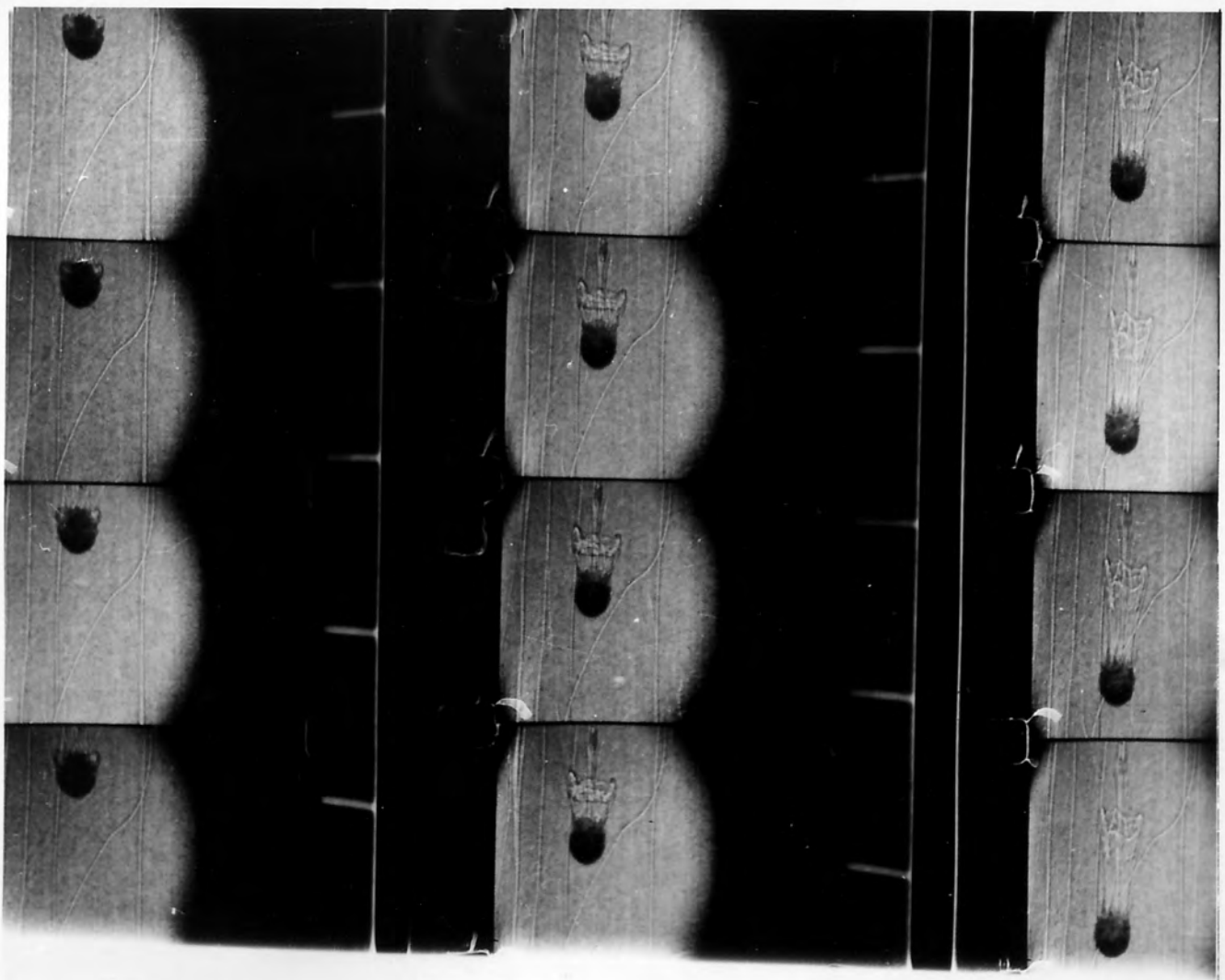

11. CONCLUSIONS

Equipment design procedures based upon non-mass transfer data and the assumption of discrete drops are of doubtful validity and may lead to large errors. For instance, this work has shown that drop size and capacity measurements made under mass transfer conditions may differ greatly from those under non-mass transfer conditions. Furthermore these measurements are dependent upon the direction of interfacial tension increase with solute concentrations; in the one case coalescence is increased, thus increasing the drop size and capacity but in the other case solute transfer results in reduced coalescence and subsequently drop size and capacity. With most common systems the former case occurs when the transfer direction is from the dispersed to continuous phase and the later one occurs for the opposite direction.

It is hoped that this study will offer more realistic design criteria. An assessment has also been made of the effect of wettability of the column internals on the mass transfer efficiency. That this may have significant effect was discussed in Section 5.3, and it is known that 'unfavourable' wetting conditions may occur in a column due to either an error in material selection or dirt deposition on surfaces inside the column.

The main conclusions of this work are as follows,

1. Non-Mass Transfer Studies

i - Drop Size Correlation - The effect which the main parameters, viz. interfacial tension, density difference, hold-up and rotor speed, have upon drop size was confirmed. Other factors were found to be important in determining d_{32}. These are

a - Dispersed phase viscosity. An increase in μ_D resulted in lower rates of break-up and coalescence, thus increasing the mean drop size.

b - Column height - The mean drop size produced in any compartment decreased with increasing number of the compartment from the dispersed phase inlet.

c - Disc wettability - d_{32} was larger for wetted than for non-wetted discs, particularly at lower rotor speeds, due to the enhanced coalescence arising from wetting of the disc surfaces.

ii - Axial Hold-Up Profile - The results obtained in this study confirm the earlier findings of Rod (79) and Strand et al. (74), i.e. hold-up increased to a maximum value at about half way up the column and then decreased towards the top.

iii - Limiting Capacity - The phenomenon of phase inversion was found to be a better criteria to define limiting capacity than the, rather ambiguous flooding phenomena. Phase inversion occurred first in the bottom compartment and travelled upwards until other compartments reached their inversion hold-up. Extraction columns can be operated efficiently near the maximum capacity limits so defined without the loss in efficiency, formerly believed to occur due to the apparent reduction in surface area caused by the increase in coalescence frequency.

2. Mass Transfer Study

i - Effect of Wetting - No significant difference was observed between the efficiency of wetted and non-wetted disc columns. The column operation was mainly dependent on the mass transfer direction and rotor speed.

ii - Direction of Mass Transfer - With the systems studied transfer from the dispersed to continuous phase enhanced coalescence and transfer in the opposite direction reduced it. The former mechanism improved mass transfer and substantially reduced axial mixing. Therefore the proper selection of transfer direction should provide improved mass transfer efficiencies in practical extractors.

iii - Mass Transfer Coefficient - The stagnant drop model gave much lower values than K_{exp}, the largest deviations being at high Peclet numbers. Better agreement was obtained with the other models, viz. circulating drop, surface stretch and fresh surface, the latter two giving similar values of transfer coefficients (less than 5% deviation). The ratio of K_{exp} to K_{theo} for oscillating and stagnant drops and fresh surface models increased linearly with increasing Peclet number. However the circulating drop model gave the best agreement with experimental values, although results were erratic when liquid paraffin was dispersed, due to the large variation in its viscosity along the column.

iv - Interfacial Area - Use of photography for interfacial area estimation may not give the effective area of transfer for use in existing mass transfer models. This applies particularly to non-discrete drop conditions as illustrated in Fig.11.1. In such cases other methods such as the 'chemical method' (231) should be used. Where fast pseudo--first order reaction accompanying liquid extraction can be used to evaluate the effective surface area. Alkaline hydrolysis of formate esters have been used successfully for this purpose (231).

3. Other Studies

i - Break-up Mechanisms Using Wetted and Non-Wetted Discs -

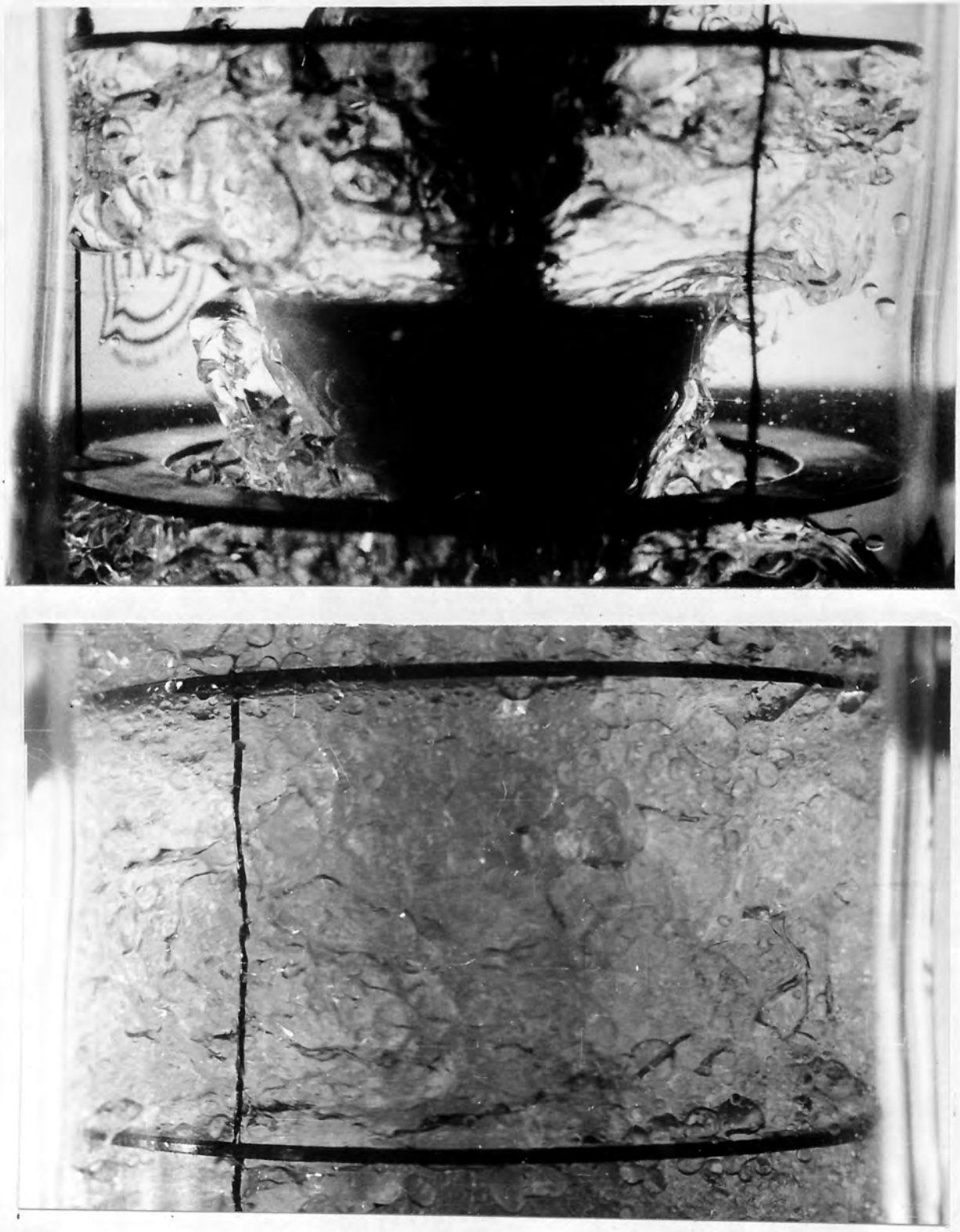

Fig.11.1 Non-Discrete Drop Conditions In A Wetted Cone Column (T → W)

Top Plate: 500 rpm, Q_c = 1.5 Litre/min, Q_d = 4 Litre/min.

Bottom Plate: 1250 rpm, Q_c = 1.5 Litre/min, Q_d = 3 Litre/min.

With non-wetted discs each discrete drop disintegrated into small drops at the periphery. With wetted discs drops coalesced on the disc surface forming a thin liquid film. Drop redispersion occurred by rim disintegration. Increase in dispersed phase flow rate resulted in a transition to sheet formation and disintegration.

ii - Single Drop Mass Transfer and Interfacial Turbulence - Nozzle Studies.

a - Forming Drops - For long formation times (> 1 min) and high concentration driving forces, three types of drop were observed, viz. pulsating, circulating and stagnant. The type of drop produced depended on the velocity of the impinging jet from the nozzle.

b - Discrete Drops - These drops were stagnant with a very distinct wake. Sometimes however they underwent a sudden pulse and a jettisoned burst of solute. This would be expected to improve mass transfer.

c - Coalescing Drops - A burst of solute, apparently in fairly large amounts, accompanied drop coalescence at the interface. Conversely the mechanism usually assumed, viz. similar to formation mass transfer, would give negligible mass transfer due to the relatively short times involved. The "density matching" technique proved useful to observe and study drop-drop coalescence as it eliminated the wake associated with moving drops. Both types of coalescence were followed by violent oscillation of the interphase or the resulting drop.

4. Miscellaneous

i - With the systems studied the interfacial tension of mixtures of two liquids with a third phase, immiscible with either component, was found to vary linearly with the mixture concentration.

ii - The viscosity of a liquid mixture of liquid paraffin and toluene or M.E.K. was found to vary exponentially with the mixture concentration.

iii - Under practical conditions, using the system toluene--acetone-water, drop oscillation was found to damp out below a drop diameter, d = 1.8 mm. The time for one drop oscillation varied from 0.04 to 0.16 sec for a drop size range of 4.0 to 10.0 mm. The ratio of major to minor axis of oscillating drops was found to be approximately 1.5 irrespective of drop size.

iv - The time of drop formation for the system T → W with acetone as solute under practical conditions, i.e. formation from the sheet periphery, was found to vary from 0.04 to 0.2 sec. for a range of drop size 3.0 to 12.5 mm. A sequence illustrating drop formation from the sheet under practical operating conditions is given Fig.11.2.

v - The time of drop-interface coalescence, under similar conditions to iv above varied from 0.006 to 0.022 for a range of drop size from 3.0 to 11.0 mm.

The results observations i through to v are plotted in Appendix 4.

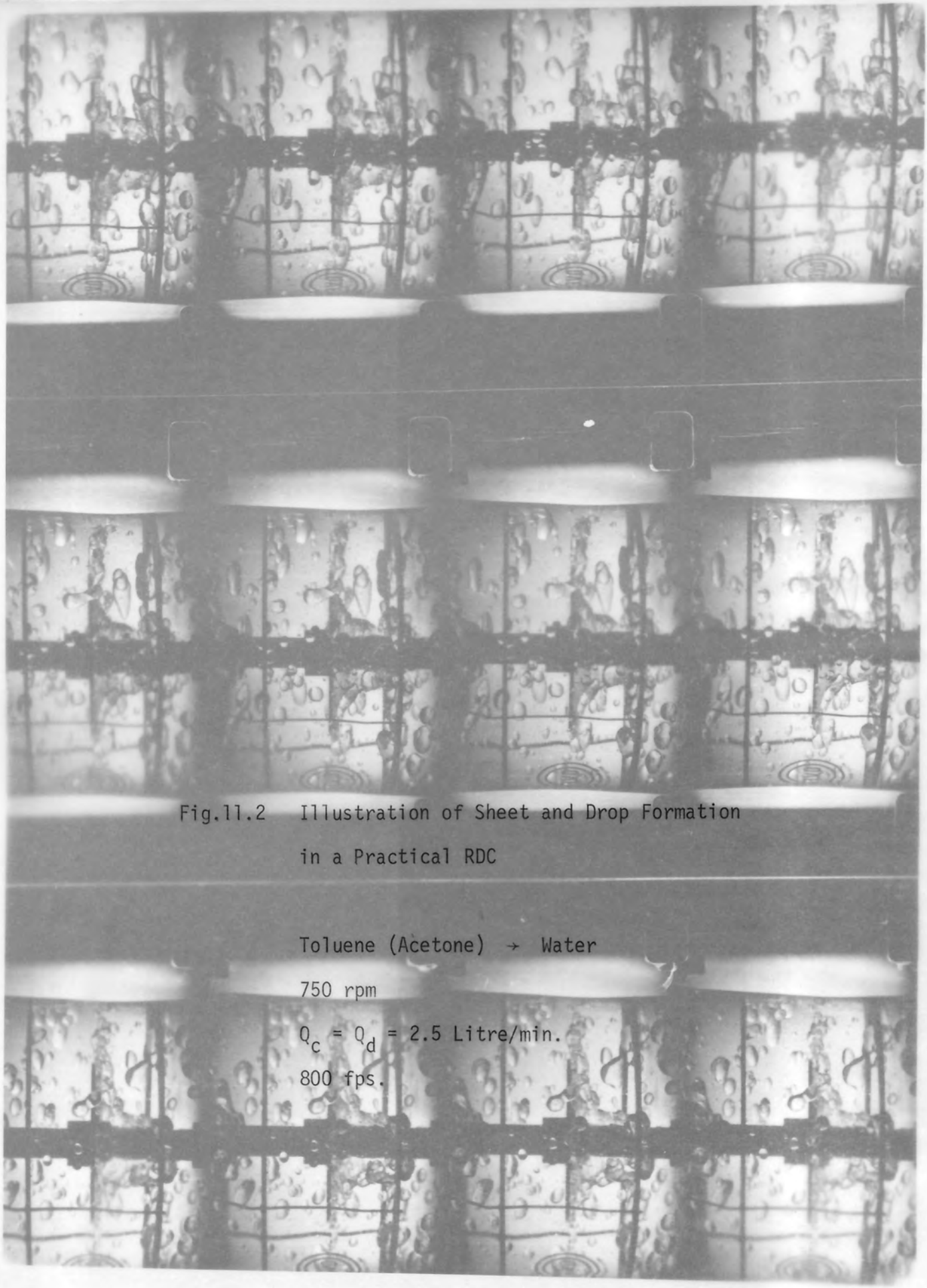

Fig.11.2 Illustration of Sheet and Drop Formation in a Practical RDC

Toluene (Acetone) → Water

750 rpm

$Q_c = Q_d$ = 2.5 Litre/min.

800 fps.

12. RECOMMENDATIONS FOR FURTHER WORK

During the course of this research several interesting areas for further research became apparent. For some of these phenomena only qualitative or limited quantitative data were obtained in the present study, and more detailed and conclusive studies would be worthwhile. Therefore the following further work is recommended.

1. Further investigation of the phenomena of phase inversion. A recent study has been made of this phenomena using different design geometries (232). However further work is needed to assess the effect of system physical properties on phase inversion rates and the validity of the model derived in Section 9.1.

2. The original rotor design, viz. cones, introduced in this study gave improved mass transfer efficiencies in some cases compared with discs. Further investigations could be carried out into the potential of the 'cone contactor' and the use of cones with smaller dimensions to improve it's hold-up characteristics.

3. Studies of the nature of flow in the vicinity of a rotating cone and its effect on droplet break-up.

4. Axial mixing has long been one of the major problems encountered in extractor operation. As shown in this study, this problem may be overcome by an appropriate choice of transfer direction. Therefore quantitative assessment of this phenomenon would be useful.

5. The two independent linear relationships of Pe vs. the ratios of mass transfer coefficients obtained for the two systems used indicate that other systems with different physical properties would produce a family of such lines which would be very useful for design purposes. Thus mass transfer studies using various systems should be carried out.

6. One of the conclusions in the present study was that estimation of the effective interfacial area by photography can be unreliable. Therefore other methods, e.g. the chemical (231) or the encapsulation (233) method could be applied with advantage to practical columns. These may prove to be more reliable, e.g. the former method was employed, for a 3.1 cm spray column and gave good results (231).

7. Mass transfer mechanisms during coalescence could be studied further using the Schlieren and density matching techniques. Since normally the mechanism assumed, i.e., as similar to that of forming drops, was suggested by the observations in Section 10.3.2, to be invalid. The potential of the 'density matching' technique is of course applicable to other studies not necessarily related to extractors.

8. Further application of the Schlieren and similar optical arrangements to study drop formation and discrete drop mass transfer mechanisms. For example, it is clear from the discussion that there are several aspects in this field, e.g. the cause of drop circulation and oscillation, yet to be fully understood.

9. In the present study the frequency of drop oscillation was measured by the analysis of high speed ciné photography. It would be of interest to extend this data and compare these values with those obtained using expressions given in the literature (234).

APPENDIX 1

Description of Cine Films

1. Films of 4 inch pilot scale RDC, at various flow rates and rotor speeds for both direction of mass transfer. (600-1000 f.p.s.)	For measurements of times of drop formation, drop coalescence, drop oscillation and major and minor semiaxis of oscillating drops. Also, illustration for drop formation from the sheet and coalescence at the liquid vortex.
2. Films of 12 inch single stage column, using wetted and non-wetted discs at various rotor speeds and flow rates. (600-1000 f.p.s.)	Illustration of droplet break-up mechanisms for wetted and non-wetted discs.
3. Films of 4 inch column section, employing density matching technique (64 f.p.s.)	Illustration of drop-drop and drop-interface coalescence mechanisms.
4. Films of 4 inch column section, employing Schlieren technique. (64 f.p.s.)	Illustration of mechanisms of forming, coalescing and discrete drops mass transfer.

APPENDIX 2

Physical Properties of Liquids Used @ ≃ 22.5°C.

Liquid	Surface Tension or Interfacial Tension With Water (*) (dyne/cm)	Density (gm./cc.	Viscosity (C.P.)	Refractive Index	M.Wt.
1. Water	73.0	1.00	1.00	1.33300	18.02
2. Toluene	34.1*	0.87	0.60	1.49430	92.13
3. Liquid Paraffin	50.0*	0.87	170.00	1.48290	≃ 360
4. Glycerin	63.0	1.26	830	1.47210	92.10
5. 60% Glycerin) 40% Water)	69.0 (26.0 with Toluene)	1.14	9.10	1.38750	-
6. 25% Toluene) 75% Liquid Paraffin)	45.0*	0.87	12.00	1.48570	-
7. 37% Toluene) 63% Liquid Paraffin)	42.75*	0.87	3.50	1.48710	-
8. Carbontetrachloride	45.0*	1.60	0.97	1.45925	153.82
9. Di-n-Butylphthalate	19.2*	1.05	19.50	1.49050	278.35
10. Acetone	23.7	0.79	0.325	1.35892	56.08
11. Methyl Ethyl Ketone	24.6	0.804	0.4	1.37740	72.11

APPENDIX 3

Details of Rotors Used

1. Stainless Steel (Non-Wetted) Discs,

   Diameter = 2.0 inches

   Thickness = 1/16 inch

2. P.t.f.e. (Wetted) Discs,

   Diameter = 2.0 inches

   Thickness = 1/16 inch

3. Polypropylene (Wetted) Cones,

   Diameter = 2.0 inches

   Height = 2.0 inches

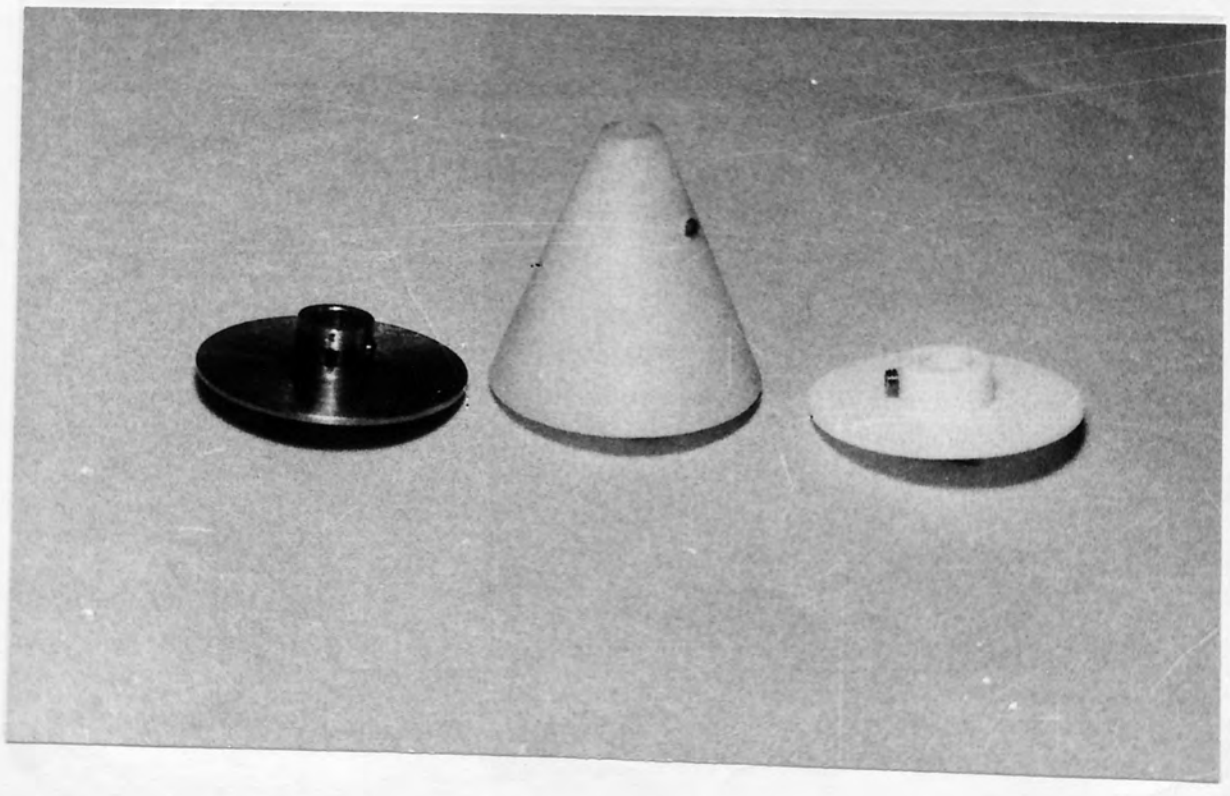

APPENDIX 4

Contents of This Appendix

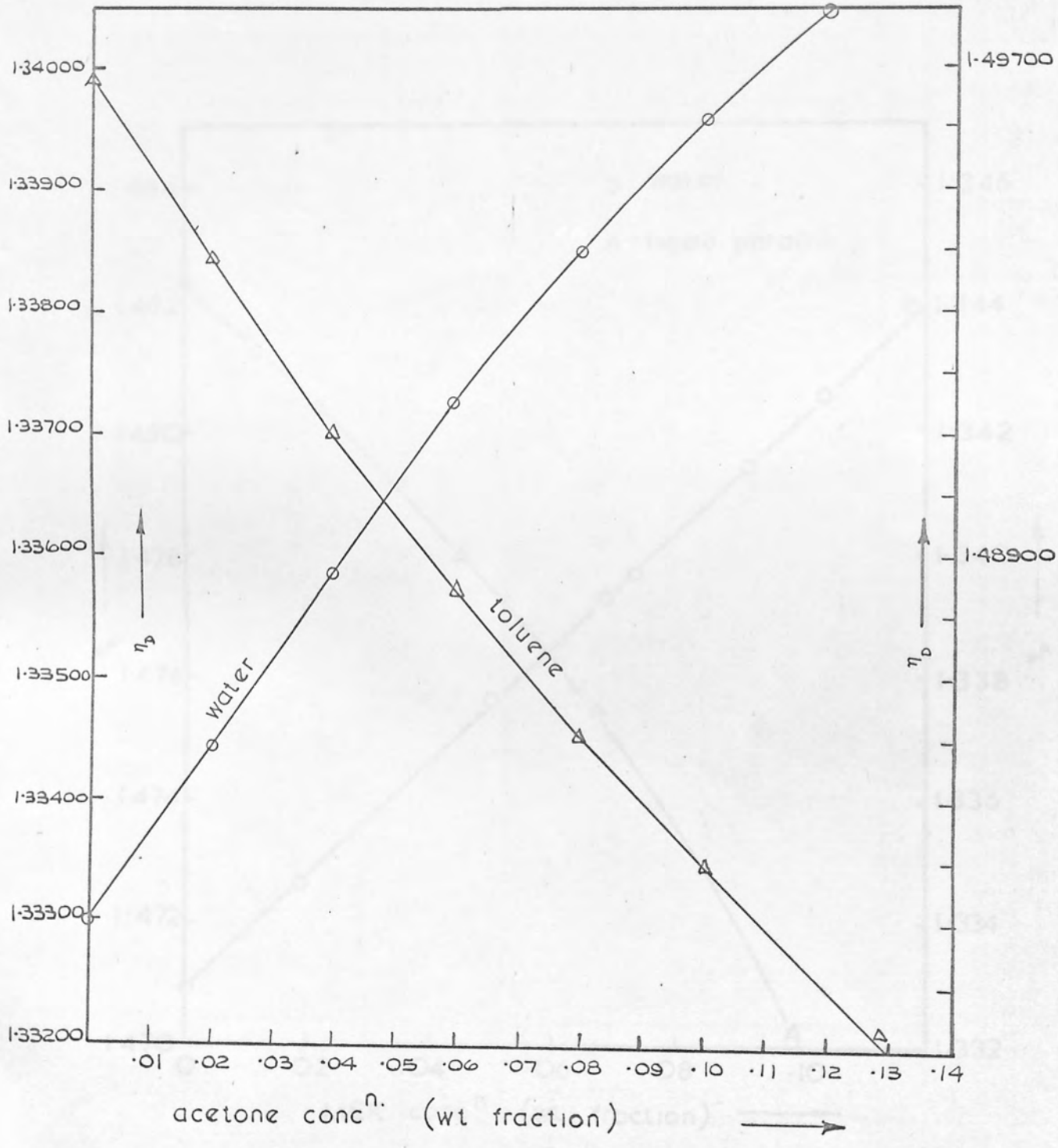

Fig. I. Solute concentration vs refractive index for toluene - acetone - water system at 22·5°c.

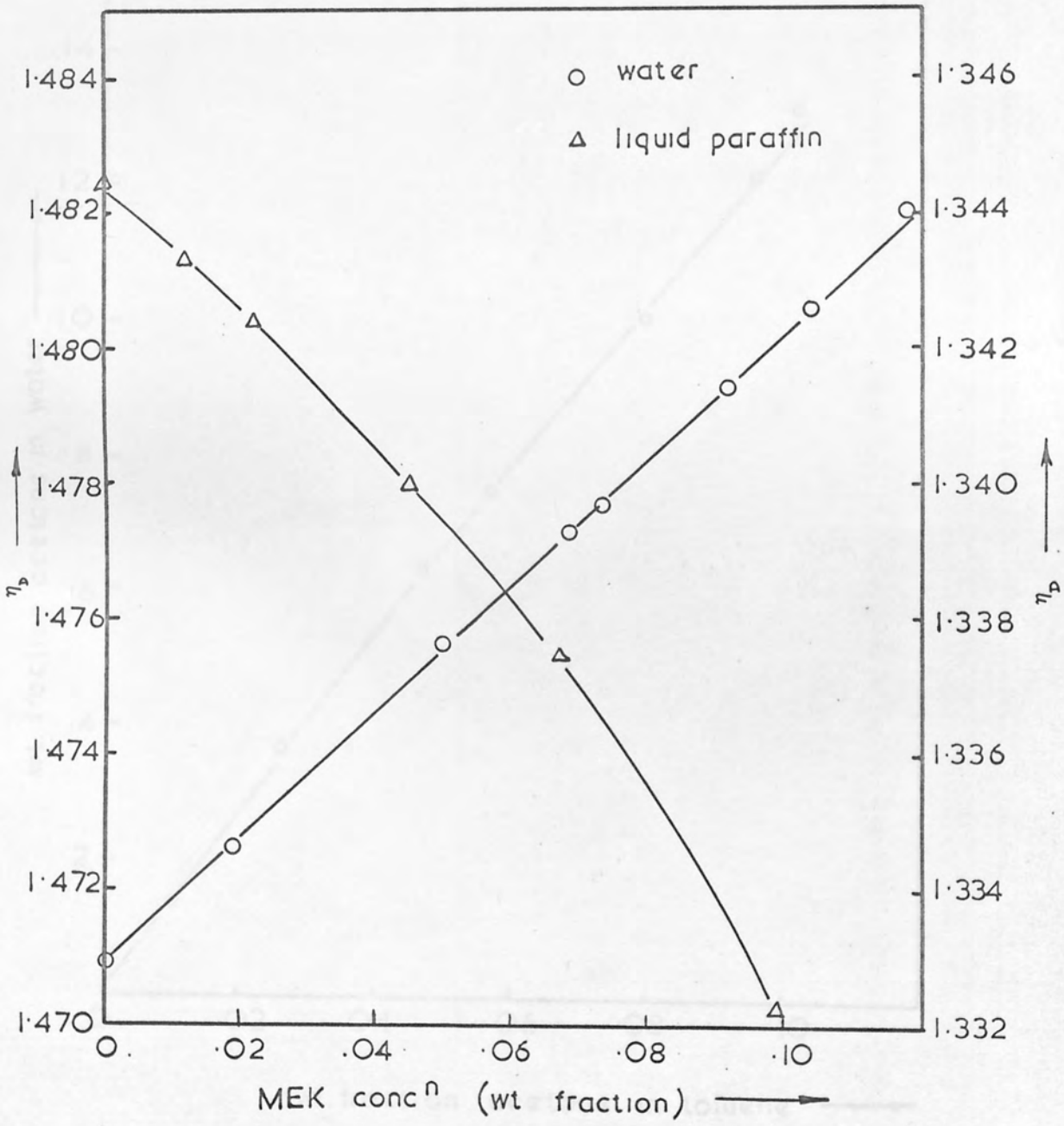

Fig. II. Solute concentration vs refractive index for liquid paraffin MEK - water system at 22·5°c

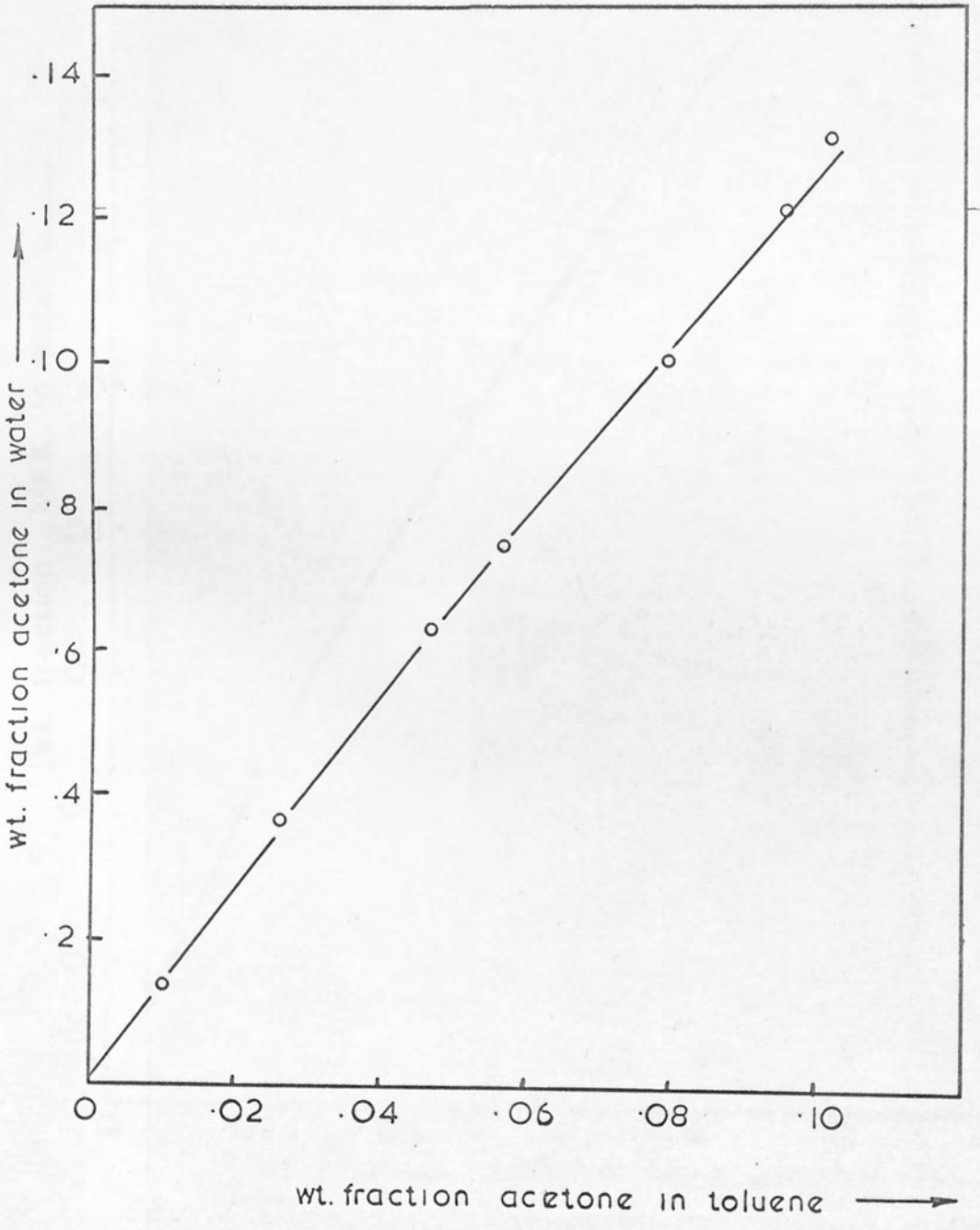

Fig. III Equilibrium diagram for system toluene acetone - water

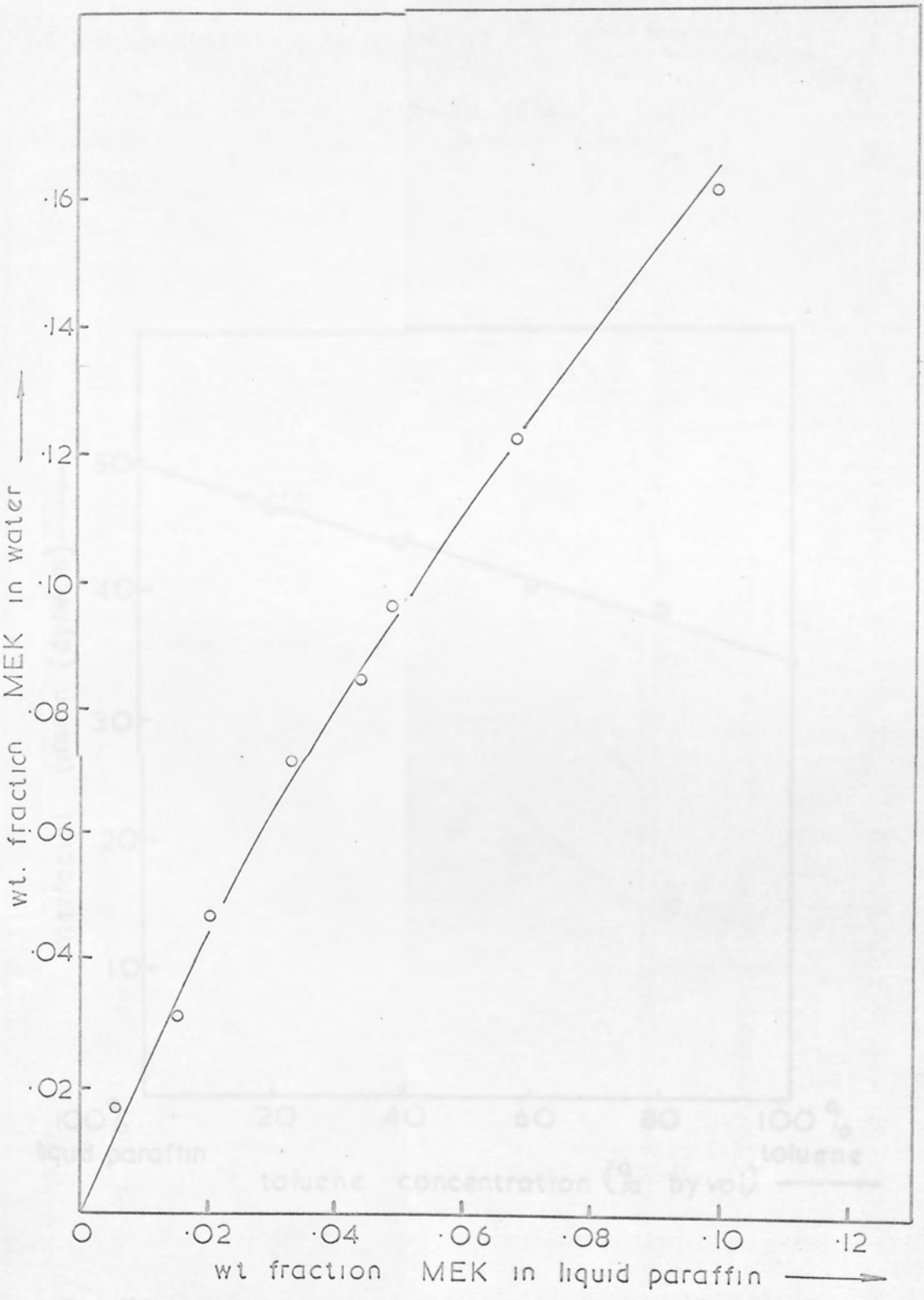

Fig. IV . Equilibruim diagram for system liquid paraffin - MEK - water

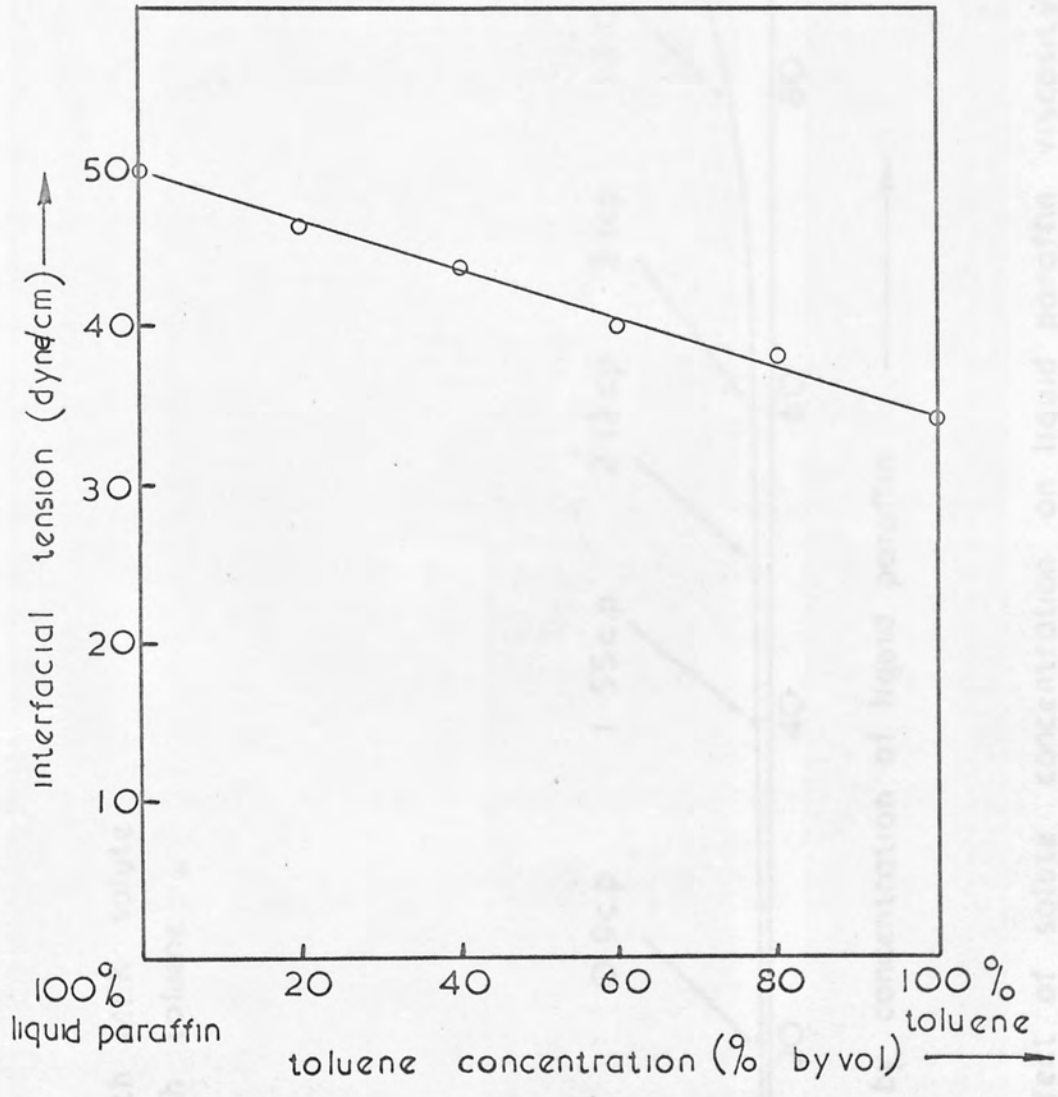

Fig. V. Variation of interfacial tension (with water) with concentration for liquid - paraffin / toluene mixtures

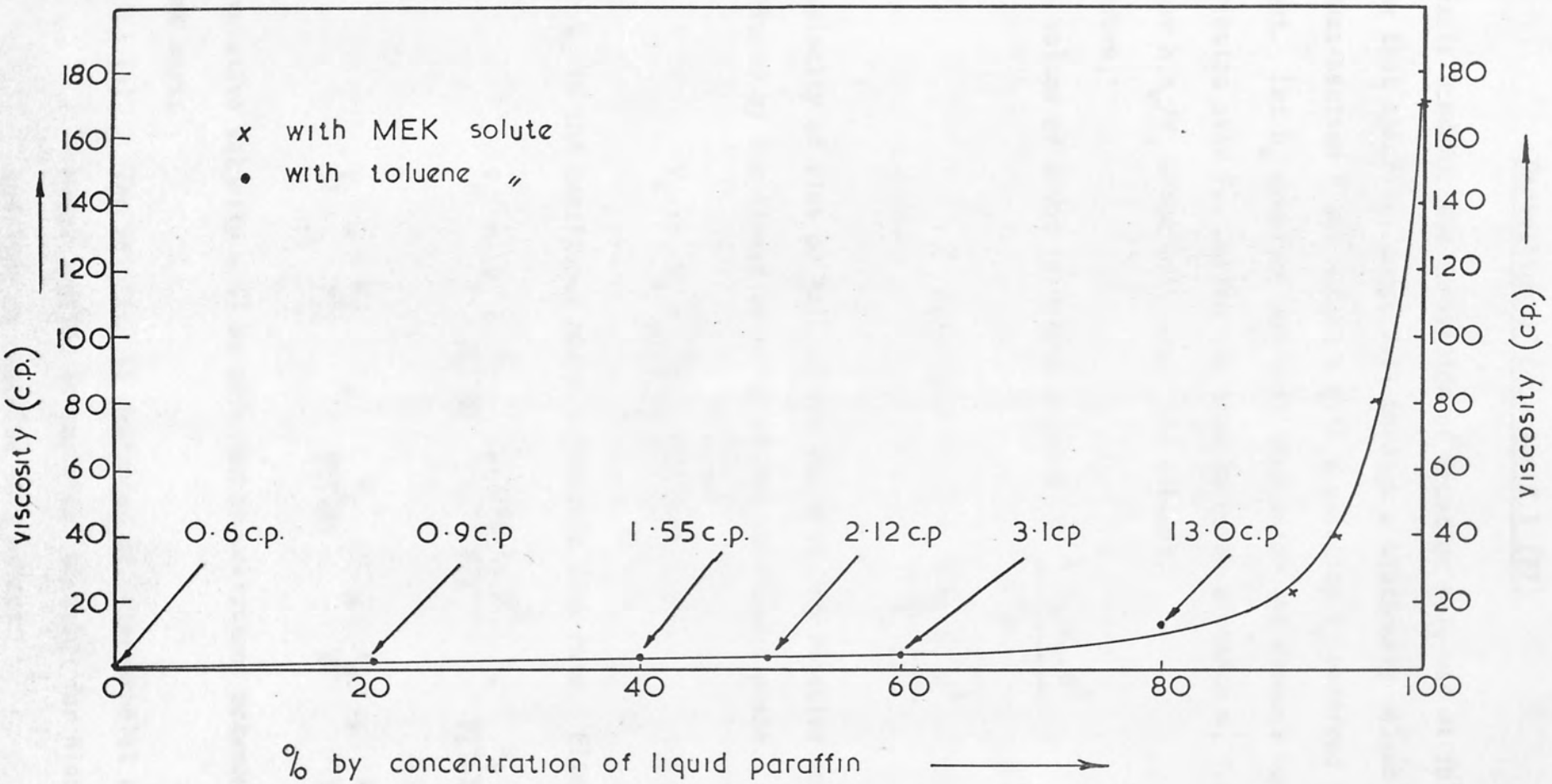

Fig. VI The effect of solute concentration on liquid paraffin viscosity at 22·5°c

APPENDIX 5

Derivation of Equation 2.1 (77)

The basis used for the derivation of Equation 2.1, was as follows:- Assume that spherical drops fall through a stationary volume element of cross-section F and height h with a velocity V_s referred to the element. Let n_k droplets per unit time enter the element equally distributed over F. During the time to cover distance h, i.e. h/V_s a further $h.n_k/V_s$ drops will enter the element.

Therefore,

Total volume of drops in volume element $= \dfrac{h.n_k.k_1.d^3}{V_s}$ (i)

$$\text{Hold-up } X = \frac{h.n_k.k_1\ d^3}{V_s.F.} \qquad \text{(ii)}$$

The velocity of rise or fall of the drops is the relative velocity V_x diminished by the linear velocity of the continuous phase.

$$V_s = V_x - \frac{W_c.}{F\ (1-X)} \qquad \text{(iii)}$$

where W_c is the continuous phase volumetric flow rate. Eliminating V_s

$$V_x = V_s + \frac{W_c}{F(1-X)} = \frac{n_k.k_1\ d^3}{F.X} + \frac{W_c}{F(1-X)} \qquad \text{(iv)}$$

$$V_x = \frac{W_d}{F.X} + \frac{W_c}{F(1-X)} = \frac{V_d}{X} + \frac{V_c}{1-X} \qquad \text{(v)}$$

The relative velocity will be affected by collisions between the droplets in two ways.

(a) The velocity is decreased by inter-droplet collisions. Misek applied an empirical equation for hindered settling to describe this effect:

$$V_{ox} = \bar{V}_o (1-X) \exp [-4.1X] \qquad \text{(vi)}$$

(b) Coalescence results in increased droplet sizes with increased velocities.

Considering first the case for equal size drops; the coalescence of two droplets of equal initial diameter d_o yields a droplet of diameter d_1, where,

$$d_1 = \sqrt[3]{2\, d_o^3} = d_o \sqrt[3]{2} \qquad \text{(vii)}$$

The droplets will split in the region of the agitator but coalesce to a final diameter $\bar{d}$. The critical diameter affecting velocity is the hydraulic mean diameter,

$$\bar{d} = \frac{\Sigma d^2}{\Sigma d} \qquad \text{(viii)}$$

If an initial number of droplets n_o require q binary collisions to reach the final size $\bar{d}$, the system will then contain q coalesced droplets and n - 2q non-coalesced droplets. Hence the final droplet size,

$$\bar{d} = \frac{(n_o - 2q)\, d_o^2 + q\, (\sqrt[3]{2}\, d_o)^2}{(n_o - 2q)\, d_o + q\, (\sqrt[3]{2}\, d_o)} \qquad \text{(ix)}$$

$$= d_o \left[\frac{n_o - q\,(2 - 2^{2}/3)}{n_o - q\,(2 - 2^{1}/3)} \right] \qquad \text{(x)}$$

Substituting $Q = q/n_o$ and evaluating

$$\bar{d} = d_o \left[\frac{1 - Q\ 0.41}{1 - Q\ 0.74} \right] \qquad \text{(xi)}$$

For the more precise case when after each coalescence the mean droplet diameter is changed and coalescence is between droplets of the mean diameter corresponding to the previous collision, assuming a large number of drops are present, Misek obtained the simplified expression,

$$\frac{\bar{d}}{d_o} = \frac{1}{(1-Q)^{0.328}} \qquad \text{(xii)}$$

Comparison of calculated values of $\bar{d}/d_o$ from Eqns.xi and xii showed that the difference between the mechanisms was small.

Since droplet size does not change over wide limits,

$$\frac{V_x}{V_{ox}} = \frac{1}{(1-Q)^{m.0.328}} \qquad \text{(xiii)}$$

where m is a function of $N_{Re} = \frac{\bar{V}_o \, d_o \, \rho}{\mu}$

as for the terminal falling velocities of rigid spheres (33).

Misek replaced the function in Equation xiii, by an approximation,

$$\text{In} \frac{V_x}{V_{ox}} = k_2.m.X = \frac{Z}{m} X \qquad \text{(xiv)}$$

assuming the number of collisions Q is proportional only to the dispersed phase hold-up (i.e. $Q = k_2 X$) and the magnitude of k_2 depends on the physical properties of the system, agitation and coalescence time.

Combining Equations v, vi and xiv,

$$\frac{V_d}{X} + \frac{V_c}{1-X} = \bar{V}_o (1 - X). \exp\left[\frac{Z}{m} - 4.1 \right] X \qquad (2.1)$$

APPENDIX 6

Contents of This Appendix

T = Toluene

W = Water

L.P. = Liquid Paraffin

TABLE I

System : Toluene/(Acetone) → Water

W = Wetted Disc Column; N.W. = Non-Wetted Disc Column.

Run No.	Comments	RPM	V_d (l/min)	V_c (l/min)	C_1 (Wt.%)	C_2 (Wt.%)	W_1 (Wt.%)	W_2 (Wt.%)
1	W.	1000	2.5	2.5	10.4	1.2	8.1	0
2	"	"	"	"	9.35	1.35	7.0	0
3	"	"	1.5	3.0	9.35	0.3	4.0	0
4	"	"	3.0	1.5	7.8	2.3	9.4	0
5	"	"	1.0	3.5	7.35	0.2	1.8	0
6	"	750	2.5	2.5	9.35	1.5	6.9	0
7	"	"	1.5	3.0	12.0	0.55	5.2	0
8	"	"	3.0	1.5	8.5	2.8	9.7	0
9	"	"	2.8	2.8	10.65	1.45	8.1	0
10	"	"	3.8	1.9	8.5	2.6	10.1	0
11	"	"	1.9	3.8	10.2	0.55	4.34	0
12	"	0	2.5	2.5	7.35	1.9	4.8	0
13	"	1250	2.2	2.2	2.15	0.3	1.6	0
14	N.W.	1000	1.5	1.5	11.2	1.8	8.3	0
15	"	"	3.0	3.0	11.2	1.9	8.3	0
16	"	"	1.5	1.5	10.5	1.7	7.8	0
17	"	"	1.0	2.0	11.6	1.15	4.7	0
18	"	"	2.0	1.0	10.95	4.0	11.9	0
19	"	"	2.0	1.0	10.07	3.3	11.7	0
20	"	750	1.75	1.75	10.35	1.7	7.6	0
21	"	"	1.75	1.75	10.35	1.4	7.9	0
22	"	500	2.2	2.2	9.65	2.1	6.7	0

TABLE I (cont'd)

K_{exp}, K_s, K_c, and K_o are the observed, stagnant drops, circulating drops and oscillating drops mass transfer coefficients respectively.

Run No.	D_{32} (cm)	X (%)	K_{exp}/K_s	K_{exp}/K_c	K_{exp}/K_o	Efficiency	Pe($\times 10^4$)
1	0.74	10.0	145.8	5.3	3.8	0.88	14.7
2	0.9	11.0	140.1	4.7	3.7	0.86	16.4
3	0.58	7.5	104.4	5.2	2.7	0.97	9.6
4	1.05	12.0	227.5	6.7	5.7	0.70	19.8
5	0.58	7.0	65.0	3.9	1.76	0.97	7.4
6	0.9	8.0	140.3	3.8	4.1	0.84	21.7
7	0.75	6.3	104.9	3.8	4.1	0.95	14.6
8	1.04	10.6	148.5	4.1	4.3	0.67	22.0
9	1.02	10.3	157.9	4.3	4.6	0.83	22.0
10	1.1	13.1	204.3	5.2	5.7	0.69	24.3
11	0.84	8.1	115.8	3.9	3.6	0.94	16.6
12	1.05	7.0	111.6	2.6	3.3	0.74	28.4
13	0.78	16.7	56.1	3.0	1.7	0.86	8.5
14	0.63	7.6	67.2	3.3	1.8	0.84	9.6
15	1.13	12.0	202.2	5.4	4.7	0.83	23.0
16	0.63	7.0	77.8	3.7	2.0	0.84	10.4
17	0.52	6.2	38.1	2.5	1.07	0.9	6.8
18	0.76	9.3	77.8	3.2	2.05	0.63	12.2
19	0.66	8.0	108.0	4.5	2.6	0.67	12.2
20	0.76	7.0	81.9	3.0	2.6	0.84	14.6
21	0.82	7.0	105.6	3.7	3.3	0.86	15.7
22	1.01	7.0	109.4	2.8	3.3	0.78	24.0

TABLE I (cont'd)

Run No.	Vortex Height (cm)	Vortex Base (cm)	Sheet Extent (cm)	Sheet Thickness (cm)
1	3.75	4.4	2.2	0.30
2	3.75	4.4	2.2	0.30
3	3.75	4.0	1.3	0.25
4	3.75	4.6	2.6	0.30
5	3.75	3.8	1.0	0.2
6	3.0	3.25	3.25	0.3
7	3.0	2.55	2.0	0.3
8	3.0	3.6	3.9	0.3
9	3.0	3.5	3.7	0.3
10	3.0	4.25	4.2	0.35
11	3.0	2.9	2.5	0.30
12	0.5	4.5	1.5	0.3
13	4.25	3.6	3.6	0.25
14	3.75	3.25	1.3	0.2
15	3.75	4.2	2.6	0.3
16	3.75	3.25	1.3	0.2
17	3.75	2.9	1.0	0.2
18	3.75	3.6	1.75	0.25
19	3.75	3.6	1.75	0.25
20	3.0	2.7	2.3	0.3
21	3.0	2.7	2.3	0.3
22	0.6	4.5	1.6	0.3

TABLE II

System : Toluene ← Water/(Acetone)

W. = Wetted Disc Column; N.W. = Non-Wetted Disc Column.

Run No.	Comments	RPM	V_d (l/min)	V_c (l/min)	C_1 (Wt.%)	C_2 (Wt.%)	W_1 (Wt.%)	W_2 (Wt.%)
23	W.	1000	2.5	2.5	4.8	6.4	6.0	7.4
24	"	"	2.5	2.5	0.42	6.1	4.4	9.7
25	"	"	1.5	3.0	1.05	6.8	7.1	9.7
26	"	"	3.0	1.5	1.3	5.3	3.9	10.5
27	"	"	1.0	3.5	1.5	3.05	3.7	4.1
28	"	750	2.5	2.5	2.2	5.0	4.75	7.25
29	"	"	1.5	3.0	1.7	4.5	5.0	6.3
30	"	"	3.0	1.5	3.0	4.9	4.8	8.2
31	"	"	2.8	2.8	0	5.5	4.3	9.4
32	"	"	3.8	1.9	0.7	5.0	2.8	11.0
33	"	"	1.9	3.8	0.5	4.2	4.4	6.05
34	"	"	2.75	2.75	0	4.6	3.45	7.6
35	"	"	1.9	3.8	0	5.1	5.3	7.6
36	"	"	3.8	1.9	0	3.4	1.3	7.6
37	"	0	2.5	2.5	1.8	3.5	4.15	5.5
38	N.W.	1000	1.5	1.5	0.3	6.0	4.1	9.4
39	"	"	1.5	1.5	0.35	6.4	4.1	9.7
40	"	"	1.0	2.0	0.35	7.4	7.1	10.3
41	"	"	2.0	1.0	0.4	4.8	1.5	10.0
42	"	750	1.75	1.75	0.25	6.4	3.95	9.7
43	"	500	2.2	2.2	0.23	6.3	4.4	10.1
44	"	"	2.2	2.2	0.2	6.1	4.6	10.1

APPENDIX 6 (cont'd)

TABLE II (cont'd)

Run No.	D_{32} (cm)	X (%)	K_{exp}/K_s	K_{exp}/K_c	K_{exp}/K_o	Efficiency	Pe($\times 10^4$)
23	0.44	17	10.3	0.8	0.55	0.76	5.3
24	0.44	18	9.6	0.78	0.5	0.83	4.9
25	0.37	17	5.1	0.58	0.26	0.92	3.07
26	0.52	23	8.2	0.64	0.425	0.61	5.2
27	0.34	10	7.2	0.8	0.37	0.98	3.2
28	0.47	12.5	18.2	1.11	0.98	0.86	7.26
29	0.4	9	10.8	0.82	0.58	0.92	5.4
30	0.56	15	15.4	0.85	0.80	0.59	8.27
31	0.53	16	13.9	0.84	0.73	0.78	7.4
32	0.62	18	18.5	0.91	0.95	0.57	9.7
33	0.44	11	12.7	0.85	0.68	0.92	6.4
34	0.62	20	16.6	1.02	0.84	0.81	7.15
35	0.47	12	11.8	0.80	0.63	0.89	6.34
36	0.66	22	19.5	1.04	0.96	0.60	8.75
37	0.5	8	16.6	0.72	0.91	0.73	11.56
38	0.34	10	6.88	0.67	0.36	0.84	3.77
39	0.34	10	7.8	0.77	0.40	0.87	3.77
40	0.53	30	4.8	0.72	0.22	0.96	2.06
41	0.48	25	6.77	0.78	0.33	0.62	3.0
42	0.33	7	12.15	0.86	0.66	0.87	5.9
43	0.47	9	18.5	1.01	1.00	0.83	8.4
44	0.47	9	16.5	0.9	0.9	0.80	8.4

TABLE III

System: Liquid Paraffin/(M.E.K.) → Water

W. = Wetted Disc Column; N.W. = Non-Wetted Disc Column.

Run No.	Comments	RPM	V_d (l/min)	V_c (l/min)	C_1 (Wt.%)	C_2 (Wt.%)	W_1 (Wt.%)	W_2 (Wt.%)
45	N.W.	1000	1.5	1.5	9.8	1.1	7.1	0
46	"	"	1.0	1.0	9.9	0.9	7.3	0
47	"	"	1.0	1.0	9.1	1.1	6.5	0
48	"	"	1.5	1.5	3.0	1.2	1.5	0
49	"	"	0.75	1.5	9.4	2.8	2.8	0
50	"	"	1.5	0.75	9.4	4.4	8.1	0
51	"	"	1.5	1.5	2.35	0.65	1.5	0
52	"	"	0.5	2.0	9.05	2.5	1.4	0
53	"	1250	0.9	0.9	8.7	3.1	4.6	0
54	"	750	1.4	1.4	8.7	4.0	4.0	0
55	"	500	2.0	2.0	8.6	5.5	2.6	0
56	"	1500	0.6	0.6	8.6	0.8	6.5	0
57	W.	1000	1.0	1.0	8.7	3.3	4.5	0
58	"	500	2.0	2.0	8.7	5.8	2.5	0
59	"	1250	0.9	0.9	9.3	2.7	5.4	0
60	"	750	1.4	1.4	9.3	4.0	4.4	0

TABLE III (cont'd)

Run No.	Mean μ_d (C.P.)	D_{32} (cm)	X (%)	K_{exp}/K_s	K_{exp}/K_c	K_{exp}/K_o	Efficiency	Pe($\times 10^4$)
45	80	0.21	15.0	135.4	12.1	0.28	0.88	159.5
46	80	0.20	11.0	124.0	13.3	0.23	0.91	132.1
47	80	0.20	11.0	106.0	11.5	0.19	0.88	131.5
48	130	0.21	15.0	78.6	7.2	0.13	0.60	250.7
49	60	0.20	9.0	34.5	3.9	0.07	0.70	95.5
50	40	0.20	13.0	24.5	2.2	0.065	0.53	78.8
51	120	0.21	15.0	107.2	9.9	0.18	0.72	231.3
52	50	0.20	6.0	29.1	3.1	0.068	0.72	83.2
53	70	0.21	16.0	27.6	4.4	0.063	0.64	78.3
54	70	0.35	12.0	116.8	5.7	0.38	0.54	257.2
55	50	0.53	8.0	223.1	3.6	0.84	0.36	566.0
56	80	0.2	14.5	56.1	12.8	0.10	0.90	62.2
57	60	0.19	17.0	18.8	3.1	0.03	0.62	64.2
58	40	0.47	10.8	93.4	2.2	0.41	0.33	306.5
59	70	0.19	21.4	20.8	4.5	0.03	0.71	56.8
60	60	0.28	14.7	57.1	4.1	0.19	0.57	149.0

TABLE IV

System : Liquid Paraffin ← Water/(MEK)

W. = Wetted Disc Column; N.W. = Non-Wetted Disc Column

Run No.	Comments	RPM	V_d (l/min)	V_c (l/min)	C_1 (Wt.%)	C_2 (Wt.%)	W_1 (Wt.%)	W_2 (Wt.%)
61	N.W.	1000	1.0	1.0	0.9	3.3	7.7	9.8
62	"	"	1.0	1.0	1.5	4.5	7.6	10.25
63	"	"	0.75	1.5	0.75	4.1	10.6	12.1
64	"	"	1.5	0.75	0.75	3.35	7.3	12.1
65	"	1250	0.9	0.9	0.4	3.6	7.1	9.95
66	"	750	1.4	1.4	0.4	2.1	8.42	10.0
67	"	500	2.0	2.0	2.0	2.9	9.3	10.05
68	W.	1000	1.0	1.0	1.75	3.3	7.9	9.3
69	"	500	2.0	2.0	1.75	2.7	8.5	9.3

TABLE IV (cont'd)

Run No.	Mean μ_d (C.P.)	D_{32} (cm)	X (%)	K_{exp}/K_s	K_{exp}/K_c	K_{exp}/K_o	Efficiency	Pe($\times 10^4$)
61	130	0.25	21.0	52.6	8.1	0.110	0.60	149.8
62	120	0.28	56.0	49.0	9.9	0.114	0.83	93.1
63	120	0.23	27.0	23.8	4.9	0.05	0.63	101.9
64	110	0.23	30.0	33.5	5.6	0.07	0.49	117.1
65	130	0.19	50.0	15.5	5.2	0.016	0.7	68.0
66	120	0.34	34.0	36.9	4.0	0.09	0.37	195.0
67	110	0.45	15.0	143.6	4.7	0.36	0.30	598.6
68	100	0.26	40.0	18.8	4.0	0.05	0.53	83.2
69	100	0.56	40.0	86.2	4.2	0.22	0.33	359.7

TABLE V

System : Toluene - Acetone - Water

Wetted Cone Column

Run No.	Comments	RPM	V_d (l/min)	V_c (l/min)	C_1 (Wt.%)	C_2 (Wt.%)	W_1 (Wt.%)	W_2 (Wt.%)
70	T → W	1000	2.0	2.0	11.25	1.5	7.9	0
71	"	500	3.0	3.0	10.15	2.55	6.20	0
72	"	1250	1.75	1.75	10.15	1.5	7.0	0
73	"	750	2.4	2.4	10.10	2.2	6.45	0
74	"	0	3.0	3.0	10.10	3.5	5.5	0
75	"	1000	2.25	1.125	10.20	3.3	10.7	0
76	"	"	1.435	2.87	10.25	0.35	4.1	0
77	"	"	1.0	3.5	11.25	0.2	2.65	0
78	"	"	2.0	2.0	10.10	1.2	7.2	0
79	"	"	1.0	2.0	10.10	0.25	4.1	0
80	T ← W	1000	2.0	2.0	0.35	7.0	3.35	9.55
81	"	500	3.0	3.0	0.2	7.45	5.35	12.2
82	"	1250	1.75	1.75	0.2	8.8	4.0	12.2
83	"	750	2.4	2.4	0.45	7.5	5.0	11.65
84	"	0	3.0	3.0	0.4	6.3	6.2	11.70
85	"	1000	2.25	1.125	0.25	5.0	1.25	10.25
86	"	"	1.435	2.87	0.25	7.4	7.05	10.30
87	"	"	1.0	3.5	0.95	3.0	3.5	4.05
88	"	"	1.435	2.87	0	7.8	7.2	10.8
89	"	"	2.25	1.125	0.2	4.8	1.2	10.0

APPENDIX 6 (cont'd)

TABLE V (cont'd)

Run No.	D_{32} (cm)	X (%)	K_{exp}/K_s	K_{exp}/K_c	K_{exp}/K_o	Efficiency	Pe($\times 10^4$)
70	0.45	12.0	13.97	0.97	0.75	0.86	6.12
71	0.84	9.0	56.4	1.55	2.7	0.75	21.9
72	0.34	12.0	6.66	0.62	0.35	0.85	4.03
73	0.53	8.0	22.8	0.95	1.24	0.78	12.2
74	1.14	8.3	80.7	1.7	3.46	0.65	32.0
75	0.45	14.0	10.6	0.78	0.56	0.67	5.56
76	0.33	7.6	11.6	0.91	0.62	0.96	5.2
77	0.25	5.0	7.7	0.69	0.36	0.98	4.26
78	0.45	11.0	16.2	1.06	0.87	0.88	6.6
79	0.26	5.0	8.6	0.79	0.41	0.97	4.12
80	0.44	18.6	22.0	2.14	1.14	0.97	3.85
81	0.52	13.7	18.9	1.01	1.01	0.81	8.72
82	0.36	25.0	8.7	1.24	0.42	0.96	2.2
83	0.41	13.7	11.75	0.88	0.63	0.85	5.5
84	0.55	13.0	14.6	0.72	0.77	0.70	9.7
85	0.4	17.0	8.5	0.82	0.44	0.64	3.9
86	0.36	14.0	6.9	0.75	0.35	0.95	3.25
87	0.24	10.0	3.9	0.55	0.16	0.98	2.27
88	0.37	15.0	7.2	0.80	0.37	0.96	3.17
89	0.4	17.0	8.1	0.78	0.42	0.63	3.9

TABLE VI

System : Toluene - Acetone - Water

Run No.	RPM	X (%)	$V_c = V_d$ (l/min)	C_1 (Wt.%)	C_2 (Wt.%)	W_1 (Wt.%)	W_2 (Wt.%)
90	1000	9.0	2.0	11.6	2.5	0	6.5
91	"	11.0	"	10.4	2.3	0	5.75
92	"	9.4	"	10.1	2.65	0	5.35
93	"	7.8	"	10.8	4.3	0	5.25
94	"	4.0	"	12.3	6.8	0	3.7
95	"	14.6	"	2.35	6.0	6.4	3.9
96	"	15.0	"	2.1	5.1	6.0	4.2
97	"	16.6	"	3.0	3.85	4.0	4.05
98	"	11.0	"	2.5	2.7	4.0	3.6
99	"	7.7	"	3.75	6.3	10.1	7.5
100	750	7.0	"	11.6	3.0	0	6.0
101	"	8.0	"	10.4	2.0	0	5.8
102	"	8.7	"	10.1	3.25	0	4.9
103	"	6.5	"	10.8	5.0	0	4.5
104	"	4.6	"	12.35	7.6	0	3.0
105	"	11.2	"	2.3	6.2	6.4	4.2
106	"	10.0	"	2.1	4.9	6.0	4.35
107	"	10.0	"	3.0	3.6	4.0	4.3
108	"	7.0	"	2.9	3.1	4.0	4.2
109	"	6.0	"	3.8	6.3	10.1	7.3
110	1250	32.0	"	5.8	3.4	0	2.2
111	0	2.5	"	11.1	7.6	0	3.1
112	750	4.0	"	10.8	7.3	0	2.9

TABLE VI (cont'd)

Comp. No. = Number of compartments used.

Run No.	Comp. No.	Efficiency	Comments
90	19	0.79	T → W
91	15	0.78	"
92	11	0.74	"
93	6	0.60	"
94	2	0.45	"
95	19	0.76	T ← W
96	15	0.60	"
97	11	0.58	"
98	6	0.55	"
99	2	0.52	"
100	19	0.75	T → W
101	15	0.75	"
102	11	0.68	"
103	6	0.54	"
104	2	0.38	"
105	19	0.65	T ← W
106	15	0.58	"
107	11	0.55	"
108	6	0.58	"
109	2	0.52	"
110	6	0.42	T → W
111	2	0.32	"
112	2	0.33	"

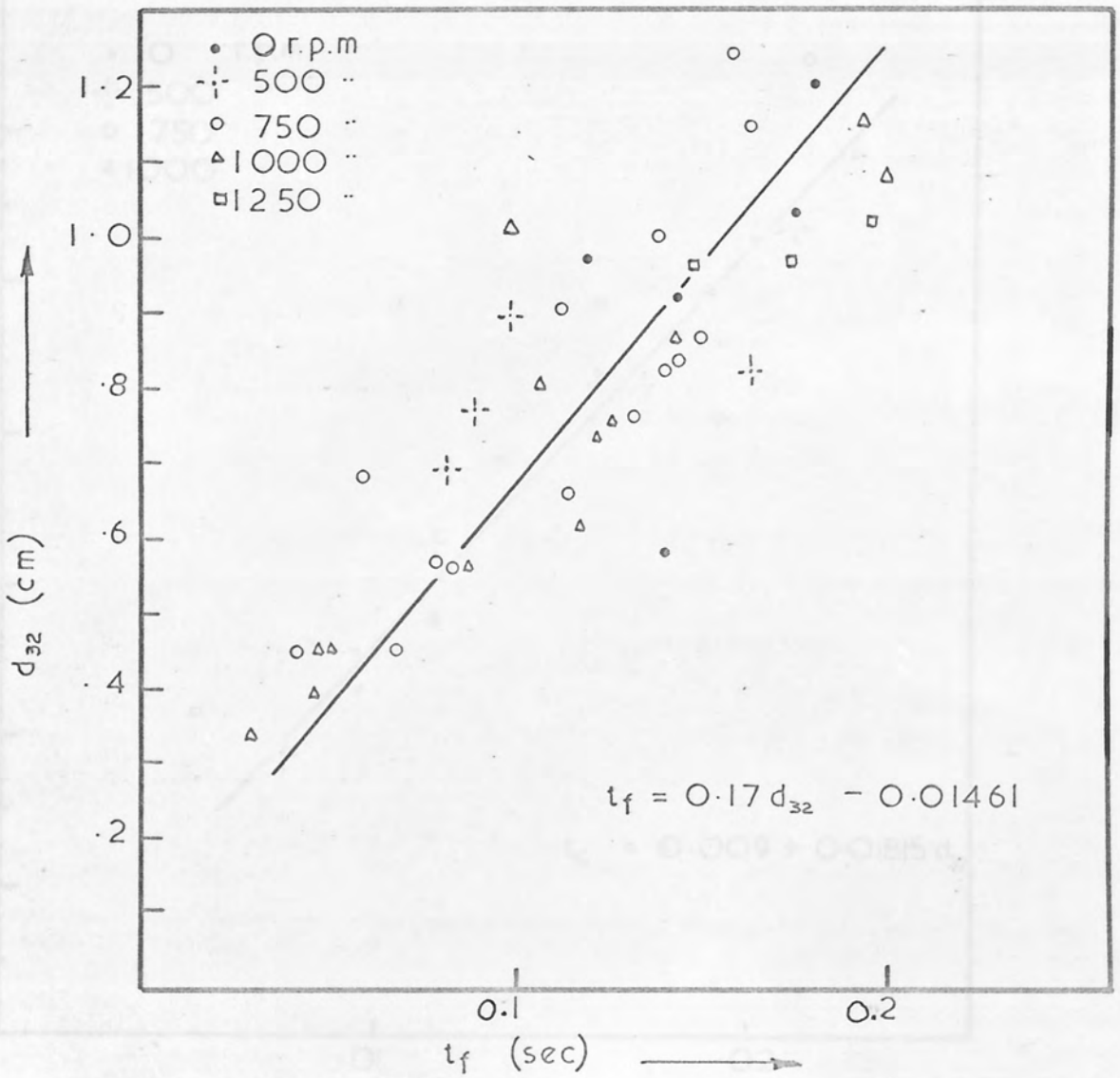

Fig. VII Correlation of drop size vs. formation time

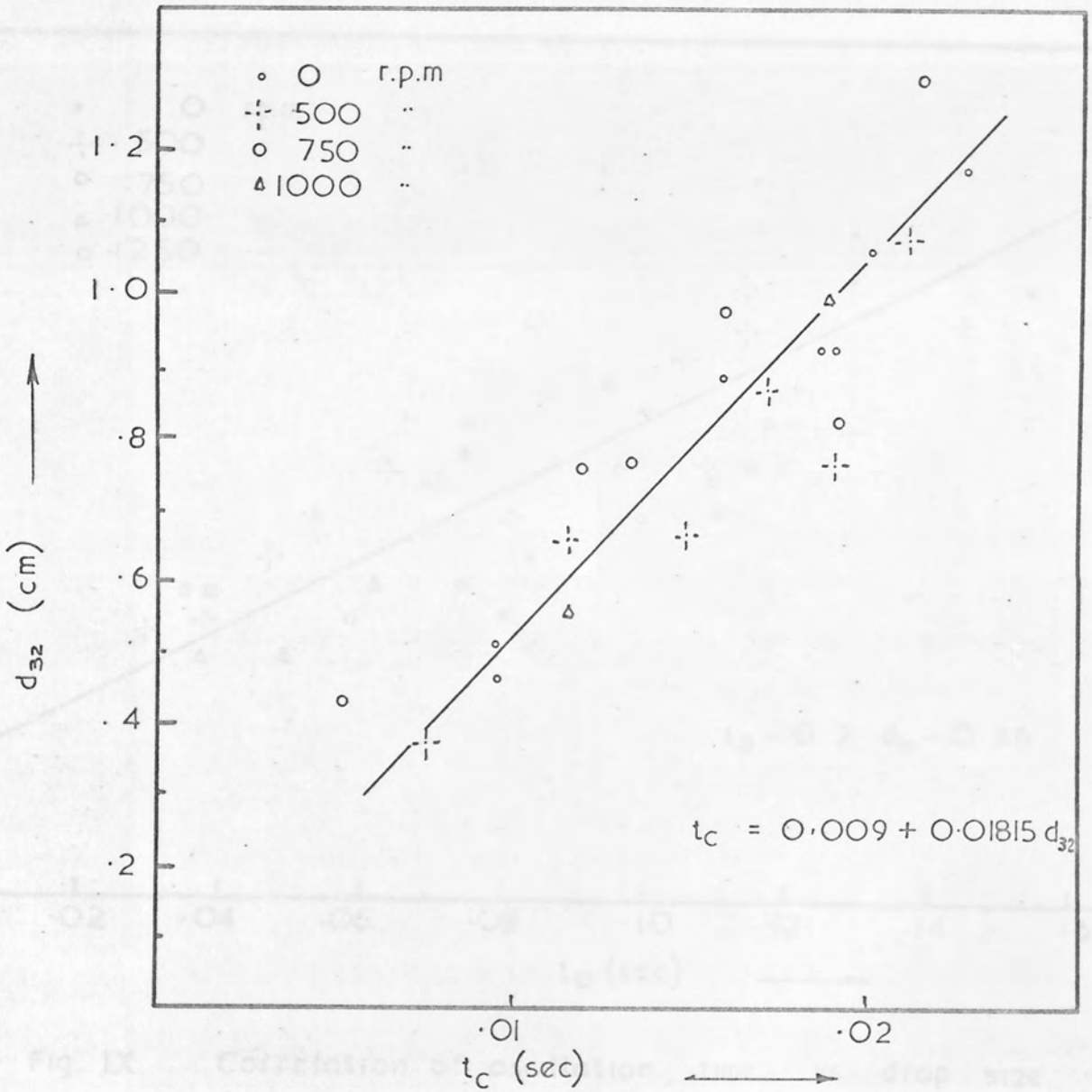

Fig .VIII Correlation of drop size vs coalescence time.

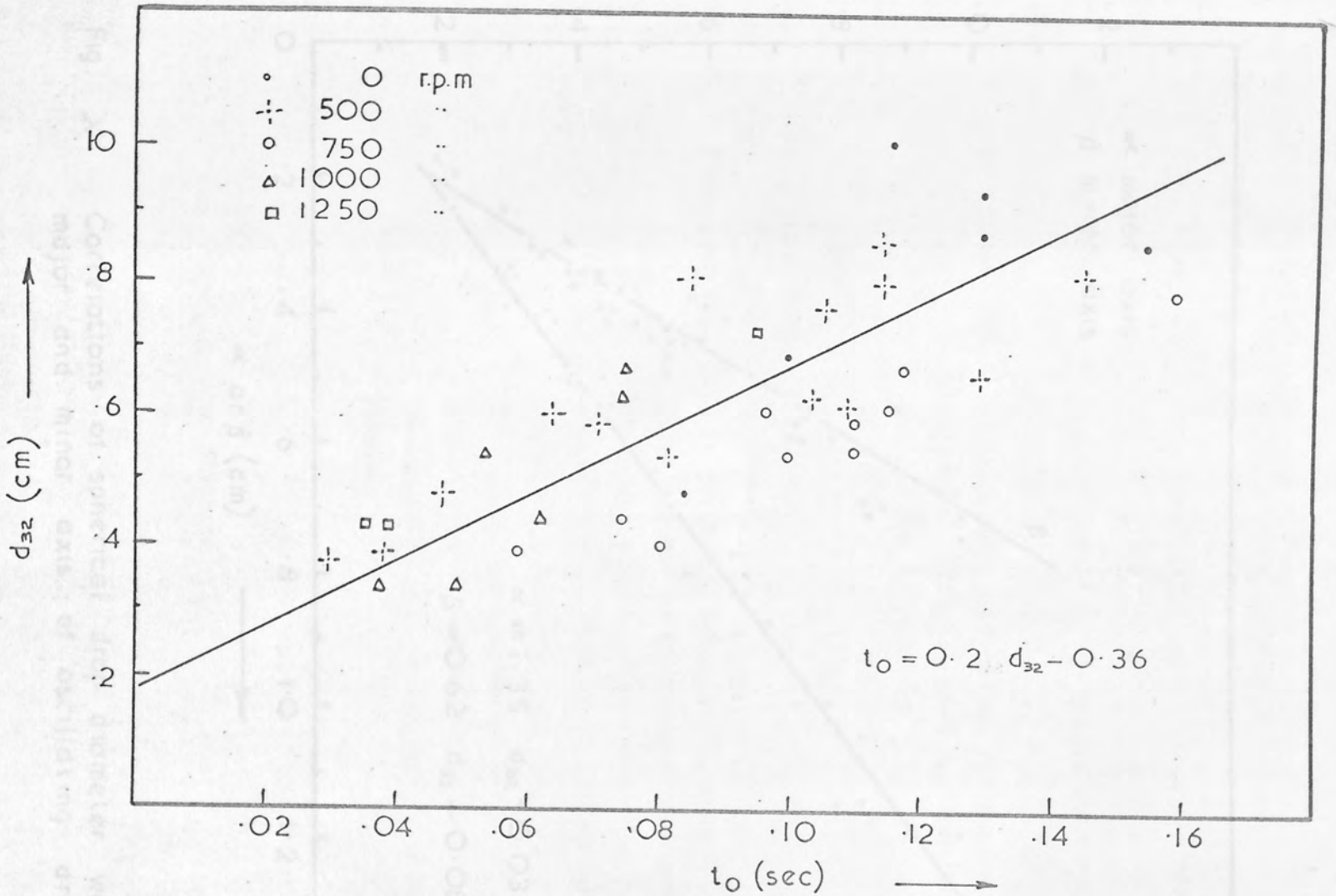

Fig. IX Correlation of oscillation time vs. drop size

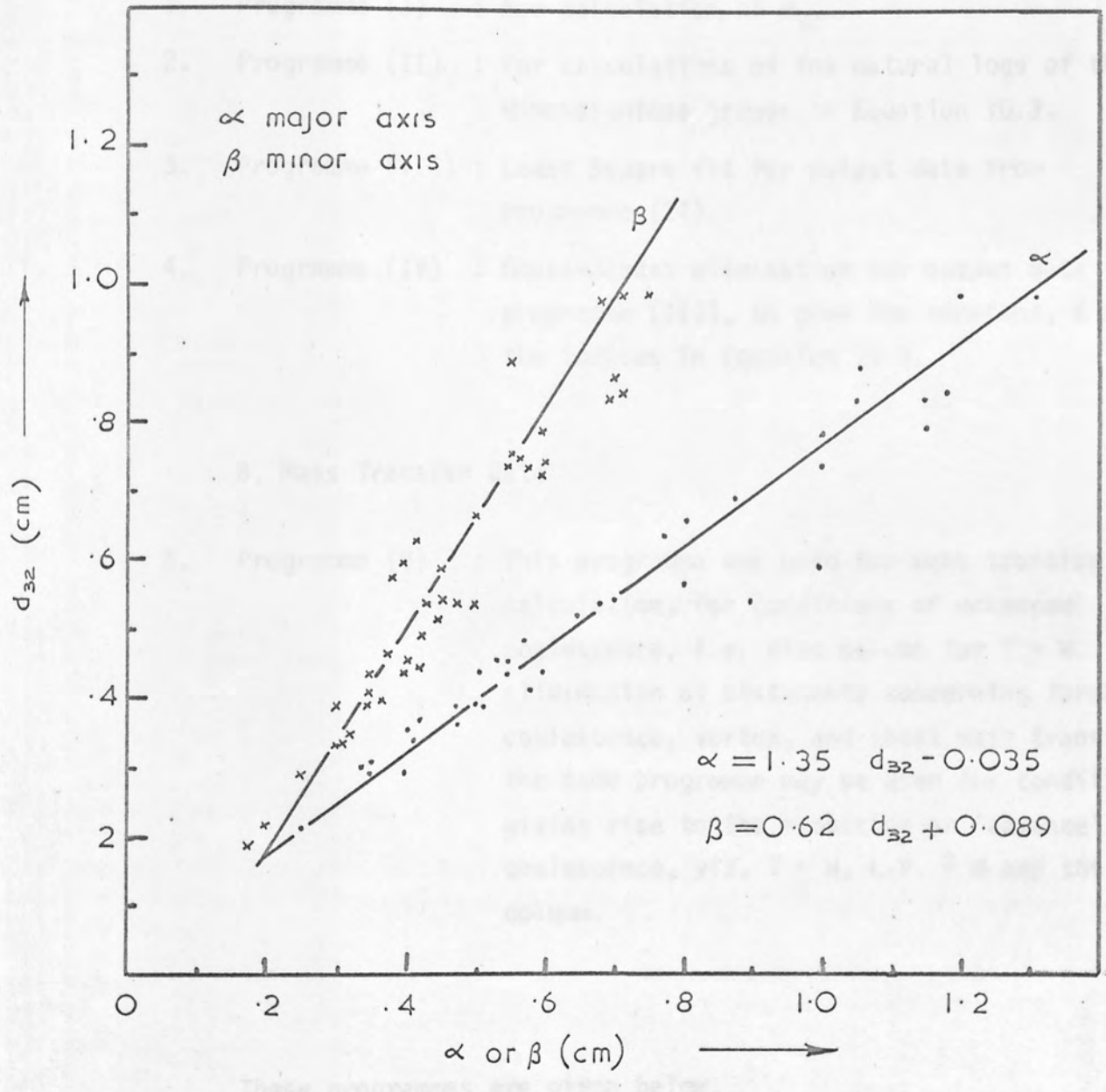

Fig. X Correlations of spherical drop diameter with major and minor axis of oscillating drops

APPENDIX 7

Computer Programmes And Calculation Procedure

A. Drop Size Correlations.

1. Programme (I) : For calculation of d_{32}.
2. Programme (II) : For calculations of the natural logs of the dimensionless groups in Equation 10.3.
3. Programme (III) : Least Square fit for output data from programme (II).
4. Programme (IV) : Gauss-Jordan elimination for output data from programme (III), to give the constant, K and the indices in Equation 10.3.

B. Mass Transfer Data

5. Programme (V) : This programme was used for mass transfer calculation, for conditions of enhanced coalescence, i.e. disc column for T → W. With elimination of statements concerning formation coalescence, vortex, and sheet mass transfers, the same programme may be used for conditions, giving rise to the reduction or 'absence' of coalescence, viz, T ← W, L.P. ⇄ W and the cone column.

These programmes are given below,

APPENDIX 7 (CONT'D.)

PROGRAMME I

```
10  DATA N1,N2,N3,N4,N5,N6,N7,N8,N9,N10,N11,N12,N13,N14,N15
11  DATA N16,N17,N18,N19,N20,N21,N22,N23,N24,N25,N26,N27,N28
20  DATA .5,1,1.5,2,2.5,3,3.5,4,4.5,5,5.5,6,6.5,7,7.5,8
21  DATA 9,10,11,12,13,14,15,16,17,18,19,20,21,22,23,24,25,26
22  DATA 27,28,30,50
30  READ R,Z,M
40  DIM N(50),D(50),X(50),Y(50)
60  FOR I=1,Z
70  READ N(I)
80  NEXT I
90  FOR I=1,Z
100  READ D(I)
110  NEXT I
120  S1=0
130  S2=0
140  FOR I=1,Z
150  X(I)=N(I)*D(I)↑2
160  Y(I)=N(I)*D(I)↑3
170  S1=S1+X(I)
180  S2=S2+Y(I)
190  NEXT I
200  W=S2/S1
202  W=W/M
210  PRINT "W=",W
220  END
```

PROGRAMME II

```
10  DATA .1E-01,.125,.875,981,5.08,10.16,5.08,7.62,19
100  INPUT F
110  DIM D(100),N(100),M(100),L(100),T(100),W(100),B(100),G(100)
115  DIM R(100),K(100),H(100),S(100),X(100),Y(100),V(100),J(100)
116  DIM A(100)
120  READ M,W,B,G,R,K,H,S,Z
130  FOR I=1,F
140  READ D(I),J(I),N(I),V(I),X(I),T(I),L(I)
150  NEXT I
160  FOR I=1,F
170  D(I)=LOG((D(I)/10)):N(I)=LOG((N(I)/60)):M(I)=LOG(M)
180  L(I)=LOG((L(I)/100)):T(I)=LOG(T(I)):W(I)=LOG(W)
190  B(I)=LOG(B):G(I)=LOG(G):R(I)=LOG(R):K(I)=LOG(K)
200  H(I)=LOG(H):S(I)=LOG(S):X(I)=LOG(X(I)):Y(I)=LOG((1-X(I)))
210  V(I)=LOG((V(I)*(1000/60))):J(I)=J(I)/Z:A(I)=1
220  NEXT I
230  FOR I=1,F
240  PRINT A(I): PRINT N(I): PRINT M(I): PRINT L(I): PRINT T(I)
245  PRINT W(I): PRINT B(I): PRINT G(I): PRINT R(I): PRINT K(I)
250  PRINT H(I): PRINT S(I): PRINT X(I): PRINT Y(I): PRINT V(I)
260  PRINT J(I): PRINT D(I)
270  NEXT I
280  END
```

PROGRAMME III

```
200  DIM A(100,20),K(100,20)
210  INPUT N,M
220  FOR R=1,N: FOR J=1,M: INPUT A(R,J): NEXT J: NEXT R
230  FOR I=1,(M-1): FOR J=1,M
240  FOR J=1,M
250  IF J>1 THEN 280
260  IF I>1 THEN 280
270  K(I,J)=N: NEXT J
280  K(I,J)=0
290  FOR R=1,N:K(I,J)=K(I,J)+A(R,I)*A(R,J)
300  NEXT R: NEXT J: NEXT I
310  FOR I=1,(M-1): FOR J=1,M
320  PRINT K(I,J): NEXT J
330  NEXT I
340  END
```

PROGRAMME IV

```
10  DIM A(20,20)
15  INPUT N
20  FOR I=1,N: FOR J=1,N+1: INPUT A(I,J): NEXT J: NEXT I
25  FOR K=1,N: FOR I=K+1,N
30  IF ABS(A(K,K))>ABS(A(I,K)) THEN  GOTO 40
35  FOR J=K,N+1:A(0,0)=A(I,J):A(I,J)=A(K,J):A(K,J)=A(0,0): NEXT J
40  NEXT I
42  IF A(K,K)=0 THEN 70
45  FOR J=N+1,K,-1:A(K,J)=A(K,J)/A(K,K): NEXT J
50  FOR M=1,N: FOR L=N+1,1,-1
55  IF M=K THEN  GOTO 65
60  A(M,L)=A(M,L)-A(M,K)*A(K,L): NEXT L
65  NEXT M: NEXT K
70  FOR I=1,N: PRINT A(I,N+1): NEXT I
75  END
```

APPENDIX 7 (CONT'D.)

PROGRAMME V

```
5  DATA 1
10  DATA .3E-04,.111E-04,5.03,5.03,.3
15  DATA .74,3.75,4.4,1.5,2.2,.9E-01,2500,10.4,.97,7.35,.35,.75
16  DATA 2500
17  DATA .1E-01,.6E-02
18  PRINT : PRINT : PRINT
20  READ R5
21  PRINT "RUN NOS.=",R5
22  PRINT
30  READ D3,D4,R,H,H1
31  READ D,L,D2,D6,D1,X,V6,C1,C2,W1,W2,M
32  READ V7
33  READ M7,M6
50  DIM K(50),U(50),P(50),F(50),O(50),C(50),G(50),Y(50),Q(50)
51  T1=-.1461E-01+(.17*D)
52  T3=.9E-03+(.132E-01*D)
53  T4=-.355E-01+(1.345*D)
54  B3=.893E-01+(.6207*D)
55  T0=(.2*D)-.36E-01
56  W=1/(3.14*T0)
60  T=((.11E05*X)/V6)*60
65  T=T/20
70  T2=(3.14*H1*((D1↑2)+D1*D2))*(60/V6)
80  L1=(((D2↑2)+(D6↑2))/2)↑.5
85  H=L/(1-(D6/D2))
90  L2=(L1*H)/D2
100  V1=.735*(.33*(H*(D2↑2)-(L2*(L1↑2)))-(H-L2)*(.95↑2))
110  T4=(V1/V6)*60
120  T2=T-(T1+T3+T4+T5)
130  A4=3.14*(D2/2)*((((D2/2)↑2)+(H↑2))↑.5)
131  A4=A4-3.14*(D6/2)*((((D/2)↑2)+(H↑2))↑.5)
140  V4=(3.14/12)*H*((D2↑2)-(D6↑3)/D2)-.735*L*(.95↑2)
150  V=(3.14/6)*(D↑3)
160  A5=6.23*((D1↑2)+(D1*R))
170  V5=3.14*H1*((D1↑2)+(D1*R))
175  B=(T1/.17)/((A5/V5)*((D↑3)/6)*3.14)
176  B1=(T3/.132E-01)/(3.14*(D↑2))
177  B=B*D*3.14
178  B1=B1*D*3.14
179  H7=2*((1+B+((B↑2)/3))↑.5):H8=2*((1-B1+((B1↑2)/3))↑.5)
181  A9=3.14*(D↑2)
182  A2=B3/B2
183  A7=(1-(A2↑2))↑.5
184  A1=LOG((1+A7)/(1-A7))
185  A1=1+((A2↑2)/(2*A7))*A1
186  A1=2*3.14*((B2/2)↑2)*A1
187  E=(A1-A9)/A9
188  PRINT "H7=",H7,"H8=",H8
189  PRINT "E=",E
190  REM      OSC. CONE AND SHEET  CONST. DIFF.  VAR. M.T.
191  S=0
192  FOR I=1,20
200  U(I)=(I*T)/T1
210  P(I)=((I*T)+T1)/T1
220  K(I)=P(I)-U(I)+B*((P(I)↑2)-(U(I)↑2))
```

APPENDIX 7 (CONT'D.)

PROGRAMME V (CONT'D.)

```
230  K(I)=K(I)+((B↑2)/3)*((P(I)↑3)-(U(I)↑3))
240  K(I)=(2/P(I))*(K(I)↑.5)
250  M1=(1/(1+M*((D3/D4)↑.5)))
260  K(I)=((D3/3.14*T1)↑.5)*M1*K(I)
270  F(I)=(6/D)*K(I)
280  E0=E+(3/8)*(E↑2)
290  E1=(E/2)+(E↑2)/4
300  E2=(E↑2)/32
310  U(I)=((I*T)+T1)*3.14*W
320  P(I)=((I*T)+T1+T2)*3.14*W
330  K(I)=((1+E0)*(P(I)-U(I)))-E1*(SIN(2*P(I))-SIN(2*U(I)))
340  K(I)=K(I)+E2*(SIN(4*P(I))-SIN(4*U(I)))
350  K(I)=(2/P(I))*(K(I)↑.5)
360  K(I)=((D3*W)↑.5)*M1*K(I)
370  O(I)=(6/D)*K(I)
375  O(I)=O(I)*(1+(E0/2))
380  U(I)=((I*T)+T1+T2)/T3
390  P(I)=((I*T)+T1+T2+T3)/T3
400  K(I)=P(I)-U(I)-B1*((P(I)↑2)-(U(I)↑2))
410  K(I)=K(I)+((B1↑2)/3)*((P(I)↑3)-(U(I)↑3))
415  K(I)=ABS(K(I))
420  K(I)=(2/P(I))*(K(I)↑.5)
430  K(I)=(D3/(3.14*T3))*M1*K(I)
440  C(I)=(6/D)*K(I)
450  U(I)=((I*T)+T1+T2+T3)*(3.14*W)
460  P(I)=((I*T)+T1+T2+T3+T4)*(3.14*W)
470  K(I)=(1+E0)*(P(I)-U(I))-E1*(SIN(2*P(I))-SIN(2*U(I)))
480  K(I)=K(I)+E2*(SIN(4*P(I))-SIN(4*U(I)))
485  K(I)=ABS(K(I))
490  K(I)=(2/P(I))*(K(I)↑.5)
500  K(I)=((D3*W)↑.5)*M1*K(I)
510  G(I)=(A4/V4)*K(I)
520  U(I)=((I*T)+T1+T2+T3+T4)*(3.14*W)
530  P(I)=((I*T)+T1+T2+T3+T4+T5)*(3.14*W)
540  K(I)=(1+E0)*(P(I)-U(I))-E1*(SIN(2*P(I))-SIN(2*U(I)))
550  K(I)=K(I)+E2*(SIN(4*P(I))-SIN(4*U(I)))
560  K(I)=(2/P(I))*(K(I)↑.5)
570  K(I)=((D3*W)↑.5)*M1*K(I)
580  Y(I)=(A5/V5)*K(I)
585  F(I)=F(I)*T1:O(I)=O(I)*T2:C(I)=C(I)*T3
586  G(I)=G(I)*T4:Y(I)=Y(I)*T5
590  Q(I)=F(I)+C(I)+O(I)+G(I)+Y(I)
600  S=S+Q(I)
601  NEXT I
604  REM     STAG. & CIRC. DROPS M.T. COEFF.  (K4 & K5)
605  V7=V7/(60*3.14*(5.03↑2))
606  V6=V6/(60*3.14*(5.03↑2))
607  V2=(V6/X)+(V7/(1-X))
608  P1=(D*V2)/D3
609  S1=(2*(3.14↑.5)*D3)/(3*D)
610  S2=.1E-02*V2
611  K4=1/((1/S1)+(M/S2))
612  S3=(.375E-02*V2)/(1+(M6/M7))
613  S4=1.13*((D4*V2)/D)↑.5
614  K5=1/((1/S3)+(M/S4))
615  K4=K4*(6/D)*(T1+T2+T3+T4+T5)
616  K5=K5*(6/D)*(T1+T2+T3+T4+T5)
```

APPENDIX 7 (CONT'D.)

PROGRAMME V (CONT'D.)

```
620  REM     OSC. CONE & SHEET  CONST. DIFF.  CONST. M.T.
630  A=((D3*W)↑.5)*M1
640  A1=((D3/(3.14*T1))↑.5)*M1
650  A3=((D3/(3.14*T3))↑.5)*M1
660  Z=T2*3.14*W
670  Z1=T4*3.14*W
680  Z2=T5*3.14*W
690  N1=(12/D)*A1*((1+B+((B↑2)/3))↑.5)
700  N=(((1+E0)*Z)-(E1*SIN(2*Z))+(E2*SIN(4*Z)))↑.5
701  N=(12/D)*(A/Z)*N
702  N=N*(1+(E0/2))
710  N2=(12/D)*A3*((1-B1+((B1↑2)/3))↑.5)
715  N3=ABS(((1+E0)*Z1)-(E1*SIN(2*Z1))+(E2*SIN(4*Z1)))
720  N3=N3↑.5
721  N3=(A4/V4)*(A/Z1)*2*N3
730  N4=(((1+E0)*Z2)-(E1*SIN(2*Z2))+(E2*SIN(4*Z2)))↑.5
731  N4=(A5/V5)*(A/Z2)*2*N4
735  N=N*T2:N3=N3*T4:N4=N4*T5
740  S1=20*(N1+N+N2+N3+N4)
750  REM     SOLID CONE & SHEET  CONST. DIFF.  CONST. M.T.
759  T4=ABS(T4)
760  N5=ABS(D3/3.14)
761  N5=(A4/V4)*M1*(2/(T4↑.5))*N5↑.5
769  T5=ABS(T5)
770  N6=ABS(D3/3.14)
771  N6=(A5/V5)*M1*(2/(T5↑.5))*N6↑.5
775  N5=N5*T4:N6=N6*T5
780  S2=20*(N1+N+N2+N5+N6)
790  REM      USE OF COMPLETE NO. OF OSCN.  I.E.  TOR=PI
800  N=((4*D3*W*(1+E0)/3.14)↑.5)*M1*(6/D)*T2
801  N=N*(1+(E0/2))
810  N3=N*(D/6)*(T4/T2)*(A4/V4)
820  N4=N*(D/6)*(T5/T2)*(A5/V5)
830  S3=20*(N1+N+N2+N3+N4)
840  REM     AS ABOVE BUT SOLID CONE & SHEET
850  S4=20*(N1+N+N2+N5+N6)
860  REM          PENETRATION     THEORY
870  S5=(A5+A4+(3.14*(D↑2)))/X
875  S5=S5*((D3/3.14)↑.5)*M1*(2/T↑.5)
880  S6=((D3/3.14)↑.5)*M1*(20*T)↑.5
885  S6=S6*((((.11E05*X)-19*(V4+V5))*(6/D)+19*(A4+A5))/(.11E05*X))
890  REM                    ONLY   OSC.        DROPS
900  S7=(6/D)*(1+(E0/2))*(21*T)
910  S7=S7*(((4*D3*W*(1+E0))/3.14)↑.5)*M1
920  REM                 SURFACE  RENEWAL
930  N1=(12/D)*A1*(2+(4/3)*B)↑.5
931  N=(6/D)*A*((2/(3.14↑.5))+.43*E)*T2
932  N2=(12/D)*A3*(2-(4/3)*B1)↑.5
933  N3=(A4/V4)*(D/6)*(T4/T2)*N
934  N4=(A5/V5)*(D/6)*(T5/T2)*N
935  N=N*(1+(E0/2))
940  S8=20*(N1+N+N2+N3+N4)
```

APPENDIX 7 (CONT'D.)

PROGRAMME V (CONT'D.)

```
950   REM                          EXP. VALUES
953   M2=(W1-W2)/(C1-C2)
954   M5=W1-(M2*C1)
955   M3=M*M2
956   M4=M*M5
960   S9=(1/(1-M3))*LOG((C1*(1-M3)-M4)/(C2*(1-M3)-M4))
970   PRINT
931   PRINT "S1=",S1
932   PRINT "S2=",S2
933   PRINT "S3=",S3
934   PRINT "S4=",S4
935   PRINT "S5=",S5
936   PRINT "S6=",S6
937   PRINT "S7=",S7
938   PRINT "S8=",S8
939   PRINT "S9=",S9
991   PRINT "K4=",K4
992   PRINT "K5=",K5
993   PRINT "P1=",P1
1000   END
```

APPENDIX 8

Typical Drop Count

Column : Non-Wetted Disc

System : Toluene-Water

RPM : 750

Hold-Up : 0.11

Compartment : 5th

Magnification: 2.0

d(mm)	n
0.5	63
1.0	26
1.5	17
2.0	7
2.5	4
3.0	3
3.5	9
4.0	7
4.5	6
5.0	4
5.5	6
6.0	2
6.5	1
	153 Total

$$d_{32} = \frac{\Sigma nd^3}{\Sigma nd^2} = 4.31 \text{ m.m.}$$

APPENDIX 8 (cont'd)

Drop Size Correlations For,

A. Non-Wetted Disc Column - This was given in Chapter 10, Equation 10.3 and Fig.10.5.

B. Wetted Disc Column

$$\left(\frac{d_{32}}{R}\right) = 2.75 \times 10^{-6}\left(\frac{NR^2\rho_c}{\mu_c}\right)^{0.42}\left(\frac{\mu_d}{\mu_c}\right)^{-0.314}\left(\frac{NR\mu_c}{\sigma}\right)^{-1.73}(X)^{0.293}$$

$$\text{EXP}\left[-0.55\,\frac{n}{z}\right] \qquad (10.5)$$

Observed d_{32}(mm)	Calculated d_{32}(mm)
3.0	2.2
1.3	1.5
1.6	1.3
3.6	2.4
1.8	1.7
1.3	1.5
4.0	2.8
3.0	2.4
1.9	1.9
1.3	1.7
5.6	5.2
4.9	4.6
4.3	4.1
2.2	2.8
2.5	3.3
3.1	3.7
4.1	3.2
2.3	2.2
1.6	1.9
8.2	13.7
5.5	6.0
3.6	3.8
2.3	3.1

APPENDIX 8 (cont'd)

B. (cont'd)

Observed d_{32}(mm)	Calculated d_{32}(mm)
9.7	10.5
5.3	4.6
1.8	2.4
6.4	5.2
5.3	5.2
3.6	3.3
2.0	2.6
7.6	6.7
7.0	6.7
3.9	4.3
2.3	3.4
6.3	6.7
7.3	7.4
2.0	2.0
4.6	3.9
6.4	4.4
5.3	4.8
2.5	5.5
1.4	1.6
3.0	3.1
3.7	3.6
7.4	3.8
2.4	2.5
3.9	2.8
5.7	3.0
6.1	3.1
0.9	1.3

APPENDIX 8 (cont'd)

C. Cone Column

$$\left(\frac{d_{32}}{R}\right) = 2.47 \times 10^{-3} \left(\frac{NR^2\rho_c}{\mu_c}\right)^{0.13} \left(\frac{\mu_d}{\mu_c}\right)^{0.2} \left(\frac{NR\mu_c}{\sigma}\right)^{-0.88} (X)^{0.35} \quad \text{EXP}\left[-0.5\,\frac{n}{z}\right] \qquad (10.6)$$

Observed d_{32}(mm)	Calculated d_{32}(mm)
6.3	4.6
6.7	5.7
4.7	6.5
5.6	7.3
7.5	8.0
4.5	3.8
5.3	4.7
5.5	5.4
6.8	6.5
3.0	3.5
5.0	4.8
4.0	4.3
6.0	5.4
7.5	6.0
2.4	3.3
3.7	4.5
5.5	5.0
6.7	5.6

NOMENCLATURE

A, a, a_r	Interfacial area
a_o	Initial radius or half axis length
a_p	Amplitude
a_w	Sheet extent for wave disintegration
a_{rw}	Sheet extent for combined wave and rim disintegration
B, b	Proportionality constants
$\Delta C, \Delta c$	Concentration driving force
C, c	Solute concentration
C, C_n	Constants (where n = 1 to 4)
C_Q	flow parameter
D, D_v	Diffusivity
D	Column diameter, Impeller diameter
D_E	Equivalent diffusivity = (Fraction resistance in dispersed phase) D_D + (Fraction resistance in continuous phase).D_C
d	Drop diameter
E, e	Eddy diffusivity
E	Energy
F	Harkin and Brown correction factor or Extraction factor = $\frac{mV_f}{V_s}$
F_B	Continuous phase axial diffusivity
F_C	Average liquid velocity
f	Mean actual interstage mixing per unit area of stator opening
g	Acceleration due to gravity

H	Compartment height
H,h	Column height or hold-up
h	Distance
h_m	Height equivalent of a stage = h_c/n
h_c	Overall column height
H_{toR}	Overall height of a transfer unit (raffinate phase)
HTU	Height of transfer unit
I	Intercept on the Φ axis (Ref.159)
i	ith stage
K,K_n	Constants (where n = 0 to 8)
K	Overall mass transfer coefficient
k	Individual mass transfer coefficient
k_{df}	Mass transfer coefficient for forming drops
L	Macroscale of turbulence or Flow rate
M	Velocity exponent
m	Equilibrium constant or Exponent in Eqn.3.47.
N	Moles per unit time, RPM or Number of drops
N_{we}	Weber number
N_{vi}	Viscosity group
N_{pe}	Peclet number
N_{toR}	Overall number of transfer units (raffinate phase)
n"	Wave number
n	Rotor speed, Number of stages, Const. in Eqn. 9.1
P	$\frac{Dv}{uh_c}$ in Equation 3.6b.
P	Energy input
ΔP	Pressure drop
Pe	Peclet number

Q	Volumetric flow rate
Q_m	Mass flow rate
R	Disc diameter or Raffinate phase flow rate
Re	Reynold's number
r	Drop radius or Disc radius
S	Stator diameter
S_o	Constant surface area
S_t or $S(\tau)$	Variable surface area
S_{drc}	Solute transferred per drop
Sc	Schmidt number
Sh	Sherwood number
S_L	Sheet thickness at cup lip.
S^*	Sheet thickness at point of free disintegration
T	Number of transfer units
t	Time
t_c	Circulation time
V	Velocity, Resultant Sheet velocity
$\bar{V}_N$	Characteristic drop velocity
V	volume, Drop Volume
v	Coalescence frequency, Velocity, Disc circumferential velocity
U	Velocity or flow rate
U_t	Terminal velocity
u	Disc radial velocity
u^*	Slip velocity
u_m	Mean radial velocity of liquid along wall of cup.
We	Weber number
w^*	Critical approach velocity

w, w'	Oscillation frequency, Angular velocity
w	Axial velocity component
X, x	Dispersed phase hold-up or Raffinate phase concentration
x	Distance
y, Y	Extract concentration
Z	Coalescence coefficient
z	h/h_c in Eqn.3.6.

Greek Letters

α	Major axis of an oscillating drop
β	Minor " " " " "
γ	Surface tension, Kinematic viscosity in Eqns.3.34 and 3.35
δ	Thickness of layer of fluid carried by the disc
ε	Amplitude of oscillation
ε_o	$\varepsilon + (3/8)\varepsilon^2$
$\zeta, \mathcal{Y}$	Microscale of turbulence
η	Liquid viscosity
θ	Time, Angle of Separation, Interfacial tension in Eqn.3.14. Half cone angle.
θ_c	Time between coalescence
λ_n	Eigen value, constant in Eqns.4.17 and 4.18.
λ	Constant in Eqn.3.6
μ	Viscosity
ξ	Dimensionless distance from wall = z/δ
π	3.14
ρ	Density
σ	Interfacial tension
τ	Dimensionless time

ν_r	Ratio of Kinematic viscosities of oil and water
ν	Kinematic viscosity
φ	Rate of drop formation
ϕ	Hold-up
ω	Angular velocity
α	$\left[\frac{\nu' - (3V/4\pi\nu')^2}{\nu'}\right]^{0.5}$, or ratio of volumetric flow rate to mean flowrate of interstage mixing (Eqn.3.67).
ν'	$(a_o + a_p \lvert \sin w't \rvert)^2$
Ψ	A function

Subscripts

A	Refers to phase A
app.	Apparent
av	Average
B	Bottom
c,C	Continuous, coalescence, column
CD,c	Circulating drop
crit.	Critical
d,D	Dispersed
dr	Drop
e,E	Extract, Efficiency
exp.	Experimental
F	Formation
f	Flooding, Final, Feed, Formation
H.B.	Harkin-Brown
h	Hold-up
i	In, Initial, Inside, Ith stage
k	Kinetic
L	Ligament
M	Middle

m	mean
min.	Minimum
max.	Maximum
N	Nozzle
o	Out, Outside
o, OD	Oscillating drop
o.c.	Overall value with respect to continuous phase
o.m.	Overall mean
p	Plug flow condition
R	Raffinate
RL,R	Release
S	Solute, Solvent, Stagnant, Slip
SD, s	Stagnant drop
S.d.	Stable drop
T	Top
vs	Refers to mean value
x	Refers to raffinate or x phase
y	Refers to extract or y phase
o	Refers to conditions at zero hold-up
1	Refers to initial condition
2	Refers to final condition

Superscripts

o	refers to no break-up and no longitudinal mixing condition in Eqn.3.6a, or initial value in Eqn.4.12.
*	Refers to equilibrium or phase inversion values.

REFERENCES

1. Treybal, R.E., Liquid Extraction, 2nd Edition (1963) McGraw-Hill.

2. Thornton, J.D., Ind.Chem., 632, Dec., 1963.

3. Thornton, J.D. and B.A. Bouyatiotis, Instn.of Chem.Eng.Symposium on Liquid-Liquid Extraction, April 1967; and Ind.Chem., 39,298 (1963).

4. Treybal, R.E., Chem.Eng.Prog., 62, 9, 67 (1966).

5. Davies, J.T., Turbulence Phenomena, Academic Press (1972), and Davies, J.T. and E. Rideal, Interfacial Phenomena, Academic Press (1963).

6. Moens, F.P. and Bos, R.G., Chem.Eng.Sci., 27, 403 (1972).

7. Danckwerts, P.V. Ind.Eng.Chem. 43, 1460 (1951).

8. Lewis, J.B. and H.R.C. Pratt, Nature 171, 1155 (1953).

9. Scheibel, E.G., Chem.Eng.Progr., 44, 681 (1948); and U.S. Patent 2,493,265 (1950).

10. Mumford, C.J., Brit.Chem.Eng., 13,7,981 (1968).

11. Molyneux, F. Chem.Proc.Eng. 502, (1962).

12. Morella, V.S. and N. Poffenberger, Ind.Eng.Chem. 42, 6, 1021 (1950).

13. Hanson, C. Brit.Chem.Eng. 10, 34 (1965).

14. Thornton, J.D. Chem.Eng.Sci. 5, 201 (1956).

15. Crawford, J.W. and C.R. Wilke, Chem.Eng.Progr. 47, 425 (1951).

16. Garner, F.H., S.R.M. Ellis and D.W. Fosbury, Trans.Instn.Chem.Engrs. 31, 348 (1953).

17. Garner, F.H., S.R.M. Ellis and J.W. Hill, A.I.Ch.E. Journal 1, 185, (1955) and Trans.Instn.Chem.Engrs. 34, 223 (1956).

18. Sobotic, R.H. and D.M. Himmelblau, A.I.Ch.E. Journal 6, 619 (1960).

19. Haynes, L.G., D.M. Himmelblau and R.S. Schechter, I. & E.C. Process Design and Development, 7, 508 (1968).

20. Buchanan, R.H., Australian J.Appl.Sci. 3, 233 (1952).

21. Treybal, R.E. Mass Transfer Operations, 2nd Edition, McGraw-Hill (1968).

22. Mar, B.W. and A.L. Babb, Ind.Eng.Chem. 51, 1011 (1959).

23. Woodfield, F.N. and G. Sege, Chem.Eng.Progr.Symp.Ser., 50(13), 14 (1954).

24. Thornton, J.D., Trans.Instn.Chem.Engrs. 35, 316 (1957).

25. Logsdail, D.H. and J.D. Thornton, Trans.Instn.Chem.Engrs. 35, 331 (1957).

26. Coggan, G.C., Instn.of Chem.Engrs.Symp. on Liquid-Liquid Extraction, April 1967.

27. Oldshue, J.Y. and Rushton, J.H. Chem.Eng.Prog., 48, 297 (1952).

28. Dykstra, J., Thompson, B.H. and Clouse, R.J., Ind.Eng.Chem., 50, 161 (1958).

29. Jones, R. Soc. of Chem.Ind., Conference on Solvent Extraction, London, 27th March, 1969.

30. Gutoff, E.B., A.I.Ch.E. Journal, 11,4, 712 (1965).

31. Reman, G.H. and Van der Vusse, J.G., Pet. Refiner, 34, 9, 129 (1955).

32. Ingham, J. Paper presented to 3rd International Congress on Chem. Eng., Marianske Lazne, September, 1969.

33. Misek, T., Coll.Czech., Chem.Comm., 28, 426 and 570 (1963).

34. Bibaud, R.E. and R.E. Treybal, A.I.Ch.E.Jour., 12, 472 (1966).

35. Mumford, C.J., Ph.D. Thesis, University of Aston (1970).

36. Thornton, J.B. and B.A. Bouyatiotis, Ind.Chemist, 39, 298 (1963).

37. Arnold, D.R., Unpublished Work, University of Aston.

38. Nagata, S., W. Eguchi, T. Yokoyama, and K. Meade, Chem.Eng. (Japan), 17, 20 (1953) and 20, 2 (1956).

39. Honekemp, J.R. and L.E. Burkhart, Ind.Eng.Chem.Proc.Design and Dev., 1,3,177 (1962).

40. Piper, H.B., M.Sc.Thesis, University of Manchester (1966).

41. Sitaramayya, T. and G.S. Laddha, Chem.Eng.Sci., 13, 263 (1960).

42. Lewis, J.B., I. Johns, and H.R.C. Pratt, Trans.Instn.Chem.Eng., 29, 126 (1951).

43. Thomas, R.J., Private Communication, University of Aston.

44. Karr, A.E. and E.G. Scheibel, Chem.Eng.Prog.Symp.Series No.10, 50, 73 (1954).

45. Schiebel, E.G., A.I.Ch.E.Jour. 2, 74 (1956).

46. Davies, G.A., G.V. Jeffreys, and M. Azfal, Brit.Chem.Eng. & Proc. Tech. 17,9, 709 (1972).

47. Leisibach, J. Chem.Eng.Tech., 3, 205 (1965).

48. Tudose, R, International Chem.Eng., 2, 156 (1962).

49. Misek, T. Chem.Eng., 68, 58 (1961) and Czechoslovakian Patent No.88, 415, A.R.D. Extractor-Technoexport, Prague and Luwa (U.K.) Literature.

50. Marek, J., T. Misek and F. Widmer, Soc.Chem.Ind.Symposium, Univ. of Bradford, (U.K.), 31st Oct., 1967.

51. Marek, J. and T. Misek, Soc. of Chem.Ind., Conference on Solvent Extraction, London, 27th March, 1969.

52. Misek, T. and J. Marek, Brit.Chem.Eng. Feb. 1970.

53. Reman, G.H., Dutch Patent, 70, 866.

54. Krishnaiah, N.M., et al., Brit.Chem.Eng., 12, 719 (1967).

55. Gouroji, I.C., A.S. Narula and M.U. Pai, Brit.Chem.Eng., 5, 67 (1971).

56. Nakamura, A and S. Hiratsuka, Kagaku Kogaku, 30, 1003 (1966).

57. Sokov, Y.F. and Z.D. Putilova, Tr.Vses Nouchn Tekn., Soveshch Protsessy Zhidkostnoi Elektraktsii i Khemosrbtsii, 2nd Ed. Leningrad pp.228 (1966).

58. Simonis, H. Process Engineering, November 1972, pp.110.

59. Kuhni, A.G., Verfahrens technik and Apparatebau, CH-4123 Allschwil-Basel, Schweiz.

60. Shell Internationale research, Maatschappij, N.V., Belgian Patent 632926 (28th Nov.1963).

61. Thomas, W.J., Trans.Instn.Chem.Engrs., 47, 304 (1969).

62. Podbielniak Inc., Division of Dresser Industries (G.B.) Ltd., Knightsbridge, London.

63. Barson, N. and Beyer, G.H. Chem.Eng.Progr. 49, 243 (1953).

64. Jacobson, F.M. and Beyer, G.H. A.I.Ch.E. Journal, 2, 283 (1956).

65. Eisenlohr, H. Ind.Chemist 27, 271 (1951).

66. Eisenlohr, H. and Scharlan, A. Pharm.Ind. 17, 207 (1955).

67. Brink, A.A. and Gericke, J.J., S.African Ind.Chemist, 18,11,152 (1964).

68. Kagan, S.Z., Trukhanov, L.G., Kostin, P.A. and Kudryarstev, S.N., Interrat.Chem.Eng. 4, 473 (1964).

69. Westerterp, K.R. and Landsman, P. Chem.Eng.Sci., 3, 55 (1954).

70. Reman, G.H. and Olney, R.B., Chem.Eng.Prog., 51, 141 (1955).

71. Kung, E.Y., and Beckmann, R.B., A.I.Ch.E.Journal, 7, 319 (1961).

72. Logsdail, D.H., Thornton, J.D. and Pratt, H.R.C., Trans.Instn. Chem.Eng., 35, 301 (1957).

73. Vermijs, H.J.A. and Kramers, H., Chem.Eng.Sci., 3, 55 (1954).

74. Strand, C.P., Olney, R.B. and Ackerman, G.H., A.I.Ch.E. Journal 8,525 (1962).

75. Misek, T., Rotacni Diskove Extraktory, Statni Nakadelstri Literatury, Prague 1964.

76. Reman, G.H., Proc.3rd World Petrol Congress, Hague, Section III, (1951), 121, and U.S. Patents, 2,601 (1952); 2,729,545 (1956); 2,912,310 (1959).

77. Misek, T., Coll.Czech.Chem.Comm., 28, 1631 (1963).

78. Rozkos, B., Reasurch Rep. 918/69 VUCHZ Praha.

79. Rod, V., Paper Presented at 3rd International Congress on Chem. Eng., Marianske Lazne, Sept.1969, and Brit.Chem.Eng., 16, 617 (1971).

80. Van de Vusse, J.G., Chem.Eng.Sci. 10, 229 (1959).

81. Reman, G.H., Joint Symposium - The Scaling-Up of Chem.Plant and Processes, Instn.of Chem.Eng., 26 (1957); and Pet.Ref., 36, 9, 269 (1967).

82. Reman, G.H., Chem.Eng.Prog., 62(9),56 (1966).

83. Quinn, J.A. and D.B. Sigloh, Can.J.Chem.Eng., 41, 15 (1963).

84. Selker, A.H. and C.A. Sleicher jr., Can.J.Chem.Eng., 298 Dec.(1965).

85. Luhning, R.W. and H. Sawistowski, Paper presented at I.S.E.C., The Hague (1971).

86. Yeh, G.C., C.A. Haynie Jun. and R.A. Mosses, A.I.Ch.E.Jour., 10, 260 (1964).

87. Juma, S.M., M.Sc. Thesis, University of Manchester (1969).

88. Jeffreys, G.V., Chem.and Proc.Eng., 49, 111 (1968).

89. Harkins, W.D. and F.E. Brown, J.Am.Chem.Soc., 41, 499 (1919).

90. Treybal, R.E. and C.B. Howarth, Ind.Eng.Chem., 42, 1174 (1950).

91. Null, H.R. and H.F. Johnson, A.I.Ch.E.Jour. 4, 273 (1958).

92. Meister, J.B., Ph.D. Thesis, Cornell Univ. New York (1966).

93. Heertjes, P.M. and L.H. de Nie, Mass transfer to drops, Recent Advances in Liquid-Liquid Extraction Edited by Hanson, C., Pergamon Press, N.Y. etc., (1971).

94. Narasinga Rao, E.V.L., R. Kumar and N.R. Kuloor, Chem.Eng.Sci., 21, 867, (1966).

95. Scheele, G.E. and B.J. Meister, A.I.Ch.E.Jour. 14, 9 (1968).

96. Wellek, R.M. et al., A.I.Ch.E.Jour., 12, 854 (1966).

97. Dixon, B.E. and A.A.W. Russel, J.Soc.Chem.Ind., Lond., 69, 284 (1950).

98. Heertjes, P.M. and L.H. de Nie, Chem.Eng.Sci., 21, 755 (1966).

99. Angelo, J.B., E.N. Lightfoot and D.W. Howard, A.I.Ch.E.Jour. 12, 751 (1966).

100. Hinze, J.O., A.I.Ch.E. Jour. 1,289 (1955).

101. Kolomogoroff Cited in Ref. (100).

102. Clay, P.H., Cited in Refs. (100 & 74).

103. Shinnar, R. and J.M. Church, Ind.Eng.Chem., 52, 3, 253 (1960).

104. Rushton, J.H. et al. Chem.Eng.Prog. 52, 515 (1956).

105. Vermeulen, T., et al. Chem.Eng.Prog., 51, 85F (1955).

106. Jeffreys, G.V. and C.J. Mumford, Paper Presented at the 3rd CHISA Congress, Marianske Lazne, Sept. (1969).

107. Jeffreys, G.V. and C.J. Mumford, Paper Presented at I.S.E.C., The Hague, (1971).

108. Thomas, R. and C.J. Mumford, Paper presented at I.S.E.C., The Hague, (1971).

109. Thornton, J.D., I.Ch.Eng.Symp.Series, Nos.26,73 and 80 (1967).

110. Levich, V.G., "Physicochemical Hydrodynamics", Prentice Hall, New Jersey (1962).

111. Madden, A.J. and G.L. Damerell, A.I.Ch.E.Jour. 8, 233 (1962).

112. Miller, R.S. et al., A.I.Ch.E.Jour. 9, 196 (1963).

113. Sleicher, C.A.Jr., A.I.Ch.E.Jour., 8, 471 (1962).

114. Olney, R.B., A.I.Ch.E.Jour., 10, 827 (1964).

115. Stainthorpe, F.P. and N. Suddall, Trans.Instn.Chem.Engrs., 42, 198 (1964).

116. Calderbank, P.H., Trans.Instn.Chem.Engrs., 36, 443 (1958).

117. Lawson, G.B., Ph.D.Thesis, University of Manchester (1967).

118. Davies, J.T. et al. Trans.Instn.Chem.Engrs., 38, 331 (1960).

119. Howarth, W.J., Chem.Eng.Sci., 19, 33 (1964).

120. Misek, T., Coll.Czech.Chem.Comm., 29, 2086 (1964).

121. Jeffreys, G.V. and G.A. Davies, "Advances in Liquid-Liquid Extraction", Edited by Hanson, C., Pergamon Press, N.Y. etc., (1971).

122. Hitit, A., Ph.D.Thesis, University of Aston (1972).

123. Smith, D.V., Ph.D.Thesis, University of Manchester, (1969).

124. Jeffreys, G.V. and J.L. Hawksley, A.I.Ch.E.Jour. 11, 413 (1965).

125. Groothus, H. and F.J. Zwiderweg, Chem.Eng.Sci., 12,288 (1960).

126. McFerrin, A.R. and R.R. Davison, A.I.Ch.E. Jour. 17, 1021 (1971).

127. Jeffreys, G.V. and G.B. Lawson, Trans.Instn.Chem.Engrs., 43, 294 (1965).

128. Sawistowski, H., 'Recent Advances in Liquid-Liquid Extraction', Edited by Hanson, C., Pergamon Press, N.Y. etc. (1971).

129. McCay, G.D.H. and S.G. Mason, J.Colloid Sci. 18, 674 (1963).

130. Heertjes, P.M. and L.H. de Nie, Paper presented at I.S.E.C. The Hague, (1971).

131. Sternling, C.V. and L.E. Scriven, A.I.Ch.E.Jour., 5,514 (1959).

132. Stemerding, S., et al., Chemie-Ingr-Tech., 35, 844 (1963).

133. Suddal, N. Ph.D.Thesis, University of Manchester (1962).

134. Westerterp, K.R. and P. Landsman, Chem.Eng.Sci., 17, 363 (1962).

135. Nagata, S., et al., Chem.Eng., Tokyo, 21, 784 (1957).

136. Misek, T. and B. Roskos, Int.Chem.Eng., 6, 130 (1966).

137. Misek, T. Paper Presented at 2nd Chisa Congress, Marienbad, Czechoslovakia (1965).

138. Miyauchi, T. et al., A.I.Ch.E.Jour. 12, 508 (1966).

139. Rushton, J.H. et al., Chem.Eng.Prog., 46, 467 (1950).

140. Sleicher, C.A., A.I.Ch.E.Jour. 5, 145 (1959).

141. Newman, A.B., Trans.Am.Inst.Chem.Engrs., 27, 310 (1931).

142. Handlos, A.E. and T. Baron, A.I.Ch.E.Jour., 3, 127 (1957).

143. Misek, T. and V. Rod., "Recent Advances in Liquid-Liquid Extraction" Edited by Hanson, C., Pergamon Press, Oxford, etc., (1971).

144. Miyauchi, T. and T. Vermeulen, Ind.Eng.Chem.Funds., 2, 304 (1963).

145. Hartland, S., and J.C. Mechlenburgh, Chem.Eng.Sci., 21, 1209 (1966).

146. Rod, V. Br.Chem.Eng., 9, 300 (1964).

147. Danckwerts, P.V., Chem.Eng.Sci., 2, 1 (1953).

148. Misek, T. and V.Rod, Paper presented at 2nd Chisa Congress, Marienbad (1965).

149. Sherwood, T.K., et al. Ind.Eng.Chem., 31, 1144 (1939).

150. West, F.P., et al, Ind.Eng.Chem., 43, 234 (1951); 44, 625 (1952).

151. Licht, W., and W.F. Pensing, Ind.Eng.Chem., 45, 1885 (1953).

152. Heertjes, P.M. and W.A. Holve, Chem.Eng.Sci., 3, 122 (1954).

153. Sawistowski, H., and G.E. Goltz, Trans.Instn.Chem.Engrs., 41,174 (1963).

154. Ilkovic, D., Colln.Czech.Chem.Comm. 6, 498 (1934).

155. Baird, M.H.I., Chem.Eng.Sci., 9, 267 (1959).

156. Beek, W.J. and H. Kramers, Chem.Eng.Sci., 16,909 (1962).

157. Groothuis, H. and H. Kramers, Chem.Eng.Sci., 4, 17 (1955).

158. Michels, H.H., Thesis, Delaware (1960).

159. Skelland, A.H.P. and S.S. Minhas, A.I.Ch.E.Jour., 17, 1316 (1971).

160. Coulson, J.H. and S.J. Skinner, Chem.Eng.Sci., 1,197 (1951).

161. Rajan, S.M. and W.J. Heideger, A.I.Ch.E.Jour., 17, 202 (1971).

162. Popovich, A.T. et al., Chem.Eng.Sci., 19, 357 (1964).

163. Ueyama, K. and H. Kida, Kagaku Kikai, 21, 188 (1957).

164. Heertjes, P.M. and L.H. de Nie, Chem.Eng.Sci., 26,697 (1971).

165. Licht, W. and J.B. Conway, Ind.Eng.Chem., 42, 1151 (1950).

166. Marsh, B.D. and W.J. Heideger, Ind.Eng.Chem. Fundamentals, 4, 129 (1965).

167. Hadamard, J. C.R. hebd. Seanc.Acad.Sci.Paris, 152, 1735 (1911).

168. Kronig, R. and J.C. Brink, Appl.Scient.Res., A2, 142 (1960).

169. Johnson, A.I. and A.E. Hamielec, A.I.Ch.E.Jour., 6, 145 (1960).

170. Skelland, A.H.P. and R.H. Wellek, A.I.Ch.E.Jour., 10,491 (1964).

171. Garner, F.H. and H. Tayeban, An.R.Soc.esp.Fis.Quim., 56B,479 (1960), and Garner, F.H. and J.J. Lane, Trans.Instn.Chem.Engrs., 37, 162 (1959).

172. Olander, D.R., A.I.Ch.E. Jour., 12, 1018 (1966).

173. Rose, P.M. and R.C. Kintner, A.I.Ch.E.Jour., 12, 530 (1966).

174. Kinard, G.E., F.S. Manning, and W.P. Manning, Brit.Chem.Eng., 8, 326 (1963).

175. Linton, M., and K.L. Sutherland, Chem.Eng.Sci., 12, 214 (1960).

176. Griffith, R.M., Chem.Eng.Sci., 12, 198 (1960).

177. Row, P.N. et al. Trans.Instn.Chem.Engrs., 43, 14 (1965).

178. Baird, M.H.I. and A.E. Hamielec, Can.J.Chem.Eng., 40, 119 (1962).

179. Hughmark, G.A. Ind.Eng.Chem.Funds., 6, 408 (1967).

180. Thorsen, G. et al., Chem.Eng.Sci., 23, 413 (1968).

181. Hendrix, C.D. et al. A.I.Ch.E.Jour., 13, 1072 (1967).

182. Elzinga, E.R. and J.T. Banchero, A.I.Ch.E.Journ.7, 394 (1961).

183. Mok, Y.I. and R.E. Treybal, A.I.Ch.E.Jour., 17, 916 (1971).

184. Schindler, H.D. and R.E. Treybal, A.I.Ch.E. Jour., 14, 790 (1968).

185. Harriott, P., Can.J.Chem.Eng., 40,60 (1962).

186. Holmes, D.B. et al., Chem.Eng.Sci., 19, 201 (1964).

187. Golden, J.O., Thesis, Iowa, 1964. Diss.Abstr.25, 1070 (1964).

188. Austin, L.J. et al., Chem.Eng.Sci., 21, 1109 (1966).

189. Adamson, A.W. Physical Chemistry of surfaces, Interscience Publishers, Inc. 1960.

190. Osipow, L.I. "Surface Chemistry" Reinhold Publishing Corp. 1962.

191. Shuttleworth, R. and Bailey, Discussion Faraday Soc., 3, 16 (1948).

192. Cassie, A.B.D. Discussion Faraday Soc., 3, 11 (1948).

193. Wenzel, R.N. Ind.Eng.Chem. 28, 988 (1936); J.Phys. and Colloid Chem., 53, 1466 (1949).

194. Jackson, M.L., Holman, K.L. and Grove, D.B., A.I.Ch.E.Journal, 8, 659 (1962).

195. Sege, G. and Woodfield, F.M. Chem.Eng.Progr. 50, 396 (1954).

196. Friedman, S.J., Gluckert, F.A. and Marshall Jr. W.R., Chem.Eng. Prog. 48, 181 (1952).

197. Fraser, R.P., Dombrowski, N. and Routley, J.H. Chem.Eng.Sci., 18, 323, (1963).

198. Fraser, R.P. and Eisenklam, P. J.Imp.Coll.Chem.Eng.Soc., 7, 53 (1953).

199. Dombrowski, N. and Johns, W.R. Chem.Eng.Sci., 18, 203 (1963).

200. Dombrowski, N. and Fraser, R.P. Phil.Trans. A247, 101 (1954).

201. Weber, C.Z., Angew.Math.Mech. 11, 136 (1931).

202. Appel, F.J. and Elgin, J.C. Ind.Eng.Chem., 29, 451 (1937).

203. Meisner, H.P. Stokes, C.A., Hunter, C.M. and Morrow, G.M. Ind.Eng.Chem. 36, 917 (1944).

204. Treybal, R.E. Ind.Eng.Chem. 51, 262 (1960).

205. Berg, C., Manders, M. and Switzer R., Am.Inst.Chem.Engr., Los Angeles Calif., March 9, 1949.

206. Osmon, F.O. and Himmelblau, D.M. Journal of Chemical and Engineering Data, 6, 551 (1961).

207. Alder, C.R. and W.R. Marshall, Chem.Eng.Prog., 47, 515 (1951).

208. Bowen, W.S., Ind.Eng.Chem., 30, 1001 (1938).

209. Herring, W.M. and W.R. Marshall, A.I.Ch.E.Jour. 1,200 (1955).

210. Lewis, H., Ind.Chemist., pps. 10,439, 499 (1934) and pp.1171 (1935).

211. Emslie, A.G. et al. Jour.of Appl.Physics. 29, 858 (1958).

212. Dixon, B.E., et al., Brit.J.Appl.Phys., 3, 115 (1952).

213. Hinze, J.O. and H. Milborn, Jour. of Appl.Mechanics, 17, 145 (1950).

214. Bar, P. Cited in Ref. (196).

215. Dombrowski, N., D. Hasson and D. E. Ward, Chem.Eng.Sci. 12, 35 (1960).

216. Hasson, D. and J. Misrahi, Trans.Instn.Chem.Engrs., 39, 415 (1961).

217. Dombrowski, N. and P.C. Hooper, Chem.Eng.Sci., 17, 291 (1962).

218. Frazer, R.P., et al., A.I.Ch.E.Jour. 8, 672 (1962).

219. Dorman, R.G., Brit.J.Appl.Phys., 3, 189 (1952).

220. Schlichting, H., 'Boundary Layer Theory', 4th Edition, McGraw-Hill, (1962).

221. Cochran, W.G., Proc.Cambridge Phil.Soc., 30, 365 (1934).

222. Browning, E., Toxicity and Metabolism of Industrial Solvents, Elsevier 1965.

223. Sterbacek, Z. and P. Tausk, Mixing in the Chemical Industry, Pergamon 1965.

224. Siedel, A., Solubilities of Inorganic and Metal Organic Compounds, Vol.II, 4th Edition, (1965).

225. Allak, A.M.A., Private Communication, University of Aston.

226. King, P.J. and E. Rhodes, Manufacturing Chem., pp.51, June 1964.

227. Carl Zeiss, Oberkochen/Wuertt, West Germany.

228. Sondes Place Research Institute, Dorking, Surrey, U.K.

229. Jeffrey s G.V., Private Communication, University of Aston.

230. Wilke, C.R. and Pin Chang, A.I.Ch.E. Jour., 1, 264 (1955).

231. Nanda, A.K. and M.M. Sharma, Chem.Eng.Sci., 21, 707 (1966).

232. Jillood, A.A.K., M.Sc.Thesis University of Aston (1973).

233. Resnick, W., Paper presented to 3rd International Congress on Chem.Eng. Marianske Lazne, Sept. 1969.

234. Vcek, P. and P. Nekovar, Paper presented at Chisa Conference 1972.